mgr inż. Michał Liput

The role of nuclear FGFR1 conditional upregulation in mitochondrial dynamics and neural differentiation during early development of hiPSC$^{Tet3G\text{-}FGFR1(SP\text{-}/NLS)}$ derived brain organoids

Rola warunkowej nadekspresji jądrowego FGFR1 w dynamice mitochondriów i różnicowaniu neuronalnym podczas wczesnego rozwoju organoidów mózgu pochodzących z linii hiPSC$^{Tet3G\text{-}FGFR1(SP\text{-}/NLS)}$

Dissertation for the academic doctoral degree
in the field of medical and health sciences
in the discipline of medical sciences

Supervisor: Prof. dr hab. n. med. Leonora Bużańska
Supervisor: Prof. Michał Stachowiak

Proceedings for a doctoral degree conferment
in Mossakowski Medical Research Institute
Polish Academy of Sciences

Warszawa 2025

Acknowledgements

I want to express my gratitude to my supervisor, Prof. dr. hab. Leonora Bużańska, for providing me with the unique opportunity to join her laboratory and for mentoring me in neural stem cells and the brain organoid field. I sincerely appreciate the opportunity to engage in her projects and for the constant support of my scientific career. I am thankful for the chance to explore innovative and challenging research approaches.

I want to thank my supervisor, Prof. Michał Stachowiak (University at Buffalo), for his scientific guidance and mentorship. It has been a great pleasure to observe his problem-solving skills, innovative approach, and passion for science. His guidance and the scientific discussions we shared have greatly shaped my journey as a researcher.

I am also very grateful to Prof. Ewa Stachowiak from the University at Buffalo for her guidance in the methodologies of brain organoids and immunocytochemistry techniques.

I want to express my gratitude to all current and former members of the Department of Stem Cell Bioengineering—especially Zuza, Erkan, and Valery—for their friendship, support, and inspiring discussions.

Special thanks go to Dr. Hanna Kozłowska, the head of the Environmental Laboratory of Laser Microscopic Techniques at IMDIK PAN, and Grzegorz Pałka for their constant professional support and assistance.

I extend special thanks to my friend Ania Balcerak (National Institute of Oncology, Warsaw) for providing plasmids, as well as for her support and guidance in molecular cloning, and to the members of Professor Stachowiak's lab at SUNY Buffalo, with whom I have collaborated.

I want to extend my heartfelt thanks to my parents and my sister. Special thanks go to my wife, Kamila - I will forever appreciate your unwavering support throughout the years and your insightful scientific feedback.

The execution of this work was made possible thanks to the financial support provided by:

- The OPUS grant from the National Science Centre (2019/35/B/NZ3/04383)
- PRELUDIUM grant from the National Science Centre (2022/45/N/NZ3/04202)
- National Science Foundation (USA) Award (CBET 2039190)
- US Fulbright Award (Michal K. Stachowiak Fulbright Distinguished Professor, Chair of Medical Sciences).

Table of contents

List of abbreviations

- **ATP** – *adenosine triphosphate*: the primary energy currency of the cell.
- **BCL11B** – B-cell CLL/lymphoma 11B (CTIP2): a transcription factor marking deep-layer cortical neurons.
- **BDNF** – *brain-derived neurotrophic factor*: recombinant neurotrophin that promotes neuronal survival, differentiation, and maturation *in vitro*.
- **BSD** – *blasticidin S-deaminase*: confers resistance to the antibiotic blasticidin for selection of edited clones.
- **ChIP-seq** – *chromatin immunoprecipitation followed by sequencing*: maps genome-wide binding sites of DNA-associated proteins.
- **CLYBL** – *Citramalyl-CoA lyase locus*: a genomic "safe-harbor" site on chromosome 13 used for stable transgene integration.
- **DMEM/F-12** – *Dulbecco's Modified Eagle Medium：Ham's F-12 nutrient mixture*: basal medium for culturing 293FT cells and various stem cell derivatives.
- **DMSO** – *dimethyl sulfoxide*: organic solvent used as vehicle control or to dissolve small-molecule inhibitors.
- **DOX** – *doxycycline*: tetracycline-analog used to induce TRE3G-driven transgene expression.
- **DPBS** – *Dulbecco's Phosphate-Buffered Saline*: balanced salt solution without Ca^{2+}/Mg^{2+}.
- **EB** – *embryoid body*: Three-dimensional aggregates of pluripotent stem cells cultured under non-adherent conditions to promote spontaneous differentiation into the three germ layers: ectoderm, mesoderm, and endoderm.
- **EDTA** – *ethylenediaminetetraacetic acid*: chelating agent used to dissociate and passage adherent stem cells.
- **EGF** – *epidermal growth factor*: recombinant protein used to support proliferation and survival of neural progenitors and NES cells.
- **FGF-2 (bFGF)** – *fibroblast growth factor 2 (basic FGF)*: recombinant growth factor used to maintain stem cell pluripotency and promote neural progenitor proliferation.

- **FGFR1** – *fibroblast growth factor receptor 1*: tyrosine kinase receptor that acts as a cell surface receptor for fibroblast growth factors or functions as a nuclear protein, playing a key role in embryonic development, neural progenitor proliferation, and differentiation.
- **GlutaMAX** – *L-alanyl-L-glutamine supplement*: stabilized dipeptide substitute for L-glutamine to reduce ammonia buildup in culture.
- **GO** – *Gene Ontology*: a structured vocabulary for annotating gene and protein functions across three domains—Biological Process, Molecular Function, and Cellular Component.
- **hCO** – *human cortical organoid*: three-dimensional, stem-cell-derived neural tissue that self-organizes into cortical-like germinal and neuronal layers *in vitro*, modeling developing human cortex.
- **hiPSC** – *human induced pluripotent stem cells*: somatic cells reprogrammed by ectopic expression of OCT4, SOX2, KLF4, and c-MYC (Yamanaka factors), expressing pluripotency markers such as OCT4, SOX2, NANOG, TRA-1-60, and SSEA-4, capable of self-renewal and differentiation into all three germ layers.
- **Hi-C** – *high-throughput chromosome conformation capture*: analysis of intra- and inter-chromosomal DNA interactions.
- **Hi-ChiP** – *ChiPseq combined with High-throughput Chromosome Conformation Capture*.
- **INFS** – *Integrative nuclear FGFR1 signaling*: the genome-wide transcriptional program coordinated by nFGFR1.
- **IPC** – *intermediate progenitor cell*: $TBR2^+$ transit-amplifying progenitors in the subventricular zone (SVZ) that undergo symmetric divisions to increase neuronal output.
- **Ki-67** – Marker of proliferation; a nuclear protein expressed in actively cycling cells.
- **LC3B** – *Microtubule-associated protein 1 light chain 3 beta*: an autophagosome membrane protein used as a mitophagy marker.
- **LC-MS/MS** – *liquid chromatography–tandem mass spectrometry*: analytical platform for identifying and quantifying proteins.
- **mApple** – *mApple fluorescent protein*: a red-fluorescent reporter used to track transgene expression.

- **MIM** – *mitochondrial inner membrane*: membrane forming cristae in mitochondria, enriched in ETC complexes and ATP synthase.
- **mitoKeima** – *mitochondria-targeted Keima*: a ratiometric fluorescent reporter for quantifying mitophagy via pH-sensitive excitation shifts.
- **MMP** – *mitochondrial membrane potential*: an indicator of mitochondrial health measured by potential-sensitive dyes (e.g. MitoTracker).
- **MOM** – *mitochondrial outer membrane*: the permeable outer bilayer of mitochondria, enclosing the intermembrane space.
- **mtDNA** – *mitochondrial DNA*: ~16.5 kb circular genome encoding 13 OXPHOS proteins, 22 tRNAs, and 2 rRNAs.
- **NES** – *neuroepithelial stem cell.*
- **nFGFR1** – *nuclear FGFR1:* (i) Endogenous hypoglycosylated receptor is transported from the cytosol to the nucleus by a Nuclear Localization Signal, providing FGF ligand, or (ii) a recombinant FGFR1(SP-/NLS) variant that lacks the signal peptide and contains a nuclear localization signal, acting as a constitutively active nFGFR1.
- **NLS** – *nuclear localization signal*: a short peptide motif added to FGFR1 to drive its constitutive nuclear import.
- **NSPC** – *neural stem/progenitor cells*: a population of neuroepithelial cells that includes both neural stem cells and neural progenitors, expressing nestin, SOX2, and PAX6 in the developing nervous system, proliferating and differentiating into neurons.
- **NT-3** – *neurotrophin-3*: recombinant growth factor used to support maturation and survival of developing neurons in organoid cultures.
- **OSVZ** – *outer subventricular zone*: expanded SVZ region in gyrencephalic brains containing oRG and IPCs, driving cortical expansion.
- **OXPHOS** – *oxidative phosphorylation*: mitochondrial process coupling electron transport to ATP synthesis via the electron transport chain.
- **PAX6** - *Paired box 6*: a transcription factor marking neuroepithelial progenitors.
- **PBS** – *Phosphate-Buffered Saline*.

- **PCA** – *principal component analysis*: a dimensionality-reduction technique that transforms data into a coordinate system where principal components (PCs) are axes capturing the most variance.
- **oRG** – *outer radial glia*: basal progenitors in the outer SVZ lacking apical contacts, capable of mitotic somal translocation and direct neuron generation.
- **PEI** – *polyethylenimine*: cationic polymer used as a transfection reagent for DNA delivery into mammalian cells.
- **PGC-1α** – *peroxisome proliferator-activated receptor γ coactivator 1-alpha*: a master regulator of mitochondrial biogenesis.
- **PGC1α-EGFP** – *peroxisome proliferator-activated receptor gamma coactivator 1α reporter fused to EGFP*: live reporter for mitochondrial biogenesis, where EGFP is driven by PGC1α promoter.
- **PINK1** - *PTEN-induced putative kinase 1*: a serine/threonine kinase that recruits Parkin to damaged mitochondria.
- **rtTA** – *reverse tetracycline-controlled transactivator*: the protein that binds TRE3G and activates transcription in the presence of doxycycline.
- **ROS** – *reactive oxygen species*: chemically reactive molecules derived from oxygen
- **RT-qPCR** – *reverse transcription quantitative polymerase chain reaction*: measures RNA expression levels via cDNA quantification.
- **SOX2** – *SRY-box transcription factor 2*: a key pluripotency and neural progenitor marker.
- **SYP** – *synaptophysin*: an integral membrane protein of synaptic vesicles; marker of presynaptic terminals.
- **SVZ** – *subventricular zone*: secondary proliferative region basal to the VZ, where IPCs amplify and migrate.
- **TALEN** – *transcription activator-like effector nuclease*: a custom endonuclease platform for targeted genome editing.
- **TBR1** – *T-box brain protein 1*: a transcription factor expressed by deep-layer cortical neurons.
- **TBR2** – *T-box brain protein 2*: a transcription factor marking intermediate neural progenitors.

- **Tet3G / TRE3G** – *third-generation tetracycline transactivator; tetracycline response element*: components of a doxycycline-inducible expression system.
- **(SP-)** – *signal peptide–lacking*: indicates removal of the N-terminal secretory signal from FGFR1 to prevent membrane targeting.
- **TMT** – *tandem mass tag*: isobaric labels used for multiplexed quantitative proteomics by mass spectrometry.
- **tRG** – *truncated radial glia*: ventricular-zone-restricted progenitors with apical junctions but no basal process, contributing to a discontinuous scaffold.
- **VZ** – *ventricular zone*: a transient proliferative layer of the developing cortex lining the lateral ventricles, enriched in neural stem cells.
- **vRG** – *ventricular radial glia*: apically located neural stem cells in the ventricular zone, undergoing interkinetic nuclear migration and asymmetric division.
- **WGCNA** – *weighted gene co-expression network analysis*: identifies modules of co-regulated proteins/genes across samples.

Streszczenie

Zapotrzebowanie energetyczne neuralnych komórek progenitorowych oraz różnicujących się neuronów podczas rozwoju zarodkowego mózgu człowieka jest bardzo wysokie w związku z nasilonymi procesami komórkowymi, takimi jak proliferacja, migracja i tworzenie synaps. Mitochondria odgrywają kluczową rolę w tym procesie, poprzez produkcję ATP, kontrolę szlaków metabolicznych związanych z różnicowaniem neuronalnym, równowagą redoks i gospodarką wapniową. Zaburzenia tych mechanizmów wiążą się z chorobami neurorozwojowymi, takimi jak schizofrenia i zaburzenia ze spektrum autyzmu.

Receptor czynnika wzrostu fibroblastów 1 (*FGFR1*), działając poprzez szlaki sygnałowe, błonowe i jądrowe, funkcjonuje jako uniwersalny regulator rozwoju zarodkowego układu nerwowego, kontrolując indukcję neuronalną i proliferację neuralnych komórek pregenitorowych, a tym samym wpływając na specyfikację budowy kory mózgu. W jądrze komórkowym jądrowa forma FGFR1 (nFGFR1) integruje sygnały rozwojowe bezpośrednio regulując geny odpowiedzialne za neurogenezę i specyfikację budowy kory mózgu wiążąc się z koaktywatorami transkrypcji takimi jak CBP, RSK1, Nurr1 i RXR. Ponadto badania wskazują na obecność FGFR1 w mitochondriach; jego rola w dynamice mitochondrialnej, biogenezie i adaptacji bioenergetycznej pozostaje jednak w dużej mierze niepoznana.

W komórkach eukariotycznych geny kodujące białka mitochondrialne są zlokalizowane zarówno w genomie jądrowym (nDNA), jak i mitochondrialnym (mtDNA). Ich współdziałanie jest kluczowe dla homeostazy komórkowej i różni się w zależności od typu komórek, obszaru mózgu oraz etapu rozwoju. W niniejszej pracy wykazano, że w modelu organoidów kory mózgu, podczas wczesnej neurogenezy, nFGFR1 wpływa na regulację aktywności obu genomów, koordynując ich wzajemne oddziaływanie.

Głównym celem niniejszej rozprawy było określenie roli jądrowej formy FGFR1 (nFGFR1) w regulacji neurogenezy i metabolizmu podczas wczesnego rozwoju kory mózgowej w ludzkich organoidach korowych (hCO), ze szczególnym uwzględnieniem jej wpływu na morfologię, funkcję mitochondriów, mitofagię oraz różnicowanie neuronalne. Postawiłem hipotezę, że warunkowa nadekspresja nFGFR1 wpływa na dynamikę mitochondrialną, różnicowanie neuronalne

i adaptację metaboliczną poprzez koordynację działania genomów jądrowego i mitochondrialnego. W celu zweryfikowania tej hipotezy, otrzymałem linię ludzkich indukowanych pluripotencjalnych komórek macierzystych (hiPSC), hiPSC$^{Tet3G\text{-}FGFR1(SP\text{-}/NLS)}$, z kasetą nFGFR1 zintegrowaną w bezpiecznym locus *CLYBL* pod promotorem indukowanym doksycykliną. Zastosowanie tej linii umożliwiło kontrolowaną nadekspresję nFGFR1, bez zaburzenia stabilności genomu. Komórki linii hiPSC$^{Tet3G\text{-}FGFR1(SP\text{-}/NLS)}$ zróżnicowowano w hodowli *in vitro* do struktur 3D: kul zarodkowych (ang. *embryoid bodies*; EB), neuroepitelialnych komórek macierzystych (ang. *neuroepithelial stem cells*; NES) oraz organoidów kory mózgu (ang. *human cortical organoids*; hCO).

W celu ustalenia, jak nFGFR1 wpływa na rozwój kory mózgowej i dynamikę mitochondriów w otrzymanych modelach *in vitro*, zastosowałem strategię badawczą, która obejmowała wieloskalowe testy funkcjonalne: analizę ekspresji genów, obrazowanie reporterów biogenezy mitochondriów i mitofagii w żywych komórkach, jak również analizy immunofluorescencyjne, analizy morfometryczne mitochondriów i rozet neuronalnych oraz proteomikę organoidów kory mózgu (hCO). Analizowałem proliferację neuronalnych komórek progenitorowych (NSPC), neurogenezę, morfologię mitochondriów, biogenezę i mitofagię mitochondriów oraz żywotność komórek i apoptozę.

Proteomika z użyciem tandemowych znaczników masowych (ang. *tandem mass tag*, TMT), przeprowadzona na 60-dniowych organoidach korowych, wykazała istotne remodelowanie proteomu po indukcji nFGFR1. Analiza WGCNA (ang. *weighted gene co-expression network analysis*) wykazała wzbogacenie modułów białkowych związanych z rozwojem neuronalnym, funkcją mitochondriów, translacją mitochondrialną, splicingiem RNA, replikacją DNA oraz autofagią. Indukcja nFGFR1 wpłynęła na zwiększenie ekspresji markerów głębokich warstw kory (TBR1, SLIT2, CUX1), białek mitochondrialnych (OXR1, TXN2, MRPL24, MRPS26), komponentów lizosomalno-autofagowych (GBA, GALC, CTSB) oraz enzymów glikolitycznych (PKM2, SLC16A3). Z drugiej strony stymulacja nFGFR1 spowodowała zahamowanie poziomu białek synaptycznych (BCL11B, SOX5, NCAM2, FOXG1, SYN2), podjednostek łańcucha transportu elektronów (NDUFA7, COX6C) oraz transportem lipidów (VPS13A, FABP5), co wskazuje na przesunięcie metabolizmu z fosforylacji oksydacyjnej na glikolizę i metabolizm glikolipidów.

Analiza *in vitro* wykazała, że indukcja nFGFR1 w organoidach korowych wpływa na zmniejszenie proliferacji progenitorów neuralnych (spadek liczby komórek $Ki67^+$ w obszarze apikalnym strefy komorowej, ang. ventricular zone) oraz zwiększenie rozmiaru rozet neuronalnych, bez zmiany ilości komórek progenitorowych $SOX2^+$ i $PAX6^+$. Indukcja nFGFR1 wpłynęła również na zwiększenie liczby neuronów warstwy głębokiej kory ($CTIP2^+$, $TBR1^+$) i obniżenie liczby progenitorów pośrednich TBR2+ w strefie podkomorowej (ang. *subventricular zone*). Ponadto, indukcja nFGFR1 spowodowala zahamowanie dojrzewania neuronalnego, poprzez istotnie obniżenie liczby komórek z ekspresją białka synapsyny 2 w warstwie korowej hCO oraz zahamowanie ekspresji synaptofizyny (*SYP*).

Ponadto, nadekspresja nFGFR1 wpłynęła na zwiększenie fragmentacji mitochondriów i zmniejszenia złożoności sieci mitochondrialnej w warstwie korowej hCO. W strefie komorowej, indukcja nFGFR1 wpłynęła na elongację mitochondriów; zmiany te sugerują, że wpływ nFGFR1 jest zależny od regionu hCO. Ponadto, nFGFR1 istotnie zwiększył poziom mitofagii, określony poprzez poziom aktywność reportera mitofagii mitoKeima, aktywację szlaku PINK1–Parkin i zwiększenie ilości autofagosomów LC3B+ w mitochondriach w warstwie korowej hCOs. Tym zmianom nie towarzyszyły zmiany na poziomie ekspresji genów i białek związanych z mitofagią, co sugeruje działanie nFGFR1 na poziomie posttranskrypcyjnym. Ponadto, indukcja nFGFR1 nie wpłynęła na stymulację szlaków biogenezy mitochondriów, określonych poprzez aktywność reportera PGC1α-EGFP i liczbę kopii mtDNA. Zaobserwowano, że nadekspresja nFGFR1 wpływa na zwiększenie ekspresji genu *MT-ATP6*, czemu towarzyszy zwiększony poziom ATP, indukcja potencjału błony mitochondrialnej oraz wzrost poziomu reaktywne formy tlenu, bez aktywacji apoptozy czy reakcji stresu oksydacyjnego.

Analiza ChIP-seq (ang. *chromatin immunoprecipitation sequencing*) wykazała, że nFGFR1 wiąże się do promotorów genów takich jak *PINK1* i *BNIP3* kodowanych przez genom jądrowy; oraz wiąże się z DNA mitochondrialnym (mtDNA), m.in. w regionach sekwencji genów *MT-ATP6* i *MT-CO3*. Wyniki te wskazują, że nFGFR1 może kontrolować ekspresję genów mitochondrialnych poprzez oddziaływanie zarówno z genomem jądrowym, jak i mitochondrialnym.

Podsumowując, praca ta wykazuje, że nFGFR1 pełni kluczową, podwójną rolę w kontroli genomu, poprzez integrację sygnałów rozwojowych

i metabolicznych. Otrzymane wyniki wskazują, że nFGFR1 koordynuje dynamikę NPSC, neurogenezę oraz kontrolę jakości mitochondriów, co wpływa na regulację wczesnej kortykogenezy człowieka. Praca ta pozwoliła na poznanie podstawowych procesów, w jaki sposób czynniki pan-ontogenetyczne regulują dynamikę mitochondriów podczas rozwoju mózgu, co w przyszłości może pozwolić na zrozumienie mechanizmów zaburzeń neurorozwojowych i nowotworów związanych z zaburzeniem aktywności FGFR1.

Abstract

During human brain neurodevelopment, neural progenitors and differentiating neurons require a dynamic energy supply to support proliferation, migration, and synapse formation. Mitochondria play a central role in these processes by supplying ATP, regulating metabolic pathways that influence cell fate decisions, and controlling redox balance and calcium signaling. Disruptions in these processes have been linked to neurodevelopmental diseases, including schizophrenia and autism spectrum disorders.

Fibroblast Growth Factor Receptor 1 (FGFR1) is recognized as a pan-ontogenic regulator involved in embryonic neural development, managing neural induction, progenitor proliferation, and cortical patterning through both cell surface and nuclear pathways. Inside the nucleus, the nuclear form of FGFR1 (nFGFR1) integrates various developmental signals by binding with transcriptional co-activators such as CBP, RSK1, Nurr1, and RXR, thereby directly controlling gene programs essential for neurogenesis and cortical specification. Additionally, growing evidence shows that FGFR1 presence is also in mitochondria; however, its role in mitochondrial dynamics, biogenesis, and bioenergetic adaptation remains largely unknown.

In eukaryotic cells, genes that encode mitochondrial proteins reside in both the nuclear (nDNA) and mitochondrial (mtDNA) genomes. Their coordination is crucial for cellular homeostasis and varies across cell types, brain regions, and developmental stages. This thesis shows that nFGFR1 orchestrates the cross-talk and coordination between these two genomic systems, actively balancing their activity during neurodevelopment.

The primary objective of this dissertation was to define the role of nFGFR1 in modulating developmental and metabolic processes during early cortical development, particularly whether nFGFR1 may influence the mitochondrial structure, function, turnover, and neural lineage specification. I hypothesized that the conditional induction of nuclear FGFR1 (nFGFR1), which models the nFGFR1 upregulation during early corticogenesis, influences mitochondrial dynamics, neural lineage commitment, and metabolic adaptation through dual targeting of both nuclear and mitochondrial genomes. To test this hypothesis, I engineered a human-induced pluripotent stem cell (hiPSC) line that contains a doxycycline-

inducible nFGFR1 cassette integrated into the CLYBL safe-harbor locus. hiPSC$^{Tet3G\text{-}FGFR1(SP\text{-}/NLS)}$ ensures controlled overexpression without causing genomic instability. The modified hiPSCs were then differentiated into embryoid bodies (EBs), neuroepithelial stem (NES) cells, and three-dimensional human cortical organoids (hCOs).

My research strategy included multi-scale functional assessments, such as gene expression, live-cell reporter imaging, immunofluorescence, morphometric analysis of mitochondria and neuronal rosettes, and proteomic analysis of hCO, to evaluate how nFGFR1 modulates cortical development and mitochondrial regulation across three developmental platforms. I examined changes in NSPC proliferation, lineage commitment, mitochondrial morphology, mitophagy, mitochondrial biogenesis, cell viability, apoptosis, and global proteomics.

TMT-based proteomics (tandem mass tag) of 60-day human cortical organoids revealed extensive proteome remodeling following nFGFR1 induction. Co-expression network analysis identified protein modules linked to neuronal development, mitochondrial function, mitochondrial translation, RNA splicing, metabolism, RNA processing, DNA replication, and autophagy. nFGFR1 increased expression of deep-layer cortical markers (TBR1, SLIT2, CUX1), mitochondrial proteins (OXR1, TXN2, MRPL24, MRPS26), lysosomal-autophagy components (GBA, GALC, CTSB), and glycolytic enzymes (PKM2, SLC16A3). Conversely, it downregulated proteins involved in synaptic function, cortical identity (BCL11B, SOX5, NCAM2, FOXG1, SYN2), electron transport chain components (NDUFA7, COX6C), and lipid transport (VPS13A, FABP5), indicating a metabolic shift from oxidative phosphorylation toward glycolysis and glycolipid metabolism.

In vitro analysis showed that nFGFR1 activation in cortical organoids reduced neural progenitor proliferation, as indicated by fewer Ki67$^+$ cells in the periluminal region of the ventricular zone, while increasing the size of neuronal rosettes without altering SOX2$^+$ or PAX6$^+$ progenitor density. This induction promoted expression of deep-layer neurons in cortical layer (CTIP2$^+$, TBR1$^+$) at the expense of intermediate progenitors in subventricular zone (TBR2$^+$). Despite enhanced neurogenesis, nFGFR1 impaired synaptic maturation, evidenced by fewer Synapsin-2 puncta and lower synaptophysin (*SYP*) expression.

Moreover, nFGFR1 caused mitochondrial fragmentation and reduced network complexity in the cortical layer. In the ventricular zone, which is populated

by glycolytic progenitor cells, it induced modest mitochondrial elongation, indicating region-specific effects on mitochondrial structure. Additionally, the mitoKeima assay revealed that nFGFR1 significantly increased mitophagy flux, coinciding with enhanced PINK1–Parkin activity and autophagosome recruitment to mitochondria in the cortical layer of hCOs. The observed effects were mainly restricted to the cortical layer. They occurred without significant changes in mitophagy-related gene or protein expression, indicating a region-specific impact of nFGFR1 or regulation via post-transcriptional mechanisms. Notably, nFGFR1 did not trigger pathways for mitochondrial biogenesis, as evidenced by no changes in PGC1α-EGFP fluorescence and mtDNA copy number; instead, it specifically enhanced the expression of the mitochondrial gene *MT-ATP6*, alongside a positive trend in the mtDNA genes *MT-ND2* and *MT-ND5*. This was accompanied by elevated ATP production, enhanced mitochondrial membrane potential, and increased ROS levels, all without inducing apoptotic or stress responses. ChIP-seq analysis revealed nFGFR1 binding at the promoters of nuclear-encoded mitochondrial genes, such as *PINK1* and *BNIP3*, and it directly binds to mitochondrial DNA (mtDNA), specifically at loci like *MT-ATP6* and *MT-CO3*. This indicates that nFGFR1 could influence mitochondrial gene expression by targeting both nuclear and mitochondrial DNA directly.

In summary, this thesis establishes that nFGFR1 plays a pivotal dual-regulatory role as a genome regulator, integrating developmental and metabolic signals to orchestrate NPSC dynamics, neuronal lineage commitment, and mitochondrial quality control, thereby shaping early human corticogenesis. This work provides foundational insights into how emerging pan-ontogenic mechanisms coordinate mitochondrial regulation during brain development, with potential implications for understanding neurodevelopmental disorders and cancers characterized by FGFR1 dysregulation.

Innovation of the dissertation

In this study, I employed TALEN-mediated editing of the CLYBL safe-harbor locus to introduce a DOX-inducible FGFR1(SP–/NLS) construct. This approach enables the conditional overexpression of nuclear FGFR1. The resulting hiPSC$^{Tet3G\text{-}FGFR1(SP–/NLS)}$ line enabled activation of nFGFR1 expression on demand and evaluation of its downstream effects across platforms, which represent three stages of development: embryoid bodies, neuroepithelial stem (NES) cells, and 3D human cortical organoids, in a highly reproducible manner. Additionally, I implemented lentiviral mitophagy (mitoKeima) and mitochondrial biogenesis (PGC1α-EGFP) reporters in neuronal models derived from the hiPSC$^{Tet3G\text{-}FGFR1(SP–/NLS)}$ line to monitor mitochondrial turnover in real-time. This live-cell imaging method demonstrates that nFGFR1 induction significantly increases mitophagy flux in cortical-layer oh hCOs, while mitochondrial biogenesis remains unchanged. In this thesis, I demonstrate the region-specific effects of nFGFR1 on cell proliferation, neuronal differentiation, mitochondrial network connectivity, and mitochondrial turnover in the cortical layer of human cortical organoids (hCOs). In this research, I conducted tandem mass tag (TMT)–based quantitative proteomics on 60-day hCO, both with and without nFGFR1 upregulation. Differential expression and network analysis showed that nFGFR1 overexpression significantly alters crucial pathways involved in neuronal function, mitochondrial dynamics, protein translation, and cellular metabolism. Overall, these innovations reveal nFGFR1 as a master nuclear regulator that integrates developmental signals with mitochondrial homeostasis. By integrating precise genome engineering, live-cell mitochondrial reporters, and global proteomic profiling, this dissertation provides the first comprehensive framework connecting nuclear FGFR1 signaling to mitochondrial dynamics, metabolism, and neural lineage specification in human cortical models.

1. Introduction

1.1. Neural stem cells, progenitors and neurogenesis

Radial glial cells, the predominant neural stem cells of the developing brain, arise from neuroepithelial progenitors, giving rise to both neurons and glial cells (Götz and Huttner, 2005). The human neocortex contains about 16 billion neurons of diverse types, which originate from an initially uniform neuroepithelium that transforms into a functionally complex, layered, gyrencephalic (folded) structure (Bershteyn et al., 2017). The greatly expanded human cerebral cortex arises from both increased progenitor cell numbers and higher proliferative output compared to other mammals (Hansen et al., 2010). At the onset of neurogenesis, neuroepithelial cells undergo rapid and symmetrical division, forming a pseudo-stratified epithelium (Lewitus et al., 2013). Mammalian brain development begins with expansion of the neuroepithelial cells (Götz and Huttner, 2005). Lehtinen et al (2011) demonstrated that cerebrospinal fluid (CSF) directly interacts with cerebral cortical progenitor cells at the apical domain and transduces diffusible mitogenic cues, known as apical complex proteins, that promote proliferation and neurogenic capacity of ventricular radial glia (vRG) (Lehtinen et al., 2011).

As neurogenesis proceeds, RG extend long basal processes toward the basal (pial) surface while retaining apical endfeet at the apical surface (ventricle) (Noctor et al., 2001). Ventricular radial glia (vRG), which express glial marker GFAP, are characterized by interkinetic nuclear migration and asymmetric division at the apical surface of the VZ (Lui et al., 2011; Taverna and Huttner, 2010). They undergo series of divisions at the apical surface of the ventricular zone (VZ), generating intermediate progenitors (IPs) and subsequently neurons (Noctor et al., 2004). After mitosis, IP daughter cells undergo asymmetric cell death, regulating total neurogenic output, genome quality, and projection-neuron subtype ratios (Hevner, 2019). However, the major pool of human radial glia populates the outer subventricular zone (OSVZ) (Lewitus et al., 2013), consisting of outer radial glia (oRG) and truncated radial glia. Outer radial glia (oRG) are characterized by a long basal process and the absence of apical junctions. Moreover, they can undergo mitotic somal translocation, enabling these cells to populate subsequent cortical layers. oRG produces intermediate progenitors and can directly generate neurons (Hansen et al., 2010). On the other hand, truncated radial glia (tRG) emerge around

mid-neurogenesis. They possess apical junctions at the ventricular surface but lose basal contact, causing them to remain restricted to the ventricular zone (VZ), forming a discontinuous scaffold. Moreover, tRG are characterized by a unique molecular signature, including downregulation of FAM107A, LIFR, and HOPX, and upregulation of CRYAB and NR4A1. Fibers of tRGs terminate on blood capillaries, with their end-feet co-localizing with CD31-positive endothelial cells within the ISVZ and OSVZ. This suggests that tRG may integrate vascular-derived signals (Nowakowski et al., 2016). In line with this, Bilgic et al. (2023) demonstrated that tRG differentiate into both ependymal and astroglial cells during cortical development in the gyrencephalic ferret (Bilgic et al., 2023).

Another type of cell, intermediate progenitor cells (IPCs), acts as a transit-amplifying progenitor that enhances neuronal output and drives the evolutionary expansion and molecular diversity of the mammalian neocortex (Martínez-Cerdeño et al., 2006). IPCs undergo symmetric division, producing two daughter cells with identical fates (Haubensak et al., 2004). It was demonstrated that IPCs derived from the VZ typically undergo one or two rounds of division. On the other hand, IPCs from more abundant oRG can undergo multiple rounds of division (Hansen et al., 2010; Noctor et al., 2007; Zhou, 2012). Additionally, after mitosis, IP daughter cells undergo asymmetric cell death, regulating total neurogenic output, genome quality, and projection-neuron subtype ratios (Hevner, 2019). Both ventricular radial glia (vRG) in the ventricular zone (VZ) and outer radial glia (oRG) in the outer subventricular zone (OSVZ) contribute to the generation of IPCs (Pollen et al. 2015). Intermediate progenitor cells (IPCs), both from the ventricular zone (VZ) and outer subventricular zone (OSVZ), proliferate within the SVZ and migrate towards cortical layers in an inside-out pattern to increase neuronal number (Fig.1). An evolutionary expansion and molecular diversity of these cortical progenitor populations contribute to the dramatic enlargement of the human neocortex and overall brain volume (Hansen et al., 2010; Pebworth et al., 2021; Pollen et al., 2015). It was demonstrated that IPCs derived from both VZ and OSVZ exclusively generate excitatory projection neurons that populate all cortical layers. Moreover, they speculated that GABAergic neurons may arise from IPCs in the cortex at late stages of neurogenesis, given the presence of GABA+ cells within the SVZ (Pebworth et al., 2021; Yu and Zecevic, 2011). Several studies have shown that intermediate progenitor cells produce chemokines, such as CXCL12, which attract

thalamocortical axons and interneurons, promoting interneuron migration and thalamocortical innervation (Abe et al., 2015; Wang et al., 2011; Wu et al., 2017). During neurogenesis, most of neural progenitors that give rise to cortical interneurons reside in the ganglionic eminences (GE) of the ventral telencephalon, as well as the preoptic area (Gelman et al., 2009; Hansen et al., 2013; Lavdas et al., 1999; Nery et al., 2002; Wichterle et al., 1999). The ganglionic eminences are subdivided into three anatomical regions, medial (MGE), lateral (LGE), and caudal (CGE), each with a distinct molecular signature and each producing different interneuron subtypes (Nery et al., 2002). NKX2-1-expressing progenitors in the MGE give rise to cortical and striatal interneurons, as well as pallidal projection neurons (Flandin et al., 2010; Marín et al., 2000; Nóbrega-Pereira et al., 2010; Sussel et al., 1999). ASCL1-expressing LGE gives rise to striatal projection neurons, olfactory bulb interneurons (Deacon et al., 1994; Ma et al., 2012; Olsson et al., 1995; Wichterle et al., 2001), whereas the caudal ganglionic eminence (CGE), which expresses COUP-TFII, gives rise to interneurons for the limbic system (e.g., hippocampus and amygdala), as well as to caudal striatal and pallidal neurons (Kanatani et al., 2008; Miyoshi et al., 2010; Nery et al., 2002). Recent single-cell RNA sequencing studies have revealed the molecular diversity of interneuron progenitors in the human ganglionic eminence (Velmeshev et al., 2021; Yu et al., 2021). Velmeshev et al. (2021) applied single-cell RNA sequencing to second-trimester human ganglionic eminence and identified two main subtypes of radial glia. These progenitors share pan-radial glial markers, such as vimentin and nestin, but are distinguished by region-specific transcription factors such as NKX2-1 in MGE and NR2F2 in CGE, as well as by novel interneuronal markers TOX3 and LMO1. They also characterize the transitional state between progenitors and lineage-committed interneurons, co-expressing DLX1 and DLX2, indicating distinct molecular signatures across different stages of interneuron development (Velmeshev et al., 2021).

Proliferative zones in the human ganglionic eminences resemble those in the cortex. The ventricular zone contains mostly radial glia expressing NSC markers, and the inner SVZ (iSVZ) is abundant in intermediate progenitor cells transitioning to neurons. Similarly to the cortex, the MGE also contains an outer SVZ (oSVZ) enriched in radial glia, IPCs, and newborn neurons. Both in the cortex and ganglionic eminences, outer SVZ progenitors share radial-glial markers such

as phosphorylated vimentin. However, unlike cortical oRG, the oRG cells appear as simple, rounded cell bodies without extended fibers or consistent radial orientation (Hansen et al., 2013).

Several studies of single-cell sequencing and lineage tracing have revealed heterogeneity among radial glia and the diverse cell types they generate. Pollen et al. (2015) identified distinct transcriptional programs in ventricular radial glia (vRG) and outer radial glia (oRG). They demonstrated that oRG cells express genes related to extracellular matrix formation, migration, and stemness, such as HOPX, FAM107A, and LIFR, suggesting that oRG directly supports the subventricular niche through local production of growth factors (Pollen et al., 2015). In another study, Delgado et al. (2022) combined genetic lineage tracing with single-cell RNA sequencing to demonstrate that individual cortical progenitors can give rise to both excitatory and inhibitory neurons, suggesting local generation of newborn GABAergic neurons. Moreover, they showed that cortical GABAergic neurons share a transcriptional signature with interneurons from the caudal ganglionic eminence (Delgado et al., 2022). Pebworth et al. (2021) applied single-cell RNA sequencing and immunohistochemical analyses to study the molecular diversity of human neural intermediate progenitor cells (nIPCs) across the subventricular zones during human mid-gestation. They identified five distinct transcriptomic subtypes that undergo a rapid change in both the number and distribution of progenitors around gestational weeks 19–20, corresponding with the onset of gliogenesis (Pebworth et al., 2021). Finally, Allen et al. (2022) revealed that VZ and OSVZ progenitors give rise to distinct astrocyte subpopulations. By performing fate mapping, they showed that cortical-plate astrocytes emerge from VZ progenitors and proliferate locally, while white-matter astrocytes derive from both VZ and OSVZ progenitors (Allen et al., 2022).

In summary, the diversity and expansion of radial glia and neural progenitors facilitate remarkable size, complexity, and cellular heterogeneity of the human neocortex. Understanding the molecular and developmental programs that govern radial glia self-renewal and neural commitment is key to understanding both cortical development and neuropsychiatric disorders, such as autism and schizophrenia.

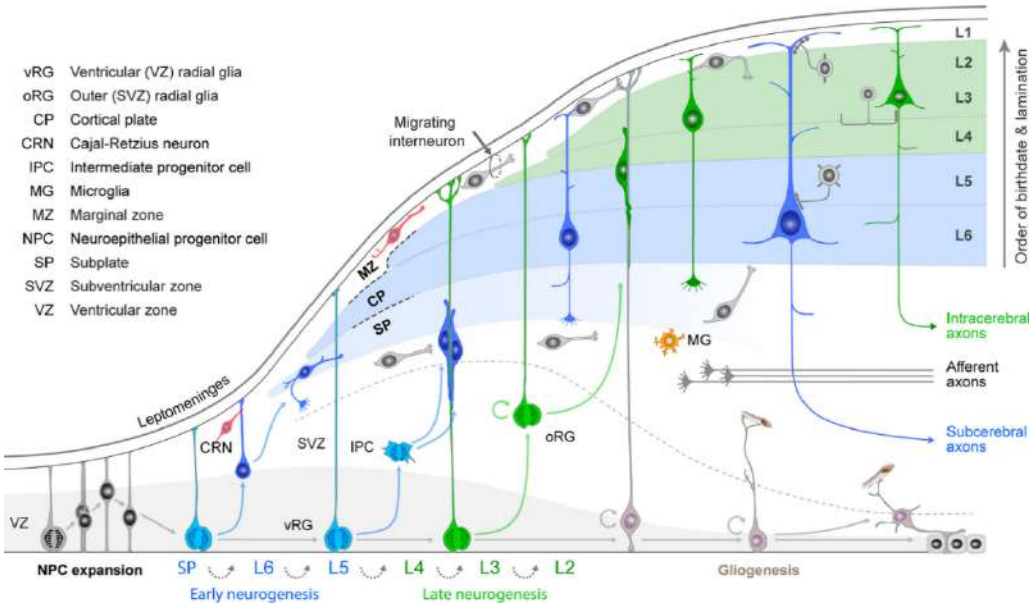

Fig.1. Schematic illustration of neurogenesis in the mammalian neocortex. *Neuroepithelial cells expand the pool of cortical progenitors before transforming into ventricular radial glia (vRGs). These cells undergo successive asymmetric divisions, producing deep- and upper-layer projection neurons, intermediate progenitors, and outer radial glia. Newly formed neurons migrate radially into the cortical plate, initially creating the preplate, which divides into the marginal zone and the subplate. Meanwhile, radial glia later switch to gliogenesis, while interneurons invade tangentially through the marginal, intermediate, and subventricular zones (Adapted from Molnár et al., 2019).*

1.2. Role of the mitochondrial dynamics and energy metabolism during neuronal development

Mitochondria are involved in a plethora of processes, including ATP production through oxidative phosphorylation (OXPHOS) and the regulation of redox metabolites such as NADH/NAD^+, ATP/ADP, ATP/AMP, and succinate/α-ketoglutarate, and synthesis of iron-sulfur (Fe-S) clusters (ISCs) (Jones et al., 2012). In addition, mitochondria play a central role in metabolic pathways, such as the citric acid cycle, fatty acid β-oxidation, amino acid metabolism, and calcium signaling (Osman et al., 2011; Stehling and Lill, 2013; Tatsuta et al., 2014), as well as in the activation of neuronal apoptosis (Benes, 2004; Gorman et al., 2000; C. Wang and Youle, 2009). Mitochondria consist of a permeable outer membrane (MOM) and an inner membrane (MIM), which form cristae that extend into the mitochondrial matrix. Cristae membranes are enriched with electron transport chain complexes and ATP synthase, facilitating efficient ATP synthesis via OXPHOS (Kühlbrandt, 2015). Human mitochondria contain their own ~16.5 kb circular DNA genome (mtDNA), which encodes 22 tRNAs, 2 rRNAs, and 13 proteins that are

subunits of the OXPHOS complexes (Anderson et al., 1981; Richter-Dennerlein et al., 2015). According to MitoCarta3.0, the human mitochondrial proteome consists of 1,136 proteins—13 encoded by the mitochondrial genome and the remaining approximately 1,123 encoded by the nuclear genome, which are translated in the cytoplasm and subsequently imported into the mitochondria (Rath et al., 2021; Schmidt et al., 2010).

Mitochondrial dynamics, involving continuous cycles of fission, fusion, and mitochondrial transport, are essential for proper brain development and neuronal survival (Scandella et al., 2023). During the transition of neural stem cells (NSCs) into neurons, mitochondria undergo morphological changes, which are accompanied by a metabolic shift from glycolysis to oxidative phosphorylation (Garone et al., 2024). These changes are tightly regulated by fission and fusion proteins, such as DRP1, MFN1/2, and OPA1 (Coelho et al., 2022; Garone et al., 2024; Son and Han, 2018). Several studies demonstrate that mitochondrial dynamics influence energy-demanding processes, such as neuronal differentiation and synaptic transmission. Alterations or loss of mitochondrial dynamics contribute to impaired neurogenesis in neurodevelopmental and neurodegenerative diseases (Devine et al., 2016; Kvajo et al., 2008; Millar et al., 2005; Norkett et al., 2016).
Mitochondrial biogenesis plays a critical role in neural stem cell (NSC) differentiation by supporting the metabolic shift from predominantly glycolytic metabolism to a state highly dependent on oxidative phosphorylation (OXPHOS). This is accompanied by increased mitochondrial mass and DNA content, along with the activation of master transcriptional regulators of mitochondrial biogenesis, including peroxisome proliferator-activated receptor-α (PPARα) and PPARγ coactivator 1-α (PGC1α) (Lin et al., 2018; Zheng et al., 2016). Mitochondrial biogenesis is tightly regulated by the coordinated activation of multiple transcription factors (TFs) and coactivators. The master regulator PGC-1α, by interacting with nuclear respiratory factors 1 and 2 (NRF1/2), induces the expression of mitochondrial transcription factor A (TFAM), which promotes mitochondrial protein synthesis, mtDNA replication, and transcription (Fontecha-barriuso et al., 2020; Gureev et al., 2019). Additional transcriptional regulators, such as PPARγ (proliferator-activated receptor gamma), PPARα, ERRα (estrogen related receptor alpha), TRα (thyroid hormone receptor), and RXRs (retinoid X receptors), interact with PGC-1α to modulate the transcriptional program required

for mitochondrial growth and function (Delerive et al., 2002; Duncan and Finck, 2008; Huang et al., 2024; Schreiber et al., 2004; Zhang et al., 2004). Conditional knockout of PGC-1α in mice leads to significant loss of dopaminergic neurons and reduced dopamine levels in the substantia nigra, suggesting that PGC-1α is essential for dopaminergic neuron survival (Jiang et al., 2016).

Upon mitochondrial dysfunction, including impaired protein import, accumulation of misfolded and unfolded proteins, the mitochondrial unfolded protein response (UPRmt) activates the transcription of nuclear genes, which function to protect mitochondria. UPRmt activates a series of chaperones and proteases that alleviate the damaging effects of mtROS. UPRmt plays a crucial role in maintaining neuronal homeostasis by regulating the survival of neurons under ischemic stress (Inigo and Chandra, 2022). Excessive production of ROS by aberrant or aged mitochondria leads to oxidative stress and damage to lipids, proteins, and nucleic acids, including mitochondrial DNA (Lenaz, 2001; Nissanka and Moraes, 2018), leading to mitochondrial fragmentation (Cid-Castro and Morán, 2021). Efficient removal of damaged mitochondria, misfolded proteins, and aggregates through multiple degradative pathways is vital for proper neuronal function and survival (Tseng et al., 2023). Multiple mechanisms of degradation of misfolded proteins have been identified, includiung ubiquitin-proteasome pathway, endolysosomal trafficking pathway, chaperone-mediated autophagy or MAGIC (mitochondria as guardian in cytosol) pathway (Kodroń et al., 2021; Lie and Nixon, 2019; Ruan et al., 2017; Tekirdag and Cuervo, 2018). Lysosome-mediated (non-selective) autophagy plays a central role in maintaining neuronal homeostasis to prevent the excess of damaged organelles over time (Stavoe and Holzbaur, 2019). By engulfing dysfunctional mitochondria into autophagosomes and fusing them with lysosomes, cells target damaged mitochondria for degradation and recycling (Feng et al., 2014; Stavoe and Holzbaur, 2019). In neurons, mitochondrial turnover via non-selective basal autophagy occurs mainly at presynaptic sites and axon terminals, ensuring proper cellular homeostasis (Goldsmith et al., 2022). Mutation or neuron-specific loss or mutation of key autophagy components triggers neurodegeneration phenotype *in vivo* (Hara et al., 2006; Komatsu et al., 2006).

Mitophagy, a selective form of autophagy, eliminates unhealthy or damaged mitochondria, thereby regulating intracellular homeostasis (Ashrafi et al., 2014; Lam et al., 2024). This process is controlled in a Parkin-dependent and -independent

manner. The PINK1/Parkin-mediated mitophagy involves PINK1-mediated phosphorylation of Parkin, which is followed by ubiquitination of outer mitochondrial membrane proteins, and recruitment of autophagy receptors such as p62 and OPTN (Geisler et al., 2010; Li et al., 2023). On the other hand, Parkin-independent mitophagy uses mitophagy receptors (BNIP3, BNIP3L/NIX, and FUNDC1), which directly bind to autophagy proteins (LC3/GABARAP) and promote mitochondrial turnover (Hanna et al., 2012; Lv et al., 2017; Poole et al., 2021; Wu et al., 2014; Xie et al., 2020a; T. Zhang et al., 2016).

Disturbed mitophagy leads to several neurodevelopmental and neurodegenerative diseases, like brain encephalopathy or neurodegenerative and neuropsychiatric diseases and age-related diseases (Barel et al., 2017; Statharakos, 2025; Wang et al., 2021). Several studies suggest a role for mitophagy in stem cell differentiation (Esteban-Martínez et al., 2017; Sin et al., 2016). In contrast to previous findings, it has been demonstrated that BNIP3L/NIX- and FUNDC1-mediated mitophagy is not critical for cardiomyocyte differentiation but is essential for mitochondrial network remodeling (Lampert et al., 2019). Efficient mitophagy is essential for neuronal development, synaptic maturation, and neuronal survival (Liu et al., 2024). Its dysfunction leads to impaired neuronal development, mitochondrial defects, and loss of dopaminergic neurons (Abed et al., 2024; Sliter et al., 2018). Excessive mitophagy has been implicated in mitophagy-mediated cell death, which was rescued by administering inhibitor URB597 (Somredngan and Thong-Asa, 2017; Subramaniam, 2020). Several studies have demonstrated that pharmacological upregulation of mitophagy, using molecules like urolithin A (UA), actinonin, and NAD+ precursors, promotes neuroprotection, preserves mitochondrial function, reduces dopaminergic neurons loss, and suppresses neurodegenerative phenotypes in both Alzheimer's and Parkinson's disease models (Dong et al., 2023; Fang et al., 2019; Georgakopoulos et al., 2017; Lautrup et al., 2019; Schöndorf et al., 2018). Lysosomes, beyond their role in autophagy, play a crucial role in the mitochondrial-lysosomal interplay. It was demonstrated that TFEB, the master regulator of lysosomal biogenesis, promotes activation of mitochondrial biogenesis by upregulating PGC-1α and NRF1/2 expression (Kim et al., 2018; Mansueto et al., 2017).

1.3. FGFR1 signaling and its role in neuronal development.

Fibroblast Growth Factor Receptor 1 (FGFR1) is a receptor tyrosine kinase essential in regulation embryonic development (Clark and Soriano, 2024; Kang et al., 2017; Kumar et al., 2021; Kurowski et al., 2019; Molotkov et al., 2017; Yamaguchi et al., 1994). Mutation or loss of FGFR1 in embryos results in severe growth retardation and defects in gastrulation (Deng et al., 1994; Li et al., 2005; Su et al., 2014; Thisse and Thisse, 2005; Yamaguchi et al., 1994). Several evidences showed its role in the early neural development and neurulation, by modulating neural induction, and neural tube closure (Deng et al., 1997; Maniou et al., 2023; Walshe and Mason, 2000). FGFR1 is highly expressed in neurogenic niches and is essential for the development of distinct brain regions by governing neural progenitor proliferation, differentiation, and regional patterning (Flandin et al., 2010; Inglis-Broadgate et al., 2005; Jukkola et al., 2006; D. K. Ma et al., 2009; Ohkubo et al., 2004; Saarimäki-Vire et al., 2007; Trokovic et al., 2003; Yoon et al., 2004).

FGFR1 is a member of the Fibroblast Growth Factor Receptor (FGFR) family, consisting of four members: FGFR -1, -2, -3 and -4 (Foldynova-Trantirkova et al., 2012; Gabler et al., 2022; Szybowska et al., 2021; Xie, et al., 2020a; Yamagishi and Okamaoto, 2009). One the FGFR1 cellular local is the plasma membrane. FGFR1 signaling in activated by ligands from the Fibroblast Growth Factor (FGF) family, such as FGF2, FGF8, FGF17, FGF21 and FGF22, and regulates neural progenitor proliferation, neuronal differentiation, synapse formation or regional brain patterning (Bosone et al., 2024; Claflin et al., 2022; Huang et al., 2024; Jacobi et al., 2015; Jensen-Cody et al., 2020; Lahti et al., 2011; Lim et al., 2015; Oberholzer et al., 2024; Ohkubo et al., 2004; Shi et al., 2018; Terauchi et al., 2016, 2017; Tomé et al., 2023; Wang et al., 2025; Woodbury and Ikezu, 2014; Yellapragada et al., 2022). Recent studies demonstrate that FGFR1 is crucial in maintaining telencephalic identity and proper cortical patterning (Gantner et al., 2021; Yellapragada et al., 2022). FGFR1 is composed of three main structural domains: an extracellular ligand-binding domain (Fig.2A), a single transmembrane domain, and an intracellular tyrosine kinase domain (Dai et al., 2019; Farrell and Breeze, 2018; Hinsch et al., 2023; Plotnikov et al., 1999). The extracellular domain comprises three immunoglobulin-like loops, Ig- I, -II, and -III, which are essential

for ligand specificity, binding and receptor autoinhibition and its activation (Groth and Lardelli, 2002; Sakaguchi et al., 1999; Sarabipour and Hristova, 2016; Szybowska et al., 2021; Wang et al., 1995). The transmembrane domain of FGFR1 anchors the receptor to the plasma membrane via single transmembrane helix and is crucial for receptor dimerization and downstream signal transduction (Comps-Agrar et al., 2015; Groth and Lardelli, 2002; Li et al., 2020; Liu et al., 2020; Peng et al., 2009). The intracellular tyrosine kinase domain of FGFR1 contains an activation loop, a catalytic loop, and a juxtamembrane segment, and is key to the initiation of a downstream cascade (Farrell and Breeze, 2018; Gędaj et al., 2024; Goetz and Mohammadi, 2013; Lin et al., 2023). Additionally, an N-terminal signal peptide regulates receptor trafficking via the secretory pathway and ensures its proper distribution at the plasma membrane (Hinsch et al., 2023; Porębska et al., 2019; Tomé et al., 2023). While FGFR1 signalling activity occurs mostly at the cell surface, several studies identified FGFR1 in the nucleus (Chioni and Grose, 2012; Coleman et al., 2014; Servetto et al., 2021) and mitochondria (Hitosugi et al., 2011; Srisakuldee et al., 2021; Xie et al., 2023; Yan et al., 2023). It was demonstrated that N-glycosylation acts as a switch for FGFR1 membrane-to-nuclear envelope translocation, where hypoglycosylated FGFR1 accumulates at the nuclear envelope and interacts with nuclear proteins in a ligand-independent manner (Gregorczyk et al., 2023).

In addition, newly synthesized FGFR1 can also be released into the cytosol from the early Golgi membrane, enabled by an atypical transmembrane domain containing polar amino acids and β-sheet structure (Dunham-Ems et al., 2006; Myers et al., 2003). The process is facilitated by proteasome p60 and FGFR1 interaction with RSK1 and generates a high mobility cytosolic protein (Dunham-Ems et al., 2006). The soluble, non-membrane FGFR1 accumulates in the nuclear chromatin (Star et al., 2009), interacts with a common transcription coregulator CBP, and together with its partners, such as RAR, Nurr1 (Baron et al., 2012; Lee et al., 2012), estrogen receptors, interacts with the promoters of the thousands of active genes (Servetto et al., 2021). The nuclear accumulation of FGFR1, unlike its membrane accumulation, is a highly regulated process (Fig.2B). While FGFR1 is translocated to the nucleus via an importin-β-dependent manner, its mitochondrial translocation mechanism remains unclear (Reilly and Maher, 2001).

It is well documented that integrative nuclear FGFR1 signaling (INFS), a pan-ontogenic mechanism, governs widespread gene reprogramming during cell development (Decker et al., 2021; Dhiman et al., 2024; X. Fang et al., 2005; Narla et al., 2017; Peng et al., 2001; Stachowiak et al., 1997, 2017; Stachowiak et al., 1996; Stachowiak and Stachowiak, 2016; Terranova et al., 2015). In the nucleus, nFGFR1 integrates signals from diverse developmental factors by interacting with CBP/CREB complex, RSK1, Nurr1, RAR, RNA polymerase II, FOXA1, miRNA, or estrogen receptors (Baron et al., 2012; X. Fang et al., 2005; Formisano et al., 2017; Narla et al., 2017; Servetto et al., 2021). Fang et al. (2005) showed that FGFR1 translocates into the nucleus, where it directly interacts with the transcriptional co-activator CREB-binding protein (CBP) and modulates its association with RSK1 by binding and releasing RSK1 from the CBP complex. This promotes RNA polymerase II recruitment and histone acetylation at the tyrosine hydroxylase (*TH*) gene promoter, enabling gene transcription activation (Fang et al., 2005). Unlike the constitutive processing of FGFR1 in the Golgi followed by its insertion into the cell membrane, the nuclear accumulation of FGFR1 is a highly regulated process, and its influence on the signaling pathway is referred to as Integrative Nuclear FGFR1 Signaling (INFS).

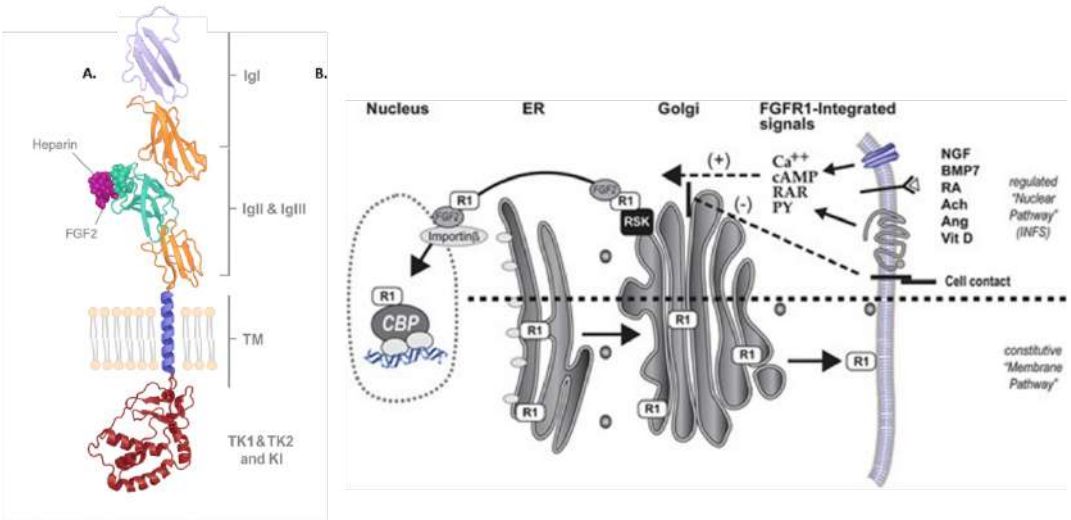

Fig.2. Protein structure and trafficking routes of FGFR1. *A. FGFR1-FGF2 complex protein structure. IgI, Immunoglobulin-like domain I (blue, PDB 2CR3); IgII and IgIII, Immunoglobulin-like domains II and III (orange, PDB 1FQ9); TM, Transmembrane domain (purple, AF-P11362-F1 predicted structure); TK1 and TK2, Tyrosine kinase subdomains and KI, kinase insert (red, PDB 4UWY); co-factor heparin facilitates FGF2–FGFR1 interaction. (adapted from Tomé et al., 2023); B. Pathways for trafficking newly synthesized FGFR1 proteins. Newly synthesized FGFR1 takes one of two routes: it either*

follows the constitutive membrane pathway, where it is glycosylated in the Golgi and trafficked to the plasma membrane, or it follows a nuclear signaling pathway. In the latter, an atypical transmembrane domain and proteasome-dependent release generate a mobile, hypoglycosylated form that enters the nucleus through importin-β. This type of nuclear accumulation is triggered by several developmental signals, including growth factors and vitamin hormones. It is facilitated by FGF-2 and RSK1, while cell–cell adhesion prevents its internalization and nuclear transport. Cytoplasmic FGFR1 exists in three pools: ER-immobile, cytosolic mobile, and membrane-bound. Its nuclear import is accelerated both by enhanced cytoplasmic-to-nuclear transport and reduced export (adapted from Stachowiak and Stachowiak, 2016).

These studies led to the formulation of a new theory for the integrated genome regulation of ontogeny in which Integrative Nuclear FGFR1 Signaling plays a broad pan-ontogenetic function (Stachowiak and Stachowiak, 2016). It was demonstrated that activation of cell-surface FGFR1 by FGF2 promotes the proliferation of neural progenitor cells. In contrast, nuclear FGFR1, through interaction with orphan nuclear receptor Nurr1, is essential for the differentiation and maturation of mesencephalic dopaminergic neurons (Baron et al., 2012). The nFGFR1 integrates diverse developmental signals and, by binding a wide range of mRNAs, microRNAs, and long non-coding RNAs, governs the progenitor-to-neuron transition and CNS development (Narla et al., 2017; Stachowiak et al., 2017; Terranova et al., 2015). Recently, the "Genome Archipelago Model" proposed that nFGFR1 acts as a master regulator of chromatin architecture and genome organization during neuronal development, by orchestrating the formation of nFGFR1-associated topologically associating domains (TADs), which serve to recruit distinct ontogenic programs (Decker et al., 2021). In addition to that, it was demonstrated that nuclear FGFR1 (nFGFR1) orchestrates genome homeostasis in a flexible, coordinated manner, ensuring stability and adaptability during neuronal development (Dhiman et al., 2024). Altered nFGFR1 signaling has been directly linked to neuropsychiatric phenotypes. Klejbor et al. (2006) demonstrated that neuronal-specific expression of a dominant negative mutant of nFGFR1 in Th(tk–)/Th(tk–) transgenic mice exhibit a schizophrenia-like syndrome, characterized by a reduction in midbrain dopaminergic neuron density and sensorimotor gating deficits (Klejbor et al., 2006). In addition, schizophrenia patient–derived cerebral organoids showed initial overexpression of nFGFR1 developing progenitors associated with premature differentiation of subcortical neurons, followed by a decline in nuclear FGFR1 in the cortical layer, coinciding with disrupted neuronal layering and connectivity (Stachowiak et al., 2017).

Role of nFGFR1 in disease - Alterations in nFGFR1 activity within the nervous system have been associated with neuropsychiatric disorders, such as schizophrenia (Narla et al., 2017; Stachowiak et al., 2017). Studies of the schizophrenia patients' iPSC and cerebral organoids revealed an overexpression of nFGFR1 in NPC, which leads to premature neuronal differentiation, followed by loss of nFGFR1 in cortical neurons and cortical malformation (Narla et al., 2017; Stachowiak et al., 2017). Excessive expression of nFGFR1 caused by the multiplication of the *FGFR1* gene has been associated with various cancers, including pancreatic (Coetzee et al., 2023; Coleman et al., 2014), osteosarcoma (Kim et al., 2022), neuroblastoma, and breast cancer (Cimmino et al., 2022; Servetto et al., 2021). In breast cancer cells, nFGFR1 interacts with estrogen receptors, causing estrogen-independent activation of a large number of genes and a neoplastic phenotype. It was demonstrated (Fig.3) that the nuclear localization of FGFR1 is associated with increased proliferation, poor prognosis, and tumor treatment resistance in cancer cells (Coleman et al., 2014; Pirou et al., 2017; Servetto et al., 2021).

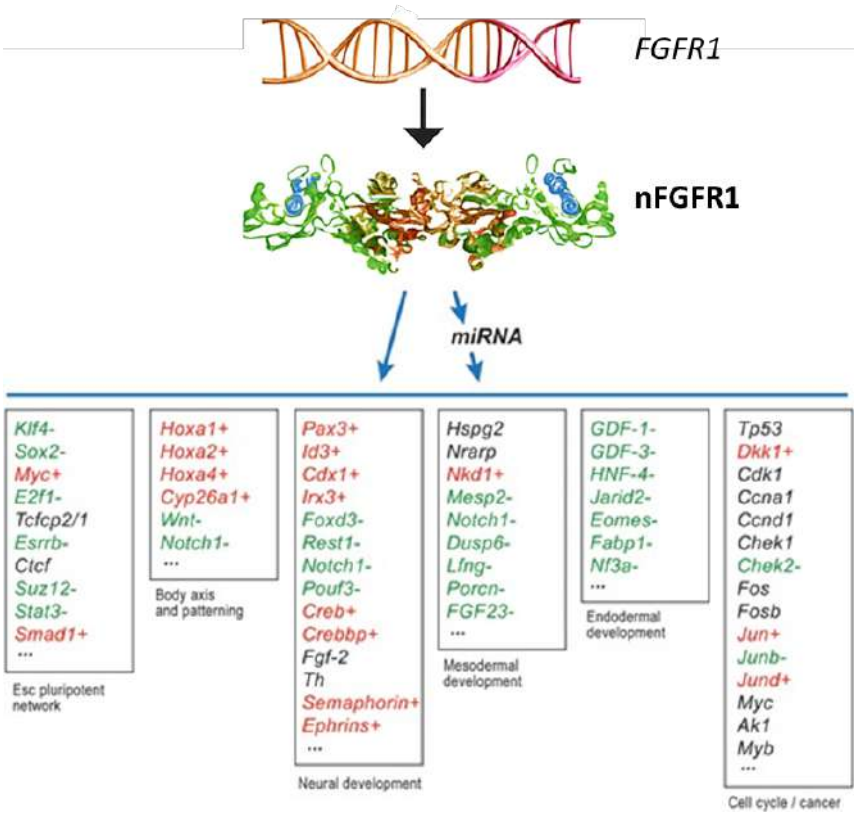

Fig.3. Pan-ontogenetic effect of INFS on developmental pathways*. In the Integrative Nuclear FGFR1 signaling the FGFR1 gene is at the top of the gene regulatory panoptogenic network that governs stem cells development, gastrulation, development of the major body axis, nervous system, muscles, and bones, by affecting downstream mRNAs genes as well as microRNAs (miRNAs) that control the cell cycle, pluripotency and differentiation. This regulation is executed by nFGFR1, which operates at the interface of genomic and epigenomic information, integrates signals from diverse developmental pathways and provides feedback regulation of those pathways (reproduced from Stachowiak* and *Stachowiak, 2016).*

1.4. Role of FGFR1 in mitochondrial dynamics, energy metabolism and cell survival

Several studies have indicated that FGFR1 signaling plays a key role in regulating both mitochondrial biogenesis and dynamics (Hu et al., 2018; Li et al., 2017; Srivastava et al., 2020; Wang et al., 2016; Yan et al., 2023). In addition to its nuclear localization, the intracellular FGFR1 was found to be located with mitochondria and could be involved in the nuclear-mitochondrial communication. FGFR1 is associated with the mitochondrial outer membrane and participates in mitochondrial metabolic functions (Hitosugi et al., 2011; Srisakuldee et al., 2021; Yan et al., 2023). Hitosugi et al. (2011) identified FGFR1 in the mitochondria, where it interacts with PDHK1 and its substrate PDHA1. Immunogold-TEM (transmission electron microscopy) confirmed FGFR1's presence in the mitochondria, while a biochemical assay of mitochondrial subfractions revealed that FGFR1 and FOP2-FGFR1 localized to the outer membrane and intermembrane and matrix spaces (Hitosugi et al., 2011; Srisakuldee et al., 2021). Recently, it was demonstrated that activation of FGFR1 by FGF21 reduced OPA1 degradation by downregulating the E3 ligase FBXW11, thereby preserving mitochondrial fusion and maintaining mitochondrial integrity under stress conditions. Conversely, inhibition of FGFR1 resulted in mitochondrial fragmentation, indicating that FGFR1 is crucial for maintaining mitochondrial dynamics (Yan et al., 2023). It was reported that FGFR1 promote mitochondrial biogenesis by activating AMP-activated protein kinase (AMPK) and microRNA let-7b-5p (Hu et al., 2018; Wang et al., 2016).

Previous studies have demonstrated that FGFR1 plays a critical role in maintaining glucose metabolism homeostasis. It was shown that activation of FGFR1 by FGF1 promoted glucose uptake in adipocytes by promoting glucose transporters GLUT4 and GLUT1 through MEK-Akt and MEK-ERK signaling

(Nies et al., 2022). It is supported by previous studies that stimulation of FGFR1 improves lipid and glucose metabolism in models of metabolic syndrome, both *in vitro* and *in vivo*, in a PI3K/AKT- and AMPK-dependent manner (Martínez-Fernández et al., 2019; Wu et al., 2022).

Growing evidence indicates that FGFR1 plays a central role in cellular energy metabolism by modulating glycolysis and lipid metabolism (Fig.4). It was shown that FGFR1 activation promotes aerobic glycolysis to meet biosynthetic demand in human epithelial cells (Lo et al., 2015). It has been demonstrated that inhibition of FGFR1 in lymphatic endothelial cells promotes a metabolic shift from glycolysis to fatty acid oxidation by reducing hexokinase 2 (HK2) expression, while promoting the expression of carnitine palmitoyltransferase 1A (CPT1A), a rate-limiting enzyme involved in fatty acid oxidation (Song et al., 2021). This supports findings, which also reported a shift from glycolysis to fatty acid oxidation upon FGFR1 inhibition (Zhen et al., 2024). Several studies demonstrated that FGFR1 signaling controls lipid homeostasis under metabolic stress. Previous studies showed that activation of FGFR1 in complex with the transmembrane protein β-Klotho through FGF21 overexpression in adipose tissue preserves phospholipid homeostasis and lipid droplet dynamics, protecting against obesity-induced metabolic stress and inflammation. In contrast, adipocyte-specific FGFR1 ablation resulted in sustained phospholipid biosynthesis and endoplasmic reticulum (ER) stress (Ye et al., 2016). Supporting this, adipocyte-specific deletion of FGFR1 led to the upregulation of hepatic lipid metabolism genes. It enhanced stress-induced hepatic steatosis and adipose lipolysis, indicating the role of FGFR1 in maintaining lipid homeostasis under metabolic stress (Yang et al., 2012).

It was reported that FGFRs activation promotes neuronal survival, axonal growth, and regeneration, by interacting with cell adhesion molecules (CAM), such as neural cell adhesion molecule (NCAM, α7 integrin, and N-cadherin) in primary neuronal and oligodendrocyte cell culture (Lom et al., 1998; Niethammer et al., 2002; Palser et al., 2009; Saffell et al., 1997). In line with the above data, stimulation of FGFR1c via FGF20 promoted survival of midbrain dopaminergic neurons through the MAPK pathway in rat midbrain cultures (Ohmachi et al., 2003). Furthermore, it was demonstrated that Hi-FGF2, but not Lo-FGF2, induces mPTP opening and cytochrome c release in rat cardiac mitochondria *in situ*; this was prevented by FGFR1 inhibition. These findings indicate that mitochondrial

FGFR1 mediates cell death in an FGF2 isoform-specific manner (Srisakuldee et al., 2021). FGFR1 signaling was also identified as a key player in regulating cellular redox balance and resistance to oxidative stress. It was demonstrated that deletion of FGFR1 reduces intracellular ROS levels and decreases the labile iron pool (LIP) in prostate cancer cells, indicating that FGFR1 plays a critical role in maintaining cellular redox balance and iron homeostasis (Lin et al., 2024). Consistently, stimulation of FGFR1/β-Klotho signaling reduces ferroptosis and neuronal cell death in a spinal cord injury model; this effect was reversed by pharmacological FGFR1 inhibition (Xu et al., 2023). Recently, Ito et al. (2025) demonstrated that FGFR1 protects motor neuron-like cells from poly-PR–induced oxidative stress by reducing ROS level and enhancing Nrf2 and heme oxygenase-1 expression (Ito et al., 2025). This is supported by previous studies showing that FGFR1 activation reduces oxidative stress by upregulating NRF2 expression (Suh et al., 2022; Yu et al., 2019).

In summary, FGFR1 is essential for mitochondrial biogenesis and dynamics and reprograms glucose and lipid metabolism to meet cellular energy demands (Fig.4). It also promotes antioxidant defenses and supresses apoptosis by modulating ROS signaling and NRF2-mediated pathways. Whether FGFR1 acts at the level of mitochondrial DNA, similar to nuclear DNA, is unknown.

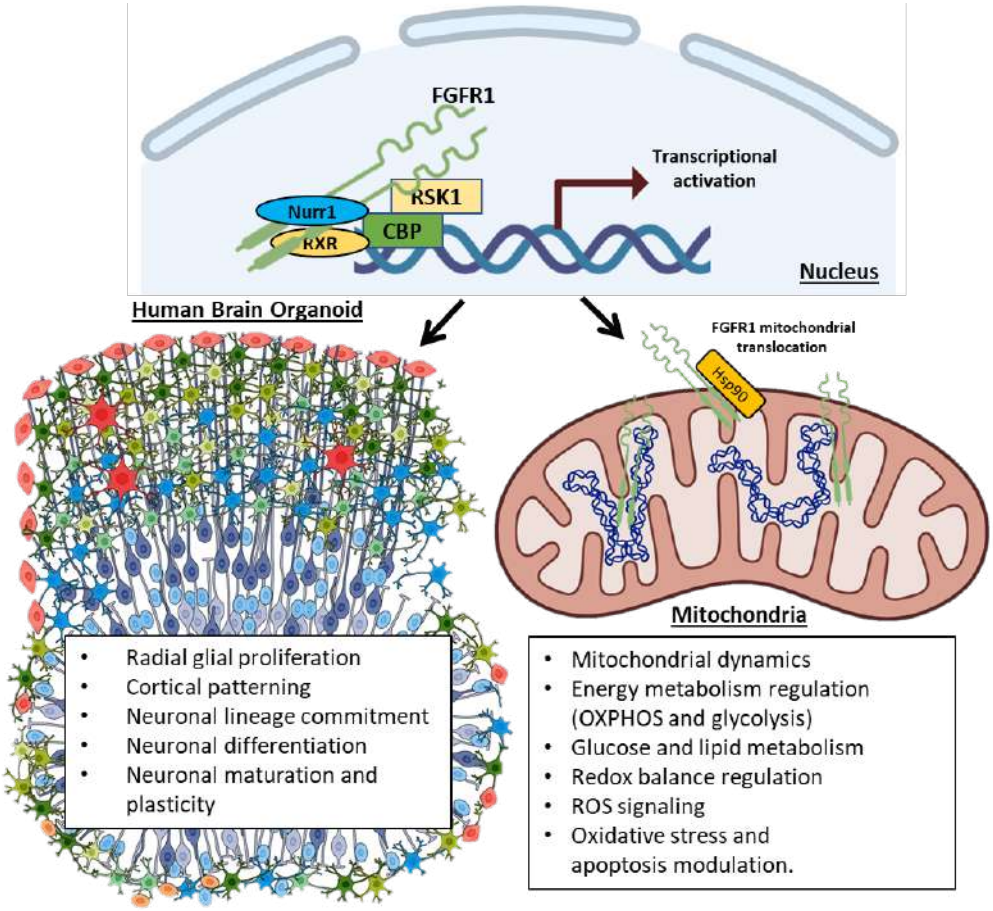

Fig.4. nFGFR1 governs neuronal development, cellular energy metabolism, and cell-survival homeostasis*. Upon nuclear translocation, FGFR1 interacts with RXR, Nurr1, CBP, and RSK1 to activate core transcriptional programs related to neuronal development (radial glia proliferation; cortical patterning, and neuronal lineage commitment), cell metabolism (glycolysis, mitochondrial dynamics, oxidative phosphorylation, and lipid metabolism), and neuronal cell survival (oxidative stress response, ROS signaling, and apoptosis). It is unknown whether FGFR1 may target the mitochondrial genome. Lacking a specific mitochondrial targeting sequence, FGFR could also translocate to mitochondrial DNA through its interaction with heat shock protein 90 (HSP90) (adapted from Di Lullo and Kriegstein, 2017).*

1.5. hiPSC-based organoid models and stem cell engineering to study human brain development

Induced pluripotent stem cells (iPSCs) revolutionized the field of disease modelling and therapeutic translational applications. This was pioneered by Shinya Yamanaka and Kazutoshi Takanashi, who first reprogrammed mouse fibroblasts into pluripotent stem cells through the ectopic expression of four transcription factors, known as “Yamanaka factors," including *OCT4*, *SOX2*, *KLF4*, and *c-MYC*. (Takahashi and Yamanaka, 2006). A similar approach was applied to successfully reprogram human somatic cells by introducing defined factors (*OCT4*, *SOX2*, *NANOG*, and *LIN28*) to establish human induced pluripotent stem cells (hiPSCs)

using the same four factors (Takahashi et al., 2007). hiPSCs express key pluripotency factors (*OCT4*, *SOX2*, *NANOG*) and surface markers (*SSEA3*, *SSEA4*, *TRA-1-60*), possess self-renewal capabilities, capacity to differentiate into all three embryonic germ layers, and closely resemble human embryonic stem cells (hESCs) (Brenes et al., 2024; Narsinh et al., 2011). iPSC can be reprogrammed from both healthy donors and patient-derived somatic cells and then differentiate into various cell types, including muscle cells (Collado et al., 2017; Metzler et al., 2022), cardiomyocytes (Balafkan et al., 2020; Li et al., 2020; Prondzynski et al., 2024), adipocytes (Guénantin et al., 2017; Hafner, 2014), and neuronal cells (Autar et al., 2022; Hiranuma et al., 2024; Liang et al., 2020, 2021).

Brain organoids are three-dimensional neural tissues derived from stem cells or progenitor cells that self-organize into distinct germinal and neuronal layers, recapitulating key aspects of the developing human cortex *in vitro* (Giandomenico et al., 2019; Koo et al., 2019; Lancaster et al., 2013; Stachowiak et al., 2017). Comparative analyses with human fetal brain tissue demonstrated that cerebral organoids recapitulate both the cytoarchitecture and gene-expression programs of the first and second trimesters of the developing cortex (Camp et al., 2015; Fleck et al., 2021).

Characteristic feature of brain organoids is the self-organization of neuroepithelial cells into SOX2/PAX6+ ventricular (VZ)-like zones, sub-ventricular (SVZ)-like zones (expressing TBR2), and cortical layers, displaying typical progenitor-zone architecture of mid-gestation human cortex (Li et al., 2024; Lui et al., 2011; Zecevic et al., 2005). Initially, neuroepithelial cells form rosette-like ventricular zones (VZ), surrounding a fluid-filled cavity (lumen), with apical distribution of N-cadherin and junction-associated protein ZO-1 (Lancaster et al., 2013). Basal to the VZ, TBR2-positive intermediate progenitor cells (IPC) accumulate in the subventricular zone (SVZ), where they undergo symmetric divisions to expand the neuronal pool (Cakir et al., 2019; Hevner, 2019; Pebworth et al., 2021). Newborn neurons migrate radially in an inside-out pattern from the VZ into the cortical plate (CP), first forming both $CTIP2^{+}TBR1^{+}$ deep-layer and $SATB2^{+}CUX1^{+}$ upper-layer neurons (Qian et al., 2020; Tsai and Gleeson, 2005).

Brain organoids can be established using either unguided (self-organizing) or directed (region-specific) differentiation protocols. In the unguided approach (often referred to as cerebral or whole-brain organoids), stem cells undergo

neuronal differentiation by removing serum and additional factors to differentiate into neuronal cells and tissues characteristic of those in the developing cortex. This type of differentiation suffers from high batch-to-batch variability and poor reproducibility (Bagley et al., 2017; Birey et al., 2017; Lancaster and Knoblich, 2014; Zhao and Haddad, 2024). Alternatively, directed protocols drive stem cells toward defined regional neuronal phenotypes by adding exogenous patterning factors, such as FGF, dual-SMAD inhibitors, or WNT modulators, during early neural induction. This method allows the production of highly reproducible, region-specific organoids (Agboola et al., 2021; Tanaka and Park, 2021).

Over the years, a wide array of protocols has enabled the generation of diverse region-specific brain organoids, such as dorsal cortical organoids (Pașca et al., 2019; Pasca et al., 2015; Yoon et al., 2019), forebrain organoids (Gomes et al., 2020; Sebastian et al., 2023), medial ganglionic eminence (MGE) organoids (Bagley et al., 2017; Sawada et al., 2024; Xiang et al., 2017), hippocampal organoids (Qian et al., 2020; Sakaguchi et al., 2015; Y. Wu et al., 2024), midbrain organoids (Becerra-Calixto et al., 2023; Chen et al., 2022; Jacob et al., 2020; Miura et al., 2020; Smits et al., 2019), cerebellar organoids (Atamian et al., 2024; Ballabio et al., 2020; Silva et al., 2020), thalamic organoids (Kiral et al., 2023; Xiang et al., 2019), hypothalamic organoids (Huang et al., 2021; Sarrafha et al., 2023), choroid plexus organoids (Pellegrini et al., 2020; Zhao et al., 2025). Assembloids are defined as self-organizing systems formed by combining region-specific organoids with other organoids or specialized cell types (e.g., endothelial cells or microglia), enabling functional studies of processes such as neuronal projections, cell migration, and circuit assembly (Pașca et al., 2022).

Understanding the functional interaction of distinct brain regions is crucial for unraveling the role of human neural circuits in brain development. Over the past few years, a different assembloid systems has been established to recapitulate inter-regional interactions and circuit-level functions: dorsal and ventral forebrain organoids were assembled to model directed interneuron migration (Bagley et al., 2017; Xiang et al., 2017), spatially arranged ventral midbrain–striatum–cortical organoids (MISCOs) system was used to study dopaminergic circuits (Reumann et al., 2023); thalamic and cortical organoids were fused, to model thalamic reciprocal axonal projections and synaptic plasticity within human circuits (Patton et al., 2024; Shin et al., 2024; Xiang et al., 2019). Recently, human ascending somatosensory

assembloids (hASA) were established by fusing somatosensory organoids, dorsal organoids, spinal cord organoids, thalamic organoids, and cortical organoids to reconstitute functional ascending sensory pathways and integrated somatosensory circuits (Kim et al., 2025). Collectively, these advanced platforms provide new insights into the roles of defined neural circuits in human brain development and neuropsychiatric disorders.

Brain organoids inherently lack immune cells such as microglia. To further enhance the organoid platform by implementing in vivo-like biomimetic conditions, brain organoids are engineered to incorporate both the vascular and immune systems. A recent study demonstrated that the xenotransplantation of human microglia into cerebral organoids suppresses interferon signaling and accelerates the emergence of synchronized oscillatory network activity, highlighting the contributions of microglia to synaptic maturation and neuroimmune homeostasis (Popova et al., 2021). On the other hand, Cakir et al. (2022) generated microglia-containing hCOs (mhCOs) by the targeted overexpression of the myeloid transcription factor PU.1 in human cortical organoids, allowing the *in situ* generation of functional microglia-like cells. They further demonstrated that microglia-like cells within mhCOs protect against amyloid-β-induced cellular and molecular damage, suppress apoptosis and ferroptosis gene programs associated with Alzheimer's disease, and assess the role of AD-risk genes on microglia through a pooled CRISPRi library (Cakir et al., 2022). Finally, it was shown that ectopic expression of *ETV2* (ETS Variant Transcription Factor 2) in cortical organoids drives the formation of complex vascular-like networks. These vascularized hCOs exhibit enhanced functional maturation and acquire key blood–brain barrier properties, including tight junctions, nutrient transporters, and trans-endothelial electrical resistance (Cakir et al., 2019).

The "village-in-a-dish" approach refers to the co-culture of hiPSC cell lines derived from multiple donors in a single dish to study inter-individual variability *in vitro* (Mitchell et al., 2020). Several studies have demonstrated the use of iPSC-derived 2D neuronal cultures from multiple donors as population-scale models to study inter-individual variability, elucidate mechanisms underlying complex disease risk loci and common genetic variation, and characterize donor-specific drug response variability (Cuomo et al., 2020; Jerber et al., 2021; Neavin et al.,

2023; Perez et al., 2022; Srivatsan et al., 2020; Wells et al., 2023; Yazar et al., 2022). However, efforts to extend the "village-in-a-dish" platform to 3D organoids have been limited due to differences in growth rates and differentiation biases among lines from different donors. Surprisingly, Antón-Bolaños et al. (2023) overcame donor-specific growth differences by dissociating cells at the neural stem cell stage and reaggregating them in equal ratios into spheroids. For the first time, they applied brain organoids from multiple cell lines, described as "Chimeroids", to study inter-individual variation in susceptibility to neurotoxic triggers, characterized by high clinical phenotypic variability (ethanol and valproic acid), uncovering donor-specific differences in cellular responses and molecular phenotypes (Bolaños et al., 2023). A similar approach was used by Parrotta et al. (2024), who developed mosaic midbrain organoids (mMOs) from four patients with progressive supranuclear palsy–Richardson syndrome (PSP-RS) to model patient-specific disease phenotypes. These mMOs were characterized by tauopathy features, such as atrophy, neuronal degeneration, neurofibrillary tangles, and tufted astrocytes (Parrotta et al., 2024). In summary, by mixing cells from multiple patients to establish 3D organoid cultures, we can develop novel, population-scale models to gain insights into patient-to-patient variability in mechanisms underlying neurodevelopmental and neurodegenerative diseases.

Lentiviral and gamma-retroviral vectors are the most commonly used delivery systems, allowing stable transgene integration and robust expression (Aiuti et al., 2013; Hacein-Bey-Abina et al., 2014; Sepehrimanesh and Ding, 2020). However, their semi-random integration into the genome can lead to unpredictable outcomes, such as transgene silencing or genomic instability (Johansson et al., 2022; Shearer and Saunders, 2015). This can be overcome by targeting genomic sites known as safe harbors. Genomic safe harbor loci are defined as specific sites in the genome that allow efficient, stable transgene integration and predictable transgene expression without affecting endogenous genes, genomic stability, or cellular phenotype (Papapetrou and Schambach, 2016). So far, several safe harbor sites have been identified in the human genome, such as AAVS1 (PPP1R12C) (Kotin et al., 1992; Ramachandra et al., 2011), CLYBL (Cerbini et al., 2015; Strittmatter et al., 2014), ROSA26 (Irion et al., 2007), CCR5 (Mummidi et al., 1998; S. Shin et al., 2020), SHS231 (Pellenz et al., 2019) or newly discovered Rogi1/2 loci (Aznauryan et al., 2022), enabling the integration of multiple transgenes into

different loci and expanding flexibility in experimental design. To take advantage of these safe harbor sites, engineered nuclease–based knock-in strategies, such as TALENs (transcription activator-like effector nucleases) and CRISPR/Cas9, introduce site-specific double-strand breaks (DSBs) and utilize a homology-directed repair mechanism (HDR) to introduce transgenes, such as fluorescence reporters or overexpression cassettes, precisely at safe harbor loci (Auer and Del Bene, 2014; Frank et al., 2013; Petazzi et al., 2022). However, hiPSC lines edited by TALENs and CRISPR/Cas9 often suffer from off-target effects, low homology-directed repair (HDR) efficiency, and transgene silencing at safe harbor loci. To minimize these unwanted outcomes, each genome-editing experiment must be carefully designed and validated (Bhardwaj and Nain, 2021; Karbassi et al., 2024; Pu et al., 2015).

By integrating state-of-the-art hiPSC genetic engineering methods with brain organoid and assembloid platforms, researchers employ single-cell RNA sequencing, neuronal lineage tracing, and CRISPR-based screening to elucidate the molecular mechanisms of human brain development (He et al., 2022; Meng et al., 2023; Sidhaye et al., 2023). He et al. (2022) developed iTracer, which combines barcoded fluorescent reporters and inducible CRISPR/Cas9, to introduce genetic "scars" for tracing clonal dynamics during cerebral organoid development. They also established the iTracer-perturb system, utilizing inducible CRISPR-mediated knockout of the TSC2 gene, and revealed that TSC2 loss alters mitochondrial metabolism and delays neuronal maturation in developing cerebral organoids (He et al., 2022). Moreover, Sidhaye et al. (2023) generated a dual-reporter SOX2::EGFP-hSYN1::dTomato hESC line by integrating EGFP (via a P2A linker) into the endogenous SOX2 gene to label neural progenitors and by inserting dTomato driven human Synapsin 1 promoter at the AAVS1 safe-harbor locus to label postmitotic neurons. They also isolated $EGFP^{+}$ neural progenitors and $dTomato^{+}$ neurons from telencephalic organoids and showed stage-specific differences in mTOR signaling and translational repression of 5′TOP ribosomal transcripts in neural progenitors (Sidhaye et al., 2023). Finally, Meng et al. (2023) generated human forebrain assembloids (hFA) by fusing ventral forebrain–human subpallial organoids (hSO) with human cortical organoids (hCO) to model interneuron migration and circuit assembly with glutamatergic neurons. By combining hFA with CRISPR loss-of-function screening, live imaging, and single-

cell RNA sequencing, they uncovered key regulators of interneuron formation and migration (Meng et al., 2023).

Collectively, the development of brain organoids and assembloid platforms, combined with state-of-the-art genetic engineering techniques, enables improved *in vitro* modeling of brain development and the identification of neurodevelopmental mechanisms and therapeutic targets for neuropsychiatric diseases (Fig.5).

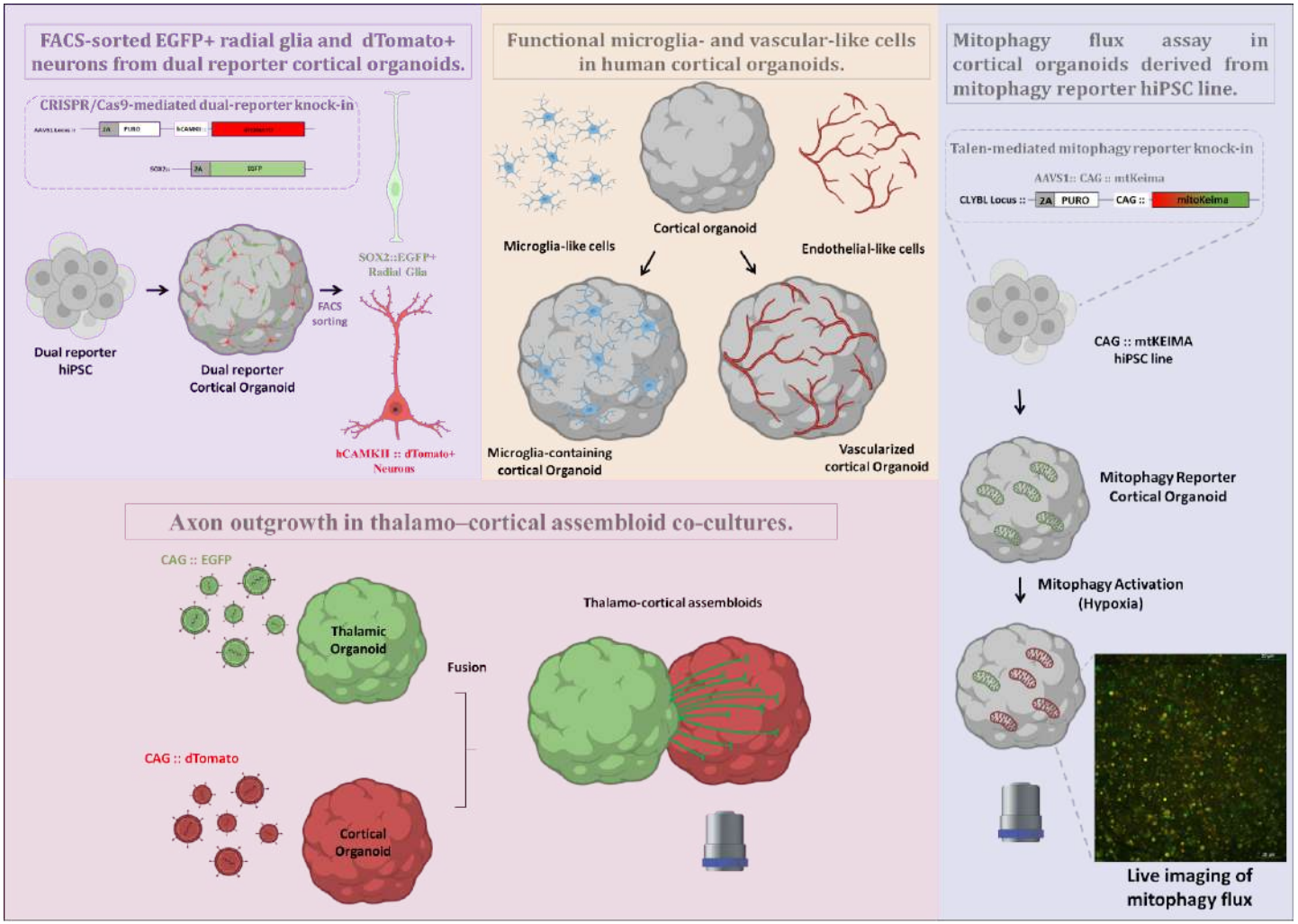

Fig.5. Schematic overview of hiPSC-derived organoid and assembloid platforms for modeling human brain development.

2. Research hypothesis

In this dissertation, I hypothesize that:

- Nuclear FGFR1 (nFGFR1), which promotes early neurogenesis in cortical organoids, influences mitochondrial dynamics, neural lineage commitment, and metabolic adaptation through dual targeting of nuclear and mitochondrial genomes.

This hypothesis is tested in a multi-platform experimental design using inducible nFGFR1 hiPSC-derived cortical organoids, embryoid bodies (EBs), and neuroepithelial stem (NES) cells, applying an integrated panel of molecular, cellular, imaging, and proteomic assays.

3. Objectives of the study

Recent discoveries highlight the importance of mitochondrial dynamics in early human brain development. However, the role of the nuclear form of FGFR1 in these processes remains underexplored. Understanding these mechanisms may provide insights relevant to both developmental biology and the identification of novel therapeutic targets for neurodevelopmental diseases, such as schizophrenia or autism.

The main objective of this dissertation is:

- To define the role of nuclear FGFR1 (nFGFR1) upregulation in modulating developmental and metabolic processes during early cortical development, through its influence on mitochondrial structure, function, turnover, and neural lineage specification.

The thesis includes the following tasks:

- Task I - To develop and characterize a doxycycline-inducible nFGFR1 hiPSC-derived *in vitro* platform.
- Task II - To investigate whether nFGFR1 modulates progenitor dynamics, neuronal differentiation, and maturation in cortical organoids.
- Task III - To investigate whether nFGFR1 regulates mitochondrial dynamics, quality control, and function in cortical organoids.
- Task IV - To investigate whether nFGFR1 regulates redox balance and cell survival in cortical organoids.
- Task V - To investigate whether nFGFR1 targets both the nuclear and mitochondrial genomes.
- Task VI - To investigate whether nFGFR1 orchestrates neurodevelopmental signaling programs.
- Task VII - To investigate whether nFGFR1 regulates cell metabolism and translational reprogramming.
- Task VIII - To investigate whether nFGFR1 modulates autophagy, oxidative stress response, and quality control pathways.

To address this objective, a combination of experimental *in vitro* models and methodologies was employed:

Embryoid Bodies (EBs):

- Analysis of germ layer differentiation using RT-qPCR and immunofluorescence (for ectoderm, mesoderm, endoderm markers).
- Evaluation of mitochondrial membrane potential (MMP), mitophagy flux (mitoKeima), and autophagosome formation (mitochondrial LC3B+).

Neuroepithelial Stem (NES) Cells:

- Analysis of gene expression via RT-qPCR (*FGFR1, NES, PAX6*), mitochondrial DNA copy number (*MT-ND1/HBB, MT-ND2/SERPINA*) via qPCR.
- Assessment of total ATP level, mitochondrial membrane potential (MMP), ROS levels, and viability assays using fluorescence and luminescence plate assays.

Cortical Organoids (hCOs):

- Assessment of proliferation, neural development, apoptosis, and mitochondrial dynamics using gene expression (via RT-qPCR) and immunofluorescence analysis.
- Live imaging for mitophagy flux (mitoKeima reporter assay) and mitochondrial biogenesis activity (PGC1α-EGFP reporter assay).
- Morphometric evaluation of neural rosette organization, mitochondrial morphology, and network connectivity.
- Whole-proteome profiling using TMT-based mass spectrometry.

These objectives aim to provide a comprehensive analysis of the role of nFGFR1 in mitochondrial regulation and neural development within a human-relevant 3D *in vitro* system.

4. Materials and methods

4.1. Reagents used in molecular biology and biochemical applications

Nucleases, ligases, polymerases:

- XbaI (New England Biolabs)
- BamHI-HF® (New England Biolabs)
- ClaI (New England Biolabs)
- SalI-HF® (New England Biolabs)
- PmeI (New England Biolabs)
- EcoRI-HF® (New England Biolabs)
- EcoRV-HF® (New England Biolabs)
- T4 DNA Ligase (New England Biolabs),
- Q5® High-Fidelity DNA Polymerase (New England Biolabs)
- Taq 2X Master Mix (New England Biolabs)
- DNA Polymerase I, Large (Klenow) Fragment (New England Biolabs)

DNA molecular weight and size standards, loading buffers:

- 1 kb Plus DNA Ladder (New England Biolabs)
- 100 bp DNA Ladder (New England Biolabs)

Small Molecules:

- Human FGF-basic (FGF-2/bFGF) Recombinant Protein (PeproTech)
- Human EGF Recombinant Protein (PeproTech)
- SB-431542 (TGF-β receptor kinase inhibitor) (MedChemExpress, MCE)
- Dorsomorphin (MedChemExpress, MCE)
- Human/Mouse/Rat BDNF Recombinant Protein (PeproTech)
- Human NT-3 Recombinant Protein (PeproTech)
- CHIR-99021 (MedChemExpress, MCE)
- Rock inhibitor (Y-27632)

Commercially available kits:

- Plasmid Mini kit (A&A Biotechnology)
- Plasmid Midi AX Endotoxin-Free (A&A Biotechnology)
- Clean-Up kit (A&A Biotechnology)
- Gel-Out kit (A&A Biotechnology)
- Total RNA Mini Plus kit (A&A Biotechnology)
- Xpure™ Cell&Tissue micro (A&A Biotechnology)
- High-Capacity cDNA Reverse Transcription Kit (Applied Biosystems™)
- Power SYBR™ Green PCR Master Mix (Applied Biosystems™)

Reagents used in microscopy-based assays:

- Hoechst (Thermo Fisher Scientific)
- MitoTracker™ Red CMXRos (Invitrogen)

4.2. Materials and reagents for culturing mammalian cell lines

Cell lines:

- Gibco™ episomal hiPSC line (Gibco™)
- Neuroepithelial-like stem (NES) cells
- 293FT Cell Line (Invitrogen™)

Reagents & drugs:

- Polyethylenimine, PEI 25K (1 μg/μl) (Sigma-Aldrich)
- Lipofectamine™ 3000 Transfection Reagent (Invitrogen™)
- Dimethyl sulfoxide, DMSO (Sigma-Aldrich)
- Dulbecco′s Phosphate Buffered Saline, without calcium chloride and magnesium chloride, DPBS (Sigma-Aldrich)
- PBS (Phosphate-Buffered Saline) Tablets (Invitrogen™)
- Phosphate-buffered saline (PBS, 10X), pH 7.4 (Thermo Scientific Chemicals)
- StemPro™ Accutase™ Cell Dissociation Reagent
- EDTA (0.5 M), pH 8.0, RNase-free (Invitrogen™)
- Trypsin-EDTA (0.5%), no phenol red (Gibco™)
- 2-mercaptoethanol (Gibco™)
- GlutaMAX™ Supplement (Gibco™)
- MEM Non-Essential Amino Acids Solution (100X) (Gibco™)
- KnockOut™ Serum Replacement (KOSR) (Gibco™)
- Antibiotic-Antimycotic (100X) (Gibco™)
- Penicilin-Streptomycin (5,000 U/mL) (Gibco™)
- Essential 8™ Medium (Gibco™)
- Essential 6™ Medium (Gibco™)
- Dulbecco's Modified Eagle Medium F12 (DMEM F12) (Gibco™)
- Neurobasal™-A Medium (Gibco™)
- Neurobasal™ Medium (Gibco™)
- B-27™ Plus Supplement without vitamin A (50X) (Gibco™)
- B-27™ Plus Supplement (50X) (Gibco™)
- N-2 Supplement (100X) (Gibco™)
- Fetal Bovine Serum (FBS), Premium (Gibco™)
- Geltrex™ Reduced-Growth Factor Basement-Membrane Matrix (Gibco™)
- Poly-L-Lysine solution (Sigma-Aldrich)
- Vitronectin (VTN-N) Recombinant Human Protein, Truncated (Gibco™)
- Poly(2-hydroxyethyl methacrylate), Poly-HEMA (Sigma-Aldrich)
- Anti-Adherence Rinsing Solution (Stemcell Technologies™)
- AggreWell™800 Plate (Stemcell Technologies™)
- Polybrene Infection / Transfection Reagent (Sigma-Aldrich)
- TAE Buffer, 10X Solution (Thermo Scientific Chemicals)
- Agarose I (Molecular Biology Grade) (Thermo Scientific™)
- 1-Propanol, HPLC Grade, 99% (Thermo Scientific Chemicals)
- Ethyl cinnamate, 98% (Thermo Scientific Chemicals)
- Triton™ X-100 (Thermo Scientific™)
- Syringe filter 0.22 μm and 0.45 μm (Genos)
- 38.5 mL Open-Top Thinwall Ultra-Clear Tube (Beckman Coulter)

4.3. Materials used in bacterial culture

Bacteria

- NEB® 10-beta Competent E. coli (New England Biolabs)
- NEB® Stable Competent E. coli (New England Biolabs)

Antibiotics

- Ampicillin Sodium (A&A Biotechnology)
- Puromycin Dihydrochloride (Gibco™)
- Geneticin™ Selective Antibiotic (G418 Sulfate) (Gibco™)
- Kanamycin Sulfate (Gibco™)

Bacterial media

- LB (A&A Biotechnology)
- LB agar (A&A Biotechnology)
- S.O.C. (Super Optimal broth with Catabolite repression) Medium (Invitrogen)

4.4. Cryosectioning

- Cryostat (Microm HM550 Thermo Scientific)
- Microtome blades (Sakura)
- O.C.T. (Optimal cutting temperature) compound (Tissue-Tek)
- Cryomold (Tissue-Tek)
- SuperFrost® Plus microscope slides(bionovo)

4.5. Plasmids

Plasmids used in this study were from the plasmid bank of the Department of Stem Cell Bioengineering, Mossakowski Medical Research Institute PAS (MMRI PAS).

- pLenti CMV GFP Puro (658-5) (Addgene #17448)
- CLYBL-TO-hNGN2-BSD-mApple (Addgene #124229)
- CLYBL-TO-FGFR1(SP-/NLS)-BSD-mApple (IMDIK PAN)
- pHAGE-mt-mKeima (Addgene #131626)
- pcDNA 3.1(-) CMV FGFR1(SP-/NLS) (gift from prof. Michal Stachowiak)
- pPGC1a_Proximal Promoter-FLuc2P (Addgene #154259)
- pLenti CMV mt-Keima Puro (658-5) (IMDIK PAN)
- pLenti PGC1A-EGFP Puro (658-5) (IMDIK PAN)

Table 1. *Primers used for cloning and sequencing.*

Name	Primer sequence (5'-3')	Product
XbaI-mKeima-F	ATTCTAGAATGTCCGTCCTGACGCCG	To ampify mKeima from pHAGE-CAG-Mkeima to pLenti-EGFP-puro
SalI-mKeima-R	AATGTCGACTTAGCCCAGCAGGGAGTG	
BamHI-E-F	ACGGGATCCATGAGCCCCAAGAAAAAGAGAAAGG	

PmeI-dlxNLS-R	CCGGTTTAAACGGGGAGGGATCAAACTCAATGATG	To ampify FGFR1 SP-/NLS from pcDNA 3.1 to CLYBL-TO-NGN2
PGC1aProxClaF	CGATCGATCCCCGTTTGCGCTTTCAAACA	To amplify PGC1a promoter to plenti EGFP vector
PGC1aProxXbaR	CGTCTAGAGTACCGGATTGCCAAGCTTT	
LNCX	AGCTCGTTTAGTGAACCGTCAGATC	Sequencing primer: Tet3G promoter
nFGFR1TK-R5	TCCAATATGGAGCTACGGGCATAC	Sequencing reverse primer for FGFR1(SP-/NLS)
SV40pA-R	GAAATTTGTGATGCTATTGC	Sequencing pA Reverse
GFPseq-R	AGCTTGCCGTAGGTGGCATC	Sequencing EGFP reverse primer
WPRE-seqR	CATAGCGTAAAAGGAGCAACA	Sequencing WPRE reverse primer

4.6. Cell culture media

Table 2. *Media composition and reagent concentrations.*

	Volume for 50 mL	**Concentration**
HEK Medium (293FT cells)		
DMEM/F-12	50 ml	-
GlutaMAX (100X)	500 µL	1:100
FBS	5 ml	1:10
P/S	500 µL	1:100
N2B27 Medium (NES cells)		
DMEM/F-12	44 ml	-
KnockOut Serum Replacement (KOSR)	5 ml	1:10
GlutaMAX (100X)	500 µL	1:100
Non-essential Amino Acids	50 µL	1:100
2-mercaptoethanol	91 µL	1:550
P/S	500 µL	1:100
N2B27 Medium (NES cells)		
DMEM/F-12	24 mL	-
Neurobasal	24 mL	-
GlutaMAX (100X)	500 µL	1:100
2-mercaptoethanol	91 µL	1:500
N2	250 µL	1:200
B27	500 µL	1:100
P/S	500 µL	1:100
NES Growth Medium (NES cells)		
DMEM/F-12 + GlutaMAX	47.5 mL	-
N2	500 µL	1:100
GlutaMAX (100X)	500 µL	1:100
B27	50 µL	1:1000

P/S	500 µL	1:100
bFGF	5 µL	10 ng/mL (1:10000)
EGF	5 µL	10 ng/mL (1:10000)
hiPSC Media (hiPSC cells)		
Essential 8 medium	48.5 ml	-
Essential 8 supplement (50x)	1 ml	1:50
P/S	500 µL	1:100
Embryoid Bodies media (Embryoid bodies)		
Essential 6 medium		
P/S		
Induction Medium (human cortical organoids)		
Essential 6	49,5	
P/S	500 µL	
SB431542 (10 mM)	50 µL	10 µM (1:1000)
Dorsomorphin (5 mM)	50 µL	5 µM (1:1000)
Differentiation medium (human cortical organoids)		
Neurobasal A	50 ml	-
B-27™ Supplement without vitamin A (50X)	1 ml	1:50
GlutaMAX (100X)	500 µL	1:100
P/S	500 µL	1:100
bFGF (10 µg/mL)	50 µL	10 ng/mL (1:1000)
EGF (10 µg/mL)	50 µL	10 ng/mL (1:1000)
BDNF (20 µg/mL)	50 µL	20 ng/mL (1:1000)
NT-3 (20 µg/mL)	50 µL	20 ng/mL (1:1000)

4.7. Mammalian cell culture

4.7.1. hiPSC cells

The Gibco™ episomal hiPSC line (catalog no. A18945; Gibco™) was derived from cord blood CD34+ progenitors via episomal expression of seven reprogramming factors: *OCT4*, *SOX2*, *KLF4*, *MYC*, *NANOG*, *LIN28*, and *SV40 T* antigen. hiPSCs were grown in a feeder-free environment on 6-well plates coated with recombinant human vitronectin. The hiPSC cells were maintained in Essential 8 medium, supplemented with penicillin/streptomycin solution. The culture medium was refreshed daily. When cells reached 70–80% confluency, they were routinely passaged using a 50 mM EDTA chelating agent at a 1:6 to 1:20 ratio. The hiPSC cultures were routinely tested to confirm the absence of mycoplasma contamination and were maintained under mycoplasma-free conditions. Media formulation is detailed in Table 2.

4.7.2. Neuroepithelial stem (NES) cells,

Neuroepithelial stem cells (NES cells) were generated using a modified version of the protocol previously described (Calvo-Garrido et al., 2021). Human induced pluripotent stem cells (hiPSCs) were cultured in complete E8 medium supplemented with Essential 8 supplement and penicillin/streptomycin, and were passaged every 3–4 days using 50 mM EDTA at ~80% confluency. Neural induction was initiated in hiPSCs on Day 0 by replacing Essential 8 medium with KOSR medium supplemented with Dorsomorphin (5 μM), SB431542 (10 μM), and CHIR99021 (3.3 μM), with daily media changes. On Day 5, cells were passaged at a 1:2 ratio onto mouse laminin-coated 6-well plates. From Day 6, the medium was changed to a 75%:25% mixture of KOSR:N2B27 media containing the same small molecules, with continued daily media changes. This ratio was adjusted to 50:50 on Day 8, followed by cell passaging using TrypLE at a 1:2 ratio into KOSR:N2B27 (25%:75%) on Geltrex-coated plates. On Day 12, cells were cultured in complete N2B27 medium supplemented with Dorsomorphin, SB431542, and CHIR99021. Finally, on Day 16, cells were gently passaged with 50 mM EDTA at a 1:2 ratio into NES growth medium enriched with EGF (10 ng/mL) and bFGF (10 ng/mL) and were maintained with media changes every other day (Fig.6B). The media formulations are detailed in Table 2.

4.7.3. 293FT cells

293FT cells were maintained on 100 mm and 150 mm tissue culture dishes pre-coated with 0.1 mg/mL poly-L-lysine. Cells were grown in DMEM/F-12 supplemented with 10% fetal bovine serum (FBS), 1% GlutaMAX, and 1% penicillin/streptomycin at 37°C in a 5% CO_2 atmosphere. Culture medium was refreshed every 2-3 days, and cells were passaged at 80–90% confluency by splitting at a 1:10–1:20 ratio. The media formulation is detailed in Table 2.

4.7.4. Generation of embryoid bodies (EBs)

Embryoid bodies (EBs) were generated as described in Latoszek et al. (2022), with slight modifications (Latoszek et al., 2022). A total of 1×10^6 human induced pluripotent stem cells (hiPSCs) were seeded in low-attachment PolyHEMA-coated plates and cultured in Essential 6 medium. The medium was

refreshed daily to support the formation of EBs. On Day 10, the EBs were transferred to wells containing slides coated with Geltrex to facilitate attachment and cell migration. By Day 21, the EBs were harvested for downstream applications (Fig.6A). The media formulation is detailed in Table 2.

4.7.5. Generation of human cortical organoids (hCOs)

The generation of human cortical organoids (hCOs) from hiPSCs was conducted according to the protocols established by Sergiu Pasca's lab (Pasca et al., 2015; Sloan et al., 2018). Embryoid Body (EB) Formation - When cells reached 70–80% confluency, intact hiPSC colonies were incubated with Accutase at 37°C for 4 minutes to dissociate them into single cells. Uniformly sized EBs were generated using AggreWell™ 800. Approximately 3×10^6 single cells were added to each AggreWell™800 well in Essential 8 medium, supplemented with the ROCK inhibitor (Y-27632). The plates were centrifuged at 100 × g for 3 minutes to settle the cells into the microwells and then incubated at 37°C with 5% CO_2. The following day, half of the medium was replaced with fresh Essential 8 medium containing Y-27632. After 48 hours, the EBs were harvested from each microwell by gently pipetting with a sterile 3 mL Pasteur pipette and transferred into polyHEMA-coated, low-attachment plastic dishes containing induction medium supplemented with SMAD pathway inhibitors: dorsomorphin (2.5 μM, Peprotech) and SB-431542 (10 μM). From day 2 to day 6, the medium was replaced daily. Neural Induction and Differentiation - On day 6, neurospheres were transferred to differentiation medium, supplemented with 20 ng/mL EGF and 20 ng/mL bFGF for the next 19 days (until day 24), with medium changes every other day. To promote the differentiation of neural progenitors into neurons, the medium was supplemented with 20 ng/mL BDNF and 20 ng/mL NT3 (Peprotech), with medium changes every other day. From day 43 onwards, only differentiation medium without growth factors was used, and the medium was replaced every 3-4 days (Fig.6C). Media formulations are displayed in Table 2.

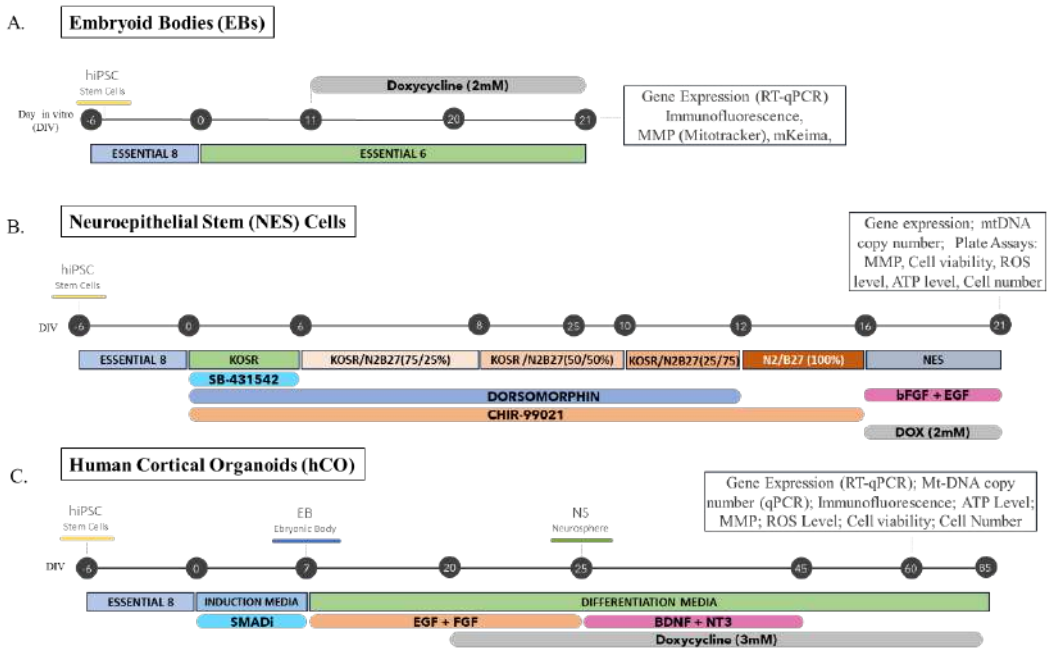

Fig.6. Experimental outline for cell culture protocols in vitro using platforms derived from the stable hiPSC$^{Tet3G\text{-}FGFR1(SP\text{-}/NLS)}$ line*; embryoid bodies (EB), neuroepithelial-like stem (NES) cells, human cortical organoids (hCOs), and nFGFR1 upregulation through doxycycline treatment.*

4.8. Cryopreservation and cryosectioning

hCOs were fixed in 4% paraformaldehyde (PFA) for 30 minutes on a shaker (100 RPM, room temperature), followed by extensive washing with 1x PBS. Organoids were sequentially incubated in 7.5% sucrose overnight, 15% sucrose for 8 hours, and 30% sucrose overnight to ensure proper infiltration and dehydration. After sucrose incubation, organoids were immersed in a gelatin/sucrose solution (7.5%/10%) for 30 minutes, embedded in the same gelatin/sucrose solution, snap-frozen in liquid nitrogen, and stored at -80°C. For immunohistochemistry, 20 µm-thick sections were prepared using a cryostat at -20°C.

4.9. Immunocytochemistry

Immunocytochemistry was performed with slight modifications as described previously (Petersilie et al., 2024; Stachowiak et al., 2017). To remove excess OCT and gelatin, cryosections were incubated in 1x PBS at 37°C water bath for 30 minutes. For permeabilization, sections were incubated in 0.5% Triton X-100 for 20 minutes at room temperature. Blocking was carried out in 10% normal goat serum (NGS) with 0.1% Triton X-100 diluted in PBS for 1 hour at room temperature. Following blocking, cryosections were incubated overnight at 4°C

with primary antibodies diluted in PBS containing 1% normal goat serum (NGS) and 0.1% Triton X-100. After overnight incubation, organoid sections were washed three times with 1x PBS for 15 minutes each on an orbital shaker (80 RPM). The sections were then incubated with secondary antibodies diluted in x1 PBS for 1 hour at room temperature in dark conditions. After secondary antibody incubation, sections were rewashed three times with 1x PBS for 15 minutes each on an orbital shaker (80 RPM). Nuclei were stained with Hoechst 33258 (2µg/mL) for 15 minutes, followed by three additional PBS washes (15 minutes each). Cryosections were mounted on glass coverslips using fluorescence mounting medium (Dako), dried overnight at room temperature, and stored at 4°C. The primary and secondary antibodies used in this study are listed in Tables 3 and 4.

Table 3. *Primary antibodies used in this study.*

Antigen	**Vendor**	**Catalog number**	**Host**	**Isotype**	**Dillution**
Ki-67	Invitrogen	MA5-41135	Rabbit	IgG	1:500
SOX2	CST	3579	Rabbit	IgG	1:400
PAX6	Invitrogen	MA1-109	Mouse	IgG1	1:200
Neun	Abcam	ab104224	Mouse	IgG2B	1:100
TBR1	CST	49661	Rabbit	IgG	1:400
Eomes	Invitrogen	14-4877-82	Mouse	IgG2B	1:300
BCL11B (CTIP2)	CST	12120	Rabbit	IgG	1:200
Synapsin-2 (SYN2)	Abcam	ab13258	Rabbit	IgG	1:200
LC3B (D11) XP®	CST	3668	Rabbit	IgG	1:200
Cleaved Caspase-3 (Asp175)	CST	9661	Rabbit	IgG	1:400
Pink1	Abclonal	A7131	Rabbit	IgG	1:200
Parkin	Abclonal	A0968	Rabbit	IgG	1:200
EGFP	Invitrogen	CAB4211	Rabbit	IgG	1:200
MAP2	Sigma-Aldrich	M4403	Mouse	IgG1	1:500
Nestin	Invitrogen	MA1-110	Mouse	IgG1	1:500
FGFR1	Abcam	Ab10646	Rabbit	IgG1	1:500
Anti-Mitochondria	Sigma-Aldrich	MAB1273	Mouse	IgG1	1:1000
OCT 3/4	Santa Cruz	sc-5279	Mouse	igG2b	1:100
SSEA4	CST	4755	Mouse	IgG3	1:400
NANOG	CST	4903	Rabbit	IgG	1:200
Alpha-Smooth Muscle Actin	Sigma-Aldrich	A2547	Mouse	IgG1	1:400
FOXA2	Invitrogen	720061	Rabbit	IgG	1:500

Table 4. *Secondary antibodies used in this study.*

Name	Vendor	Catalog number	Antigen	Concentration
Alexa Fluor™ 488	Invitrogen	A-21121	Mouse IgG1	1:500
Alexa Fluor™ 488	Invitrogen	A-21141	Mouse IgG2b	1:500
Alexa Fluor™ 488	Invitrogen	A-11008	Rabbit IgG	1:500
Alexa Fluor™ 546	Invitrogen	A-21123	Mouse IgG1	1:500
Alexa Fluor™ 546	Invitrogen	A-21143	Mouse IgG2b	1:500
Alexa Fluor™ 546	Invitrogen	A-11035	Rabbit IgG	1:500
Alexa Fluor™ 647	Invitrogen	A-21245	Rabbit IgG	1:500

4.10. Image acquisition

Image acquisition was performed using a Zeiss Cell Observer SD microscope (Zeiss) equipped with a Yokogawa Spinning Disk system and four diode lasers (405 nm, 488 nm, 561 nm, and 635 nm). Tiled images, composed of multiple smaller image tiles stitched together, were acquired to capture the entire region of hCO cryosections. For image acquisition, a 20× (NA 1.4) or 40× (NA 1.2) objective was used based on the desired resolution and field of view. For each tile, Z-stack images were obtained by capturing 30–50 optical sections at different focal planes, with a Z-stack interval of 0.7-2 µm. The tiled Z-stacks were processed into extended focus depth (EFD) images using ZEN software for further analysis.

4.11. Isolation of nucleic acids

Total RNA was extracted from hiPSC, NES cells, EBs, and hCO cells using Total RNA Mini Plus (A&A Biotechnology). Total DNA was extracted from NES cells using Xpure™ Cell&Tissue micro kit (A&A Biotechnology). RNA was purified using Clean-Up RNA Concentrator kit (A&A Biotechnology). After purification, RNA integrity was assessed by electrophoresis on 2% agarose gels. The concentration of RNA and DNA was determined by using NanoDrop ND-1000 spectrophotometer (Thermo Fisher Scientific). The DNA was used in the mtDNA copy number analysis (qPCR). The RNA was converted into cDNA in the RT reaction using the High-Capacity RNA-to-cDNA™ Kit (Thermo Fisher Scientific)

on a thermal cycler (Biotech INC). Next, cDNA was used to analyze gene expression (RT-qPCR).

4.12. Primer design

All primers used in these studies are based on the human reference genome GRCh38 and were designed using PrimerQuest software (https://www.idtdna.com/pages/tools/primerquest), analyzed both *in silico* and *in vitro*. Primer sequences were validated for specificity and efficiency *in silico* with Primer-BLAST (https://www.ncbi.nlm.nih.gov/tools/primer-blast/) and UCSC In-Silico PCR (https://genome.ucsc.edu/cgi-bin/hgPcr). The sequences of primers for the selected genes are listed below. Experimentally determined PCR efficiency (E%) was in the range of 1.92–2.15. Candidate reference genes were assessed for expression stability by analyzing their Ct values with NormFinder (https://www.moma.dk/software/normfinder) and BestKeeper (https://www.gene-quantification.de/bestkeeper.html). The most stable gene identified by these programs was then selected as normalization controls for RT-qPCR gene expression analyses. The primer sequences used in this study are provided in Table 1 (cloning and sequencing), Table 5 (mtDNA copy number), and Table 6 (gene expression).

4.13. Quantitative real-time PCR (qPCR; mtDNA copy number)

For qPCR, 10 ng of DNA was loaded with 0.25 μM of forward and reverse primers, and PowerUp™ SYBR™ Green Master Mix (Applied Biosystems) on a LightCycler® 480 II system (Roche). The amplification reaction consisted of a hot start at 95 °C for 3 minutes, followed by 45 cycles of denaturation at 95 °C for 10 seconds, annealing at 60 °C for 30 seconds, and extension at 72 °C for 30 s. The mtDNA copy number was calculated as (1) *MT-ND1/HBB* and (2) *MT-ND5/SERPINA1* ratio; the following equation was used: relative mitochondrial DNA content = $2 \times 2^{\Delta CT}$, where ΔCT was calculated using the formula ($\Delta CT = nDNA_{CT} - mtDNA_{CT}$). Primer sequences used in this study are listed in Table 5.

4.14. Reverse transcription quantitative real-time PCR (RT-qPCR)

Quantitative real-time PCR (RT-qPCR) was performed using 10 ng of cDNA, 0.2 μM of each primer, and PowerUp™ SYBR™ Green Master Mix

(Applied Biosystems) on a LightCycler® 480 II system (Roche). The amplification protocol consisted of an initial incubation at 50°C for 2 minutes and 95°C for 2 minutes, followed by 40 cycles of 95°C for 15 seconds and 60°C for 1 minute, with a final extension at 95°C for 5 minutes and 65°C for 1 minute. Gene expression was quantified using the ΔCt method with *GAPDH* as the reference gene. Stability of the reference gene was confirmed using BestKeeper and NormFinder software. Results are presented as $2^{-\Delta\Delta Ct}$ values relative to *GAPDH*. Primer sequences used in this study are listed in Table 6.

Table 5. *Sequences of primers used for relative mt-DNA copy number.*

Gene	**Forward Primer (5'-3')**	**Reverse Primer (5'-3')**
MT-ND1	AACATACCCATGGCCAACCT	AGCGAAGGGTTGTAGTAGCCC
HBB	GAAGAGCCAAGGACAGGTAC	CAACTTCATCCACGTTCACC
MT-ND5	CATTACTAACAACATTTCCCCCGC	GGCTGTGAGTTTTAGGTAGAGGG
SERPINA1	CAGTGAATAAATGAGGCGTACATCC	GACTGTTTCTCATGCCTCTGGAAAG

Table 6. *Sequences of primers used for gene expression analysis.*

Gene	**Forward Primer (5'-3')**	**Reverse Primer (5'-3')**
ATF4	CAACAACAGCAAGGAGGAT	CATCCAACGTGGTCAGAAG
EOMES	TCACCCAGAGTCTCCTAATAC	ACTATCATCTGGGTGTTGTTG
BCL11B	CAGTGTCAGTTGTCAGGTAAA	TCCAGGTAGATGCGGAAG
PINK1	GGTCGACTACCCTGATGT	CAGGGTACAGGGATAGTTCT
SQSTM1	CCCTGAGGAACAGATGGA	GACTGGAGTTCACCTGTAGA
BNIP3	ACAGTCTGAGGAAGATGATATTG	TTTAAAGAGGAACTCCTTGGG
SOX17F	GTGGACCGCACGGAATTTG	GGAGATTCACACCGGAGTCA
CXCR4F	CCCTCCTGCTGACTATTCCC	TAAGGCCAACCATGATGTGC
TBXTF	TATGAGCCTCGAATCCACATAGT	CCTCGTTCTGATAAGCAGTCAC
MEF2C	CCAACAAGCTGTTCCAGTAT	CCTTCTTTCTCAACGTCTCC
MAP2	GACCTAAGCCATGTGACATCCA	AATTTTCACACGTCCGCCAC
SOX2	5GTGGAAACTTTTGTCGGAGA	TTATAATCCGGGTGCTCCTT
PAX6	CAGGCCAGCAACACACCTAG	GCAGAGCGCTGTAGGTGTTT
NES	AAGGGCAAATCTGGGGGTTG	GGGAGTCCTGGATTTCCTTCC
GAPDH	GGGCTCTCCAGAACATCATCC	GGTCCACCACTGACACGTTG
MT-ATP6	AAGGACGAACCTGATCTCT	TGGGTGGTTGGTGTAAATG
MT-ND2	GCTAAGCTCGCACTGATTT	CTGTGGAACGAGGGTTTATT
MT-ND5	CGCCTGAGCCCTATCTATTA	GACCTGTTAGGGTGAGAAGA
PPARGC1A	CCCAGAGTCACCAAATGAC	TCCAGAGAGTTCCACACTTA
SYP	GATGTAGTCTGGTCAGTGAAG	GGTGGAGACCTAGGGTATAG
BAX	GGGCTGGACATTGGACTTCCT	CCGCCACAAAGATGGTCACG
BCL2	ATCGCCCTGTGGATGACTGAG	AGGGCCAAACTGAGCAGAGTC
TBR1	CTCAGTTCATCGCCGTCACC	AGCCGGTGTAGATCGTGTCATA

4.15. Lentiviral particle production and concentration

Lentiviral particles were produced as described in Tiscornia et al. (2006), with slight modifications (Tiscornia et al., 2006). Human embryonic kidney 293FT cells were maintained in DMEM/F12 media supplemented with GlutaMax and 10% FBS. For transfection, cells were seeded on poly-lysine-coated 15-cm plates. At 85-90% confluency, 293FT cells were co-transfected with packaging plasmids psPAX2 (Addgene, 12260) and pMD2.G (Addgene, 12259), along with the lentiviral transfer vector, using 1 mg/mL polyethylenimine (PEI) transfection reagent at a DNA: PEI ratio of 1:3. After 48 and 72 hours, the supernatant containing lentiviral particles was collected, filtered through a 0.45 μm syringe filter, and concentrated by ultracentrifugation in 38.5 mL Open-Top, round-bottom ultracentrifugation tubes (Cat. 344058, Beckman and Coulter) using a swinging bucket rotor (SW-28) at 80 000 g for 2 hours. The supernatant was then discarded, and the viral pellet was resuspended in 1x PBS. It was snap-frozen in liquid nitrogen and stored at -80°C.

4.16. Mito-Keima mitophagy reporter

To track mitophagy flux *in vitro*, the pH-dependent fluorescent mitophagy reporter mt-Keima was used as previously described (Sun et al., 2017; Yang et al., 2022). Mito-Keima is a dual-excitation ratiometric fluorescent protein resistant to lysosomal proteases. At mitochondrial pH (pH 8.0), shorter-wavelength excitation predominates, while in acidic lysosomes (pH 4.5), it shifts to longer-wavelength excitation. The mito-Keima (546 nm / 488 nm) ratio, divided by the total mitochondrial area, reflects mitophagy flux. To generate the mitophagy reporter, the mt-Keima sequence containing the mitochondrial targeting sequence (MTS) was amplified by PCR from the plasmid pHAGE-mt-mKeima (Addgene #131626) using primers with flanking BamHI and SalI restriction sites (Fig.7A). The amplified mt-Keima DNA was cloned into the BamHI and SalI sites of the pLenti CMV-GFP-PGK-Puro (658-5) lentiviral transfer vector (Addgene #17448). Successful cloning was verified using colony PCR and Sanger sequencing. Lentiviral particles were produced as described in Section 4.15. Stable mitophagy reporter hiPSC line. hiPSCs were transduced with lentiviral particles containing mt-Keima. Briefly, hiPSCs were maintained in Essential 8 media supplemented with penicillin/streptomycin. When cells reached 80-90% confluency, they were

passaged using EDTA. Lentiviral particles were added to the cell suspension in Essential 8 media containing polybrene (10 μg/mL) and 10 μM ROCK inhibitor (Y-27632), and the cells were plated on vitronectin-coated plates. For positive selection, cells were maintained in media containing 0.5–1 mg/mL puromycin for 5–7 days. Expression of the fluorescent protein was verified using fluorescence microscopy or flow cytometry (data not shown in the study). Stable mitophagy reporter hiPSC lines were cryopreserved or processed for further experiments. hCO Mitophagy Flux Imaging Assay. At day 56 of differentiation, hCOs were transduced by incubating in fresh differentiation medium containing mito-Keima lentiviral particles and polybrene (10 μg/mL) for 48 h. After 48 hours, the medium was replaced with differentiation medium lacking virus, and the organoids were maintained for an additional 10 days to allow for robust reporter expression. For live imaging, 60-day hCOs were transferred to a glass-bottom 35 mm cell culture imaging dish (Ibidi). Live-cell imaging of mitophagy flux was performed using a spinning-disk confocal microscope with 488 nm and 546 nm excitations (Fig.7B).

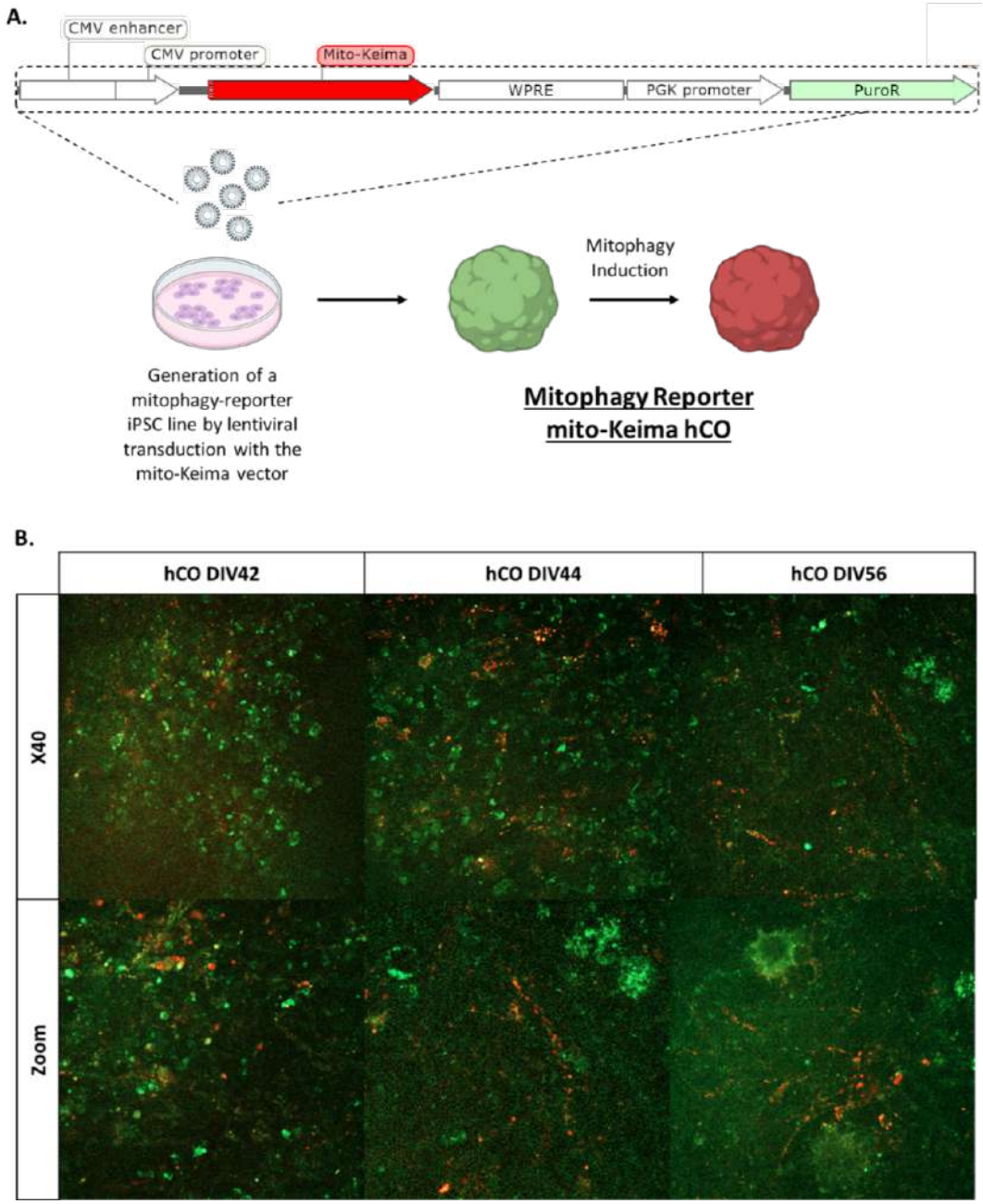

Fig.7. Generation and validation of a mito-Keima mitophagy reporter hiPSC line. *A. Diagram of the lentiviral construct (pLenti-CMV-Mito-Keima-WPRE-PGK-PuroR); B. Experimental outline for generating the mito-Keima hiPSC reporter line; C. Live-cell time-lapse imaging of Mito-Keima (pH-sensitive fluorescence) in hCOs was performed on days in vitro (DIV) 42, 44, and 56. MitoKeima expression indicates mitochondrial pH levels, with the green signal representing neutral mitochondria and the red signal showing acidic mitochondria (commonly found in lysosomes). The top row displays low magnification (×40); the bottom row features zoomed views. Scale bar: 20 µm.*

4.17. PGC-1alpha(p)-EGFP mitochondrial biogenesis reporter hiPSC line

A live-cell reporter system for monitoring mitochondrial biogenesis *in vitro* was developed as previously described (Nilsson et al., 2015). This system utilizes

the promoter sequence of the master regulator of mitochondrial biogenesis, peroxisome proliferator-activated receptor gamma coactivator 1 alpha (*PPARGC1A*), to control the expression of green fluorescent protein (*EGFP*). The level of EGFP expression serves as an indicator of mitochondrial biogenesis activity. The sequence of the human PGC-1α proximal promoter (-500 to +52) was amplified by PCR from the plasmid pPGC1a Proximal Promoter-FLuc2P (Addgene #154259) using primers with flanking ClaI and XbaI restriction sites. The PGC-1α proximal promoter DNA was cloned into the ClaI and XbaI sites of the pLenti CMV-GFP-PGK-Puro (658-5) lentiviral transfer vector (Addgene #17448). Successful cloning was verified using colony PCR and Sanger sequencing. Lentiviral particles were produced as described in Section 4.15. Stable mitochondrial biogenesis reporter hiPSC line. hiPSCs were maintained in Essential 8 media supplemented with penicillin/streptomycin. When cells reached 80-90% confluency, they were passaged using EDTA. Lentiviral particles containing PGC-1α(p)-EGFP reporter were added to the cell suspension in Essential 8 media containing Polybrene (8 µg/mL) and 10 µM ROCK inhibitor (Y-27632), and the cells were plated on vitronectin-coated plates. For positive selection, cells were maintained in media containing 0.5-1 mg/mL puromycin for 5-7 days. Expression of the fluorescent protein was verified using fluorescent microscopy. Stable mitochondrial biogenesis reporter hiPSC lines were cryopreserved at -80^{0}C or processed for further experiments.

hCO PGC-1α(p)-EGFP mitochondrial biogenesis (MB) Assay - At day 56 of differentiation, hCOs were transduced by incubating in fresh differentiation medium containing mito-Keima lentiviral particles and polybrene (10µg/mL) for 48 h. After 48 hours, the medium was replaced with differentiation medium without virus, and the organoids were maintained for an additional 2 weeks to allow robust reporter expression. For live imaging, hCOs were transferred to a glass-bottom 35 mm cell culture imaging dish (Ibidi). Live-cell imaging of the MB assay, where EGFP fluorescence indicates PGC1α activity, was conducted using a spinning-disk confocal microscope with 488 nm excitation (Fig.8).

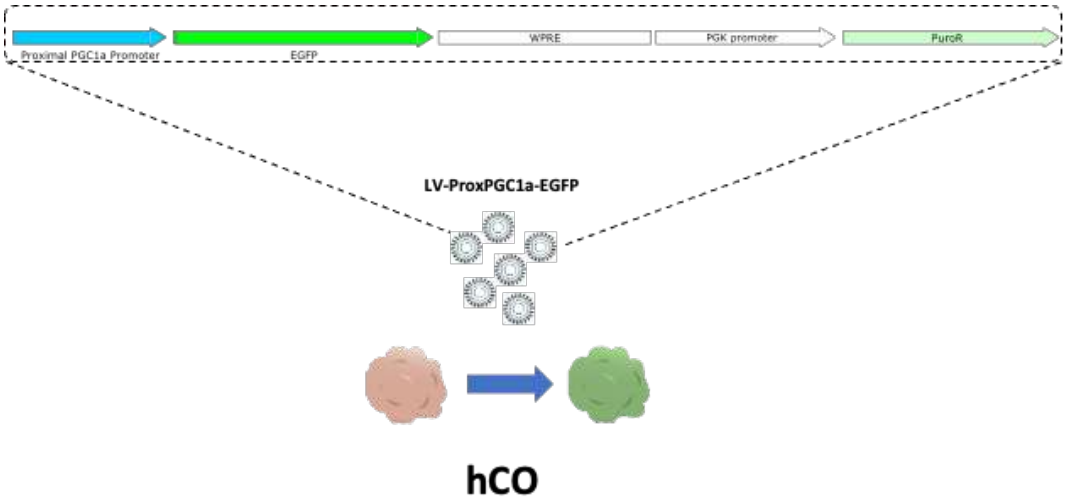

Fig.8. Lentiviral PGC1α-EGFP reporter for tracking mitochondrial biogenesis. *A. Diagram of the pLenti-Proximal-PGC1α-EGFP-WPRE-PGK-PuroR construct. The proximal PGC1α promoter, where EGFP intensity reflects PGC1α transcriptional activity and consequently mitochondrial biogenesis; B. Workflow for generating PGC1α-EGFP reporter hCOs: At DIV 56, organoids are transduced with Proximal-PGC1α-EGFP lentivirus. Live confocal imaging is conducted approximately 10 days later to assess GFP fluorescence as an indicator of mitochondrial biogenesis.*

4.18. Generation of an inducible nuclear FGFR1 hiPSC line via TALEN-mediated knock-in at the CLYBL safe harbor locus

A TALEN-mediated knock-in of FGFR1(SP-/NLS)-mApple into the CLYBL locus of human induced pluripotent stem cells (hiPSCs) was performed as previously described, with slight modifications (Cerbini et al., 2015; Fernandopulle et al., 2018). Transfection Procedure - Human iPSCs were passaged two days before transfection using 50 mM EDTA to achieve ~80–90% confluency within 48 hours. For reverse transfection, Lipofectamine 3000 (Thermo Fisher Scientific) was used according to the manufacturer's protocol. TALEN plasmids (0.75 µg each) and donor plasmid (1.5 µg) were diluted in Opti-MEM medium, mixed with Lipofectamine 3000 reagent, and incubated for 15 minutes to form transfection complexes. During the incubation period, hiPSCs were dissociated with Accutase for 4 minutes to create a single-cell suspension. The transfection complexes were added directly to 2×10^5 hiPSCs resuspended in Essential 8 medium supplemented with 10 µM ROCK inhibitor (Y27632). Cells were plated onto vitronectin-coated 6-well plates and incubated for 24 hours. After incubation, the medium was replaced with fresh Essential 8 medium. Enrichment of mApple+ Cells - To obtain pure mApple+ colonies, cells were first manually picked based on mApple

fluorescence. For further enrichment, hiPSCs were sorted using fluorescence-activated cell sorting (FACS) with mApple as the gating parameter. FACS-sorted cells were seeded onto Geltrex-coated 24-well plates and cultured in Essential 8 medium. Recovered cells were manually picked and expanded for downstream applications.

4.19. Live-cell imaging of mitophagy flux using mito-Keima reporter

Live ratiometric mito-Keima imaging was performed as described previously, with minor modifications. Imaging was conducted in embryoid Bodies (EBs) and human cortical organoids (hCOs) using analogous methods. Images were acquired with a Cell Observer SD (Zeiss) with a CO_2/O_2 incubation chamber, Yokogawa Spinning Disk system, four diode lasers (405 nm, 488 nm, 561 nm, and 635 nm), and an LD Plan-Neofluar 40×/0.6 Korr objective. For live imaging, hEBs and hCOs were cultured on 35 mm cell culture imaging dishes with a coverslip bottom (Ibidi). Mito-Keima was imaged in two channels using sequential excitations at 488 nm (green) and 546 nm (red), with emissions collected in the 600–695 nm range (Kinnart et al., 2024; Yang et al., 2022). Mitophagy calculations were performed using Fiji software on a pixel-by-pixel basis. Prior to thresholding, images from both channels were converted to 8-bit format, followed by background subtraction and application of smoothing functions in Fiji. The total mitochondrial area was determined by segmenting and thresholding the emission area at an excitation wavelength of 458 nm. This area was quantified using the “Analyze Particles” plugin (parameters: “Mean”, “Area Fraction”). Similarly, the total lysosomal area was determined by segmenting and thresholding the emission area at an excitation wavelength of 561 nm and quantified using the same plugin. To accurately segment the high mito-Keima (546/488) ratio area, the "AND" function in the Image Calculator plugin was applied. This operation combined the total mitochondrial area (image 1) and the total lysosomal area (image 2) on a pixel-by-pixel basis, ensuring precise overlap segmentation. The parameter "high mito-Keima (546/488) ratio area/total mitochondrial area" was used as an index of mitophagy. This was quantified using the “Analyze Particles” plugin (parameters: Mean, Area Fraction).

4.20. Live-cell imaging of mitochondrial biogenesis in human cortical organoids

Human cortical organoids (hCOs) were generated as described in Section 4.7.5 and maintained in differentiation medium until day 56 *in vitro* (DIV 56). To visualize mitochondrial biogenesis, organoids were transduced for 48 hours with a third-generation lentivirus encoding the PGC-1α proximal promoter reporter (PGC-1α(p)-EGFP), in the presence of polybrene (10 µg/mL). 48 hours later, the medium containing viral particles was replaced with fresh differentiation media, and organoids were cultured for an additional 10 days to allow reporter expression.

For live imaging, single organoids were transferred to 35 mm glass-bottom dishes containing pre-warmed differentiation medium and placed in a temperature-controlled incubation chamber (37 °C, 5% CO_2) of the Cell Observer SD spinning-disk confocal microscope (Zeiss). The system was equipped with a Yokogawa CSU-X1 scan head, diode lasers at 405, 488, 561, and 635 nm, and LD Plan-Neofluar 20×/0.6 Korr and 40×/0.6 Korr objectives. EGFP was excited at 488 nm, and emission was collected at 500–550 nm with identical detector gain and laser power across all samples. Z-stacks (1 µm interval, total depth 120 µm) were acquired from three non-overlapping fields per organoid; Raw 8-bit Z-stack images were converted into a single-plane image using the Extended Depth-of-Focus (EDF) projection tool in ZEN software. Raw 8-bit image stacks were imported into FIJI (v2.15). A rolling-ball background subtraction (radius = 50 px) and a mild 2-pixel Gaussian blur were applied uniformly. Maximum-intensity projections were generated for quantitative analyses. Regions of interest (ROIs) were manually drawn around the neuronal soma and primary dendritic segments of EGFP-positive cells. Mean fluorescence intensity (MFI) for each ROI was extracted with the "Measure" function and exported to GraphPad Prism 9. Statistics. Three independent organoids per condition served as biological replicates. For each condition, a minimum of 300 ROIs were analysed (Control, $n = 313$; doxycycline-induced PGC-1α overexpression, $n = 297$). Data distribution was non-parametric (Shapiro–Wilk); therefore, two-tailed Mann–Whitney tests were applied. Results are presented as mean ± standard deviation (SD); $p < 0.05$ was considered significant; ns- non-significant.

4.21. Measurement of mitochondrial membrane potential (MMP) in EBs

Mitochondrial membrane potential (MMP) was assessed in embryoid bodies (EBs), using Mitotracker CMXRos, a dye that selectively accumulates in mitochondria with an intact membrane potential. On Day 10, EBs were plated onto Geltrex-coated Ibidi glass-bottom 3.5 cm plates to facilitate cell attachment in Essential 6 media supplemented with either 2 mM doxorubicin (DOX or DMSO as a control. On Day 21, cells were incubated with media containing 50 nM Mitotracker CMXRos for 30 minutes at 37°C and 5% CO_2, followed by a wash with PBS (1x) to remove excess dye. Image acquisition was performed using a Zeiss Axio Observer microscope equipped with a spinning disk confocal system and a controlled CO_2 chamber. A 546 nm laser and 40x magnification were used to capture z-stack images, which were processed to generate extended depth-of-field (EDF) images. MMP was quantified as the mean gray intensity of Mitotracker fluorescence in 8-bit images using FIJI software.

4.22. Measurement of neural rosette and lumen morphology

Morphological analyses were conducted on high-resolution phase-contrast (or immunofluorescence) images of neural rosettes captured at 20× magnification. Image processing and quantification utilized FIJI (ImageJ v1.52p), using calibrated spatial units (µm and µm²). The Rosette area was measured by manually outlining the entire ring of polarized progenitors and applying the Measure → Area function in FIJI (µm²). The lumen area was determined by manually selecting the central region within each rosette—identified by membrane markers (e.g., ZO-1, N-cadherin)—and measuring its area with the same tool (µm²). Basal area (rosette minus lumen area) was determined by subtracting the lumen area from the rosette area, resulting in the net area of neural rosette (µm²). Rosette perimeter and lumen perimeter were each obtained by tracing the boundary of the respective region and using FIJI's *Measure → Perimeter* function. Micrometers (µm) were used as the unit of measurement. APD-normalized area - To address shape irregularity and facilitate size-independent comparisons, the "area per diameter" (APD) normalization for both rosette and lumen was calculated accordingly:

APD-normalized rosette area = $A_{rosette}/(P_{rosette}/2\pi)^2$

APD-normalized lumen area = $A_{lumen}/(P_{lumen}/2\pi)^2$

where A is the measured area (μm²) and P is the corresponding perimeter (μm); **P/2π** represents the equivalent circular "radius," and squaring this term yields a circular area scaling factor. All measurements were performed on at least ten rosettes per biological replicate, and mean ± SD values were calculated for each experimental condition.

4.23. Mitochondrial network analysis

Mitochondrial network connectivity was quantified in human cortical organoid sections using a semi-automated, image-based workflow in FIJI (ImageJ) with the Mitochondria Analyzer plugin, as detailed previously (Chaudhry et al., 2020). Briefly, z-stacks were acquired on a Zeiss Cell Observer SD spinning-disk confocal microscope (Yokogawa module; Plan-Neofluar 63×/1.4 NA oil objective) under controlled CO_2/O_2 conditions and processed into extended-depth-of-focus images for 2D analyses or analyzed in 3D. Preprocessing included background subtraction (radius 1 μm), sigma filtering (radius 0.1 μm, σ = 2.0), local contrast enhancement (block size = 64, slope = 2.0 for 2D), and gamma correction (γ = 0.80 for 2D), followed by adaptive thresholding (block size = 2.25 μm, C = 28) in batch mode. Mitochondrial morphology and network parameters—including total and mean mitochondrial area and perimeter, aspect ratio, form factor, fragmentation index, branch count and length, junction number, branch end points per cell, and mean branch diameter—were extracted on a per-cell basis across cortical plate (n = 53 areas for Control, n = 47 areas for DOX) and ventricular zone regions (n = 35 areas for Control, n = 40 areas for DOX). Statistical comparisons between the control and overexpression groups were performed using two-tailed Mann–Whitney tests on data pooled from three independent experiments (Fig.9). Mitochondrial parameters analyzed in this study are described in Table 7.

Table 7. *Mitochondria parameters used in this study*

Parameter (Units)	Description
Total Area (μm²)	The total area of all mitochondrial objects in a cell, reflecting overall mass.
Total Perimeter (μm)	Total length of mitochondrial boundaries, reflecting membrane complexity.

Mean Perimeter (µm)	Average boundary length for each mitochondrion, indicating typical shape complexity.
Aspect Ratio (unitless)	The ratio of the major to minor axis of each mitochondrion indicates the level of elongation.
Form Factor (unitless)	Measure of circularity ($4\pi \cdot$area / perimeter^2), with lower values indicating elongation.
Mitochondrial Fragmentation Index (µm² per object)	Total mitochondrial area divided by object count, where higher values indicate fragmentation.
Branches (count)	Number of individual branch segments in the mitochondrial network per cell.
Total Branch Length (µm)	Sum of all branch segment lengths, reflecting network extension.
Mean Branch Length (µm)	Average length of branch segments, indicating typical branch extension.
Branch Junctions (count)	number of nodes where two or more branch segments meet, indicate network complexity.
Branch End Points (count)	Number of terminal tips of branches, reflecting network fragmentation.
Mean Branch Diameter (µm)	Average width of branch segments, indicating structural thickness.

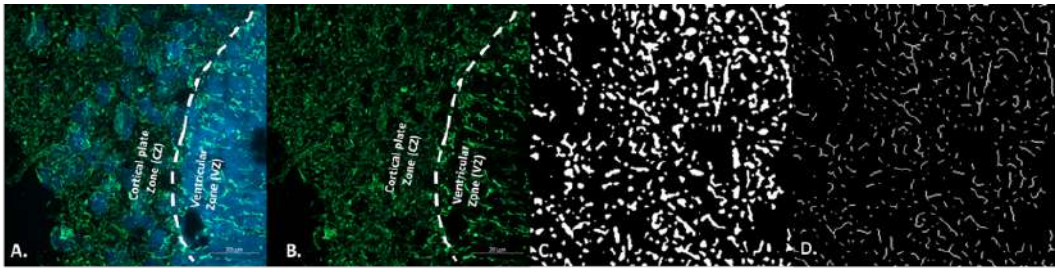

Fig.9. Mitochondrial morphology and network connectivity using the "Mitochondria Analyzer" plugin in human cortical organoids (hCOs). *Representative images of mitochondrial network segmentation and skeletonization in cortical plate (CP) and ventricular zone (VZ) regions of 60-day hCOs; A. confocal image of mitochondria (green) in a section spanning the cortical zone (CZ) and ventricular zone (VZ) in hCO. The dashed line indicates the CP–VZ boundary. Nuclei are counterstained with Hoechst (blue). Scale bar = 20 µm; B. Binary mask after mitochondrial segmentation using the Mitochondria Analyzer plugin using FIJI software; C. Skeletonized mitochondrial network.*

4.24. Fluorescence intensity analysis

Fluorescence intensity in randomly selected regions of interest (ROIs) was analyzed using Fiji (ImageJ). Preprocessing steps included applying a Gaussian blur and performing background subtraction to enhance image quality. The mean gray value was measured using the "Measure" function, and background noise was accounted for by subtracting the mean gray value of the background from the measured values. Analyses were performed on multiple sections of organoids generated from three independent experiments for each condition. Fluorescence

intensity measurements were performed using Fiji software. Images were first converted to an 8-bit format, after which ROIs, approximately 225 square pixels in size, were selected. This approach was used to analyze the fluorescence intensity of cleaved caspase-3 (an apoptosis marker), FGFR1 (reflecting nuclear and mitochondrial accumulation of FGFR1), MAP2, as well as PINK1 and PARKIN (mitophagy markers). Analyses were performed on multiple sections of organoids generated from three independent experiments for each condition. Statistical comparisons between experimental groups were conducted using two-tailed Mann–Whitney tests.

4.25. Immunocytochemistry quantification

Immunocytochemistry quantification was performed on 20 μm-thick cryosections of human cortical organoids (hCOs), following a previously established protocol (Pașca et al., 2019) with minor modifications. I quantified cell densities of markers TBR1, TBR2, NEUN, PAX6, SOX2, KI67, CTIP2, SYNAPSIN-2, MAP2, mitochondrial protein, and LC3B within defined regions of interest (ROIs) of at least 225 μm², positioned around proliferative zones and cortical zone regions. Boundaries between the ventricular zone (VZ), subventricular zone (SVZ), and cortical layer (CZ) were delineated based on expression patterns of PAX6, TBR2, TBR1, and the orientation and density of Hoechst-stained nuclei. Immunostainings were conducted using primary antibodies against KI67 (Abcam), NEUN (Millipore), TBR1 (Abcam), TBR2 (Invitrogen), CTIP2 (Abclonal), SYNAPSIN-1 (Abcam), MAP2 (Invitrogen), TOM20 (Millipore), and LC3B (Cell Signaling Technology). Specifically, I assessed KI67-positive proliferating cells within the apical VZ (n = 37 control and n = 45 DOX areas), NEUN-positive postmitotic neurons (n = 142 control and n = 175 DOX areas), TBR1-positive deep-layer cortical neurons (deep-layer cortical neurons, n = 69 control and n = 76 DOX areas), TBR2-positive intermediate progenitors within the SVZ (n = 62 per condition), and CTIP2-positive layer V/VI projection neurons in the cortical zone (n = 118 control and n = 116 DOX areas). Synaptic density was quantified by analyzing SYNAPSIN-2 puncta colocalizing with MAP2-positive neuronal processes (n = 37 control and n = 33 DOX areas). For mitophagy analysis, mitochondrial marker and lysosomal marker LC3B puncta colocalization were measured to indicate mitophagic events (n = 60 control and n = 61 DOX areas).

Quantifications were performed across at least three independent experiments per condition. Statistical significance was assessed using non-parametric Mann-Whitney tests.

4.26. Plate-based assays in NES cells

4.26.1. Measurement of mitochondrial membrane potential (MMP) in NES Cells

Mitochondrial membrane potential (MMP) was assessed in NES cells labeled with Mitotracker CMXRos, a dye that selectively accumulates in mitochondria with intact membrane potential. NES cells (200 cells/well) were seeded on Geltrex-coated black 96-well plates in NES media with either 2 mM DOX or DMSO as a control. On Day 4, cells were incubated with media containing 50 nM Mitotracker CMXRos for 4 hours at 37°C and 5% CO_2, followed by a wash with PBS (1x) to remove excess dye. Fluorescence was measured using a plate reader (Fluoroskan Ascent FL, Labsystems) with an excitation wavelength of 579 nm and an emission wavelength of 599 nm. Results were normalized to cell number using Hoechst staining as per the manufacturer's protocol and are presented as a percentage ratio of the test sample to the control.

4.26.2. Measurement of reactive oxygen species (ROS) levels

Reactive oxygen species (ROS) levels were quantified in NES cells using DCFH-DA (dichloro-dihydro-fluorescein diacetate), a cell-permeable fluorogenic dye that becomes fluorescent upon oxidation by ROS. NES cells (200 cells/well) were seeded on Geltrex-coated black 96-well plates in NES media with either 2 mM DOX or DMSO as a control. On Day 4, cells were incubated in media containing 1 µM DCFH-DA (Sigma-Aldrich) for 3 hours at 37°C and 5% CO_2, followed by a wash with PBS (1x) to remove excess dye. Fluorescence was measured using a plate reader (Fluoroskan Ascent FL, Labsystems) with an excitation wavelength of 485 nm and an emission wavelength of 538 nm. Results were normalized to cell number using Hoechst staining, according to the manufacturer’s protocol, and results are presented as a percentage ratio of the test sample to the control.

4.26.3. Measurement of ATP levels in NES cells

ATP levels were quantified in NES cells using the CellTiter-Glo® 3D Cell Viability Assay (Promega), which measures luminescence proportional to the amount of ATP present. NES cells (200 cells/well) were seeded on Geltrex-coated white 96-well plates in NES media with either 2 mM DOX or DMSO as a control. On Day 4, the CellTiter-Glo® 3D reagent was prepared according to the manufacturer's instructions and added directly to each well in a 1:1 ratio with the cell culture medium. Cells were incubated at room temperature for 15 minutes on a shaker at 120 RPM to allow cell lysis, followed by a 30-minute incubation in the dark to stabilize the luminescent signal. Luminescence was measured using a plate reader (Fluoroskan Ascent FL, Labsystems). Data was normalized to cell number using Hoechst staining, according to the manufacturer's protocol, and results are presented as a percentage ratio of the test sample to the control.

4.26.4. Measurement of cell viability

Cell viability was assessed in NES cells using the Resazurin assay, a fluorometric method that evaluates metabolic activity as an indicator of cell viability. Resazurin, a non-fluorescent compound, is reduced to the fluorescent product resorufin in metabolically active cells. The method was performed as described previously, with slight modifications (Augustyniak et al., 2019; Pamies et al., 2018). NES cells (200 cells/well) were seeded in NES media on Geltrex-coated black 96-well plates and treated with either 2mM DOX or DMSO as a control. On Day 4, cells were incubated with media containing 100 µg/mL Resazurin for 3 hours at 37°C in a humidified incubator with 5% CO_2. Following incubation, cells were washed with 1x PBS to remove excess dye. Fluorescence was measured using a plate reader (Fluoroskan Ascent FL, Labsystems) with an excitation wavelength of 544 nm and an emission wavelength of 590 nm. Results were normalized to cell number using Hoechst staining, according to the manufacturer's protocol, and are presented as a percentage ratio of the test sample to the control.

4.27. Proteomics (TMT Labeling and LC-MS/MS)

4.27.1. Sample preparation

Samples were extracted using the Sample Preparation by Easy Extraction and digestion protocol. In brief, samples were solubilized in concentrated trifluoroacetic acid (cell pellet/TFA 1:4–1:8 (v/v)) and incubated for 2 – 10 min at room temperature. Next, samples were neutralized with 2 M Tris-base buffer using a 10-fold volume of TFA and further incubated at 95°C for 5 min after adding Tris(2-carboxyethyl) phosphine (final concentration, 10 mM) and 2-chloroacetamide (final concentration, 40 mM). Turbidity measurement determined protein concentration at 360 nm, adjusted to the same concentration using a sample dilution buffer (2 M Tris-Base/TFA 10:1 (v/v)), and then diluted 1:4-1:5 with water. Digestion was carried out overnight at 37°C using trypsin at a protein-to-enzyme ratio of 100:1. Digestion was terminated by the addition of trifluoroacetic acid (TFA) to a final concentration of 1%. The resulting peptides were labeled using an on-column TMT labeling protocol. TMT-labeled samples were compiled into a single TMT sample and concentrated using a SpeedVac concentrator. Peptides in the compiled sample were separated into eight fractions by off-line basic reversed-phase using the Pierce High pH Reversed-Phase Peptide Fractionation Kit (Cat: 84868; Thermo Fisher Scientific).

4.27.2. Liquid chromatography-mass spectrometry measurement

Prior to the liquid chromatography (LC-MS) measurement, the peptide fractions were resuspended in 0.1% TFA and 2% acetonitrile in water. Chromatographic separation was performed on an Easy-Spray Acclaim PepMap column (50 cm length × 75 μm inner diameter; Thermo Fisher Scientific) at 55°C by applying 120 min acetonitrile gradients in 0.1% aqueous formic acid at a flow rate of 300 nl/min. An UltiMate 3000 nano-LC system was coupled to a Q Exactive HF-X mass spectrometer via an easy-spray source (all Thermo Fisher Scientific). The Q Exactive HF-X was operated in TMT mode with survey scans acquired at a resolution of 60,000 at m/z 200. Up to 15 of the most abundant isotope patterns with charges 2-5 from the survey scan were selected with an isolation window of 0.7 m/z and fragmented by higher-energy collision dissociation with normalized collision energies of 32, while the dynamic exclusion was set to 35 s. The maximum

ion injection times for the survey scan and dual MS (MS/MS) scans (acquired with a resolution of 30,000 at m/z 200) were 50 and 130 ms, respectively. The ion target value for MS was set to 3e6 and for MS/MS was set to 1e5, and the minimum AGC target was set to 8e2. Sample preparation and proteomics analysis were conducted in the Proteomics Core Facility of the IMol Polish Academy of Sciences in Warsaw.

4.28. Bioinformatics analysis

4.28.1. Data Preprocessing and differential expression analysis

The data were processed with MaxQuant v. 2.2.0.0, and the peptides were identified from the MS/MS spectra searched against Uniprot Human Reference Proteome (UP000005640, with gene count 20644, downloaded on February 27, 2025) using the build-in Andromeda search engine. Reporter ion MS2-based quantification was applied with reporter mass tolerance = 0.003 Da and min. reporter PIF = 0.75. Cysteine carbamidomethylation was set as a fixed modification and methionine oxidation, and protein N-terminal acetylation were set as variable modifications. For in silico digests of the reference proteome, cleavages of arginine or lysine followed by any amino acid were allowed (trypsin/P), up to two missed cleavages were allowed. The FDR was set to 0.01 for peptides, proteins. Match between runs was enabled. Other parameters were used as pre-set in the software. Reporter intensity corrected values for protein groups were loaded into Perseus v.2.0.6.0. Standard filtering steps were applied to clean up the dataset: reverse (matched to decoy database), only identified by site, and potential contaminant (from a list of commonly occurring contaminants included in MaxQuant) protein groups were removed. Protein groups were further filtered to include only those with a minimum of one unique peptide. Reporter intensity corrected values were log2 transformed. Protein groups with at least one valid values at least one group were kept. From one to six missing values in each sample were imputed from a normal distribution. The values were normalized by median subtraction within TMT channels. To explore global variation between Control and DOX-treated samples, Principal Component Analysis (PCA) was performed on proteomics data. PCA was performed on the normalized dataset, and the first two principal components (PC1 and PC2) were selected to visualize major sources of variation. To determine proteins differentially regulated, Student’s t-test (two-sided,

permutation-based FDR = 0.05, S0 = 0.1, n = 3) was performed. The table was exported from Perseus and formatted to its final form in Microsoft Excel 2016.

4.28.2. Weighted gene co-expression network analysis (WGCNA)

Weighted Gene Co-expression Network Analysis (WGCNA) was conducted in R (v4.4.2) using the WGCNA, openxlsx, and ggplot2 packages (Ghafouri-Fard et al., 2023; Short et al., 2023; Wang et al., 2023). Proteomics intensity data from 60-day human cortical organoids treated with 3 mM doxycycline (nFGFR1 induction) or DMSO control (n = 3 per group) were imported from Excel and pre-processed by removing proteins with > 50 % missing values and imputing remaining gaps via row means. Low-variance proteins (bottom 20 %) were filtered out, retaining the top 80 % most variable features. The cleaned matrix was transposed so that samples were rows and proteins columns, then checked for good samples and genes using WGCNA's goodSamplesGenes function. A soft-thresholding power β was selected based on scale-free topology criteria ($R^2 > 0.9$) via pickSoftThreshold, and an adjacency matrix was computed and converted into a Topological Overlap Matrix (TOM). Hierarchical clustering of 1 – TOM identified co-expression modules using dynamic tree cutting, with a module eigengene dissimilarity cutoff of 0.25. Module–trait relationships were assessed by correlating module eigengenes with the binary doxycycline versus control trait, with significance determined by Student's t-test. Finally, network dendrograms, module color plots, and module–trait heatmaps were visualized with ggplot2, and module assignments and hub protein lists were exported for downstream interpretation.

4.28.3. Volcano Plot

Proteomics data from cortical organoids treated with 3 mM doxycycline or DMSO control were visualized as a volcano plot in R (v4.4.2) using the tidyverse package for data manipulation, openxlsx for Excel import, ggplot2 for plotting, and ggrepel for non-overlapping labels. First, protein $\log_2$ (fold changes) and $-\log_{10}$ (p-values) from paired t-tests comparing DOX versus control were read in and annotated against certain categories, such as the "MitoCarta3.0" proteins list, to classify each protein as "Mito" or "NonMito". Proteins meeting thresholds of $\log_2 FC \geq 0.2$ and $-\log_{10} p \geq 1.3$ were labeled as up- or downregulated. Proteins that

did not meet these criteria were marked “Other”. The top ten most significantly up- and downregulated mitochondrial proteins were selected for labeling. Vertical and horizontal cutoff lines (±0.2 log_2FC, $p = 0.05$) and text annotations were added in ggplot2, points were colored by regulation class, and the top 20 proteins were annotated with geom_text_repel. The final plot clearly highlights global expression changes and mitochondrial-specific regulation in response to nFGFR1 induction.

4.28.4. Heatmap (hierarchical clustering)

Hierarchical clustering and heatmap visualization of differentially expressed proteins were performed in R (v4.4.2) using the openxlsx package to import quantitative proteomics data and lists of differentially expressed and top 20 proteins, dplyr and reshape2 for data wrangling, pheatmap for heatmap generation, ggplot2 and ggrepel for custom X-axis labeling, and cowplot for aligning the heatmap with its labels. After filtering for proteins present in the DEP list, removing those with >50% missing values, and imputing remaining gaps by row means, expression values for control (C1–C3) and nFGFR1-induced (NLS1–NLS3) samples were log_2-transformed and row-scaled. Pairwise Euclidean distances among proteins and among conditions were computed, and hierarchical clustering was performed with the Ward D2 linkage method. The scaled matrix was reordered according to the resulting dendrograms, and pheatmap was used to render the heatmap (rows and columns clustered, no overlapping X-axis labels). A separate ggplot2 panel with ggrepel labels for the top 20 DEP proteins was generated and aligned beneath the heatmap via cowplot.

4.28.5. Gene ontology (GO) enrichment analysis

Gene Ontology (GO) enrichment analysis was performed in R (v4.4.2) using the tidyverse package for data manipulation, openxlsx for Excel import, clusterProfiler for enrichment testing, and org.Hs.eg.db for human gene annotation; ggplot2 and ggrepel were employed for visualization. Briefly, proteins significantly upregulated (log_2FC ≥ 0.2, $P \leq 0.05$) and downregulated (log_2FC ≤ –0.2, $P \leq 0.05$) in doxycycline-treated versus DMSO control organoids were separated into two gene lists. UniProt identifiers for each list were converted to Entrez Gene, and GO enrichment was conducted for Biological Process (BP), Cellular Component (CC), and Molecular Function (MF) ontologies using enrichGO with Benjamini–

Hochberg correction (pAdjustMethod = “BH”, pvalueCutoff = 0.05, qvalueCutoff = 0.05). Enriched terms ($P \leq 0.05$) were exported for further analysis and plotted as faceted bar charts of the top ten terms per ontology, with term counts colored by $-\log_{10}$(p-value).

4.29. Statistical analysis

Data are presented as means ± standard deviations. Experiments were conducted with 3–5 independent experiments, with a minimum of three replicates. Normality of the data was evaluated using the Shapiro–Wilk and Kolmogorov–Smirnov tests. Statistical analyses were performed using GraphPad Prism 9. Statistical significance was determined through Mann–Whitney U tests, one-way ANOVA, with appropriate post-hoc corrections. Significance is denoted as: $*P \leq 0.05$; $**P \leq 0.01$; $***P \leq 0.001$; $****P \leq 0.0001$.

5. Results

5.1. Engineering a TET-On hiPSC line for controlled nuclear FGFR1 expression via CLYBL safe harbor targeting

To establish a platform for inducible nuclear FGFR1 expression, I engineered a human induced pluripotent stem cell (hiPSC) line via TALEN-mediated gene editing targeting the CLYBL safe harbor locus on chromosome 13. CLYBL locus was selected due to its strong transgene expression across both pluripotent and differentiated cell states as well minimal epigenetic silencing (Liu et al., 2009). Previous study showed that CLYBL-targeting TALENs, constructed using the pZT backbone, achieved approximately 25% NHEJ-mediated gene editing efficiency in human HEK293T cells (Cerbini et al., 2015).

The recombinant transgene, FGFR1(SP-/NLS), was designed to localize FGFR1 exclusively to the nucleus by removing the endogenous signal peptide (SP-) to prevent translocation to the membrane, and by adding a C-terminal nuclear localization signal (NLS) to ensure constitutive nuclear accumulation and function as a transcriptional regulator rather than as a membrane-bound receptor. This configuration mimics the function of the nuclear variant of FGFR1, which has been previously shown to regulate chromatin architecture and gene expression in neuronal development (Decker et al., 2021; Terranova et al., 2015).

I designed a donor construct, CLYBL-Tet3G-FGFR1(SP-/NLS)-BSD-NLS-mApple, to include three core elements: (1) a doxycycline-inducible FGFR1(SP-/NLS) transgene driven by a TRE3G promoter; (2) a floxed Blasticidin resistance and nuclear mApple (BSD-NLS-mApple) selection cassette under the EF1α promoter; and (3) a reverse tetracycline-controlled transactivator (rtTA, Tet3G) under the constitutive CAG promoter (Fig.10A). Successful generation of this construct was verified by Sanger sequencing prior to cell transfection (Fig.10B). The knock-in procedure was performed via Lipofectamine 3000-based transfection of TALEN plasmids and the donor construct into hiPSCs at approximately 80–90%. Following transfection, cells underwent selection with G418 and FACS sorting to isolate mApple-positive clones, which were manually picked and expanded. PCR analysis confirmed the successful integration of the construct at the CLYBL locus (Fig.10D), and fluorescence microscopy validated nuclear mApple expression in edited hiPSCs (Fig.10E).

The resulting hiPSC$^{Tet3G\text{-}FGFR1(SP\text{-}/NLS)\text{-}BSD\text{-}NLS\text{-}mApple}$ line maintained classic pluripotent stem cell morphology and expressed pluripotency markers, including OCT4, NANOG, SSEA4, and SOX2, as confirmed by immunofluorescence (Fig.11-12). The pluripotency was validated through embryoid body (EB) formation assays, which demonstrated successful differentiation into all three germ layers. Significantly, FGFR1 overexpression was inducible and functional across various differentiated states. After doxycycline treatment, I observed robust nuclear FGFR1 protein expression in neuroepithelial stem cells (NES), embryoid bodies (EB), and human cortical organoids (hCO). It was confirmed by immunofluorescence, which showed increased fluorescence intensity of FGFR1 and qPCR analysis revealing FGFR1 gene expression (Fig.16). This supports the utility of the engineered hiPSC line as a versatile tool for studying the effects of nuclear FGFR1 in the early and advanced stages of human neural development.

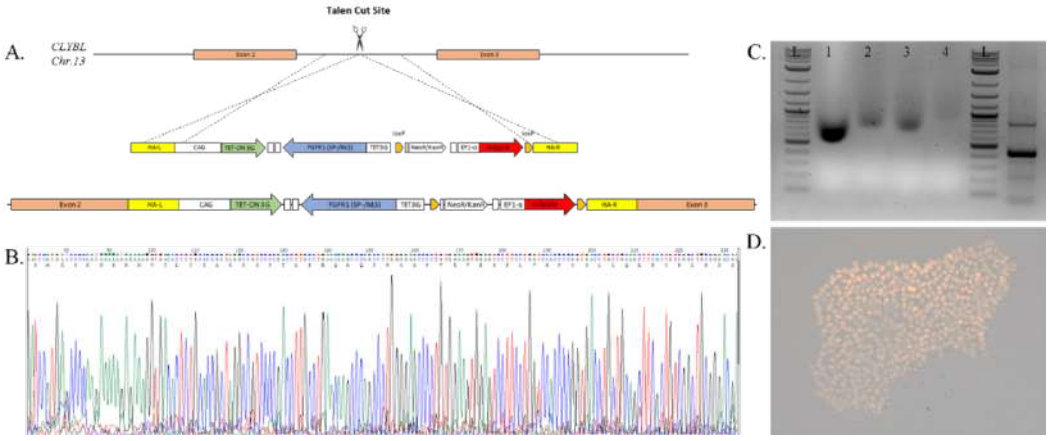

Fig.10. Establishment of a human iPSC line with doxycycline-inducible FGFR1 (SP-/NLS) integrated into the CLYBL safe harbor locus. *A. Schematic illustration of the targeting vector CLYBL-Tet3G-FGFR1(SP-/NLS)-BSD-NLS-mApple; B. Sanger sequencing confirms the targeting construct; C. PCR electrophoresis verifies the successful genomic insertion at the CLYBL locus in safe-harbor targeted iPSC clones (L- 1kb plus ladder; 1-2: WT bands; 3-4:- mApple band); D. Representative fluorescent images of EIFa-driven mApple expression in CLYBL targeted iPSC clone. Scale bar = 20 µm.*

5.2. Pluripotency and differentiation potential of the engineered hiPSC Line

To evaluate the pluripotency and differentiation capacity of the engineered hiPSC line, I conducted embryoid body (EB) assays, followed by immunofluorescence and RT-qPCR analyses on day 21 of differentiation. The immunofluorescence confirmed the expression of lineage-specific markers from the

three germ layers: NES and SOX2 for ectoderm, α-SMA for mesoderm, and FOXA2 for endoderm (Fig.13). The findings were further verified through quantitative RT-PCR analysis. Markers for ectoderm (*NES*, *PAX6*), mesoderm (*TBXT*, *CXCR4*), and endoderm (*SOX17*, *CXCR4*) were significantly upregulated in EBs compared to undifferentiated hiPSCs ($P \leq 0.05$, Mann–Whitney). Notably, *SOX17* and *PAX6* demonstrated particularly strong induction, indicating robust commitment to endodermal and ectodermal lineages. Moreover, the increased expression of mesodermal markers, such as *TBXT,* confirmed mesodermal differentiation. These results demonstrate that the genetic modification, including the integration of an expression cassette containing FGFR1(SP-/NLS) into the CLYBL safe harbor locus of the hiPSC cell line, does not impair the tri-lineage differentiation potential of the hiPSC line and may slightly favor endodermal and ectodermal fates.

To further investigate the functional impact of nuclear FGFR1 (nFGFR1) upregulation. Next, EBs were treated with doxycycline (DOX) or vehicle control on day 11 and cultured until day 21 (Fig.14). Among all markers evaluated, only *PAX6* - an ectodermal marker - was significantly upregulated following nFGFR1 induction ($P \leq 0.0001$), indicating enhanced neural lineage specification. Expression changes of other lineage-associated markers (e.g., *NES* for ectoderm; *TBXT* and *ACTA2* for mesoderm; *SOX17*, *FOXA2*, and *CXCR4* for endoderm) were not statistically significant ($P > 0.05$).

These results suggest that while increased expression of nFGFR1 does not impair differentiation potential, it may subtly bias hiPSC differentiation toward the ectodermal lineage, particularly the neural ectoderm, as indicated by the selective upregulation of *PAX6*. Thus, nFGFR1 may influence lineage commitment dynamics without disrupting overall pluripotency.

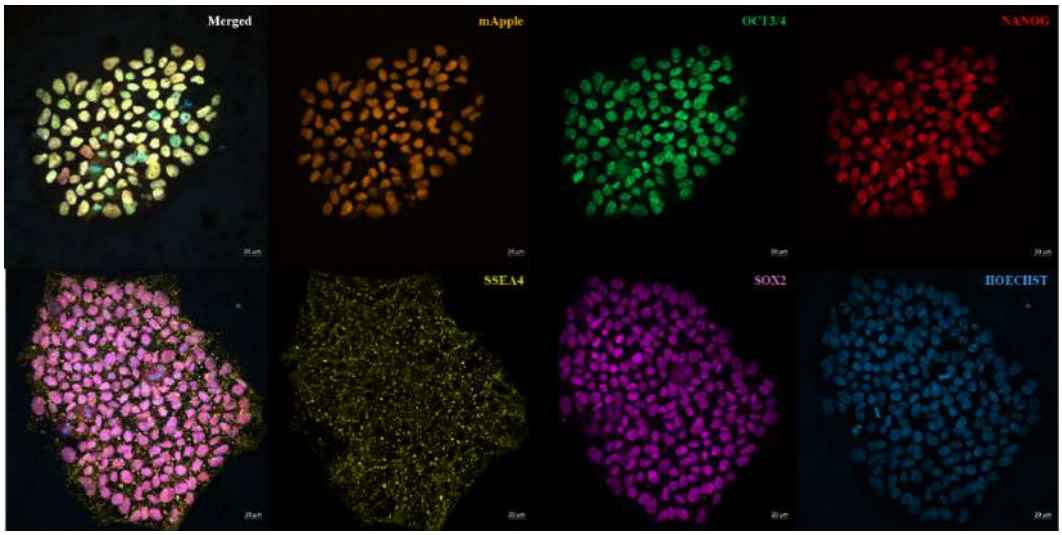

Fig.11. Key pluripotency markers are expressed in the hiPSC$^{Tet3G\text{-}FGFR1(SP\text{-}/NLS)}$ line. *Representative immunofluorescence images demonstrate consistent expression of the mApple selection marker, along with pluripotency markers OCT3/4, NANOG, SSEA-4, and SOX2 in the established CLYBL-FGFR1(SP-/NLS-mApple) hiPSC line. Nuclei were visualized using Hoechst staining. Scale bar = 20 µm.*

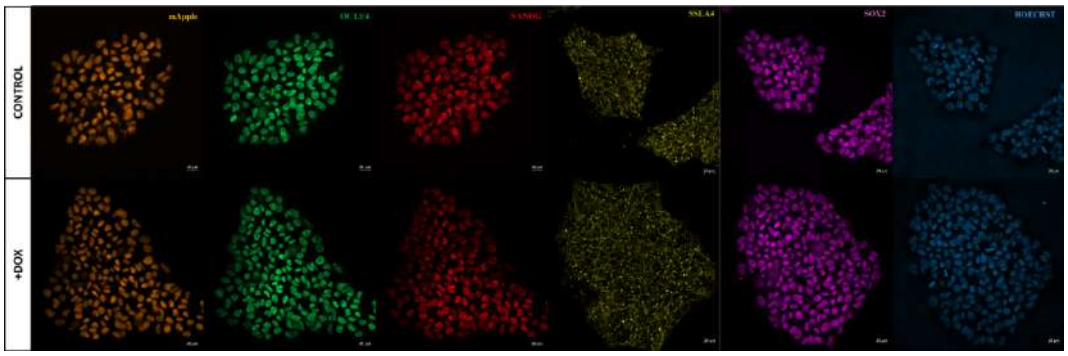

Fig.12. ***Expression of core pluripotency markers following conditional upregulation of nFGFR1 in the hiPSC$^{Tet3G\text{-}FGFR1(SP\text{-}/NLS)}$ line****. Representative immunofluorescence images comparing control and doxycycline-induced (DOX) conditions in the CLYBL-FGFR1(SP-/NLS-mApple) hiPSC line. Images show the expression of the mApple selection marker, as well as pluripotency markers OCT3/4, NANOG, SSEA-4, and SOX2. Nuclei were visualized using Hoechst staining. Scale bars = 20 µm.*

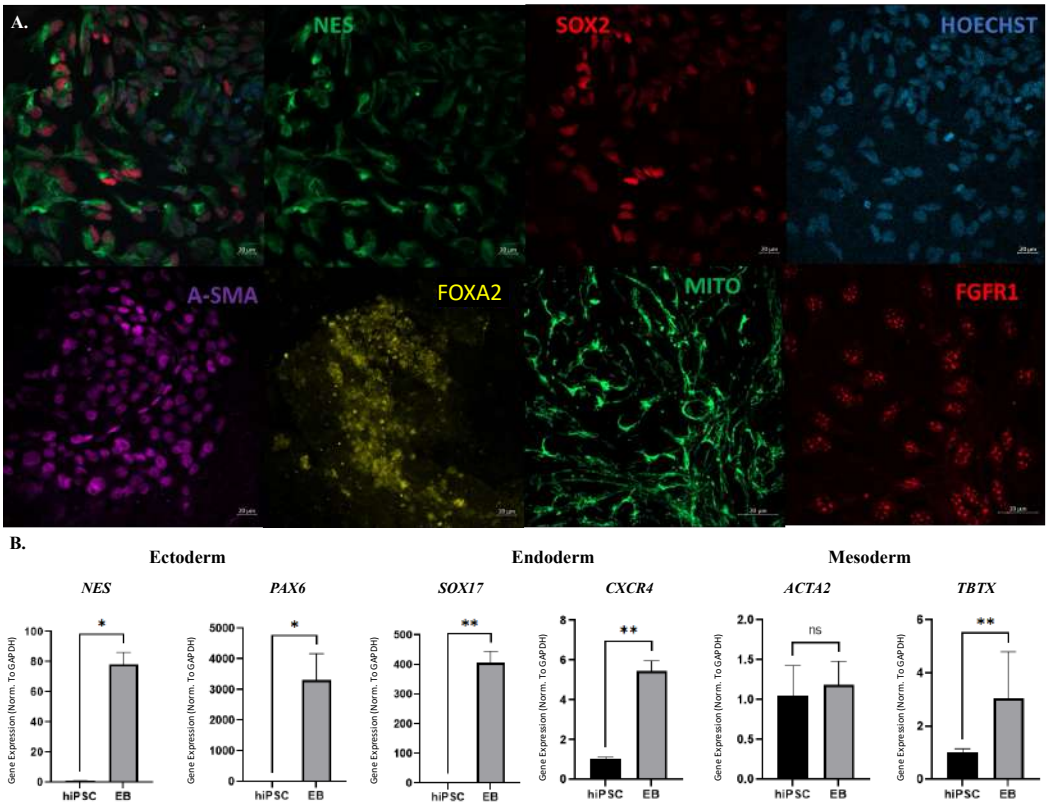

Fig.13. Spontaneous differentiation of embryoid bodies derived from hiPSC$^{Tet3G\text{-}FGFR1(SP-/NLS)}$ line into the three germ layers: ectoderm, mesoderm, and endoderm. *A. Immunofluorescence characterization of embryoid bodies (EBs) demonstrating lineage-specific markers: NES and SOX2 for ectoderm, α-SMA for mesoderm, and FOXA2 for endoderm. Cells also expressed a mitochondrial marker and FGFR1. Nuclei were visualized using Hoechst staining. Scale bar = 20 µm; B. RT-qPCR analysis showing relative gene expression levels of ectodermal (NES, PAX6), mesodermal (ACTA2, TBXT, CXCR4), and endodermal (CXCR4, SOX17) markers in differentiated EBs compared to undifferentiated hiPSCs. Data are presented as fold-change (2^-ΔΔCT) normalized to hiPSCs; mean ± SD (N = 3 independent replicates). Statistical significance determined using two-tailed Mann-Whitney test; *P ≤ 0.05, **P ≤ 0.01, ns—not significant.*

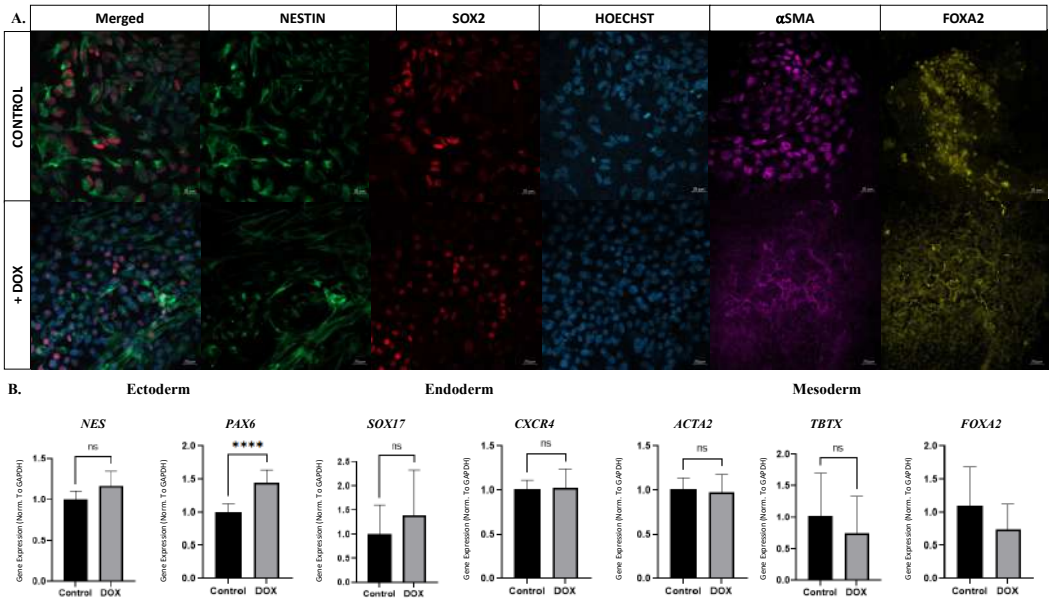

Fig.14. Evaluation of trilineage differentiation potential in embryoid bodies (EBs) derived from a stable hiPSC$^{Tet3G\text{-}FGFR1(SP\text{-}/NLS)}$ line following doxycycline treatment. *A. Immunofluorescence analysis shows the expression of lineage-specific markers in Control and doxycycline-upregulated nFGFR1(DOX) EBs: Nestin and SOX2 (ectoderm), α-SMA (mesoderm), and FOXA2 (endoderm). The nuclei were counterstained with Hoechst. Scale bars = 20 µm; B. RT-qPCR analysis reveals the relative expression levels of lineage markers NES, PAX6 (ectoderm), ACTA2, TBXT, CXCR4 (mesoderm), and FOXA2, CXCR4, SOX17 (endoderm) in Control and DOX-treated EBs. The data is presented as fold-change (2^-ΔΔCT) normalized to controls, with mean ± SD (N = 3 independent experiments). A two-tailed Mann-Whitney test was used to determine statistical significance; ****P ≤ 0.0001, ns—not significant.*

5.3. Differentiation into neuroepithelial stem (NES) cells

To determine whether the stable integration of the FGFR1(SP-/NLS)-mApple transgene into the CLYBL safe harbor locus impacts neural differentiation potential, I differentiated the engineered hiPSCs into neuroepithelial stem (NES) cells using the small molecule-based protocol adapted from Calvo-Garrido et al. (2021). Briefly, neural induction was initiated by sequential exposure to dorsomorphin, SB431542, and CHIR99021 in defined media transitions (KOSR to N2B27) over 16 days, followed by expansion in NES growth medium supplemented with EGF and bFGF (Calvo-Garrido et al., 2021). At the end of the differentiation protocol, immunofluorescence staining revealed strong expression of NES cell markers NES (Nestin) and SOX2, confirming successful induction of a neuroepithelial phenotype. Nuclear expression of mApple confirmed robust expression of the integrated transgene at the CLYBL locus. Additionally, FGFR1 protein was detected, validating the presence and potential functional contribution of the nuclear-targeted FGFR1. Robust expression of mitochondrial surface protein further demonstrated the structural and metabolic integrity of the NES cell population (Fig.15A). To evaluate the transcriptional changes associated with neural induction, I performed RT-qPCR analysis on NES cells and undifferentiated hiPSCs. The expression of two hallmark neuroectodermal markers, *NES* (Nestin) and *PAX6*, were significantly upregulated in NES cells compared to the undifferentiated hiPSCs ($P \leq 0.05$, Mann–Whitney test; Fig.15B).

These results demonstrate that integration of the FGFR1(SP-/NLS)-mApple construct into the CLYBL locus does not impair the ability of hiPSCs to undergo neural differentiation. In contrast, the significant upregulation of *NES* and *PAX6* gene expression, along with strong protein-level marker expression, suggests that the engineered line retains full neuroectodermal differentiation potential. The data

further support the suitability of the CLYBL locus for safe and stable expression of functional transgenes in lineage-specific differentiation settings.

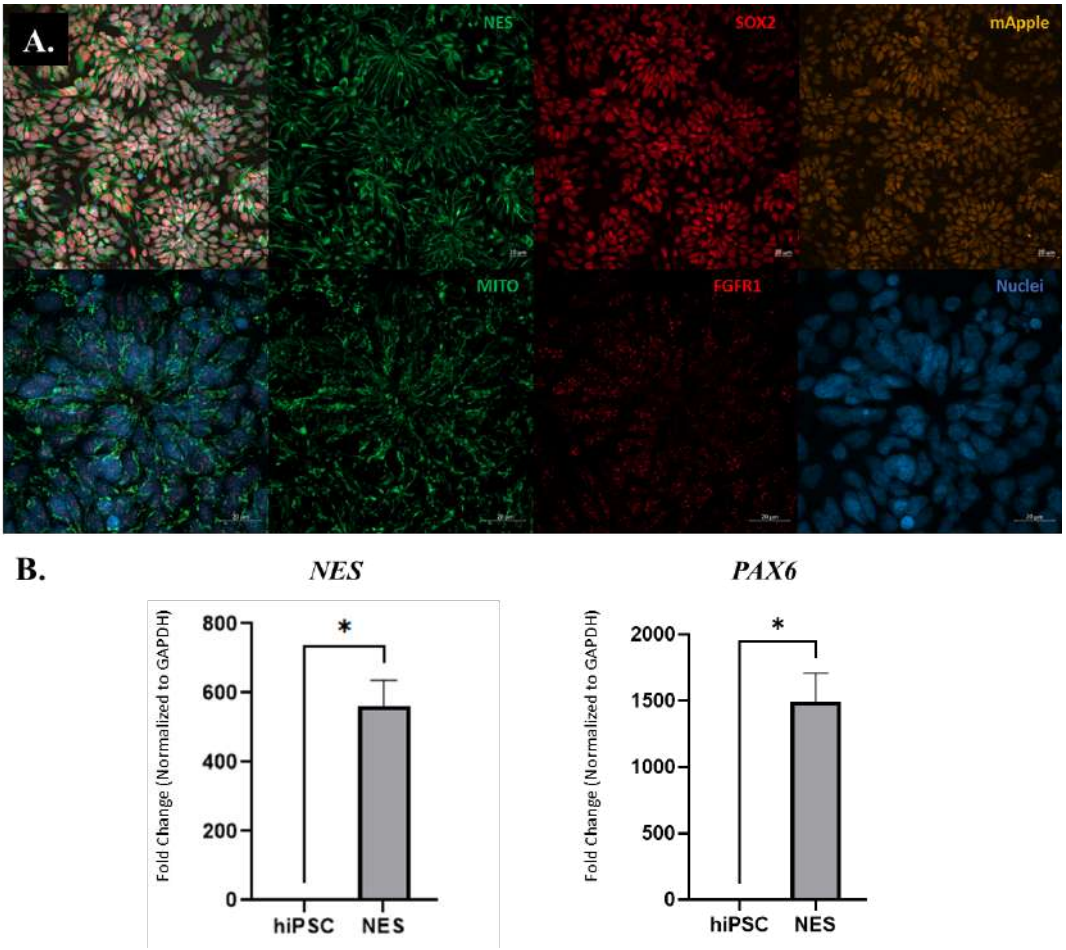

Fig.15. Induction of a stable hiPSC$^{Tet3G\text{-}FGFR1(SP\text{-}/NLS)}$ line into neuroepithelial stem (NES) cells. *A. Immunofluorescence characterization confirms successful differentiation into NES cells, demonstrated by the expression of neural stem cell (NSC) markers Nestin (NES), SOX2, FGFR1, mitochondria (MITO), and the selection marker mApple. Nuclei are stained with Hoechst. Scale bars = 20 µm. B. RT-qPCR analysis compares NSC-specific marker expression (NES, PAX6) in differentiated NES cells and undifferentiated hiPSCs. Data are shown as fold change (2^-ΔΔCT), normalized to hiPSCs, and presented as mean ± SD (N = 3 independent replicates). Statistical analysis is performed using the two-tailed Mann-Whitney test; *P ≤ 0.05.*

5.4. Doxycycline-inducible nFGFR1 expression confirmed in multiple cell types

To validate the functionality of the engineered doxycycline-inducible nuclear FGFR1 (nFGFR1) system, I examined its expression across three stem cell-derived differentiation platforms: embryoid bodies (EBs), neuroepithelial-like stem (NES) cells, and human cortical organoids (hCOs). The inducible nFGFR1 cassette was targeted to the CLYBL safe harbor locus using TALEN-mediated homologous

recombination. Nuclear FGFR1 expression was activated by the addition of doxycycline (2-3 mM) to the media in three *in vitro* cultures derived from an engineered hiPSC$^{Tet3G\text{-}FGFR1(SP\text{-}/NLS)}$ line: embryoid bodies (EBs), neuroepithelial stem (NES) cells, and human cortical organoids (hCO).

I generated NES cells following the method outlined by Calvo-Garrido et al. (2021), with some modifications. The NES cells were cultured on plates coated with Geltrex in NES growth medium supplemented with EGF (10 ng/mL) and bFGF (10 ng/mL). To stimulate nFGFR1 expression, the cells were passaged gently at a 1:2 ratio using 50 mM EDTA, and 2 mM DOX (with DMSO as a control) was incorporated into the fresh medium, with the media refreshed daily. On the fifth day, the NES cells were harvested for further assays. Embryoid bodies were generated using the method described in Latoszek et al. (2022), with some modifications (Latoszek et al., 2022). On day 10, EBs were placed on Geltrex-coated slides to promote attachment and cell migration. To induce nFGFR1, 2 mM doxycycline was added on day 11 (or DMSO as a control), and the media was changed daily. EBs were harvested on day 21 for further analyses. I generated human cortical organoids (hCOs) from hiPSCs using a modified protocol from the Sergiu Pasca lab. In brief, colonies were dissociated at 70–80% confluency into single cells, resulting in the formation of uniform embryoid bodies. Neural differentiation was induced by culturing the spheroids in suspension with SMAD inhibitors. Starting on day 8, the medium was replaced with differentiation medium containing EGF and bFGF for 20 days, followed by the introduction of laminal specification factors BDNF and NT3 for the next 18 days. After day 45, hCOs were maintained in media that lacked growth factors. For doxycycline induction, 3 mM DOX (or DMSO as a control) was added into the differentiation medium. The medium with DOX was changed daily until day 25, and then every other day until hCO collection. Due to preliminary dose–response experiments (data not shown) and the limited drug penetration caused by the size of the hCOs, the doxycycline concentration was increased from from 2 mM to 3 mM and harvested the hCOs at day 60 (for RNA, IHC, and proteomics, mitoKeima), and day 72 (PGC1α-EGFP).

To assess if nFGFR1 is successfully upregulated in different *in vitro* models, I evaluated FGFR1 expression following doxycycline treatment via immunofluorescence analysis (Fig.16A). A significant increase in nuclear FGFR1 intensity was observed in EBs ($P \leq 0.0001$) and in hCOs ($P = 0.0044$), confirming

that the effective induction of FGFR1 occurred in various developmental platforms at protein level. (Fig.16C). Additional RT-qPCR analysis showed that FGFR1 expression in EBs rose 12-fold ($P \leq 0.0001$) and increased nearly 6-fold ($P \leq 0.0001$) in hCOs. I also observed a rising trend in FGFR1 expression in NES and hiPSC cells following the addition of doxycycline, although this was not subjected to statistical analysis (Fig.16B). These results confirm transcriptional activation of the FGFR1 transgene across pluripotent and neural cell types.

A schematic overview of my experimental timelines and downstream assays for each platform is provided in Fig.17. These include a range of functional assessments. In EBs, lineage specification was evaluated by RT-qPCR and immunofluorescence for ectoderm, mesoderm, and endoderm markers, alongside mitochondrial membrane potential (Mitotracker CMXROS), mitophagy flux (mitoKeima), and LC3B+ autophagosome recruitment. In NES cells, assays included gene expression analysis (*FGFR1*, *NES*, *PAX6*), mitochondrial DNA copy number (qPCR: *MT-ND1/HBB*, *MT-ND2/SERPINA*), mitochondrial membrane potential (Mitotracker), ATP production (CellTiter), ROS levels (DCFDHA), cell viability (Resazurin), and cell count (DAPI). In hCOs, effects of nFGFR1 were assessed using RT-qPCR for neural, metabolic, and mitochondrial genes; immunofluorescence was used to access cortical, apoptotic, and mitochondrial proteins; live imaging for mitophagy (mitoKeima) and mitochondrial biogenesis (PGC1α-EGFP); morphometric analysis of neural rosettes and lumens; and global proteomic profiling using TMT-based quantitative mass spectrometry. These assays provided a comprehensive, platform-specific evaluation of nFGFR1's role in cell fate, metabolism, and mitochondrial regulation.

Together, my findings confirm that the doxycycline-inducible FGFR1 expression system enables precise, robust, and reproducible control of nFGFR1 expression across different human stem cell-derived *in vitro* platforms. This system thus provides a powerful tool for dissecting FGFR1-dependent mechanisms in early human development and neural maturation.

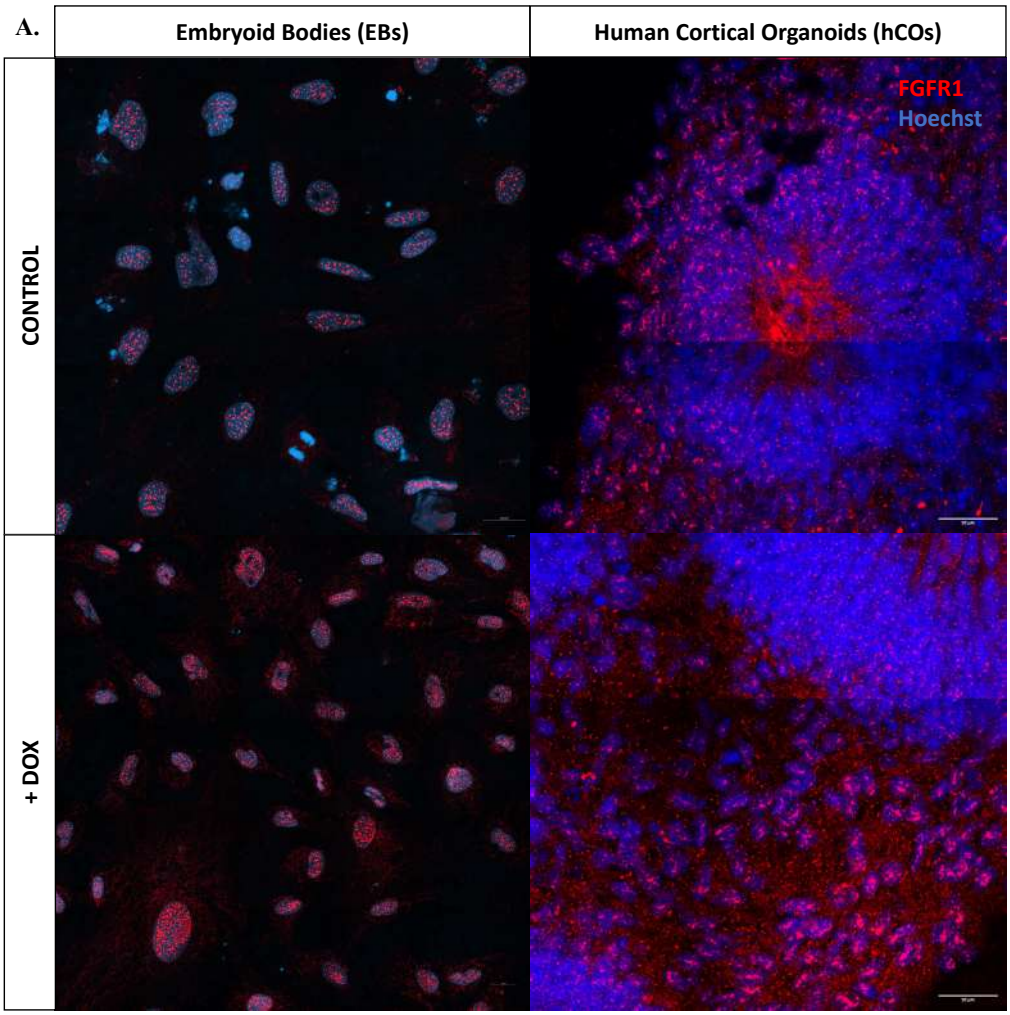

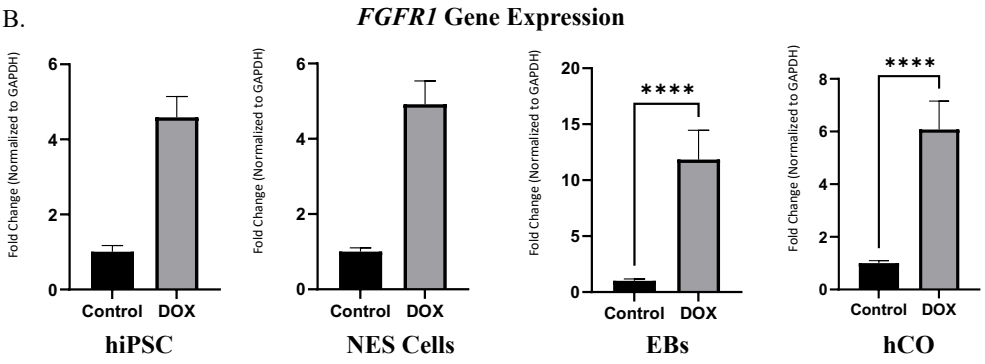

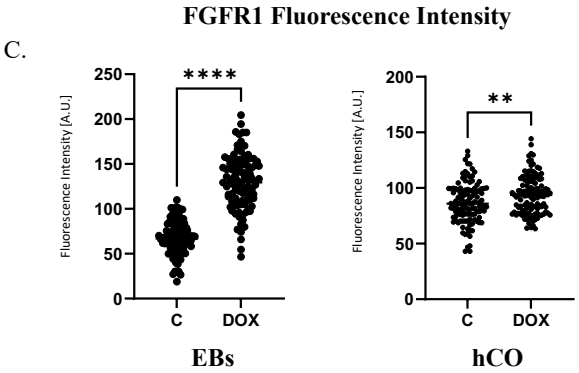

Fig.16. Evaluation of conditional nFGFR1 upregulation following doxycycline treatment across different in-vitro platforms derived from the stable hiPSC$^{Tet3G\text{-}FGFR1(SP-/NLS)}$ line*. A. Immunofluorescence staining reveals FGFR1 protein localization in embryoid bodies (EBs) and human cortical organoids (hCOs) under both control and doxycycline (DOX) treated conditions. Nuclei are stained with Hoechst. Scale bars = 20 µm; B. RT-qPCR analysis of FGFR1 gene expression was conducted on hiPSCs, EBs, NES cells, and hCOs (Control vs DOX). Data is shown as fold-change (2^-ΔΔCT) normalized to controls, reported as mean ± SD (N ≥ 3 independent replicates). Statistical significance was assessed using the two-tailed Mann-Whitney test; ****P ≤ 0.0001, ns—not significant; C. Quantitative analysis of fluorescence intensity of FGFR1 within Hoechst-stained nuclei in EBs and hCOs under both control and DOX conditions. The average fluorescence intensity was calculated from three independent experiments (EB: n = 100 areas/group; hCO: n = 120 areas/group). Statistical significance was evaluated using the Mann-Whitney test (EB: P ≤ 0.0001; hCO: P = 0.0044).*

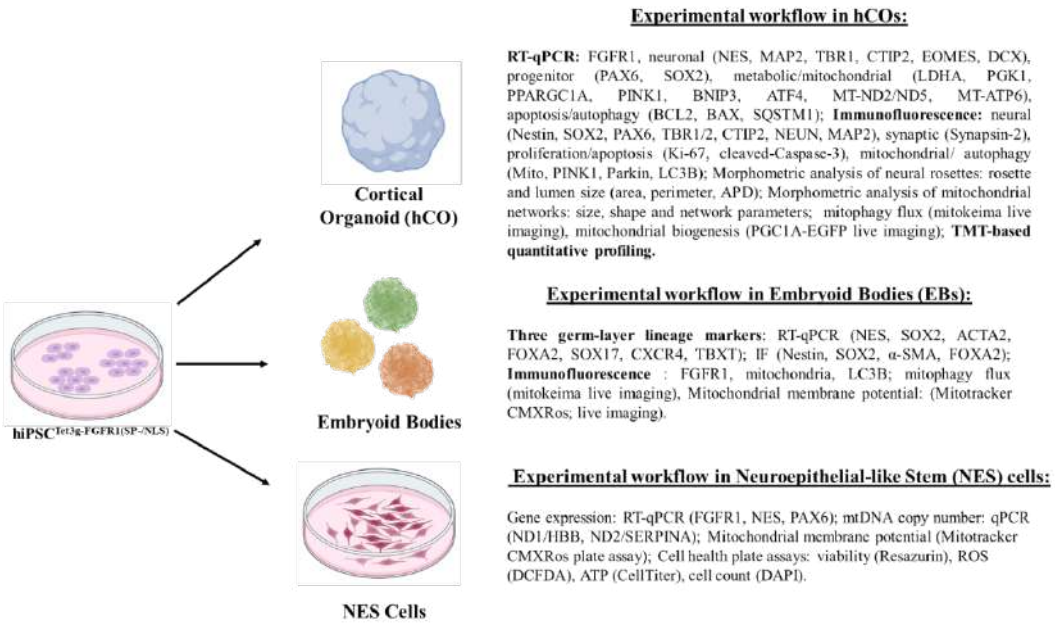

Fig.17. Outline experimental procedures for nFGFR1 induction and subsequent analysis using three hiPSC-derived platforms. *A schematic overview illustrates the differentiation of the engineered hiPSC line into (i) embryoid bodies (EBs), (ii) neuroepithelial stem (NES) cells, and (iii) human cortical organoids (hCOs). Doxycycline was administered in each in vitro model to induce nFGFR1 expression, with samples collected at specific time points for RNA, proteomic, and imaging assays.*

5.5. Establishment of human Cortical Organoids to study nFGFR1-mediated neurogenesis

To investigate the role of nuclear FGFR1 (nFGFR1) in neural progenitor proliferation and differentiation during early human corticogenesis, I employed a three-dimensional human cortical organoid (hCO) model. Cortical organoids derived from human induced pluripotent stem cells (hiPSCs) provide a robust and physiologically relevant *in vitro* platform that recapitulates the spatial, temporal, and cellular features of the developing human cortex (Lancaster et al., 2013; Stachowiak et al., 2017).

I generated hCOs using established protocols (Pașca et al., 2019; Sloan et al., 2018). hiPSCs were maintained in feeder-free conditions in stem cell medium until they reached 70–80% confluency. Embryoid bodies (EBs) were formed by enzymatic dissociation using Accutase and then seeded into AggreWell™ 800 plates to ensure uniform size and structure. After 48 hours, EBs were transferred to low-attachment plates and cultured in induction medium supplemented with the SMAD pathway inhibitors dorsomorphin and SB-431542 to induce neural fate through dual inhibition of BMP and TGF-β signaling. By day 6, the resulting neurospheres were cultured in neurogenic medium containing EGF and bFGF to promote progenitor proliferation and cortical expansion. On day 25, EGF and bFGF were replaced with brain-derived neurotrophic factor (BDNF) and neurotrophin-3 (NT3) to support neuronal differentiation and maturation. From day 45 onward, organoids were maintained in neural differentiation medium without exogenous growth factors, with medium changes every 2 to 3 days (Fig.6C).

The cortical organoids generated in this study exhibited a highly organized, stratified architecture that closely recapitulates key aspects of early human corticogenesis. As illustrated in Fig.18, these structures displayed distinct neuroepithelial zones, including a prominent ventricular zone (VZ), characterized by the presence of PAX6-expressing neural stem/progenitor cells (NSPCs). These transcription factors are well-established markers of radial glial progenitors and early neuroepithelial cells, playing critical roles in neurogenesis and cortical patterning (Nowakowski et al., 2017; Qian et al., 2017). Basal to the VZ, the intermediate subventricular zone (SVZ) is enriched with TBR2+ (also known as EOMES) intermediate progenitor cells, which indicate the transition from radial

glia to committed neurogenic progenitors. These progenitors are essential for generating upper-layer cortical neurons and represent a hallmark of cortical layer expansion in the human brain (Hevner et al., 2006; Molnár et al., 2019).

As noted in the Stachowiak lab's previous studies (Stachowiak et al., 2017), the external region of the organoids exhibited features of an early cortical zone (CZ), where neurons at different stages of maturation could be identified. The expression of TBR1, a marker of deep-layer excitatory neurons, along with CTIP2 (BCL11B), associated with layer V cortical neurons, and NeuN, a general marker of mature neurons, collectively indicated successful neuronal differentiation and laminar identity. The presence of MAP2 (microtubule-associated protein 2), a dendritic marker, further confirmed the establishment of mature neuronal morphology and dendritic arborization by day 60 of differentiation.

I observed that hCO constitutively expressed the mApple fluorescent protein, which confirms the integration of the inducible cassette. Consistent with previous studies from the Stachowiak lab, immunostaining for Ki-67, a marker of actively cycling cells, showed that the proliferative activity was mainly found in the apical region of the ventricular zone (E. K. Stachowiak et al., 2017). This finding reflects the spatial regulation of progenitor proliferation observed in the embryonic cortex (Fig.18). Neuronal maturation was observed through the punctate expression of the presynaptic marker synapsin-2 within the cortical region, indicating the early stages of synaptogenesis and network formation. This is consistent with previous studies demonstrating synaptic maturation in long-term cultured organoids (Quadrato et al., 2017). Finally, in my analysis of apoptosis using cleaved caspase-3 immunolabeling, I found sparse apoptotic cells in the outer cortical regions. In contrast, the centers of the organoids exhibited higher caspase activity, indicating the presence of a necrotic core. This is a known limitation in dense three-dimensional cultures due to limited nutrient diffusion (Bhaduri et al., 2020; Qian et al., 2017).

Taken together, these results confirm that the cortical organoids accurately recapitulate the molecular, spatial, and functional features of early human cortical development, providing a powerful *in vitro* platform for modeling corticogenesis and disease-related perturbations.

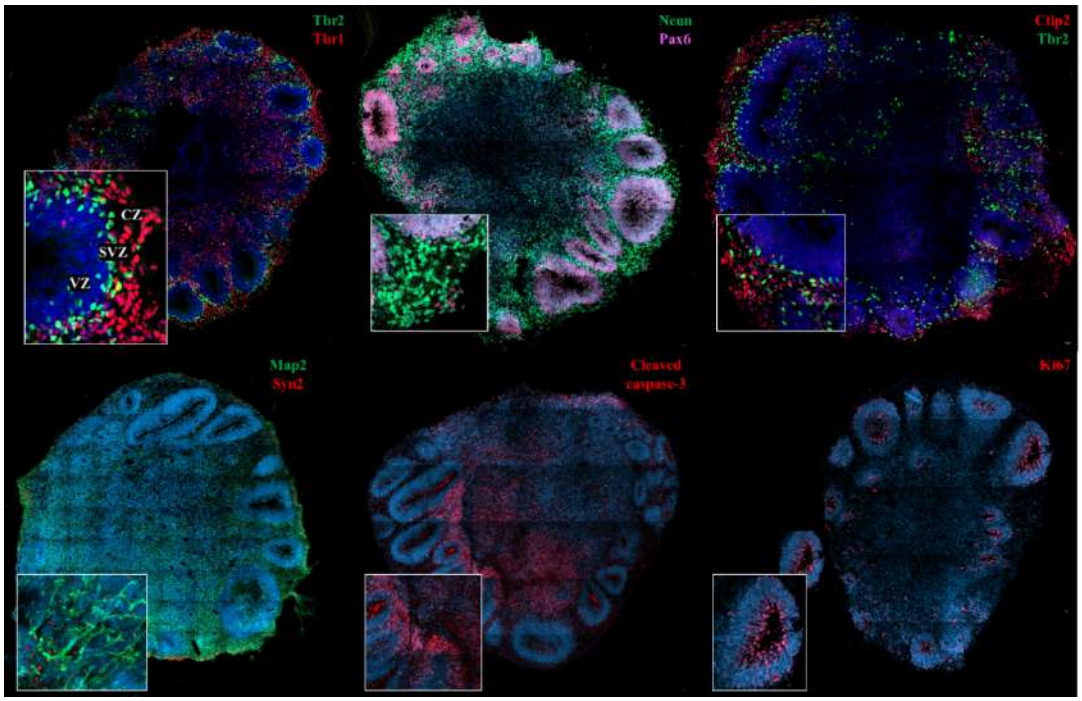

Fig.18. Characterization of 60-day human cortical organoids generated from hiPSC$^{Tet3G\text{-}FGFR1(SP\text{-}/NLS}$ line. *Representative immunofluorescence images of hCOs derived from the hiPSC$^{Tet3G\text{-}FGFR1(SP^{-}/NLS)}$ line, immunolabeled for proliferation (Ki67), cortical progenitor (Pax6), neuronal (Tbr1, Tbr2, Ctip2, Neun), and apoptosis markers (cleaved caspase 3); nuclei were counterstained with Hoechst (blue). Insets indicate distinct regions within a neuronal rosette (ventricular zone (VZ), subventricular zone (SVZ,) and cortical layer (CZ)) displayed at higher magnification. Scale bars: 20 µm.*

5.6. nFGFR1 reduces neural progenitor proliferation and rosette expansion in cortical organoids

Emerging evidence indicates that nuclear FGFR1 (nFGFR1) acts as a transcriptional regulator, playing crucial roles in early neurodevelopment by influencing progenitor proliferation and cortical tissue patterning (Stachowiak et al., 2017; Stachowiak et al., 2009; Stachowiak and Stachowiak, 2016). Previous studies showed that nFGFR1 promotes neural progenitor cells to exit the cell cycle, facilitating neuronal migration and differentiation (E. K. Stachowiak et al., 2009). To explore this function in a hCO-specific context, I examined the effects of nFGFR1 upregulation on the proliferation of neural progenitors, their density, and the architecture of neuronal rosettes in hCOs. It was shown that increased expression of nFGFR1 reduces proliferative activity and promotes significant morphometric changes in neuroepithelial rosettes, suggesting a role in regulating cortical morphogenesis.

Proliferation marker protein Ki-67 is expressed during all active phases of the cell cycle (G_1, S, G_2, and M) but is absent in quiescent (G_0) phase (Gerdes et al., 1983; Scholzen and Gerdes, 2000). I observed progenitor cells in the apical area of a neuronal rosette that are express elevated levels of Ki-67 protein, as they undergo mitotic divisions (Fig.19A). As these progenitors start to delaminate and move outward, Ki-67 levels decrease. These cells are likely in late G_1 or early S phase, close to exit the cell cycle to initiate differentiation (Miller et al., 2018).

Immunofluorescence analysis (Fig.19B) for proliferation marker protein Ki-67 revealed a notable reduction in the density of Ki-67+ cells in the periluminal region of the VZ of neuronal rosettes following nFGFR1 induction ($P \leq 0.0001$; Mann-Whitney test). This finding suggests that nFGFR1 overexpression significantly suppresses progenitor proliferation in the VZ, driving these cells toward cell-cycle exit and promoting their premature neuronal differentiation.

Despite the reduction in proliferation in the periluminal area following nFGFR1 upregulation, the overall density of neural progenitor markers remained stable. The $SOX2^+$ cell density showed no significant difference in the VZ ($P=0.2115$; Fig.20B). Similarly, no changes in $PAX6^+$ cell density were observed between the control and DOX-treated groups ($P = 0.0942$; Fig.21B), suggesting that nFGFR1 does not suppress the progenitor pool or alter progenitor identity.

Next, I assessed the morphometric parameters of neural rosettes and the apical lumen, revealing that they undergo structural remodeling upon activation of nFGFR1. Interkinetic nuclear migration translocates the nuclei of neural progenitor cells radially in an inside-out pattern between the apical and basal surfaces, forming the pseudostratified ventricular zone (Kosodo et al., 2011; Miyata et al., 2015). To test whether nFGFR1 activation would induce measurable remodeling of the pseudostratified ventricular zone, I performed quantitative morphometric analyses of neural rosettes and their apical lumens following doxycycline-driven nFGFR1 upregulation (Fig.22A). I observed that the total rosette area increased markedly from 1896 μm² to 2635 μm² ($P = 0.0001$), while the basal rosette area (reflecting rosette area minus lumen area) expanded from 1777 μm² to 2343 μm² ($P = 0.0002$). This indicates an enlargement of the progenitor-rich neuroepithelial zones following doxycycline induction (Fig.22B–C). Additionally, a significant increase in the rosette perimeter was observed (166.9 μm vs. 196.9 μm; $P \leq 0.0001$), reflecting an enlarged and more complex rosette geometry (Fig.22E). Interestingly,

the APD-normalized rosette area, which reflects shape irregularities, showed a slight but significant reduction following nFGFR1 upregulation (2.76 vs. 2.67; *P = 0.0440*; Fig.22D). This indicates that while rosettes may become larger, they tend to lose their circularity or uniformity.

Finally, I observed a significant twofold increase in the lumen area following doxycycline induction (139.7 μm² to 254.1 μm²; *P ≤ 0.0001*), which coincided with an increase in the lumen perimeter. (49.4 μm to 70.9 μm; *P ≤ 0.0001*). Additionally, a reduction in the APD-normalized lumen area was noted, indicating a less uniform shape (*P = 0.0018*; Fig.22F–H). However, the total number of rosettes per hCOs did not differ significantly between control and DOX-treated conditions (*P = 0.7033*; Fig.22I), suggesting that nFGFR1 specifically promotes the expansion of the existing rosette structures rather than enhancing rosette formation.

In summary, these findings indicate that nFGFR1 upregulation reduces progenitor proliferation in the periluminal region, as evidenced by the reduction of $Ki67^+$ cells, without altering progenitor identity. This coincides with the enlargement of the lumen and rosette area, indicating an increased pool of radially migrating progenitors exiting the cell cycle to undergo differentiation. Collectively, these data support a model in which nFGFR1 signaling drives a coordinated shift from progenitor proliferation toward premature differentiation in the neuronal rosette of developing hCOs.

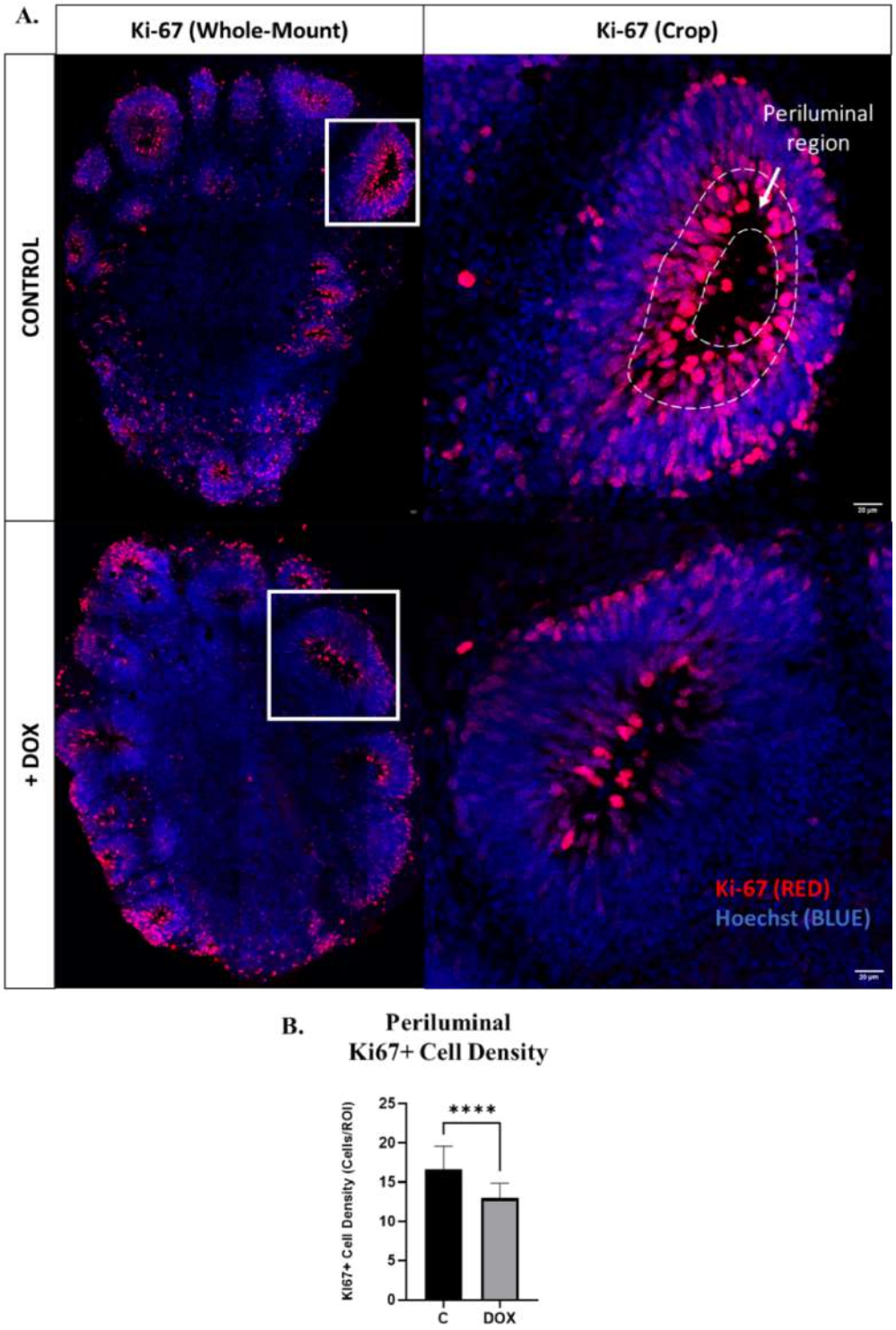

Fig.19. Quantitative assessment of Ki-67+ cells in the apical region of the ventricular zone (VZ) of human cortical organoids (hCO) after nFGFR1 induction. *A. Immunofluorescence analysis of 60-day-in-vitro human cortical organoid (hCO) sections, comparing control (C) and doxycycline-treated (DOX) hCOs, reveals that Ki-67⁺ proliferating cells (red) are primarily located in the periluminal area of the ventricular zone (VZ). Nuclei were counterstained with Hoechst (blue). The white dashed line indicates the peri-luminal region. Scale bars = 20 µm; B. Quantification of Ki-67⁺ cell density in the periluminal VZ of control (n = 34 areas) versus DOX (n = 41 areas) organoids across three independent experiments. Data show mean ± SD; P ≤ 0.0001 (Mann–Whitney test).*

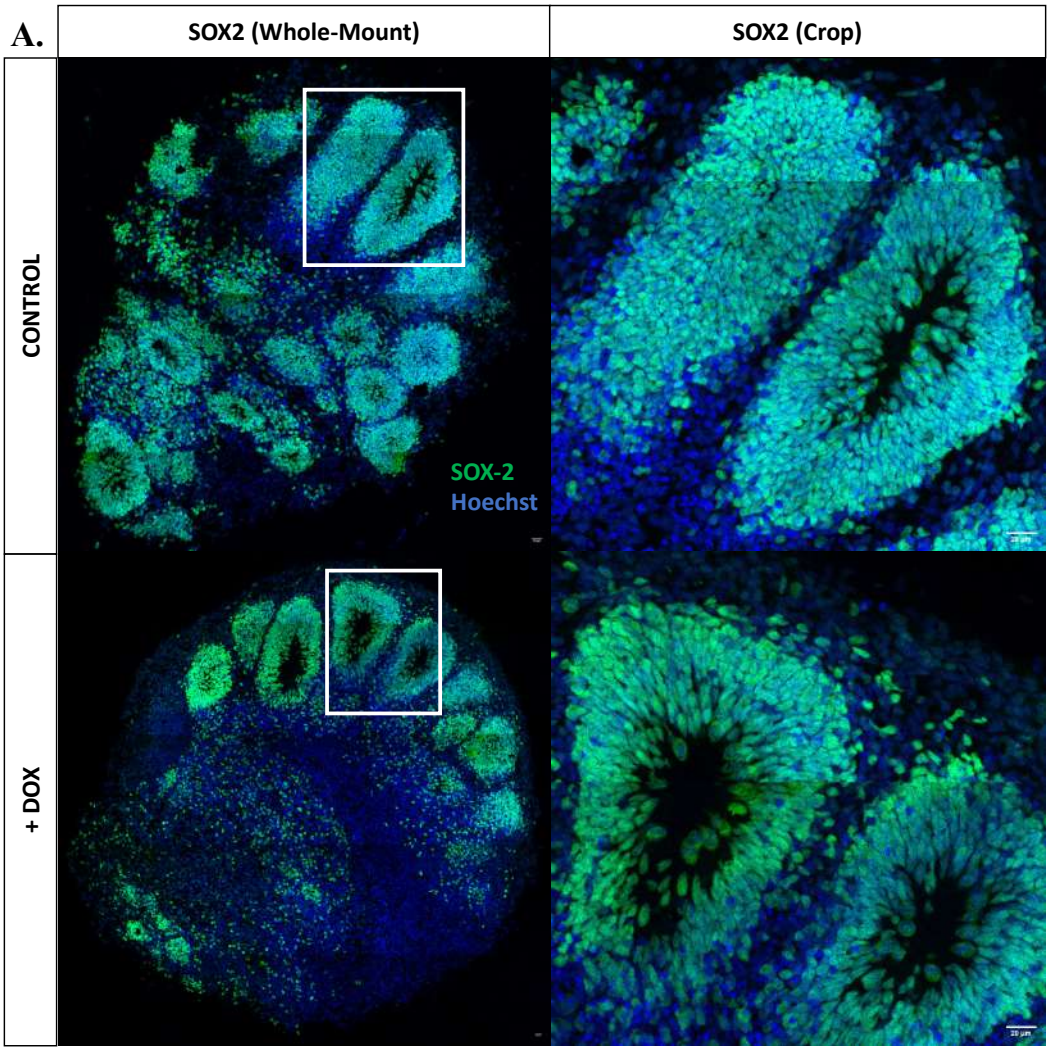

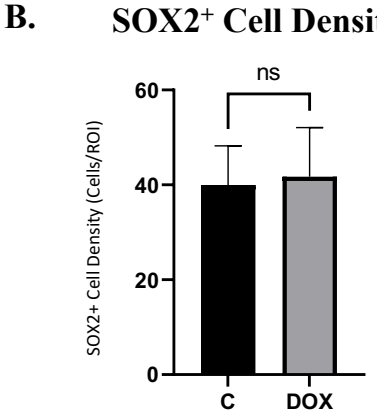

Fig.20. Evaluation of cell density of SOX2⁺ cells in the ventricular zone (VZ) of human cortical organoids (hCO) after nFGFR1 upregulation. *A. Representative immunofluorescence images showing SOX2 expression (green) in the ventricular zone for both control (C) and doxycycline-treated (DOX) 60 DIV hCOs. Nuclei were counterstained with Hoechst (blue). White boxes indicate VZ regions shown at higher magnification in. Scale bars: 20 µm. B. Quantification of SOX2⁺ cell density within ventricular zones of the neuronal rosette was conducted from three independent experiments per condition (Control: n = 150 areas; DOX: n = 158 areas). Statistical significance was determined using the Mann–Whitney test (P = 0.2115). Data presented as mean ± SD.*

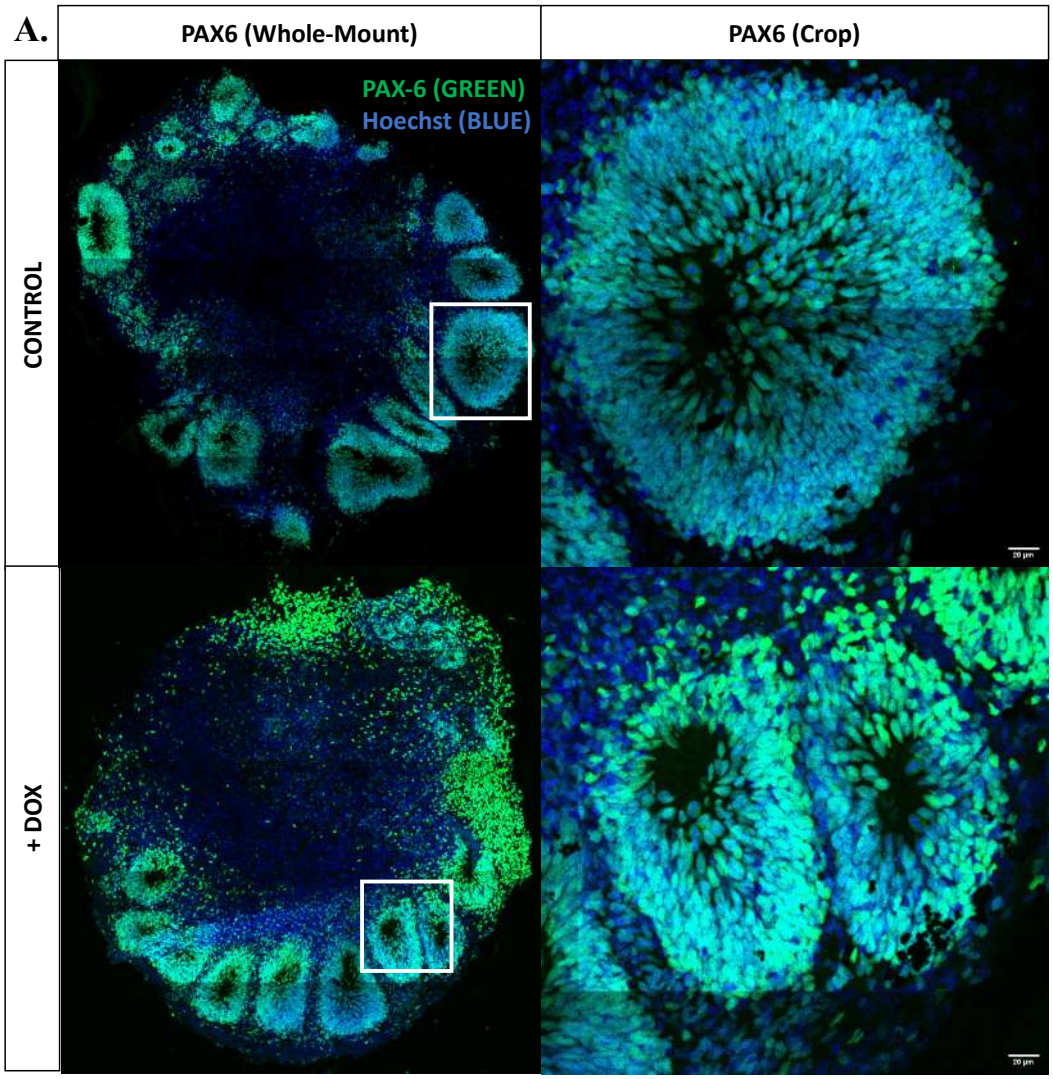

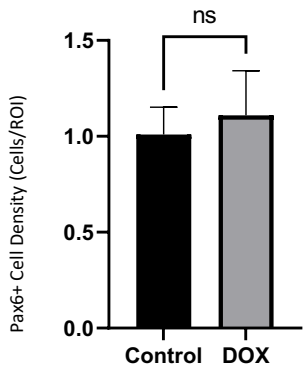

Fig.21. Assessment of cell density of PAX6⁺ cells in the ventricular zone (VZ) of human cortical organoids (hCO) following nFGFR1 activation. *A. Representative immunofluorescence images showing PAX6⁺ cells (green) in the ventricular zone of 60 DIV hCOs under both control and doxycycline-treated (DOX) conditions. Nuclei are stained with Hoechst (blue). White boxes highlight VZ areas shown at higher magnification. Scale bars = 20 µm. B. The density of PAX6⁺ cells was quantified in ventricular zones of neuronal rosettes across three independent experiments (Control: n = 85 areas; DOX: n = 95 areas). Results are shown as mean ± SD; Mann–Whitney test, P = 0.0942 (ns).*

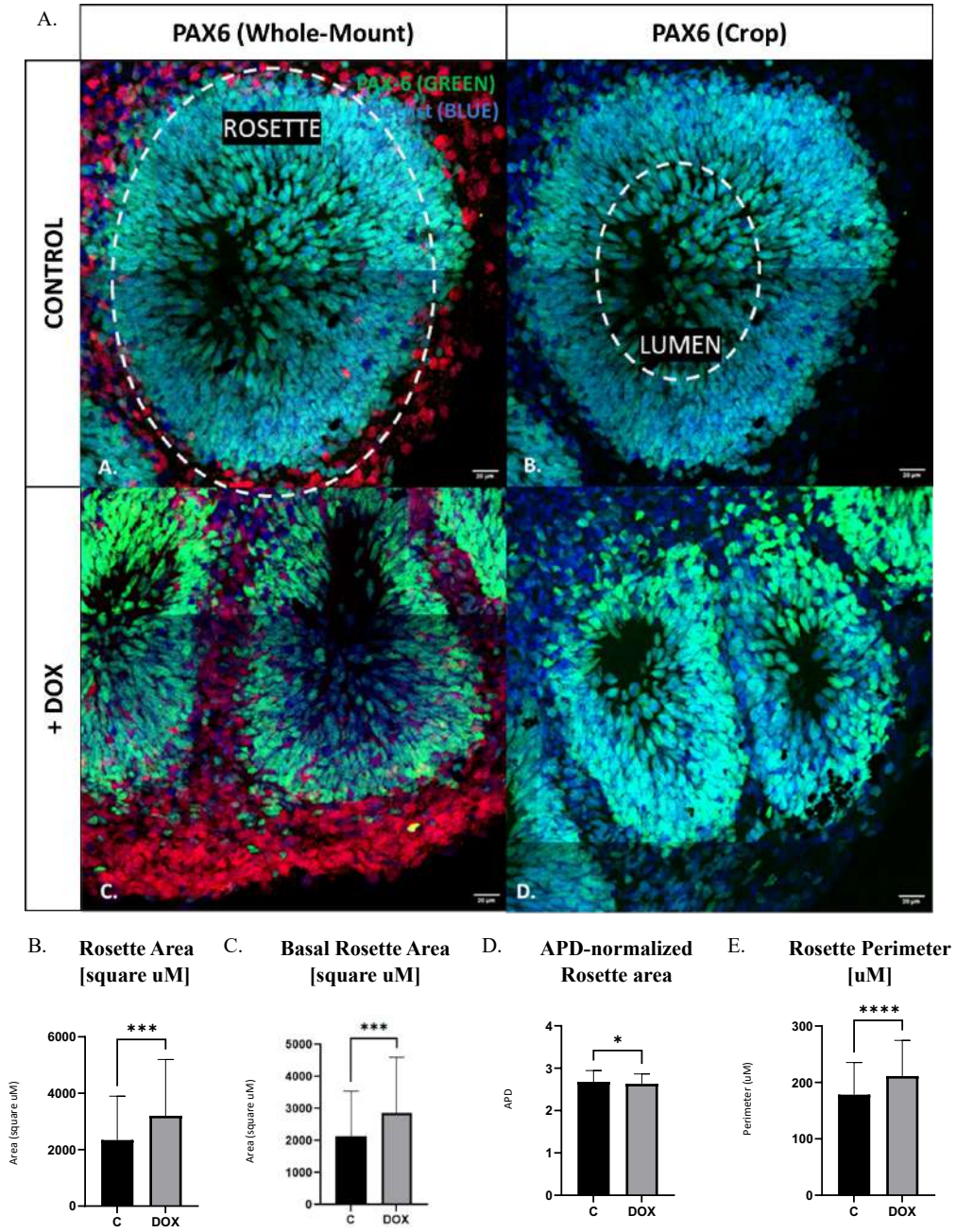

Fig.22. Quantitative assessment of size metrics for neuronal rosettes and lumens in human cortical organoids (hCOs) after nFGFR1 upregulation. *A. Representative immunofluorescence images of PAX6⁺ cells (green) in ventricular zone rosette structures from 60 DIV hCOs, comparing control (C) and doxycycline-treated (DOX) conditions. Dashed lines indicate total rosette (white) and lumen (inner circle) regions. Nuclei were stained with Hoechst (blue). Scale bars = 20 µm; B. Total rosette area (µm²). Quantitative measurements from three independent experiments per condition (Control: n = 81 rosettes; DOX: n = 112 rosettes) are presented as mean ± SD. Two-tailed Mann–Whitney tests were used for statistical comparisons, p = 0.0001; C. Basal rosette area (, µm²), p = 0.0002; D. APD-normalized rosette area (unitless), p = 0.0440; E. Rosette perimeter length (µm), ****P ≤ 0.0001; F. Lumen area (µm²), ****P ≤ 0.0001; G. APD-normalized lumen area (unitless), p = 0.0018; H. Lumen perimeter length (µm), ****P ≤ 0.0001: I. Rosette number per organoid section (Control: n = 10 organoids; DOX: n = 9 organoids), ns—not significant (p = 0.7033).*

5.7. nFGFR1 promotes differentiation of post-mitotic and deep-layer cortical neurons

I examined neuronal marker expression in human cortical organoids following nFGFR1 induction to evaluate its impact on cortical neuron differentiation. NeuN, also known as Rbfox3, is a neuron-specific nuclear protein that indicates post-mitotic neuronal differentiation (Gusel'nikova and Korzhevskiy, 2015). To assess whether nFGFR1 induction enhances cortical neuron differentiation, I quantified $NeuN^+$ cell density in the cortical zone (CZ) of human cortical organoids following nFGFR1 activation (Fig.23A). A significant increase in $NeuN^+$ post-mitotic neurons within the CZ region of hCOs was observed following nFGFR1 activation ($P \leq 0.0001$; Fig.23B), indicating that nFGFR1 promotes neuronal differentiation in the cortical layer of hCO.

CTIP2 (encoded by BCL11B) is a zinc-finger transcription factor that directs the specification of subcerebral projection neurons in cortical layers V–VI during neocortical development (Chen et al., 2008). To determine whether nFGFR1 activation influences the differentiation of deep-layer neurons, the density of $CTIP2^+$ cells was analyzed in the cortical zone of hCOs (Fig.24A). A significant increase in the density of $CTIP2^+$ deep-layer neurons was observed, indicated by the rise in $CTIP2^+$ cell density in the CZ region of hCOs following nFGFR1 activation ($P \leq 0.0001$; Fig.24B). Surprisingly, it coincided with a significant decrease in *CTIP2* RNA expression in hCO after nFGFR1 upregulation ($P = 0.0008$; Fig.24C). This suggests potential post-transcriptional regulation or a region-specific effect of nFGFR1. Together, these findings indicate that nFGFR1 activation promotes the differentiation of deep-layer neurons in the cortical zone of hCOs by post-transcriptionally modulating CTIP2 expression.

5.8. nFGFR1 enhances the expression of $TBR1^+$ cells and affects intermediate progenitors

TBR1 is a T-box transcription factor that specifies post-mitotic projection neurons in cortical layer VI and plays a crucial role in establishing deep-layer identity (Bedogni et al., 2010). In contrast, TBR2 (EOMES) is a T-box transcription factor expressed in intermediate progenitors of the subventricular zone, where it regulates their proliferation and neurogenic potential (Sessa et al., 2008).

To determine whether nFGFR1 overexpression shifts the balance between intermediate progenitor maintenance and neuronal differentiation, I quantified both $TBR1^+$ deep-layer neurons and $TBR2^+$ intermediate progenitors in hCOs following nFGFR1 conditional upregulation (Fig.25A). A significant increase in $TBR1^+$ cell density was observed within the cortical layer of hCO following nFGFR1 activation ($P \leq 0.0001$; Fig.25B). This was supported by RT-qPCR, which revealed a 2-fold increase in *TBR1* mRNA ($P \leq 0.0001$; Fig.25C). In contrast, the population of $TBR2^+$ intermediate progenitors was significantly reduced in the subventricular zone of hCO ($P \leq 0.0001$; Fig.21D), aligning with the decreased *EOMES* (TBR2) RNA expression in hCO following doxycycline administration ($P = 0.0040$; Fig.25E).

These findings suggest that the activation of nFGFR1 directs a transition from the maintenance of the intermediate progenitor pool to the differentiation of deep-layer neurons. This underscores the pivotal role of nFGFR1 in orchestrating laminar fate specification during human corticogenesis in the hCO model.

5.9. nFGFR1 impairs synaptic maturation in hCO cortex despite promoting neuronal differentiation

Although nFGFR1 signaling is known to support neurogenesis, its role in synapse formation remains poorly understood. Recent work demonstrates that different FGF receptors, including FGFR1, can exert divergent effects on excitatory and inhibitory synaptogenesis, influencing the balance and maturation of neural circuits (Dabrowski et al., 2015; Dabrowski and Umemori, 2016; Tomé et al., 2023). To explore this in human cortical development, we examined how increased expression of nFGFR1 affects synaptic maturation in cortical organoids.

Synapsin-2, encoded by *SYN2*, is a neuron-specific phosphoprotein that regulates synaptic vesicle dynamics and neurotransmitter release, which are crucial for presynaptic maturation and plasticity. Synaptophysin, encoded by the *SYP* gene, is a glycoprotein located in the synaptic vesicle membrane and serves as a key marker of presynaptic terminals, mediating vesicle biogenesis and recycling (Feliciano et al., 2017; Thiel, 1993). To determine whether nFGFR1 upregulation modulates presynaptic site plasticity and synaptic maturation, I quantified synapsin-2 protein in the cortical layer of hCOs and measured synaptophysin mRNA

expression (Fig.26C). While nFGFR1 positively influences neuronal differentiation, I observed that its upregulation has a negative impact on synaptic maturation. Through immunofluorescence analysis, a significant decrease in synapsin-2^+ puncta density within $MAP2^+$ neuronal processes was observed in the cortical layer of hCOs after increased expression of nFGFR1 ($P \leq 0.0001$; Fig.26B). In line with this, a notable decrease in *SYP* mRNA levels in hCOs was noted following doxycycline treatment ($P = 0.0188$; Fig.26C). Together, these findings demonstrate that while nFGFR1 induction drives neuronal differentiation, it impairs synaptic maturation, underscoring a dual role for nFGFR1 in balancing neurogenesis with the establishment of functional connectivity. Synaptic deficits reflect those in neuropsychiatric disorders like schizophrenia, where nFGFR1 signaling is dysregulated.

5.10. nFGFR1 modestly increases pan-NSC Nestin but does not alter expression of the pan-neuronal marker MAP2

MAP2 is a protein specific to neurons that stabilizes microtubules within the dendrites of postmitotic neurons and serves as a universal pan-neuronal marker for neuronal differentiation (Caceres et al., 1984; DeGiosio et al., 2022). To determine whether nFGFR1 upregulation affects overall neuronal differentiation, I measured MAP2 levels in hCOs after doxycycline induction and found that the immunofluorescence intensity in the CZ of hCO remained unchanged following nFGFR1 activation ($P = 0.3557$; Fig.27A-B). In line with this, there was no significant alteration in *MAP2* gene expression ($P = 0.3865$; Fig.27C).

NES (Nestin), a commonly used pan-neural stem cell marker, is a key intermediate filament protein primarily found in neural stem and progenitor cells, playing a crucial role in maintaining cytoskeletal integrity during early neurogenesis (Bernal and Arranz, 2018; Lendahl et al., 1990). A modest but significant increase in *NES* (Nestin) mRNA levels was observed after doxycycline treatment in hCO ($P = 0.0079$), which suggests that nFGFR1 supports the maintenance of neural stem cell identity (Fig.27C). *DCX* (Doublecortin) is a microtubule-associated protein that plays a critical role in neuronal migration and initial neurite growth (Ayanlaja et al., 2017). Meanwhile, *MEF2C* is a MADS-box transcription factor vital for controlling embryonic brain development, neuron

formation, and neuron survival (Barker et al., 2021). The transcript levels of both *DCX* (*P = 0.9372*) and *MEF2C* (*P = 0.1615*) showed no significant changes following the conditional upregulation of nFGFR1 (Fig.27C). Together, these findings indicate that nFGFR1 upregulation moderately impacts neural stem cell identity while leaving core neuronal differentiation pathways intact.

Collectively, these results demonstrate that increased expression of nFGFR1 in hCOs promotes the differentiation of deep-layer cortical neurons ($NeuN^+$, $CTIP2^+$, $TBR1^+$), reduces the pool of TBR2+ intermediate progenitors, and impairs synaptic maturation. Importantly, these effects occur without significant alterations in the expression of general neuronal markers such as *MAP2* and *DCX*, highlighting a selective, region-specific effect of nFGFR1 upregulation in human cortical development.

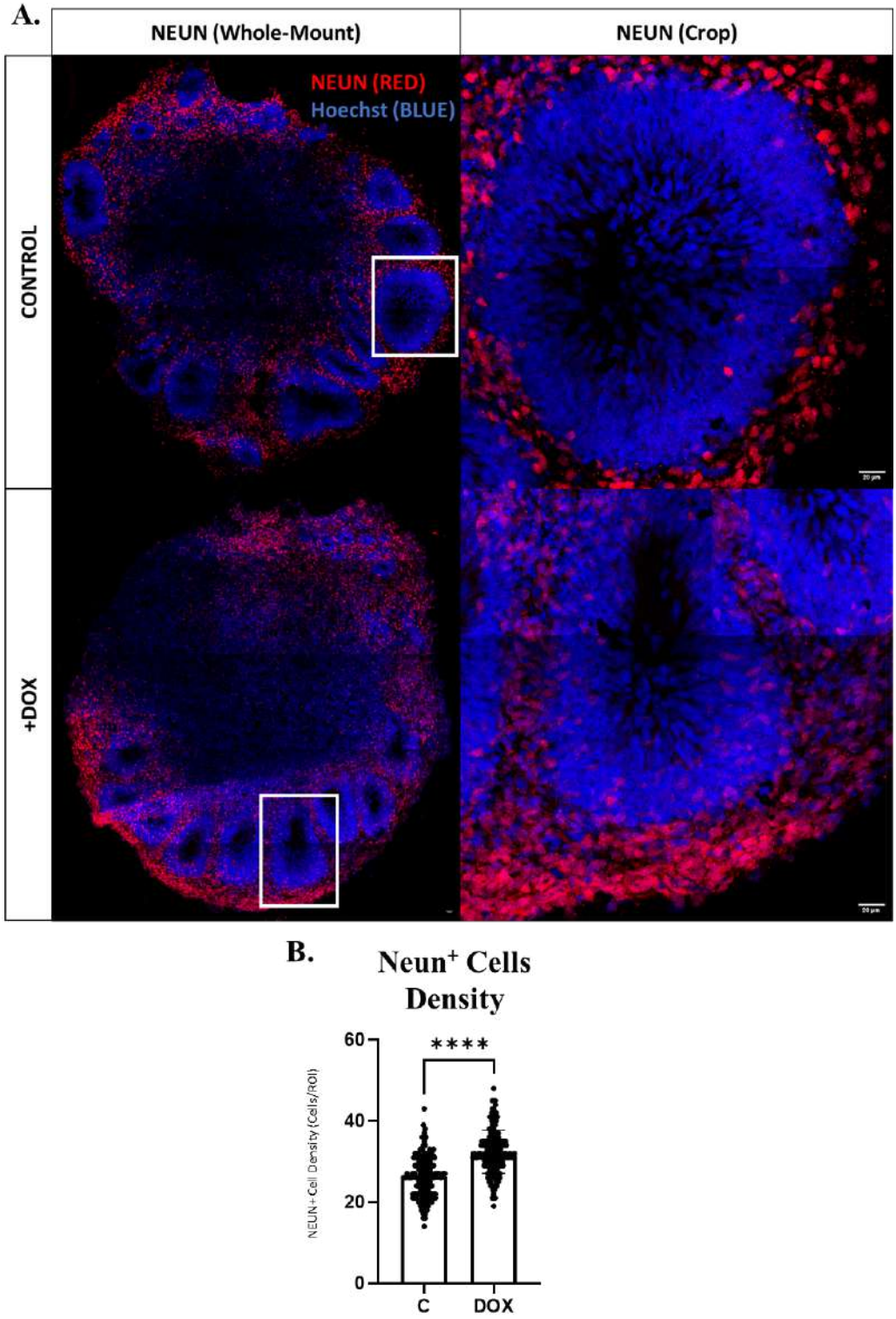

Fig.23. Measurement of NeuN+ cortical neurons in the cortical zone (CZ) of human cortical organoids (hCOs) after nFGFR1 upregulation. *A. Representative immunofluorescence images of NeuN⁺ neurons (red) in the cortical plate of 60 DIV human cortical organoids, under control (C) and doxycycline-treated (DOX) conditions. Nuclei are counterstained with Hoechst (blue). White boxes indicate regions shown at higher magnification in the panels on the right. Scale bars = 20 µm; B. Quantification of NeuN⁺ cell density in the cortical layer. Data are presented as means ± SD across cortical zones from three independent experiments per condition (n = 142 areas for Control, n = 175 areas for DOX). Statistical analysis was conducted using a non-parametric Mann-Whitney test (P ≤ 0.0001).*

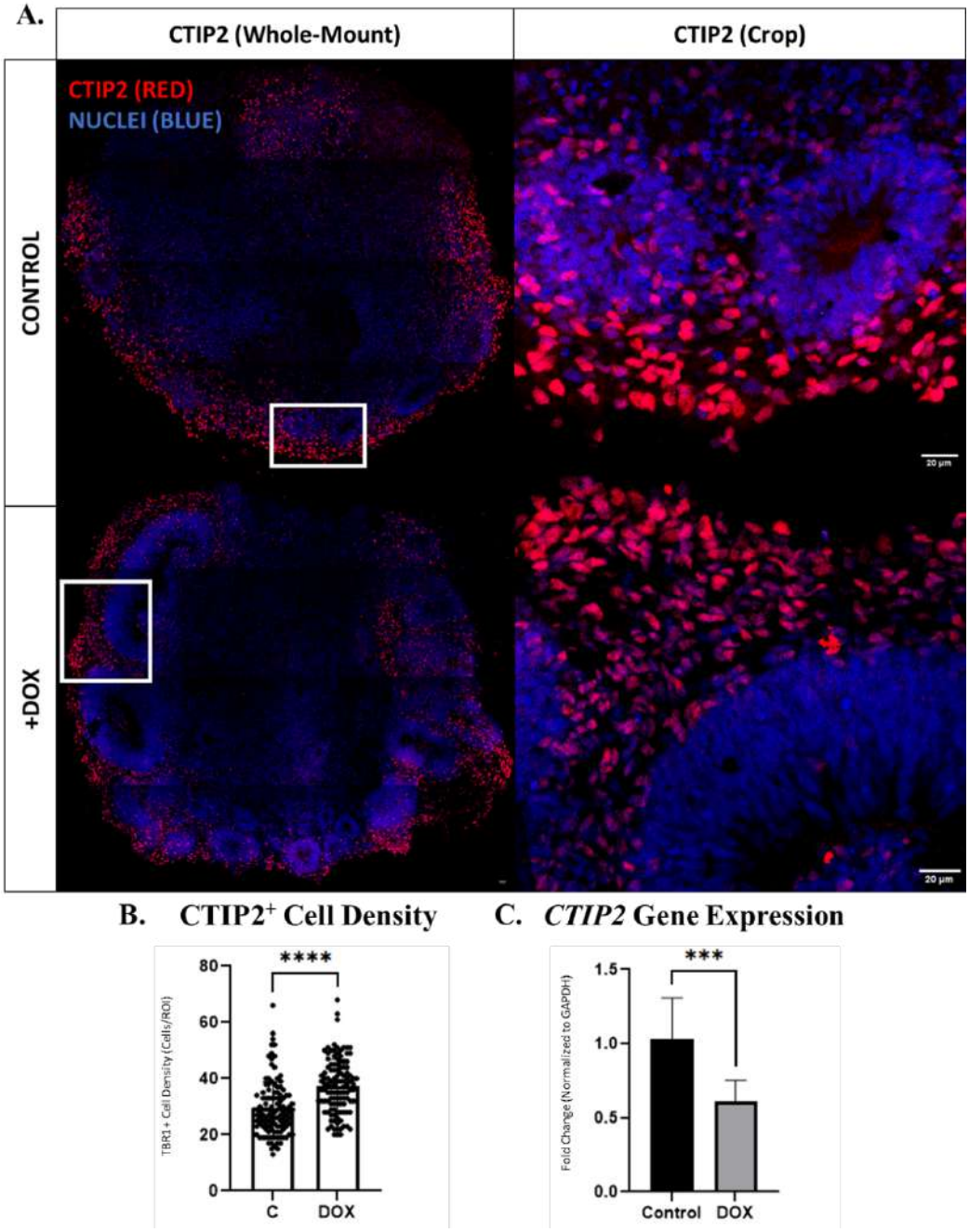

Fig.24. Assessment of Ctip2+ deep-layer neurons in the cortical layer of human cortical organoids (hCOs) following nFGFR1 activation. *A. Representative immunofluorescence images of CTIP2⁺ cells (red) in the cortical plate of 60 DIV human cortical organoids under control (C) and doxycycline-treated (DOX) conditions. Nuclei are counterstained with Hoechst (blue). White boxes indicate regions shown at higher magnification in panels. Scale bars = 20 µm; B. Quantification of CTIP2⁺ cell density in the cortical plate (Control: n = 118 areas; DOX: n = 116 areas) from three independent experiments. Data are mean ± SE; ****P ≤ 0.0001 (Mann–Whitney test); C. RT-qPCR analysis of CTIP2 mRNA levels in 60-day hCOs treated with 3 mM doxycycline (DOX) or DMSO (Control). Expression was normalized to GAPDH; results are presented as the mean ± SD (N=3). Statistical analysis was conducted using a non-parametric Mann-Whitney test (P = 0.0008).*

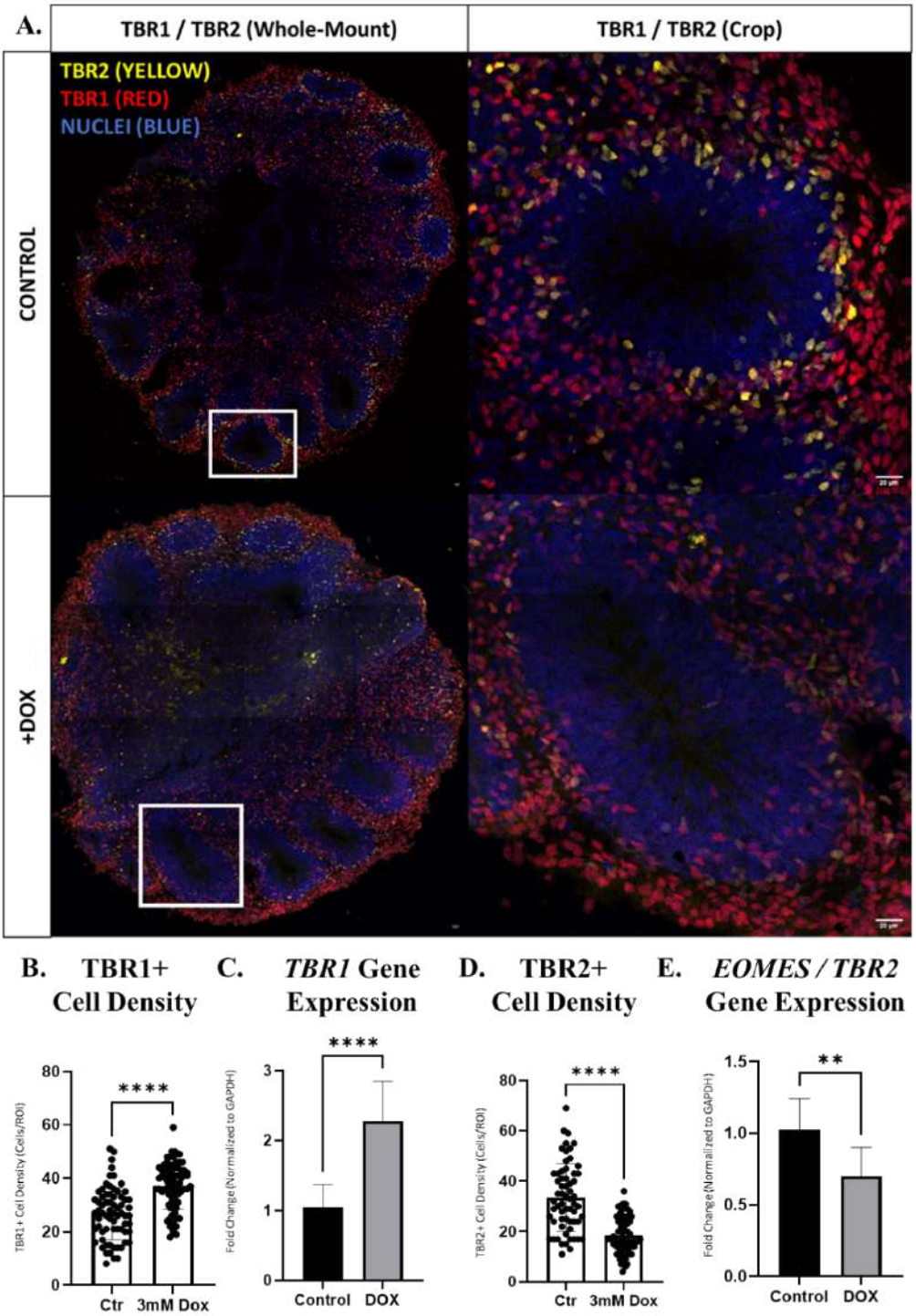

Fig.25. ***Evaluation of Tbr2+ intermediate progenitors in the subventricular zone (SVZ) and Tbr1+ deep-layer neurons in the cortical layer of human cortical organoids (hCOs) after nFGFR1 upregulation***. *A. Representative immunofluorescence images of 60 DIV hCO sections under control (Ctr) and doxycycline-treated (DOX) conditions. TBR2⁺ intermediate progenitors are shown in yellow in the subventricular zone (SVZ), while TBR1⁺ deep-layer neurons are depicted in red in the cortical plate. Nuclei are counterstained with Hoechst (blue). White boxes indicate regions shown at higher magnification. Scale bars = 20 µm; B. Quantification of TBR1⁺ neuron density in the cortical plate (Control: n = 69 areas; DOX: n = 76 areas) across three independent experiments. Data are mean ± SD; ****P ≤ 0.0001 (Mann–Whitney test); C. RT-qPCR analysis of TBR1 mRNA in 60-day hCOs treated with 3 mM doxycycline (DOX) or DMSO (Control). Expression was normalized to GAPDH; mean ± SD of three replicates from*

*three independent experiments; ****P ≤ 0.0001 (Mann–Whitney test); D. Quantification of TBR2⁺ progenitor density in the SVZ (Control: n = 62 areas; DOX: n = 62 areas) across three independent experiments. Data are mean ± SD; ****P ≤ 0.0001 (Mann–Whitney test); E. RT-qPCR analysis of EOMES (TBR2) mRNA in 60-day hCOs treated with 3 mM doxycycline (DOX) or DMSO (Control). Expression normalized to GAPDH; mean ± SD (N=3); p = 0.0040 (Mann–Whitney test).*

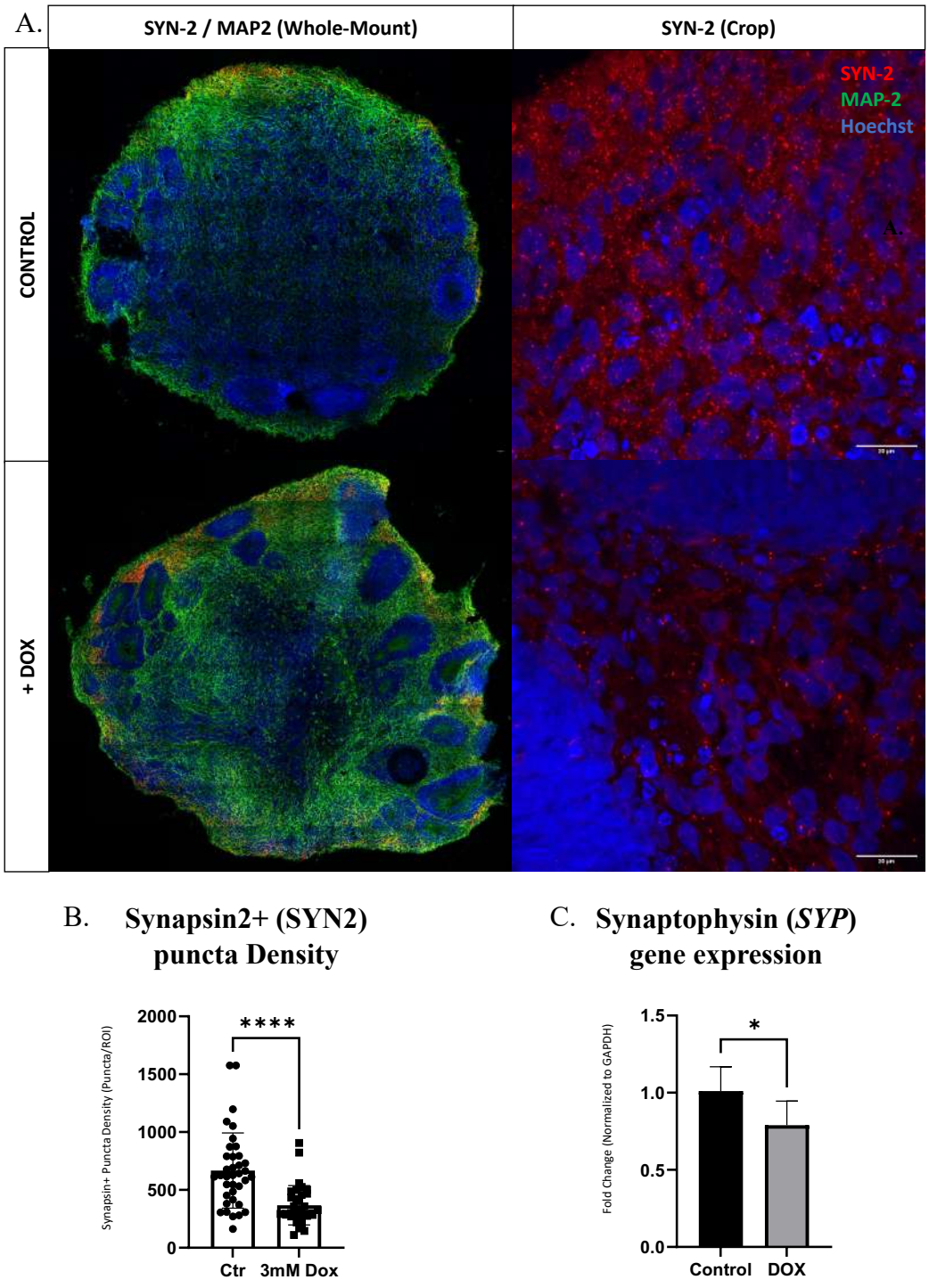

Fig.26. Measurement of synaptic maturation in hCO after nFGFR1 activation. *A. Representative immunofluorescence images show Synapsin-2 (red) puncta within MAP2⁺ neuronal processes (green) in the cortical plate of 60-day-old human cortical organoids, under both control (Ctr) and doxycycline-treated (DOX) conditions. Nuclei are*

counterstained with Hoechst (blue). White boxes outline regions displayed at higher magnification. Scale bars = 20 µm; B. Quantification of Synapsin-2 puncta overlapping with MAP2⁺ processes in cortical plate regions (Control: n = 37 areas; DOX: n = 33 areas) across three independent experiments. Data are presented as mean ± SD. P ≤ 0.0001 (Mann–Whitney test); C. RT-qPCR analysis of synaptophysin (SYP) mRNA levels in 60-day hCOs treated with doxycycline (DOX) or DMSO (control). Expression was normalized to GAPDH; the results are presented as mean ± (N=3); P = 0.0188 (Mann–Whitney test).

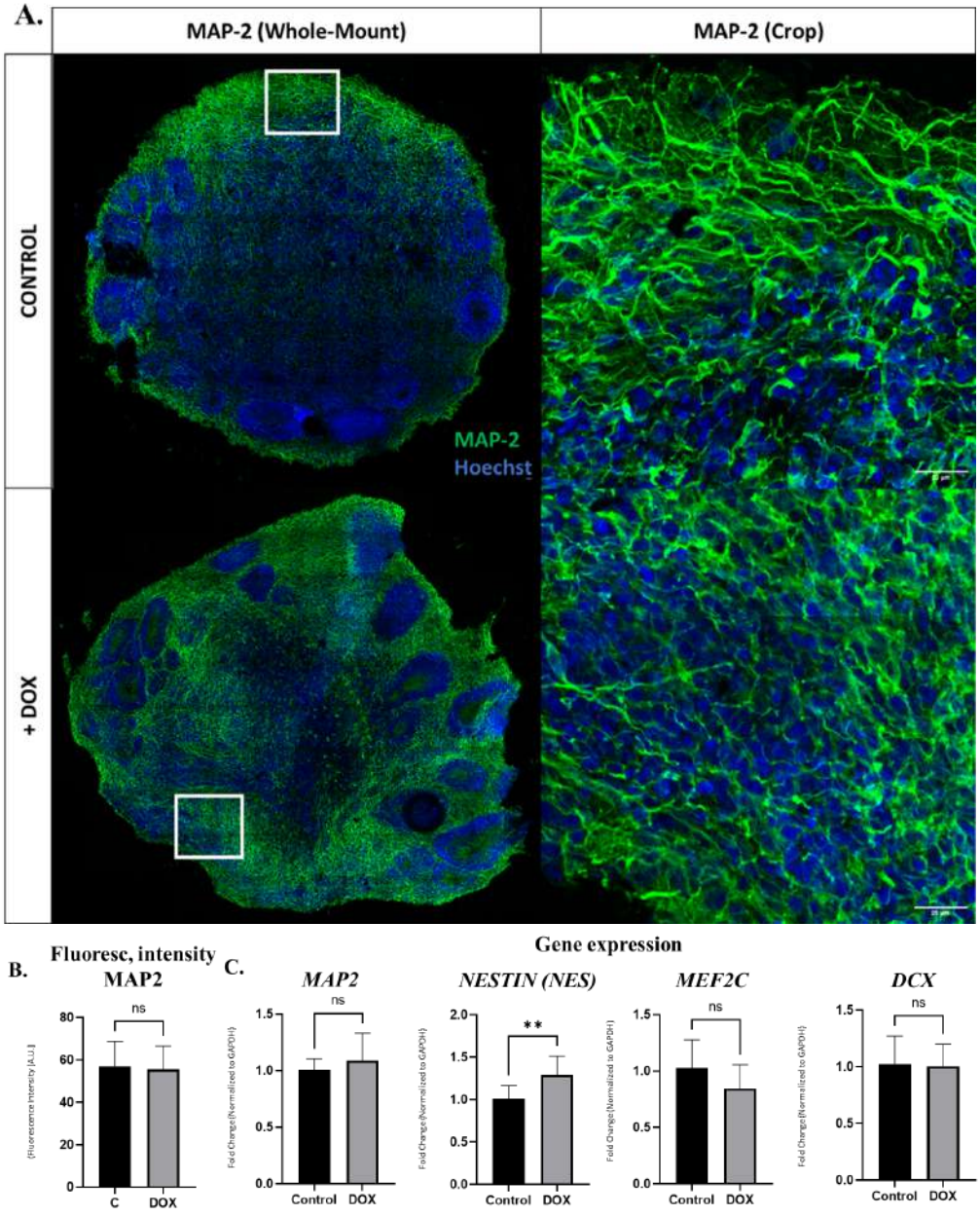

Fig.27. Assessment of pan-NSC and pan-neuronal markers in hCO after nFGFR1 induction. *A. Representative immunofluorescence of MAP2⁺ neurons (green) in 60-day hCO cortical plates under control (C) and doxycycline-treated (DOX) conditions. Nuclei are stained with Hoechst (blue). White boxes indicate regions shown at higher magnification. Scale bars = 20 µm; B. Quantification of MAP2 fluorescence intensity across cortical plate regions (Control: n = 90 areas; DOX: n = 92 areas) from three independent experiments. Data are represented as mean ± SD; p = 0.3557 (Mann–Whitney test); C. RT-qPCR analysis of NSC marker NES (Nestin) and neuronal genes MAP2, DCX, and MEF2C in 60-day hCOs treated with doxycycline (DOX) or DMSO (Control).*

Expression normalized to GAPDH; Data are presented as mean ± SD of three replicates from three independent experiments. NES: p = 0.0079; MAP2: p = 0.3865; DCX: p = 0.9372; MEF2C: p = 0.1615 (Mann–Whitney test).

5.11. nFGFR1 modulates mitochondrial morphology and network connectivity in a region-specific manner during cortical development

Mitochondrial morphology and dynamics are closely linked to neurodevelopmental states, with fused, branched networks supporting oxidative metabolism in differentiated neurons and fragmented forms predominant in glycolytic progenitors (Khacho and Slack, 2018; Liu et al., 2024; Romero-Morales et al., 2022). Recent studies have implicated FGFR1 in controlling mitochondrial structure and function, including fusion dynamics through OPA1 degradation and permeability transition (Srisakuldee et al., 2021; Yan et al., 2023).

To determine how nuclear FGFR1 (nFGFR1) affects mitochondrial structure, I conducted high-resolution imaging and quantitative morphometric analysis of the mitochondrial morphology and network connectivity in the ventricular and cortical areas of human cortical organoids (hCOs). Mitochondrial morphology and network structure closely reflect the metabolic needs of cells and their differentiation stages. In human cortical organoids (hCOs), the ventricular zone (VZ) contains neural progenitors that depend on glycolysis, while the cortical zone (CZ) consists of differentiating post-mitotic neurons that utilize oxidative metabolism. To evaluate how nuclear FGFR1 (nFGFR1) affects these region-specific mitochondrial properties, I conducted high-resolution confocal microscopy combined with semi-automated analysis using the Mitochondria Analyzer plugin (Fig.9). Images were acquired from both cortical and ventricular zones and processed using segmentation and skeletonization pipelines. This allowed for the extraction of mitochondrial metrics, including number, morphology, and branching complexity (Fig.28).

In the CZ, I found that nFGFR1 upregulation resulted in a significant reduction in mitochondrial numbers ($P = 0.0042$). A notable decrease in the total mitochondrial area ($P = 0.0008$), total perimeter ($P = 0.0013$), and mean perimeter per mitochondrion ($P = 0.0005$, Fig.29B) was also observed. These morphological changes were accompanied by a decrease in network complexity. I found that the total branch length decreased following nFGFR1 upregulation ($P \leq 0.0001$). Additionally, it was noted that the mean branch length ($P = 0.0002$) and the number

of branch junctions (*P = 0.0003*) were reduced (Fig.29D). Moreover, the form factor, which indicates elongation and regularity, was significantly decreased (*P = 0.0016)*. Importantly, the mitochondrial fragmentation index increased after nFGFR1 expression increased (*P = 0.0006*), suggesting a transition toward a more fragmented and less interconnected mitochondrial network (Fig.29C). These changes suggest that nFGFR1 overexpression disrupts mitochondrial fusion and network integration in the CZ region of hCO, which could potentially impact oxidative energy metabolism and mitochondrial homeostasis.

In contrast, I observed that mitochondria in the ventricular zone showed only modest structural changes following the upregulation of nFGFR1 (Fig.30A). The total number of mitochondria and mitochondrial area remained unchanged (*P = 0.0791* and *P = 0.0617*, respectively). On the other hand, a significant increase was observed in total perimeter (*P = 0.0327*) and aspect ratio (*P = 0.0014*), indicating a more elongated shape (Fig.30B-C). Additionally, there was an increase in total branch length (*P = 0.0186*) and in mean branch length (*P = 0.0493*) following nFGFR1 upregulation (Fig.30D). Furthermore, the form factor increased as well (*P = 0.0201*), suggesting a more regular mitochondrial structure. In contrast, parameters such as mean perimeter, fragmentation index, and branch junctions remained unchanged after the doxycycline treatment. The results show that in the ventricular area of hCO, primarily composed of glycolytic neural progenitors, nFGFR1 promotes mild mitochondrial elongation and connectivity, indicating improved fusion dynamics and metabolic efficiency.

Together, these results reveal that the conditional upregulation of nFGFR1 has a region-specific impact on mitochondrial structure within the hCO. In the differentiating neurons of the cortical plate, nFGFR1 causes fragmentation of mitochondria and decreases network connectivity, while in the ventricular zone, it modestly promotes mitochondrial elongation and branching (Fig.28B). This spatial divergence likely indicates the different metabolic states and maturation profiles of progenitor and neuronal cell populations and underscores the importance of nFGFR1 in regulating mitochondrial adaptation throughout neurodevelopment.

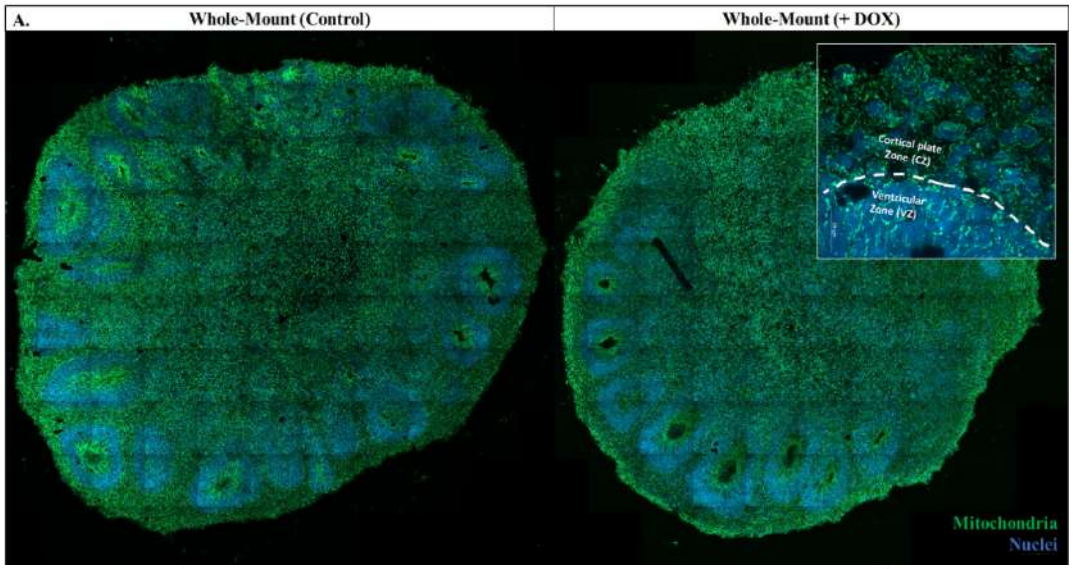

B. Mitochondrial Parameter		Cortical Plate Zone (CZ)		Ventricular zone (VZ)	
		Significance	FC	Significance	FC
Size predictors	Count (uM)	****	Down	NS	
	Total Area (square uM)	***	Down	NS	
	Total Perimeter (uM)	**	Down	*	Up
	Mean Perimeter (uM)	***	Down	NS	
Shape predictors	Aspect Ratio (AR)	ns		**	Up
	Form Factor (FF)	**	Down	*	Up
Branching metrics	Branches	***	Down	NS	
	Total Branch length (uM)	****	Down	*	Up
	Mean branch length (uM)	***	Down	*	Up
	Branch junctions	****	Down	NS	
	Branch end points	**	Down	NS	
	Mean branch diameter (uM)	***	Down	NS	

Fig.28. Assessment of mitochondrial shape and network connectivity in different areas of human cortical organoids (hCOs) following nFGFR1 activation*. A. Representative fluorescent images of mitochondria (green) and nuclei (Hoechst, blue) in 60-day hCO sections under control (C) and doxycycline-treated (DOX) conditions. The panels show tile-scan whole-section views of hCOs at 40x magnification; Insets show distinct regions within a neuronal rosette, ventricular zone (VZ), and cortical zone (CZ), displayed at higher magnification. Scale bars = 100 µm; B. Summary of mitochondrial metrics extracted by Mitochondria Analyzer; significance is determined by the Mann–Whitney test: *P ≤ 0.05, **P ≤ 0.01, ***P ≤ 0.001, ****P ≤ 0.0001. In the CZ, doxycycline treatment decreased mitochondrial count, area, perimeter, form factor, branch number, total and mean branch length, junctions, endpoints, and diameter. In the VZ, total perimeter, aspect ratio, form factor, total and mean branch length increased; other parameters remained unchanged.*

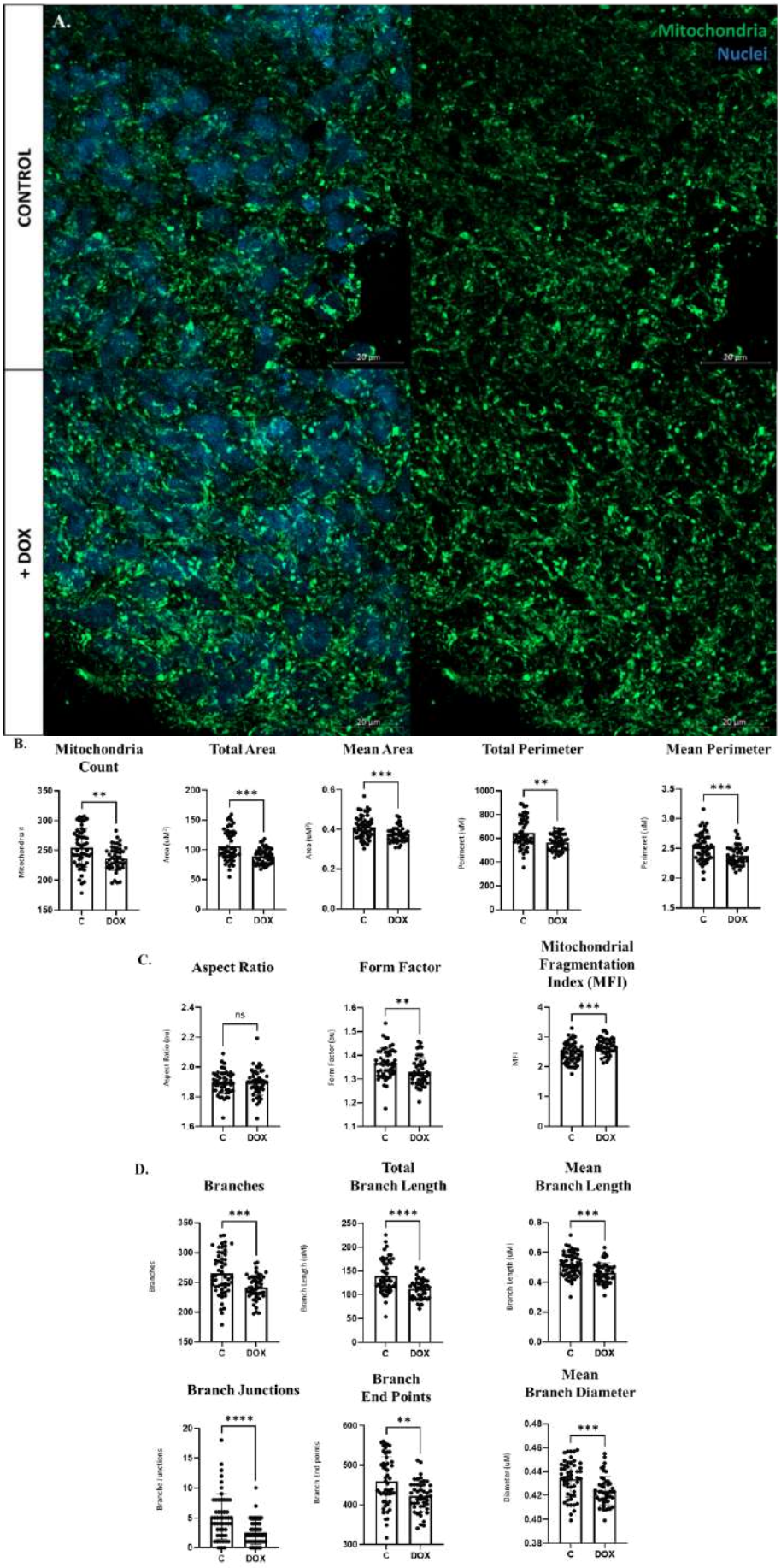

Fig.29. Assessment of mitochondrial morphology and network connectivity parameters in the cortical layer (CZ) of human cortical organoids (hCO) after nFGFR1 upregulation. *A. Representative ×63 confocal images of mitochondria (green) and Hoechst-labeled nuclei (blue) in the CZ of 60-day hCO sections under control (C) and doxycycline-treated (DOX) conditions. Scale bars = 20 μm; B. Size predictors include the quantification of mitochondrial count, total area, total perimeter, and mean perimeter using the Mitochondria Analyzer plugin. All metrics showed a significant reduction in DOX compared to the control (Count: ****P ≤ 0.00001; Total Area: ***P ≤ 0.0001; Total Perimeter: **P ≤ 0.001; Mean Perimeter: ***P ≤ 0.0001); C. Shape metrics reveal a reduced form factor (p ≤ 0.001) while the aspect ratio remains unchanged (ns) following nFGFR1 upregulation; D. Branching metrics branch count, branches per mitochondrion, total branch length, mean branch length, branch junctions, branch end points, and mean branch diameter) are significantly lower after nFGFR1 induction (***P ≤ 0.0001; ****P ≤ 0.00001; **P ≤ 0.001, as indicated). Data are presented as mean ± SD from three independent experiments (Control: n = 53 ROIs; DOX: n = 46 ROIs). Statistical significance was assessed using two-tailed Mann–Whitney tests.*

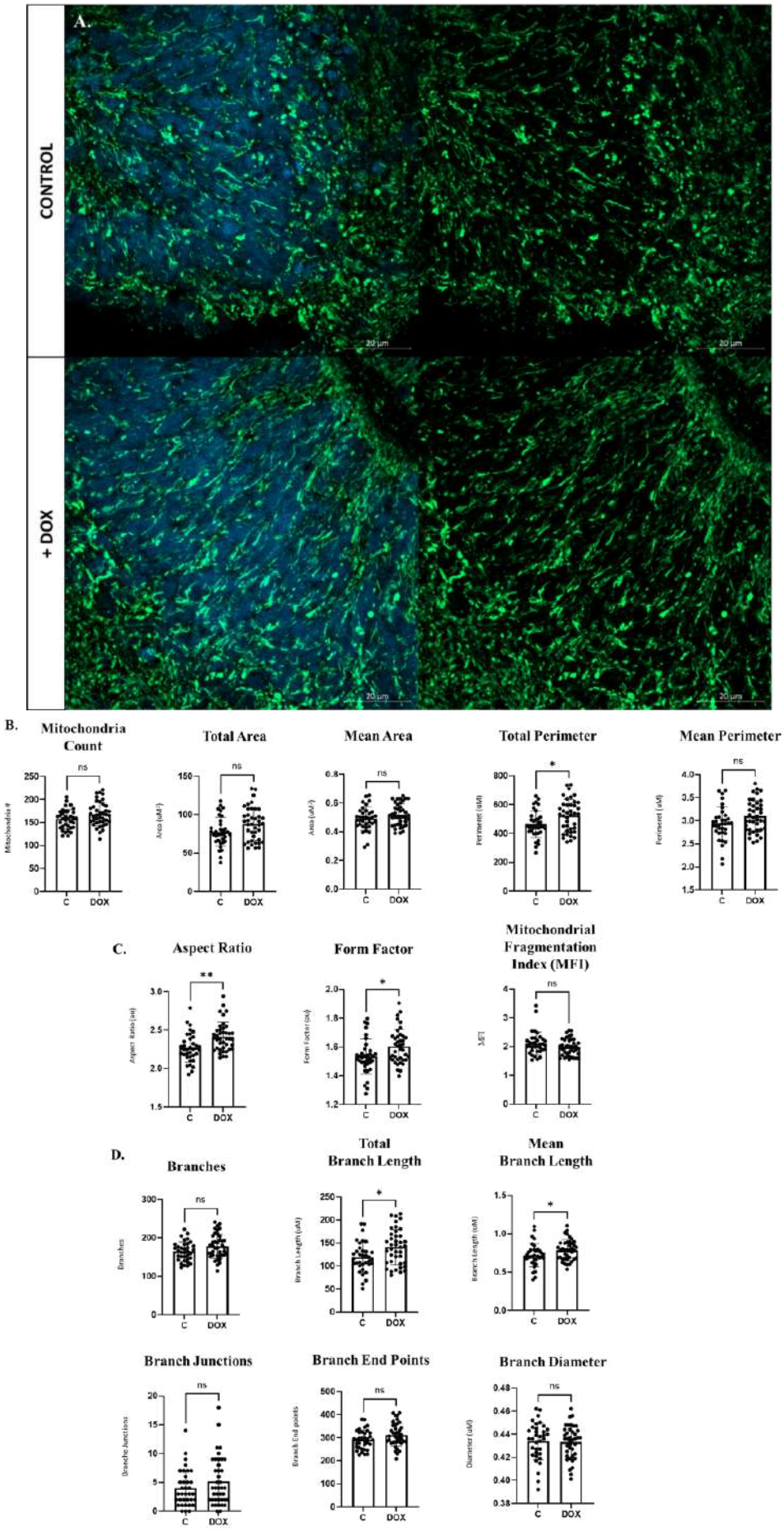

Fig.30. Evaluation of mitochondrial morphology and network connectivity parameters in the ventricular zone (VZ) of human cortical organoids (hCO) after nFGFR1 upregulation. *A. Representative ×63 fluorescence images showing mitochondria (green) and Hoechst-stained nuclei (blue) in the VZ of 60-day hCO sections, comparing control (C) and doxycycline-treated (DOX) conditions. Scale bars = 20 μm; B. Size metrics reveal a significant increase in total perimeter ($P \leq 0.05$), while mitochondrial count, total area, and mean perimeter show no changes; C. Shape metrics. The aspect ratio ($P \leq 0.01$) and form factor ($P \leq 0.05$) demonstrate a significant increase following doxycycline treatment; D. Branching metrics: Total branch length and mean branch length show a significant increase ($p \leq 0.05$), while branch count, junctions, endpoints, and mean branch diameter exhibit no significant changes. Results from three independent experiments (Control: n = 35 ROIs; DOX: n = 40 ROIs) are presented as mean ± SD. The two-tailed Mann–Whitney test was used to determine statistical significance (*$P \leq 0.05$; **$P \leq 0.01$; ***$P \leq 0.001$; ****$P \leq 0.0001$; ns, not significant).*

5.12. nFGFR1 Enhances Region-Specific Mitophagy via PINK1–Parkin Activation

Mitophagy, the selective degradation of mitochondria via the autophagy–lysosome pathway, plays a crucial role in maintaining mitochondrial quality during neurodevelopment. Recent studies have implicated FGFR1 signaling in regulating mitochondrial turnover and homeostasis, with evidence linking FGFR1 to OPA1-dependent fusion, lysosomal engagement, and Parkin-mediated degradation pathways (Srisakuldee et al., 2021; Yan et al., 2023). To evaluate how nuclear FGFR1 (nFGFR1) influences mitophagy in a neurodevelopmental context, I utilized a ratiometric mitoKeima reporter system, combined with live-cell imaging, immunofluorescence, and gene expression analyses in human cortical organoids (hCOs) and embryoid bodies (EBs). MitoKeima is a dual-excitation, pH-sensitive fluorescent protein that localizes in mitochondria, enabling the distinction between cytoplasmic mitochondria and those engulfed by lysosomes. A stable hiPSC$^{\text{CMV-mitoKeima}}$ line expressing mitoKeima was generated using lentiviral particles carrying a CMV-mitoKeima construct. Next, hCOs were generated from this line, and images were acquired at various time points using a spinning disk confocal microscope. Emissions at 488 nm (neutral mitochondria) and 546 nm (acidic, lysosome-localized mitochondria) were captured, and mitophagy flux was quantified as the 546/458 nm fluorescence ratio, calculated on a pixel-by-pixel basis using Fiji (Fig.7B). An abundant expression of mitochondrially targeted green fluorescent protein was noticed, indicating healthy mitochondria in the cytoplasm. In contrast, fewer red puncta were observed, reflecting the presence of mitochondria within acidic autolysosomes. These observations demonstrate that the mito-Keima

system reliably reports mitophagy flux, without reducing reporter expression throughout differentiation in our hCO model.

To evaluate the impact of nFGFR1 on mitophagy flux, EBs and hCOs were transduced with lentiviral particles carrying the mitoKeima reporter on day 16 for EBs and day 56 for hCOs, followed by live imaging four days later. I observed a significant increase in mitophagy flux under nFGFR1 induction in both developmental platforms (Fig.31A-B). A significant increase in the 546/488 ratio was observed in hCOs ($P = 0.0004$; Fig.31D) and in EBs ($P = 0.0085$; Fig.31C) following nFGFR1 activation, indicating an increase in lysosomal degradation of mitochondria across both developmental models.

To validate the mitoKeima flux assay, I analyzed the colocalization of LC3B (an autophagosome marker) and a mitochondrial surface protein that reflects mitochondrial autophagosome engagement (Fig.32A). In hCOs, a 2-fold increase in the density of LC3B+ mitochondrial puncta was observed (median: 111.0 vs. 56.0; $P \leq 0.0001$; Fig.32C) after nFGFR1 upregulation, which indicates active mitochondrial sequestration into autophagosomes. A similar, though less pronounced, increase was noted in EBs ($P=0.0085$; Fig.32B). These findings support the idea that nFGFR1 enhances mitophagic flux by facilitating the recruitment of autophagosomes into mitochondria.

Next, I assessed whether nFGFR1 influences the activation of the PINK1–Parkin pathway, a core mechanism for mitophagy initiation. Upon mitochondrial depolarization, PINK1 accumulates on the outer mitochondrial membrane and recruits the cytosolic E3 ubiquitin ligase Parkin. This enzyme then ubiquitinates various mitochondrial substrates to trigger their selective autophagic degradation (Narendra et al., 2010; Narendra and Youle, 2011). I observed an increase in PINK1 fluorescence in the CZ region of hCOs following nFGFR1 upregulation ($P = 0.0193$; Fig.33C). This was accompanied by the upregulation of Parkin in the cortical layer ($P \leq 0.0001$; Fig.33B), which indicates that nFGFR1 promotes the activation of the PINK1–Parkin pathway in a region-specific manner in the hCO.

However, gene expression analysis using RT-qPCR revealed no significant differences in transcript levels for *PINK1* ($P = 0.0770$), *SQSTM1* (p62) ($P = 0.8633$), or *BNIP3* ($P = 0.6665$) after nFGFR1 activation in hCOs (Fig.34). This suggests that nFGFR1-driven mitophagy functions mainly through post-

transcriptional and region-specific mechanisms, especially within the cortical layer of hCOs, without extensive transcriptional remodeling of mitophagy-related genes.

Collectively, these data indicate that nFGFR1 increased expression induces mitophagy flux by enhancing the recruitment of mitochondrial autophagosomes and promoting the activation of the PINK1–Parkin pathway. These effects are spatially restricted to the cortical zone of hCOs, suggesting that nFGFR1 promotes selective mitochondrial turnover without altering whole-organoid RNA gene expression. This region-specific mitophagic activation could be a compensatory response to mitochondrial dysfunction or reduced respiration, and potentially, reflects nFGFR1-induced shift from oxidative phosphorylation to glycolytic metabolism.

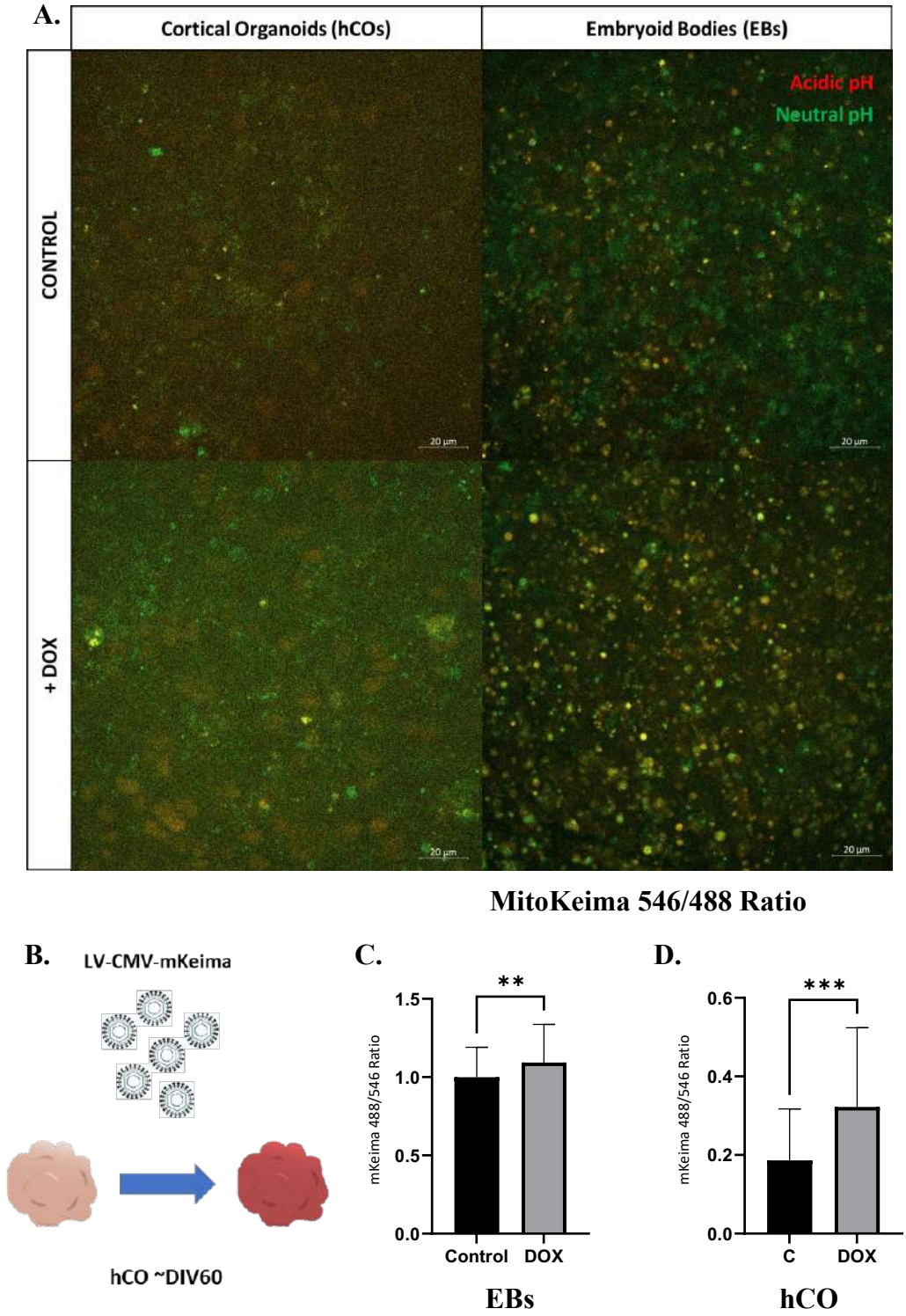

Fig.31. Assessment of mitophagy flux using the mitoKeima reporter assay in embryoid bodies (EBs) and human cortical organoids (hCOs) after nFGFR1 upregulation. *A. Live-cell confocal imaging of mito-Keima in 60-day human cortical organoids (hCOs) and embryoid bodies (EBs) was conducted after both control (C) and doxycycline-treated (DOX) conditions. Neutral mitochondria emit green fluorescence (488 nm excitation), while mitochondria engulfed in lysosomes (acidic) emit red fluorescence (546 nm). Scale bars = 20 µm; B. Experimental outline: At DIV 56, hCOs were transduced with a CMV-driven mito-Keima lentivirus approximately 10 days prior to imaging; EBs were transduced 5 days before imaging, followed by live-cell imaging; C. Quantification of mitophagy flux in EBs is expressed as the ratio of high-pH (546 nm) mito-Keima area to*

the total mitochondrial area (546 nm / 488 nm). Data are presented as mean ± SD (Control: n = 66 ROIs; DOX: n = 66 ROIs); p = 0.0085 by Mann–Whitney test; C. Quantification of mitophagy flux in hCOs using the same ratio metric. Data are presented as mean ± SD (Control: n = 36 ROIs; DOX: n = 45 ROIs); p = 0.0004 by Mann–Whitney test.

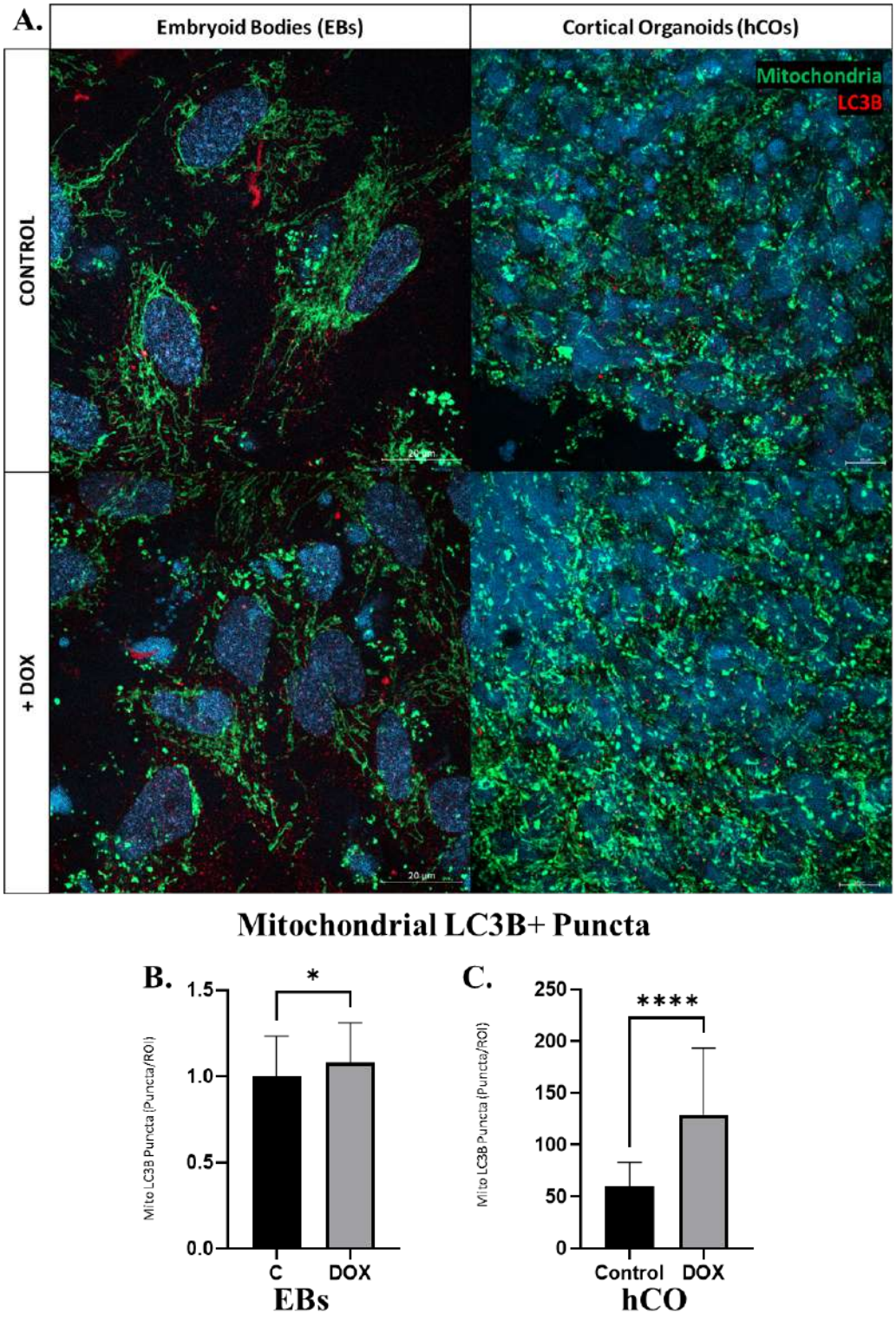

Fig.32. Quantitative assessment of LC3B+ puncta in embryoid bodies (EBs) and the cortical layer of human cortical organoids (hCO) after the upregulation of nFGFR1. *A. Representative confocal images of 21-day embryoid bodies (EBs) and 60-day human cortical organoids (hCOs) co-stained for mitochondria (MAB1273, green) and*

*autophagosome marker LC3B (red) under control and doxycycline-treated (DOX) conditions. Scale bars = 20 µm; B. Quantification of LC3B⁺ puncta co-localized with mitochondria in EBs (Control: n = 70 ROIs; DOX: n = 73 ROIs). Mitochondrial LC3B puncta were identified by thresholding the mitochondrial channel to define mitochondrial masks and measuring LC3B pixels within these masks. Data are normalized to control and presented as mean ± SD (*P = 0.0316; Mann–Whitney test); C. Quantification of LC3B⁺ puncta co-localized with mitochondria in hCOs (Control: n = 60 ROIs; DOX: n = 61 ROIs). DOX induces a robust increase in mitochondrial LC3B recruitment. Data are normalized to control and presented as mean ± SD (****P ≤ 0.0001; Mann–Whitney test).*

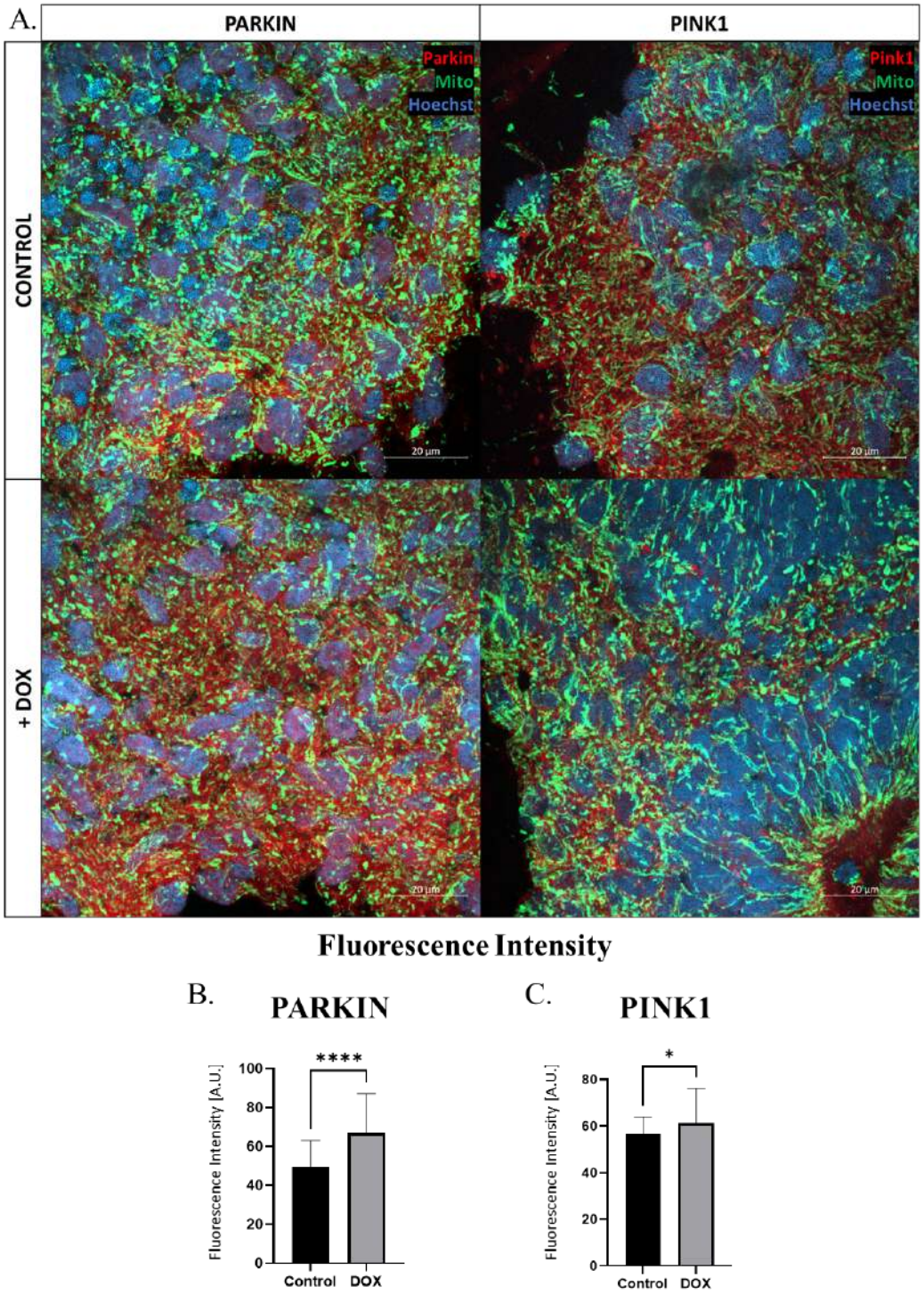

Fig.33. Immunofluorescence analysis of PINK1–Parkin signaling in the cortical layer of hCOs after FGFR1 upregulation. *A. Fluorescence images of Parkin (red) and PINK1 (green) immunostaining in 60-day hCO sections for both control (C) and doxycycline-treated (DOX) conditions. Nuclei are stained with Hoechst (blue). Scale bars = 20 µm; B. The measurement of Parkin fluorescence intensity in the cortical layer (CZ) of hCOs (Control: n = 72 ROIs; DOX: n = 73 ROIs; mean ± SD) indicates that DOX treatment significantly increases Parkin levels (****P ≤ 0.0001, Mann–Whitney test); C. The measurement of PINK1 fluorescence intensity in the cortical layer (CZ) of hCOs (Control: n = 72 ROIs; DOX: n = 78 ROIs; mean ± SD) shows that PINK1 expression significantly increases after nFGFR1 activation (*p = 0.0193, Mann–Whitney test).*

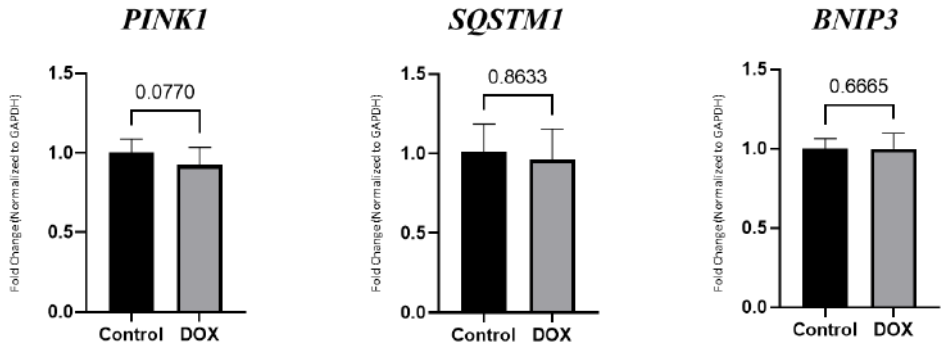

Fig.34. mRNA expression of mitophagy genes in human cortical organoids (hCO) after nFGFR1 upregulation*. RT-qPCR analysis of mitophagy-related transcripts PINK1 (PTEN-induced kinase 1), SQSTM1 (p62), and BNIP3 (BCL2/adenovirus E1B 19 kDa protein–interacting protein 3) was performed in 60-day hCOs treated with doxycycline (DOX) or DMSO (control). Expression levels were normalized to GAPDH, and the data is presented as mean ± SD from three technical replicates across three independent differentiations. No significant differences were observed (PINK1: p = 0.077; SQSTM1: p = 0.863; BNIP3: p = 0.937; BNIP3L: p = 0.667; Mann–Whitney test).*

5.13. nFGFR1 does not impact mitochondrial biogenesis despite increasing mtDNA-encoded ATP6 Expression

Mitochondrial biogenesis, facilitated by the upregulation of nuclear-encoded transcriptional regulators such as PGC-1α and TFAM, is a vital process during neuronal differentiation, supporting increased energy demands and synaptic maturation (Khacho and Slack, 2018). FGFR1 has recently been implicated in the regulation of mitochondrial dynamics and homeostasis via the upregulation of microRNA let-7b-5p, linking it to non-canonical control of mitochondrial remodeling (Hu et al., 2018). To investigate whether nuclear FGFR1 (nFGFR1) drives mitochondrial biogenesis in a human neurodevelopmental context, I performed PGC1α-reporter imaging, mitochondrial gene expression analysis, and mtDNA quantification in cortical organoids and neural progenitors.

I used a live-cell reporter system based on the mitochondrial biogenesis master regulator PGC1α to monitor real-time activity. The proximal promoter region of the *PPARGC1A* gene was cloned upstream of EGFP in a lentiviral vector to generate this reporter vector. To verify the functionality of the reporter system, hiPSCs were transduced with the PGC1α(p)-EGFP vector and then selected with puromycin to generate a stable hiPSC PGC1α(p)-EGFP reporter cell line (Fig.8).

On day 56 of differentiation, hCOs were transduced with lentiviral particles containing the PGC1α-EGFP reporter and cultured them until day 72, followed by live imaging using high-resolution spinning disk confocal microscopy (Fig.35A-B). Although I observed a robust expression of the PGC1α-EGFP reporter, there was no significant difference in EGFP fluorescence intensity following nFGFR1 upregulation in hCOs, both in the dendrites ($P = 0.5448$; Fig.35C) and soma regions ($P = 0.4366$; Fig.35D). Additionally, no significant change in the expression of the *PPARGC1A* gene was found ($P=0.6048$; Fig.35E), which encodes the PGC1α protein, in response to nFGFR1 activation. This indicates that nFGFR1 does not induce PGC1α-regulated mitochondrial biogenesis.

To determine whether nFGFR1 regulates mitochondrial biogenesis at the gene expression level, I conducted RT-qPCR analysis of mitochondrial genes in hCOs following nFGFR1 upregulation (Fig.36A). The expression of *MT-ATP6*, a mitochondrial-encoded ATP synthase subunit, was significantly elevated. This coincides with increased ATP production upon the addition of doxycycline,

suggesting that nFGFR1 enhances ATP production ($P \leq 0.05$; Figure 38C). However, no significant changes in the expression of the mt-DNA coded genes *MT-ND2* ($P = 0.1359$) and *MT-ND5* ($P = 0.2973$) were found following nFGFR1 upregulation, although there is a modest trend of upregulation (Fig.36A).

I then quantified the mtDNA copy number through qPCR, measured as the ratios of mitochondrial genes *MT-ND1* and *MT-ND5* to nuclear reference genes *HBB* and *SERPINA1* (Fig.36B). I did not observe significant changes in the *MT-ND1/HBB* ($P = 0.6218$) or *MT-ND5/SERPINA1* ($P = 0.8381$) ratios, indicating that nFGFR1 activation does not affect mtDNA copy number.

Together, these findings indicate that while nFGFR1 does not activate broad mitochondrial biogenesis or increase mtDNA replication, it selectively upregulates *MT-ATP6*, potentially contributing to enhanced mitochondrial energy output. This points to a specific modulatory role for nFGFR1 in fine-tuning mitochondrial efficiency rather than expanding mitochondrial content.

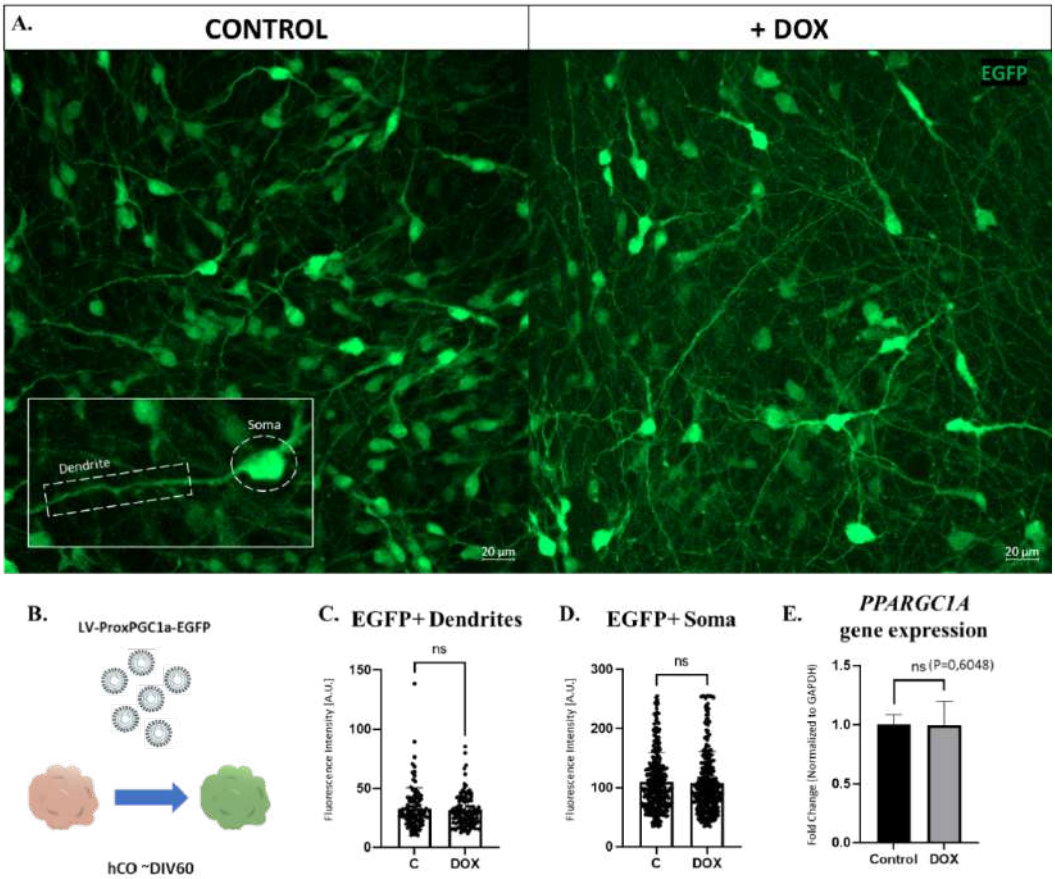

Fig.35. Assessment of mitochondrial biogenesis in hCO and EBs following nFGFR1 upregulation. *A. Live fluorescent imaging reveals the PGC1α-EGFP reporter fluorescence in 72-day hCOs under both control and doxycycline (DOX) conditions. The expression of*

EGFP, driven by the proximal PGC1α promoter, acts as an indicator of mitochondrial biogenesis. The inset shows regions of interest for intensity measurement: the dendrite (dashed rectangle) and soma (dashed circle). Scale bars = 20 µm; B. Experimental outline: At DIV 56, hCOs were transduced with Proximal-PGC1α-EGFP lentivirus, and live imaging was performed approximately two weeks later; C, D. Quantification of EGFP fluorescence intensity in dendritic (C) and somatic (D) compartments of hCO neurons (Control: n = 111 ROIs; DOX: n = 117 ROIs; mean ± SE) revealed no significant differences. Data are presented as mean ± SD (dendrites: p = 0.5448; soma: p = 0.4366; Mann–Whitney test); E. RT-qPCR analysis of PPARGC1A (PGC-1α) mRNA in 60-day hCOs (Control vs DOX), normalized to GAPDH. Data are presented as mean ± SD of three technical replicates from three independent experiments; no significant change was observed (p = 0.6048, Mann–Whitney test).

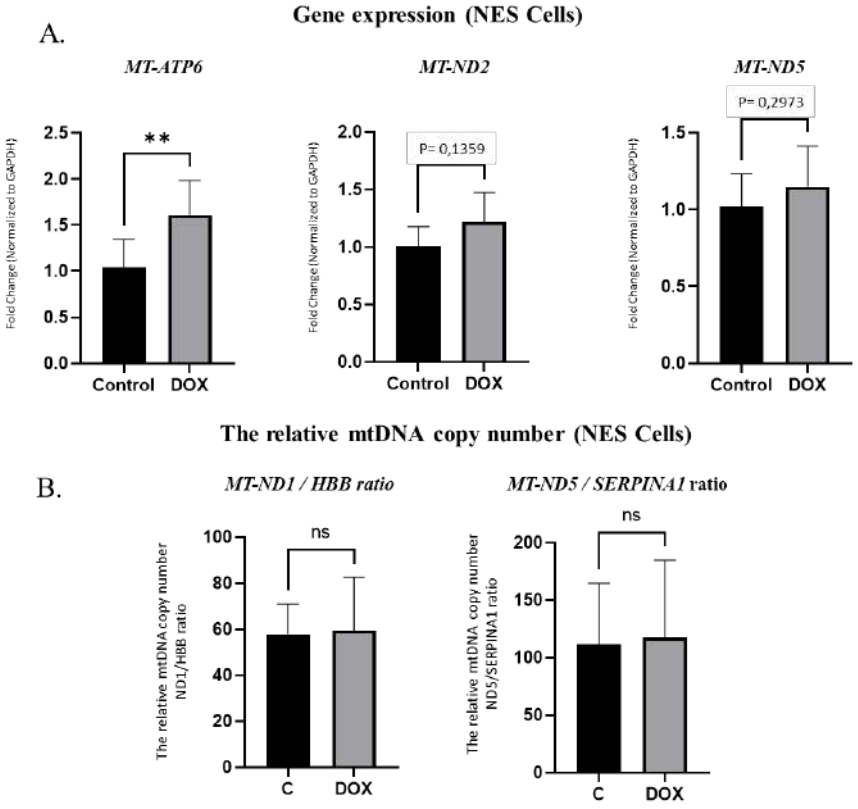

Fig.36. Assessment of mRNA levels of mitochondrial genes encoded by MT-DNA and mtDNA copy number in hCOs and NES cells following the upregulation of nFGFR1. *A. RT-qPCR analysis of mitochondrial transcripts MT-ATP6, MT-ND2, and MT-ND5 was conducted on 60-day hCOs treated with doxycycline (DOX) or a DMSO control. The expression levels were normalized to GAPDH. Results are presented as mean ± SD from three technical replicates across three independent experiments. Statistical analysis was performed using a non-parametric Mann-Whitney test: MT-ATP6 (P = 0.0056), MT-ND2 (P = 0.1359), MT-ND5 (P = 0.2973); B. Quantification of mtDNA copy number in NES cells (DIV 5) was performed by qPCR, using the MT-ND1/HBB and MT-ND5/SERPINA1 ratios. Results are expressed as mean ± SD from three technical replicates across five independent experiments, presented as a percentage relative to the control group. Statistical analysis was conducted using the non-parametric Mann-Whitney test: ND1/HBB (P=0.6218), ND5/SERPINA1 (P=0.8381); ns: non-significant.*

5.14. nFGFR1 regulates cellular redox balance without triggering apoptosis

Fibroblast growth factor receptor 1 (FGFR1) plays a crucial role in maintaining cellular responses to oxidative stress, mitochondrial function, and survival signaling. It has been shown to prevent ferroptosis through activation of the FGFR1/β-Klotho axis and to modulate apoptotic signaling under oxidative conditions (Xie et al., 2020b; Xu et al., 2023). To determine whether nuclear FGFR1 (nFGFR1) regulates redox balance and energy metabolism during early human neural development, I assessed mitochondrial activity, reactive oxygen species (ROS) accumulation, and apoptotic markers in NES cells, embryoid bodies, and cortical organoids.

I measured ROS levels using the DCFDHA fluorescence assay, which detects the oxidant-induced conversion of a non-fluorescent probe into a fluorescent signal. There was a significant increase in ROS levels in NES cells, suggesting that oxidative stress was elevated due to nFGFR1 upregulation ($P = 0.0002$; Fig.38A). Furthermore, cell viability, evaluated through the Resazurin assay which measures the conversion of resazurin to the fluorescent compound resorufin, was notably elevated in NES cells upon increased expression of nFGFR1 ($P \leq 0.0001$; Fig.38B). ATP production also showed an increase, as assessed by the CellTiter luminescence assay, which measures intracellular ATP levels ($P \leq 0.0001$; Fig.38C). To evaluate mitochondrial function, mitochondrial membrane potential (MMP) was assessed in two *in vitro* models. In NES cells, MMP was quantified using a fluorescence plate-based assay with Mitotracker CMXROS, while in embryoid bodies (EBs), MMP quantification was performed using Mitotracker-labeled EBs visualized via fluorescence microscopy. Both models exhibited a significant increase in fluorescence intensity upon FGFR1 induction (NES: $P = 0.0207$; EB: $P \leq 0.0001$; Fig.39), reflecting improved mitochondrial polarization and functionality.

Although ROS levels increased, hCOs showed no signs of enhanced apoptosis. I did not observe any significant change in fluorescence intensity within the cortical layer following nFGFR1 upregulation ($P = 0.0991$; Fig.37A-B). These findings were supported by RT-qPCR analyses of key apoptotic regulators (Fig.37C). While the expression of the anti-apoptotic gene *BCL2* was slightly elevated ($P = 0.0019$), the expression of the pro-apoptotic gene *BAX* ($P = 0.1903$), the *BCL2/BAX* ratio

(*P = 0.3865*), and the integrated stress response marker *ATF4* (*P = 0.1135*) remained stable following nFGFR1 induction. This indicates that nFGFR1 does not trigger apoptotic and stress-response pathways.

These findings indicate that nFGFR1 elevates reactive oxygen species while simultaneously improving mitochondrial function and energy production without triggering apoptosis or metabolic stress, potentially by upregulating the anti-apoptotic factor BCL2. This suggests a neuroprotective role of nFGFR1 during neural differentiation in hCO.

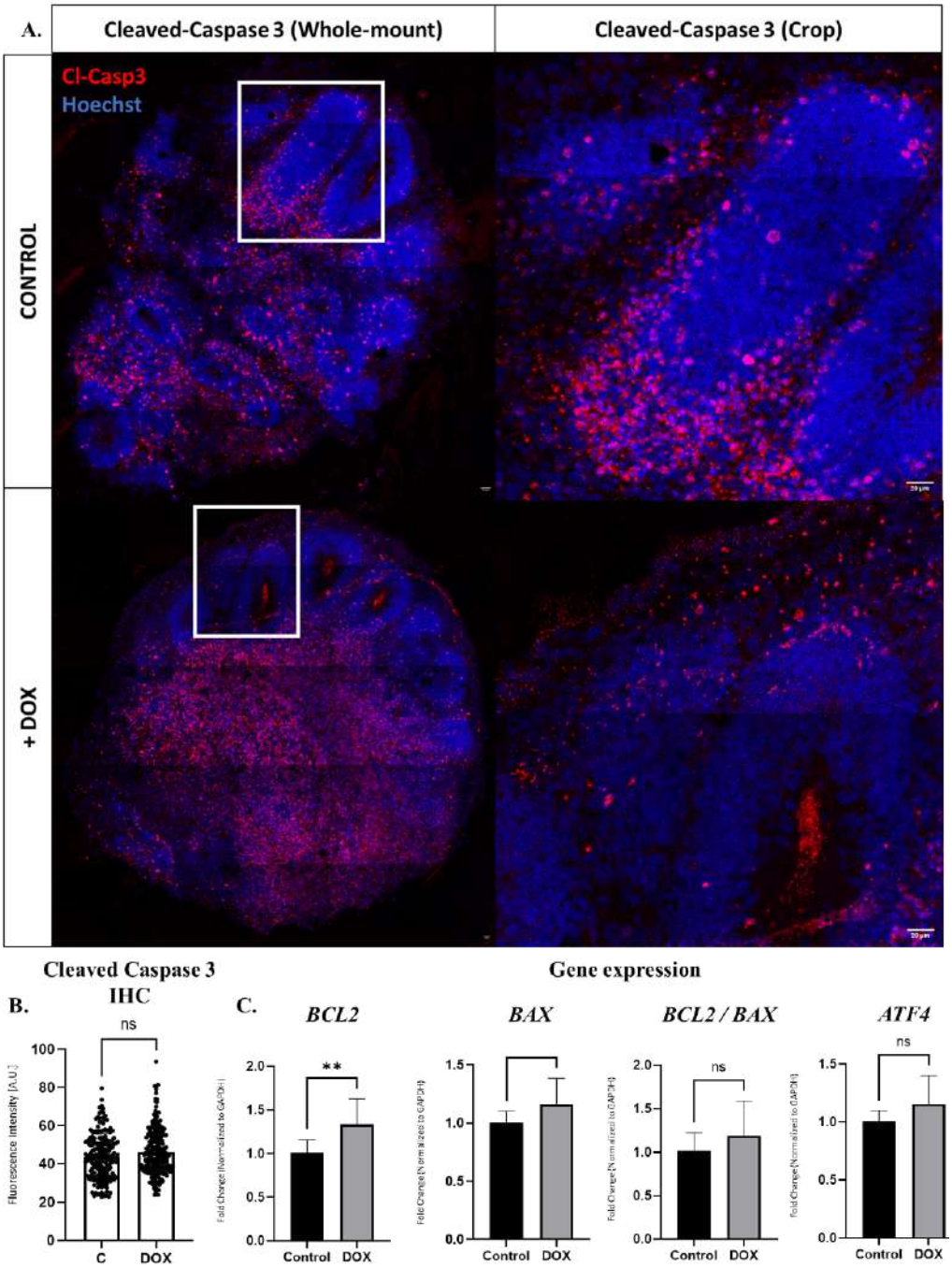

Fig.37. Evaluation of apoptosis and integrated stress response (ISR) in hCOs after nFGFR1 upregulation. *A. Representative fluorescence images showing cleaved caspase-3 (red) immunostaining in the cortical plate of 60-day hCOs under control (C) and doxycycline (DOX) conditions. White rectangles indicate regions shown at higher magnification. Nuclei are stained with Hoechst (blue). Scale bars = 20 µm; B. Quantification of cleaved–caspase–3 fluorescence intensity in the cortical plate (Control: n = 200 ROIs; DOX: n = 229 ROIs) was performed across three independent experiments. Data are presented as mean ± SD; no significant difference was observed (p = 0.0991, Mann–Whitney test); C. RT-qPCR analysis was performed on transcripts related to apoptosis and the integrated stress response (ISR), focusing on BCL2 (anti-apoptotic), BAX (pro-apoptotic), the BCL2/BAX ratio (apoptosis indicator), and ATF4 (ISR marker) in 60-hCOs treated with doxycycline (DOX) or DMSO as the control. The expression levels were normalized to GAPDH. Statistical analysis was performed using the non-parametric Mann-Whitney test: BCL2 (P=0.0019), BAX (P=0.1903), BCL2/BAX ratio (P=0.3865), and ATF4 (P=0.1135).*

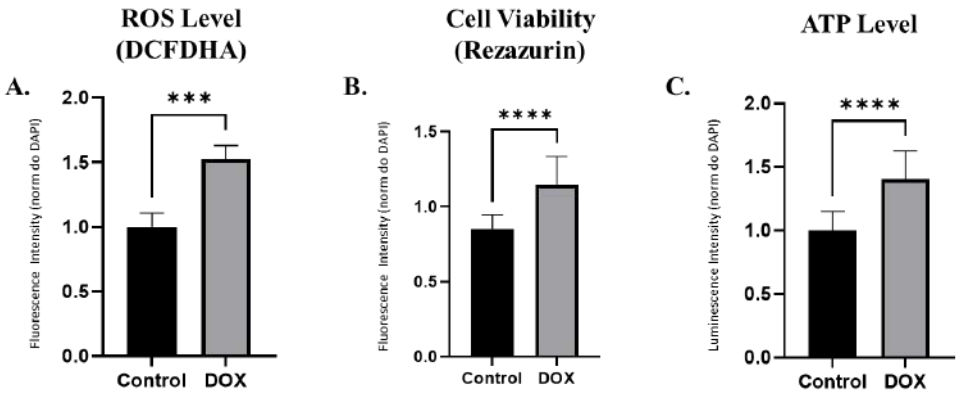

Fig.38. Assessment of ROS levels (A), cell viability (B), and ATP levels (C) in NES cells following nFGFR1 activation. *A. ROS production in NES cells treated with doxycycline (DOX) or a DMSO (control), was assessed by DCFH-DA fluorescence, with results normalized to cell count (Hoechst). The data are presented as mean ± SD from two technical replicates across four independent experiments; p = 0.0002 (Mann–Whitney test). B. Cell viability in NES cells treated with doxycycline (DOX) or DMSO (control) was assessed by resazurin reduction and normalized to cell number. Data are presented as mean ± SD from four replicates across four independent experiments; ****P ≤ 0.0001 (Mann–Whitney test); C. Intracellular ATP levels in NES cells after 4-day DOX or DMSO (control) treatment were measured using CellTiter-Glo luminescence and normalized to cell number. Data are presented as mean ± SD from four replicates in four independent experiments; ****P ≤ 0.0001 (Mann–Whitney test).*

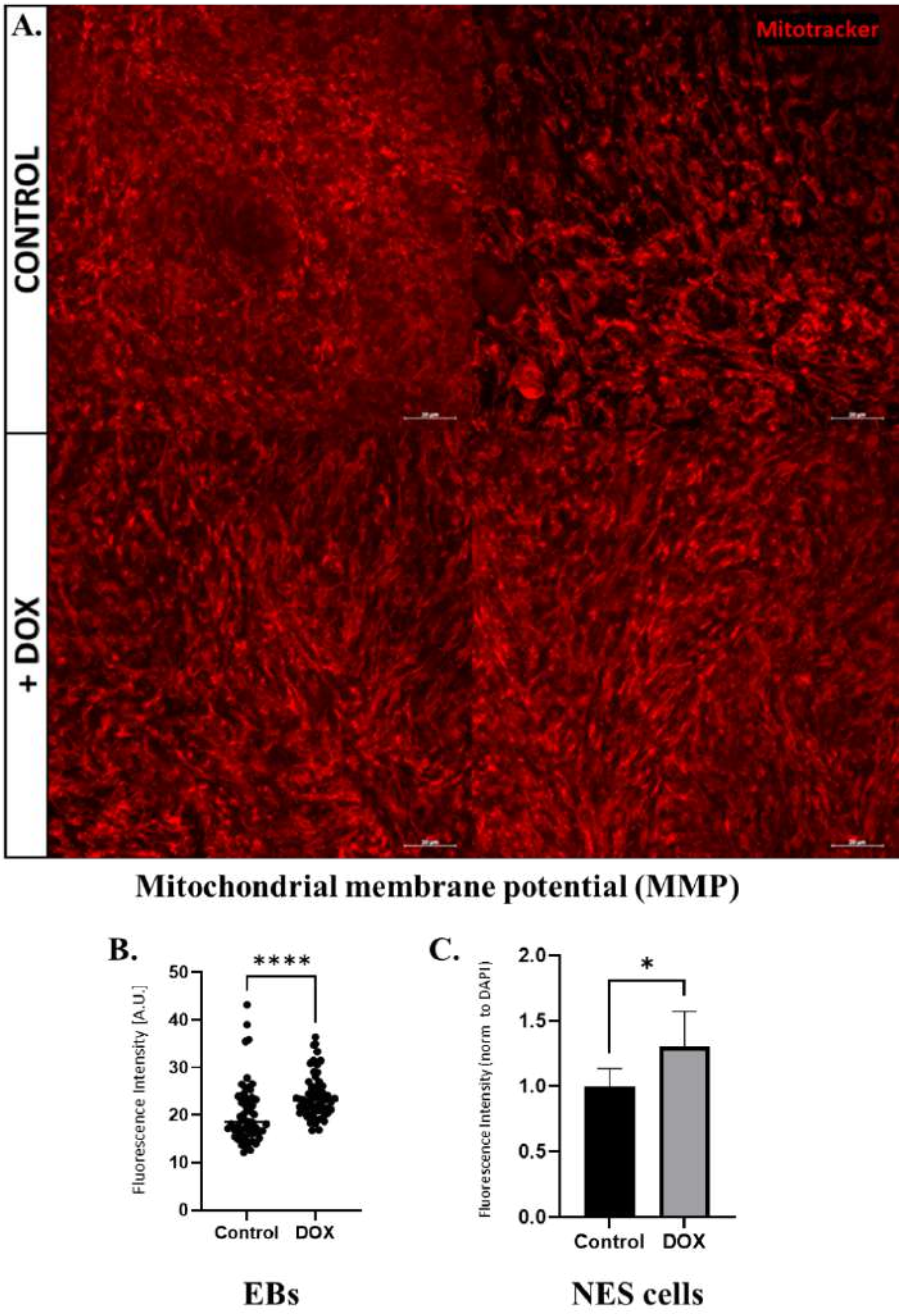

Fig.39. Examination of mitochondrial membrane potential (MMP) in the EB and NES cell models following nFGFR1 activation. *A. Representative live-cell images display mitochondria labeled with MitoTracker™ Red CMXRos (in red) within 21-day human embryoid bodies (EBs) under both control and doxycycline (DOX) conditions. Scale bars = 20 μm; B. Quantification of MitoTracker fluorescence intensity in EBs (Control: n = 60 ROIs; DOX: n = 62 ROIs) from three independent experiments. Higher fluorescence indicates elevated MMP. Data are presented as mean ± SD (****P ≤ 0.0001; Mann–Whitney test); C. MMP in NES cells treated with 2 mM DOX or DMSO (control) for 4 days was measured using MitoTracker fluorescence and normalized to cell number (Hoechst). Data are presented as mean ± SD from two technical replicates across four independent experiments (P = 0.0207; Mann–Whitney test).*

5.15. Dual nuclear and mitochondrial DNA targeting by nuclear FGFR1

Beyond its canonical membrane-associated signaling, FGFR1 has been shown to translocate to the nucleus, where it functions as a transcriptional regulator involved in developmental gene expression programs and chromatin remodeling (Decker et al., 2021; Narla et al., 2017; Stachowiak and Stachowiak, 2016; Terranova et al., 2015). In parallel, emerging evidence indicates that FGFR1 may also localize to mitochondria and modulate mitochondrial dynamics and stress responses through direct interactions with the organelle (Srisakuldee et al., 2021). To explore these dual roles in a human neurodevelopmental context, we examined the subcellular localization and genomic interactions of nFGFR1 in embryoid bodies (EBs) and NSPCs.

To determine whether nFGFR1 has dual regulatory roles in human neural models, I assessed its subcellular localization in the nucleus and mitochondria and FGFR1 binding to nuclear-encoded mitochondrial genes and mitochondrial DNA, using ChIP-seq. I used nuclear immunofluorescence (IF) imaging to determine whether that addition of doxycycline enhance FGFR1 accumulation in the nucleus of both EB and hCO models (Fig.40). Quantitative fluorescence analysis revealed a significant two-fold increase in nuclear FGFR1 intensity in EBs ($P \leq 0.0001$; Mann–Whitney test) and a significant upregulation in hCOs ($P = 0.0044$). I then performed RT-qPCR, which showed a 12-fold increase in FGFR1 transcript levels in EBs ($P \leq 0.0001$) and a six-fold increase in hCOs ($P \leq 0.0001$) upon doxycycline induction (Fig.16B). Together, these data confirm that doxycycline effectively activates nuclear FGFR1 expression.

Next, I assessed whether increased nuclear FGFR1 expression coincides with its mitochondrial translocation by quantifying FGFR1 fluorescence intensity within perinuclear mitochondria following doxycycline induction. I chose the EB model because it has loosely packed cells, larger nuclei, and less compact mitochondrial networks, making it more suitable for colocalization studies than hCO model. I observed that FGFR1 appeared as distinct puncta within perinuclear mitochondria under control conditions (Fig.40B). Quantitative assessment showed that, following doxycycline treatment, FGFR1 intensity in these mitochondria increased 1.9-fold

($P \leq 0.0001$; Mann–Whitney test). These findings confirm that nuclear upregulation of FGFR1 coincides with its translocation to and accumulation in mitochondria.

To assess whether nFGFR1 directly interacts with regulatory elements of genes associated with mitochondrial function, I examined ChIP-seq (Chromatin Immunoprecipitation followed by high-throughput Sequencing) data using an antibody against FGFR1 from the nuclei of human neural progenitor cells (NPCs). I found that nFGFR1 associates with the promoter regions of various nuclear-encoded genes essential for mitochondrial function. This includes *PINK1* (Fig.41A), as well as *BNIP3* and *FUNDC1* (data not shown in this study), all of which are key in regulating mitophagy. Surprisingly, nFGFR1 did not bind to the promoter of the *PPARGC1A* gene (PGC-1α), known as the master regulator of mitochondrial biogenesis. This suggests that its role is more focused on quality control and mitochondrial maintenance rather than biogenesis. It was further demonstrated that nFGFR1 also binds directly to mitochondrial DNA (mtDNA). The circular genome map of the mitochondrial genome (Fig.41B, provided by Dr. Georgi Marinov) shows that nFGFR1 binds directly to specific loci in mtDNA, including *MT-ATP6* and *MT-CO3*. This suggests that nFGFR1 may indirectly influence mitochondrial gene expression through nuclear regulation and direct interaction with mitochondrial DNA.

In summary, these data establish that nFGFR1 exhibits dual targeting behavior - it localizes in the nucleus (1) and within the mitochondria (2), and directly binds to both nuclear and mitochondrial genomes. Its engagement with mitophagy and mitochondrial function-related genes, along with mtDNA itself, positions nFGFR1 as a multifunctional regulator of mitochondrial homeostasis. This implicates nuclear FGFR1 as a key player in coordinating cellular energy metabolism and organelle quality during human neuronal differentiation.

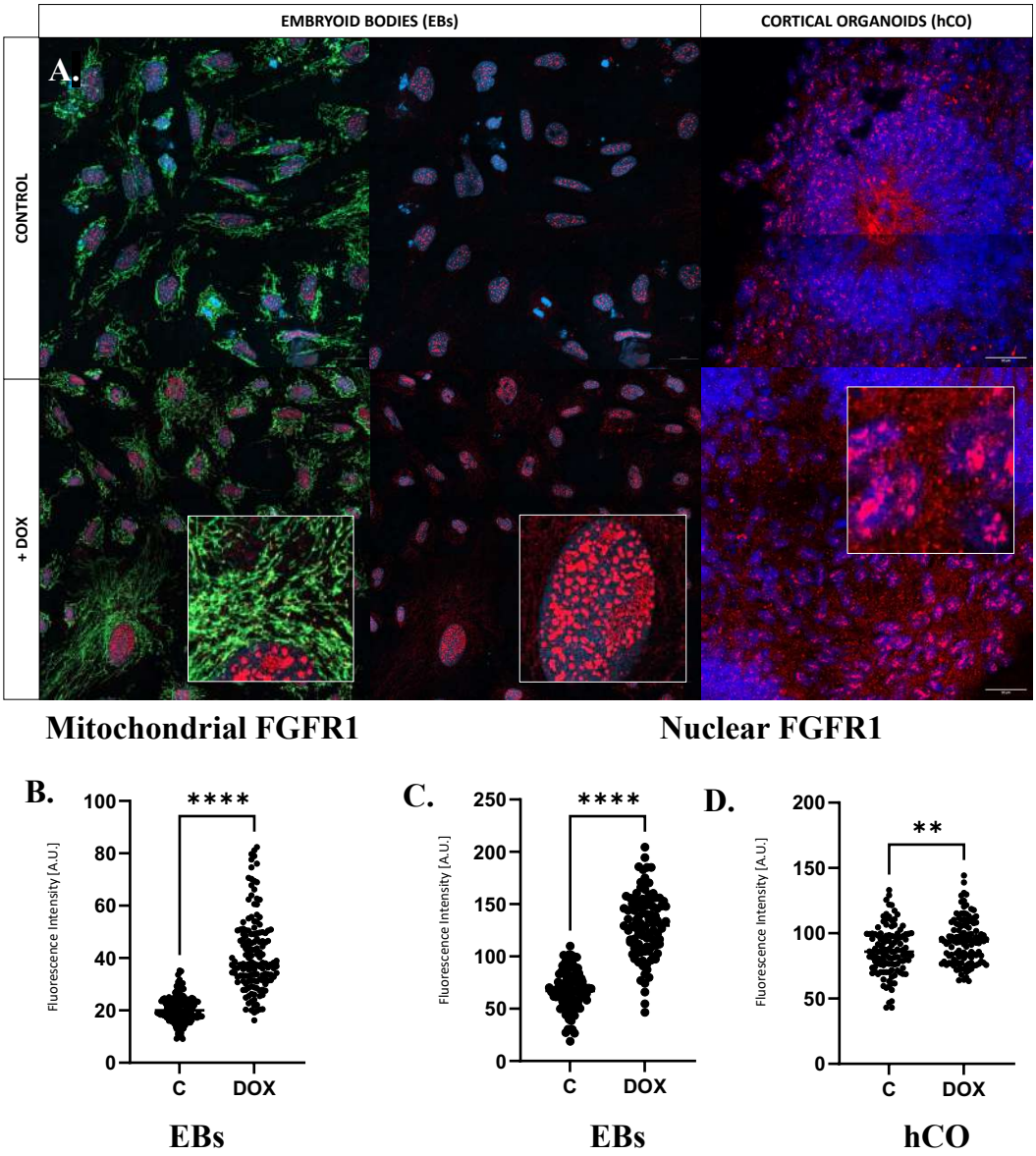

Fig.40. Accumulation of FGFR1 in nuclear and mitochondrial sites after nFGFR1 exposure upregulation. *A. Representative confocal images illustrate FGFR1 (red) and mitochondria (green) in 21-day embryoid bodies (EBs) and 60-day human cerebral organoids (hCOs) under both control (C) and doxycycline (DOX) conditions. Nuclei are counterstained with Hoechst (blue). Insets reveal FGFR1 puncta that colocalize with perinuclear mitochondria, and FGFR1 accumulation in nuclear speckles. Scale bars represent 20 µm; B. Measurement of perinuclear mitochondrial FGFR1 fluorescence in EBs (Control: n = 151 ROIs; DOX: n = 151 ROIs) across three independent experiments. Results are shown as mean ± SD (P ≤ 0.0001, Mann–Whitney test); C. Quantification of nuclear FGFR1 fluorescence in EBs (n = 100 ROIs per condition) and in the cortical layer of hCOs (n = 100 ROIs per condition), across three independent experiments. The data is presented as mean ± SD (EBs: P ≤ 0.0001; hCOs: P = 0.0044; Mann–Whitney test).*

A. ***PINK1 [1p36.12]***

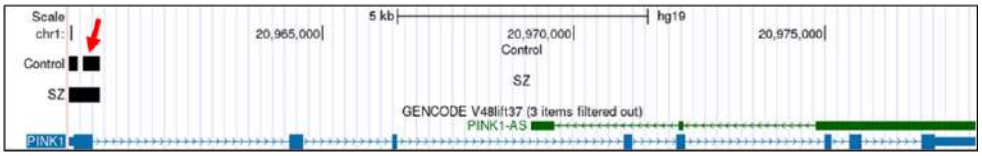

B. Mitochondrial DNA

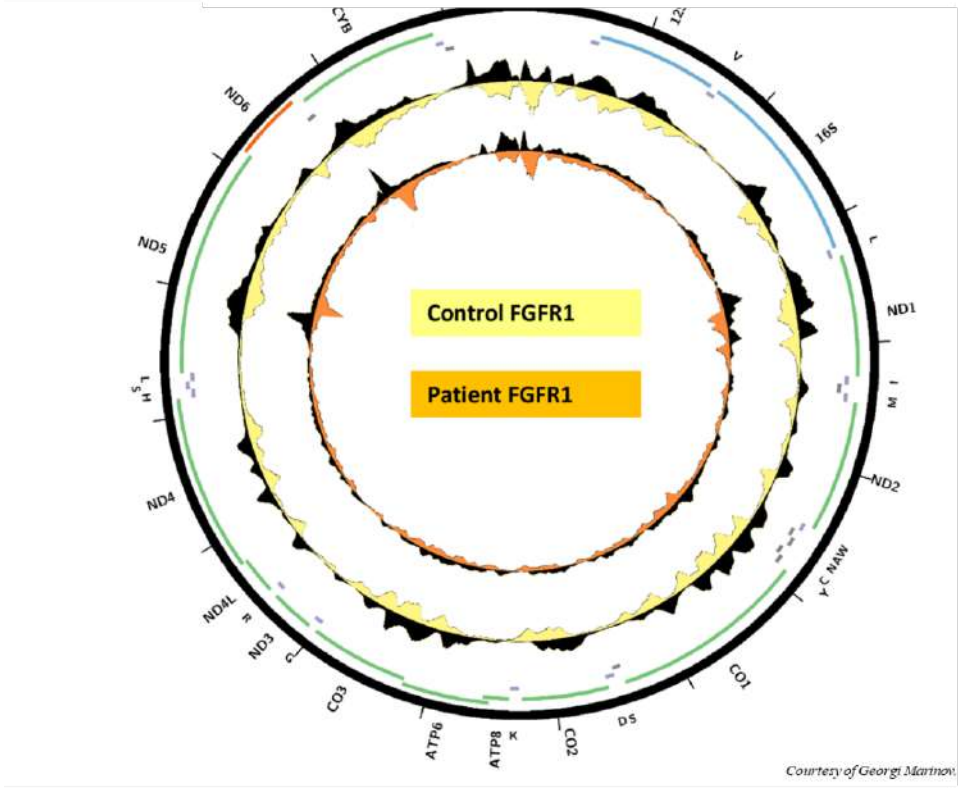

Fig.41. ChIP-seq analysis in human neural progenitor cells (NPC). *A. Genome browser visualization of FGFR1 ChIP–seq peaks at the nuclear-encoded PINK1 locus on chromosome 1. A red arrow indicates a strong concentration of FGFR1 binding peak directly overlapping the PINK1 promoter, demonstrating specific binding by nFGFR1; B. circular plot of mitochondrial DNA (mtDNA) illustrates FGFR1 binding density. The outer circle labels the 13 mtDNA genes, while the density tracks reflect FGFR1 occupancy in control (yellow) and schizophrenia patient-derived (orange) chromatin, indicating that FGFR1 is associated with the mitochondrial genome (courtesy of Georgi Marinov).*

5.16. nFGFR1 orchestrates widespread proteomic remodeling in human cortical organoids

FGFR1 is increasingly recognized not only for its role in neural development but also as a global regulator of gene expression, metabolism, cellular homeostasis, and the development and metastasis of cancer cells (Chaudhuri et al., 2024; Coetzee et al., 2023; Dhiman et al., 2024; Servetto et al., 2021). Recent evidence shows that nuclear FGFR1 (nFGFR1) can reprogram metabolic pathways, reshape the transcriptome, and modulate chromatin and proteomic landscapes to support differentiation and stress adaptation (Stachowiak et al., 2021; Terranova et al., 2015; Francavilla et al., 2017). To determine the downstream proteomic targets of nFGFR1, quantitative mass spectrometry was performed on hCOs following nFGFR1 overexpression.

In my experimental workflow (Fig.42), I utilized tandem mass tag (TMT)-based quantitative mass spectrometry to compare DMSO-treated organoids (control) with nFGFR1-overexpressing 60-day cortical organoids treated with DMSO (control) or 3 mM doxycycline (DOX) for 40 days. Principal Component Analysis (PCA) demonstrated a clear separation between control and DOX-treated samples (Fig.43A). PC1 represented 34.8% of the overall variance, while PC2 contributed an additional 26.9%. These findings suggest that nFGFR1 activation results in considerable proteomic changes (Fig.43B-C).

Through differential expression analysis, I identified 660 proteins that were significantly differentially expressed (DEPs) among a total of 5503 proteins (Fig.45). Out of these, 110 proteins showed upregulation and 87 displayed downregulation following doxycycline treatment ($P \leq 0.05$). Key upregulated proteins included FGFR1, NUCKS1, TGFBRAP1, TMSB10, and HIST1H1C, which are linked to chromatin remodeling and signal transduction. In contrast, significantly downregulated proteins such as SPOCK1, CAMKV, GRIA2, and SLC1A3 indicated a reduction in synaptic function and alterations in the extracellular matrix regulation. A heatmap of hierarchical clustering was generated from z-score normalized reporter intensity data. Distinct clusters corresponding to the control and nFGFR1 conditional upregulation were clearly observed, separating the samples (Fig.46). Additionally, the top 20 differentially expressed proteins are displayed on the axis, including GRIA2, SLC1A3, OPCML, SERPINI1, SPOCK1,

CAMKV, HPCA, TTC9, MYO5B, and SOX5 (downregulated), as well as FAM120C, HIST1H1C, FBLN2, PPP1R14C, TMSB10, FGFR1, PPP1R1B, NUCKS1, TGFBRAP1, and TUBA4A (upregulated). Notably, FGFR1 emerges as one of the most significantly upregulated proteins, emphasizing the pronounced upregulation of nFGFR1.

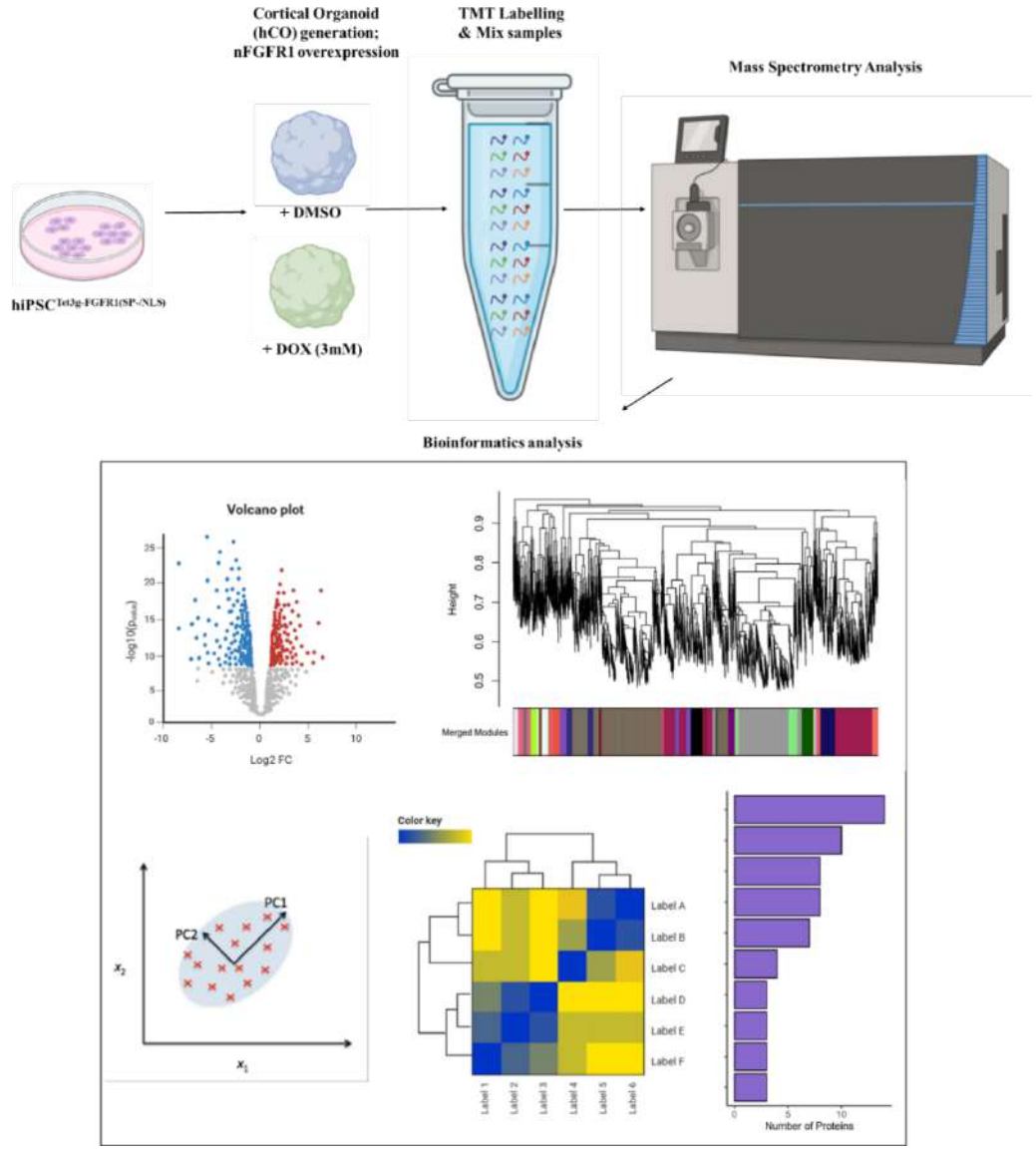

Fig.42. Workflow and data analysis for quantitative proteomics of nFGFR1 activation in hCOs*. Human cortical organoids (hCOs), derived from hiPSC*$^{CLYBL\text{-}Tet3G\text{-}FGFR1(SP\text{-}/NLS)\text{-}mApple}$*, were treated with doxycycline (3 mM) or DMSO from day 20 to day 60. After treatment, they were snap-frozen and subjected to TMT labeling and LC–MS/MS analysis (top). The resulting proteomic data were then processed using PCA (bottom left), hierarchical clustering, and heatmap visualization (bottom center), as well as weighted gene co-expression network analysis (WGCNA) for module detection (top right, dendrogram and color bar). Additionally, volcano plotting and pathway enrichment analyses were performed for differentially expressed proteins (DEP; bottom right bar graph).*

Weighted gene co-expression network analysis (WGCNA) is a powerful systems biology approach that constructs weighted correlation networks to identify modules of co-expressed proteins and hub genes associated with specific phenotypes (Ghafouri-Fard et al., 2023; Short et al., 2023; Wang et al., 2023). To investigate co-regulated protein networks, I utilized WGCNA on my proteomic dataset to identify nFGFR1-responsive protein modules and delineate the functional pathways driven by nFGFR1 upregulation. In this analysis, proteomics data were grouped into separate modules, with the "Bisque4" and "Maroon" modules showing the strongest correlation following nFGFR1 conditional upregulation (Fig.44A). GO enrichment analysis for "Bisque4" (781 proteins), revealed processes related to neuronal projection (GO:0010975), axonogenesis (GO:0007409), and the synaptic vesicle cycle (GO:0099504). On the other hand, the "Maroon" module (777 proteins) showed enrichment for mitochondrial energy-related terms such as ATP synthesis coupled electron transport (GO:0042773) and cellular respiration. Other significant modules include "Darkgrey," which is associated with ribosome biogenesis (GO:0042254) and DNA replication (GO:0006260), alongside "Antiquewhite4," linked to RNA splicing (GO:0000375) and mitochondrial translation (GO:0032543; Fig.44B-D). Moreover, modules such as "Midnightblue" and "Mediumpurple3" demonstrated enrichment for autophagy (GO:0016236), telomere maintenance (GO:0032206), and mitochondrion organization (GO:0007005) (not shown in this study). Gene ontology enrichment analysis identifies whether predefined GO categories are overrepresented in a gene list, which allows for the biological interpretation of proteomics data (Tomczak et al., 2018). The functional annotation of DEPs through Gene Ontology (GO) terms showed that the upregulated biological processes were associated with mitochondrial gene expression (GO:0140053), lysosome organization (GO:0007040), and vesicle budding (GO:0006900) (Fig.47A). Additionally, cellular components such as the vacuolar lumen (GO:0005775) and mitochondrial protein-containing complex (GO:0098798) also exhibited significant enrichment (Fig.47B). The identified molecular functions included cadherin binding (GO:0045296), ribosome structural constituents (GO:0003735), and hydrolase activities (GO:0016798) (Fig.47C). Conversely, the downregulated proteins were enriched in processes such as oxidative phosphorylation (GO:0006119), the electron transport chain (GO:0022900), and the ATP biosynthetic process

(GO:0006754) (Fig.47D). Additionally, there was a reduction in mitochondrial components, including the respiratory chain complex (GO:0098803) and the NADH dehydrogenase complex (GO:0030964) (Fig.47E). nFGFR1 suppression affected molecular functions such as proton transmembrane transporter activity (GO:0015078), NADH dehydrogenase activity (GO:0008137), and oxidoreductase activity (GO:0016655), which indicate compromised mitochondrial respiration and redox balance (Fig.47F).

In summary, the proteomic data reveals that the conditionally increased expression of nuclear FGFR1 significantly influences protein expression in cortical organoids. This leads to an increase in mitochondrial gene expression and lysosomal activity, alongside a reduction in oxidative phosphorylation and synaptic signaling components. Such alterations indicate a metabolic and structural reprogramming that promotes biosynthesis and degradation rather than energy production, which may be responsible for the altered neuronal differentiation and maturation seen in organoids following nFGFR1 conditional upregulation.

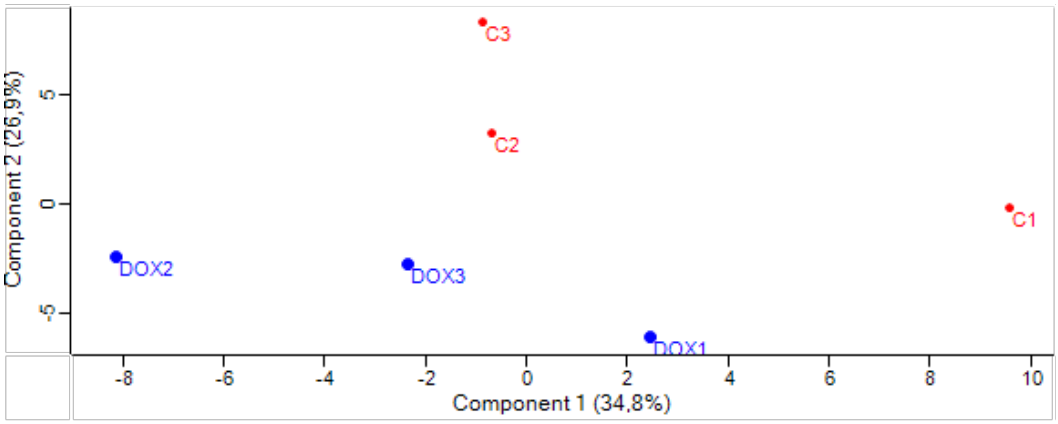

Fig.43. Principal component analysis (PCA) of proteomic profiles in human cortical organoids (hCOs) following nFGFR1 conditional upregulation. *PCA was conducted on log_2-transformed protein intensity values normalized by median subtraction; samples treated with doxycycline (red) and the DMSO control (blue) form two distinct clusters, with PC1 explaining 34.8% of the variance and PC2 accounting for 26.9%.*

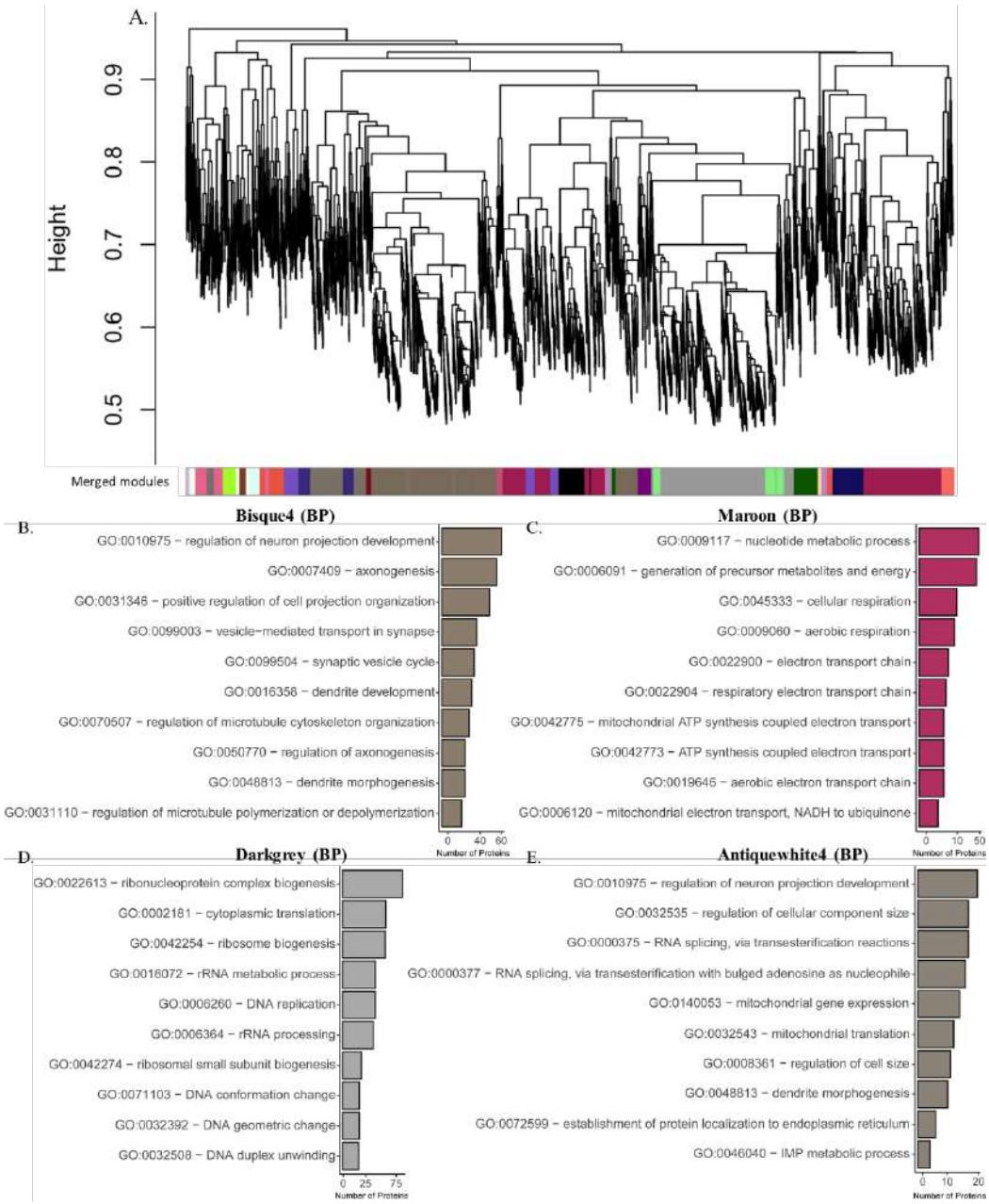

Fig.44. Weighted correlation network analysis (WGCNA) identifies co-expression modules after nFGFR1 upregulation in hCOs. *A. Hierarchical clustering dendrogram of 5,503 proteins from 60-day hCOs (DOX vs. control) identifies 24 co-expression modules (color bar). Modules were defined using the dynamic tree-cut method and merged based on module correlation (p, q ≤ 0.05); B. Gene ontology "Biological Process" (GO-BP) enrichment for the Bisque4 module (781 proteins) revealed significant enrichment in neuron development, axonogenesis, synaptic vesicle cycling, and dendrite morphogenesis (p, q ≤ 0.05); C. GO-BP enrichment for the Maroon module (777 proteins) indicated a significant enrichment of energy metabolism processes, including cellular respiration, the electron transport chain, and ATP synthesis (p, q ≤ 0.05). Enrichments were calculated using a Fisher's exact test with Benjamini–Hochberg correction (p, q ≤ 0.05). D. GO-BP enrichment for the Darkgrey module (687 proteins) demonstrated significant enrichment of terms associated with ribosome biogenesis, rRNA processing, cytoplasmic translation, and DNA replication (p, q ≤ 0.05); E. GO-BP enrichment for the Antiquewhite4 module (366 proteins) revealed significant enrichment of processes related to neuron projection regulation, RNA splicing, mitochondrial gene expression, and protein localization to the*

endoplasmic reticulum. Enrichments were calculated using a Fisher's exact test with Benjamini–Hochberg correction (p, q ≤ 0.05).

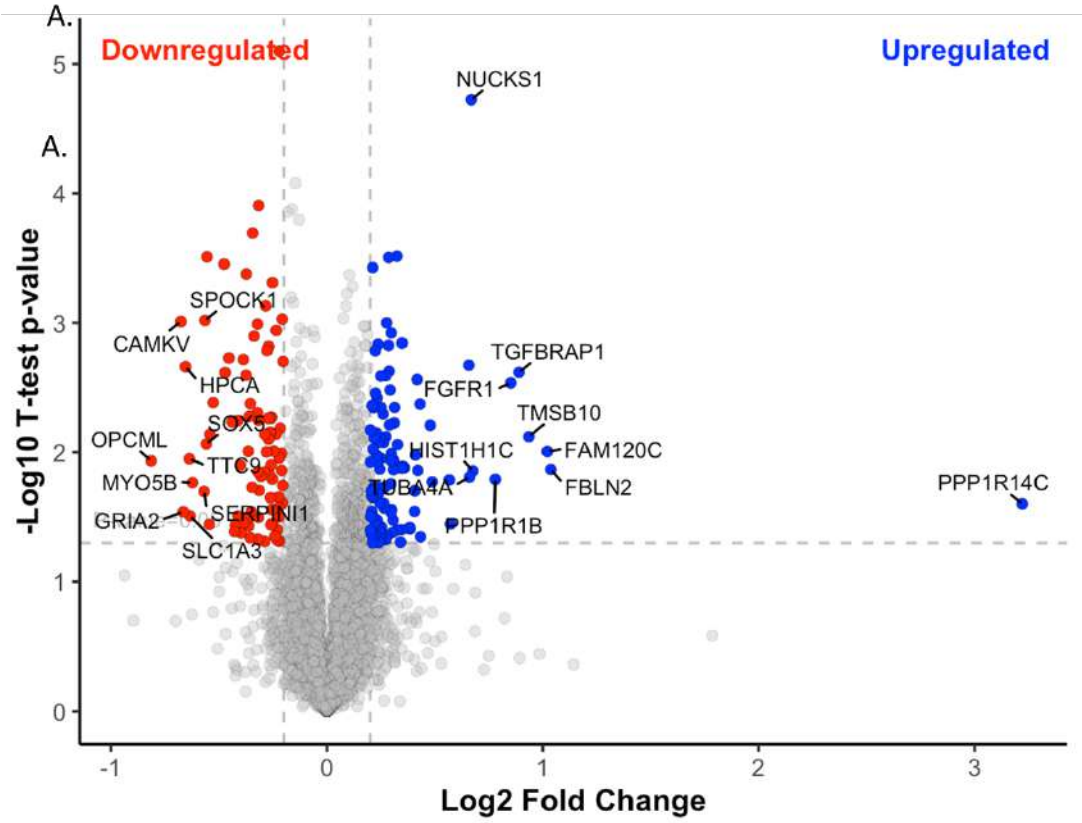

B.

	Proteins
Downregulated (p>0,05; FC<-0,2)	87
Downregulated Trend	2516
Upregulated (p>0,05; FC>0,2)	110
Upregulated Trend	2790

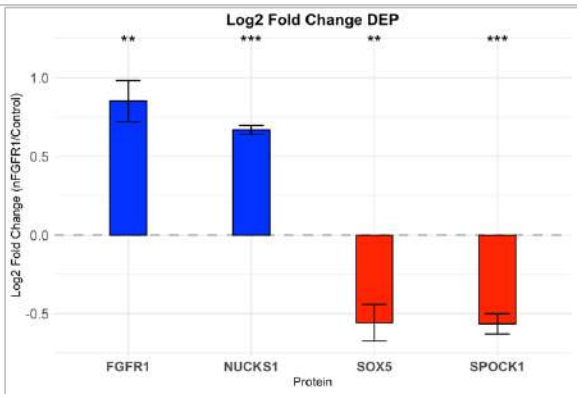

Fig.45. Differentially expressed proteins (DEPs) in hCOs after nFGFR1 upregulation. *A. Volcano plot. Each point corresponds to one of 5,503 quantified proteins. The x-axis displays log_2 fold change (DOX vs. control), where positive values reflect upregulation and negative values denote downregulation. The y-axis illustrates $–log_{10}$ p-values from two-tailed t-tests, with greater values indicating stronger statistical validation. Vertical dashed lines represent ±0.2 log_2 fold-change, while the horizontal dashed line marks $–log_{10}$ (0.05). Proteins that meet both criteria thresholds (log_2 FC ≥ 0.2; P ≤ 0.05) are highlighted in blue (upregulation) or red (downregulation) and annotated by names; B. Protein Expression Trend. Table classifies each protein into one of four categories based on its log_2 fold-change (FC) and p-value from the proteomics analysis: Significantly Upregulated (Log_2FC ≥ 0.2; P ≤ 0.05); Significantly Downregulated (Log_2FC ≤ –0.2; P ≤ 0.05); Positive Trend (0 < Log_2FC); Negative Trend (Log_2FC < 0); C. Plot for Top 4 DEP proteins Plot. Bar graph showing log_2 fold changes (mean ± SD) for the four most differentially expressed*

*proteins: FGFR1 and NUCKS1 (up), SOX5 and SPOCK1 (down). P ≤ 0.01, **P ≤ 0.001, p *** ≤ 0.0001*

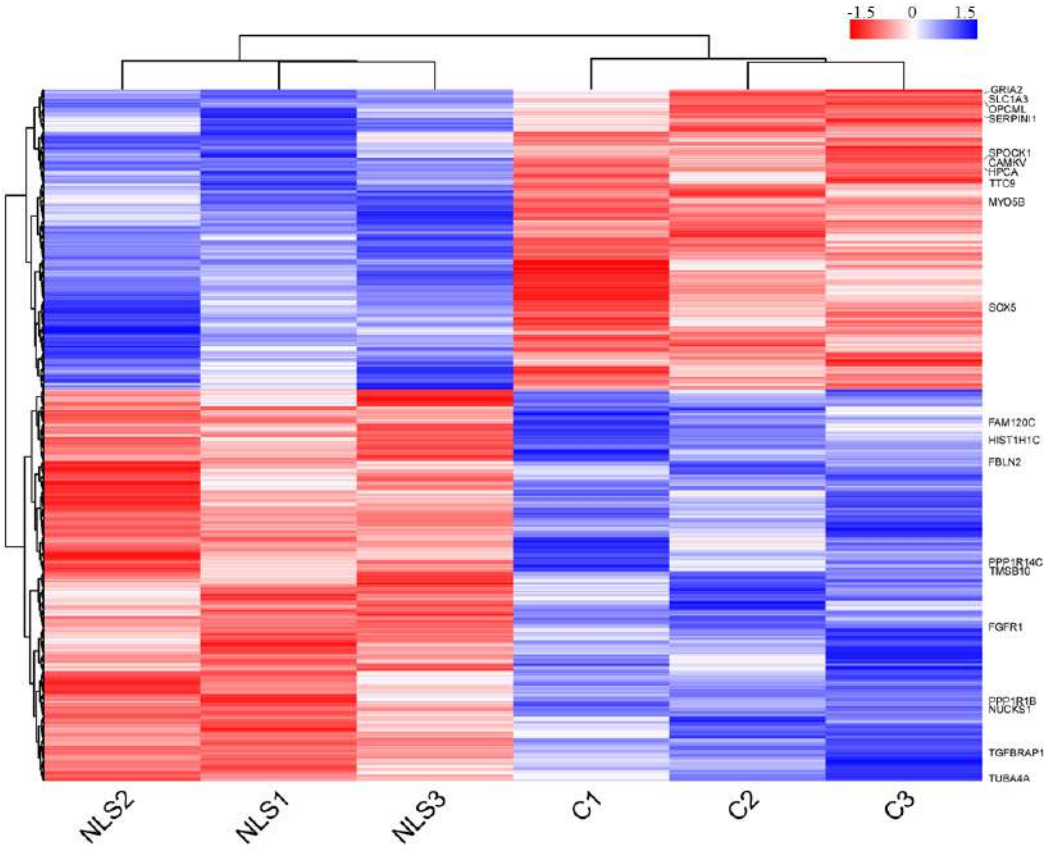

Fig.46. Hierarchical Clustering Heatmap for differentially expressed proteins (DEPs) in 60-day hCOs after nFGFR1 upregulation. *The heatmap presents a hierarchical clustering analysis of differentially expressed proteins (DEPs) in hCO, treated with either 3 mM doxycycline (DOX) or DMSO (Control). Z-score normalized expression values were utilized to cluster both genes and samples applying Ward's method. The samples were divided into two experimental conditions: C (control) and NLS (nFGFR1 upregulation). A total of 660 DEPs are represented in the heatmap. The red–blue color scale reflects relative protein abundance, with red and blue indicating up- and down-regulated proteins, respectively. To enhance clarity, sample labels are bolded, and the gene names of the Top 20 DEPs are emphasized. The clustering reveals distinct expression patterns between treatment groups, underscoring the transcriptional changes caused by nFGFR1 upregulation.*

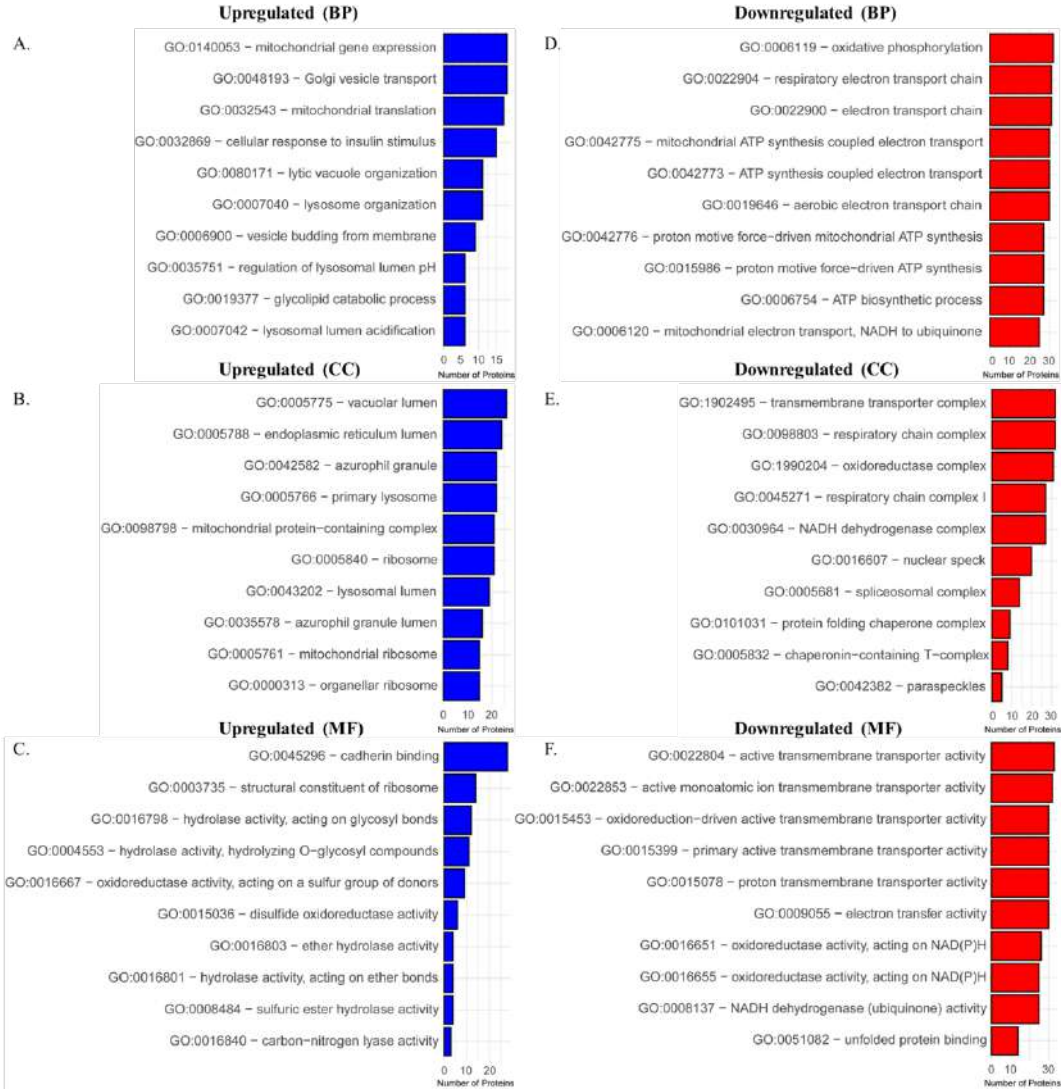

Fig.47. Gene Ontology (GO) enrichment analysis for differentially expressed proteins (DEPs) after nFGFR1 activation in 60-day hCOs. *Proteins exhibiting log_2 FC > 0 and an p-value ≤ 0.05 were classified as significantly upregulated or downregulated following DOX or DMSO (Control) treatment. Distinct lists of upregulated and downregulated differentially expressed proteins (DEPs) were analyzed for enrichment across three Gene Ontology (GO) categories: Biological Process (BP), Cellular Component (CC), and Molecular Function (MF). The bars represent the number of DEPs corresponding to each GO term. Enrichment analysis was performed using Fisher's exact test with Benjamini–Hochberg correction (q ≤ 0.05). Panels A–C display upregulated DEPs, while D-F show downregulated DEPs.*

5.17. Dual modulation of neurogenic and synaptic pathways by nFGFR1 in cortical organoids

FGFR1 signaling is essential for regulating neuronal subtype identity, axon targeting, and the assembly of functional neural circuits during early brain development (Gantner et al., 2021; Stachowiak and Stachowiak, 2016; Tomé et al., 2023; Vaccarino et al., 1999). Recent studies shows that FGFR1 governs forebrain

patterning and synaptic connectivity by fine-tuning neurodevelopmental gene expression programs. To assess how nuclear FGFR1 (nFGFR1) impacts these developmental processes, I performed ontology-guided proteomic analyses on human cortical organoids, focusing on pathways involved in neuronal development (GO:0048666), forebrain development (GO:0030900), axonogenesis (GO:0007409), and synaptic proteins (GO:0045202).

In total, I identified 836 proteins associated with neuronal development (GO:0048666). Among these, 15 were significantly upregulated, while 26 were downregulated following nFGFR1 induction in hCOs (Fig.48). The key downregulated proteins included BCL11B, SOX5, and NCAM2, which play crucial roles in neuronal subtype specification, migration, and synapse formation, respectively. Additionally, the upregulated proteins such as FGFR1 (including transduced FGFR1(SP-/NLS), TBR1 (linked to the differentiation of cortical excitatory neurons), and SLIT2 (involved in axon guidance) indicate the activation of alternative neurogenic mechanisms. Furthermore, GO enrichment analysis (Fig.49) of downregulated proteins revealed enrichment of terms such as forebrain development (GO:0030900), telencephalon development (GO:0021537), and hindbrain development (GO:0030902). On the other hand, the upregulated proteins were enriched in processes such as limb development (GO:0060173) and lysosome organization (GO:0007040).

In the subset of 157 proteins annotated under forebrain development (GO:0030900), I found that seven proteins were upregulated while nine were downregulated (Fig.50). The suppressed expression of BCL11B and FOXG1 suggests disrupted cortical patterning and telencephalic identity, while elevated levels of TBR1 and SLIT2 imply a selective enhancement of neuronal fate commitment and axon guidance. Additionally, GO enrichment analysis identified terms such as forebrain development (GO:0030900), telencephalon development (GO:0021537), pallium development (GO:0021543), and cerebral cortex development (GO:0021987), which were represented in both my upregulated and downregulated gene groups (Fig.51). This suggests a dual regulation - simultaneously activating and impairing distinct neurodevelopmental sub-pathways following nFGFR1 conditional increased expression.

In the context of axonogenesis (GO:0007409), I identified 156 proteins, with six being upregulated and five downregulated (Fig.52). The reduced expression

of EPHA4, PARD3, FOXC1, and BCL11B suggests a disruption in axonal guidance, polarity, and differentiation. However, the upregulation of SLIT2, ECE1, and BAIAP2 indicates compensatory mechanisms that facilitate axon extension and cytoskeletal dynamics remodeling. Additionally, GO enrichment analysis revealed a significant downregulation of axonogenesis (GO:0007409) and related terms, such as neuron projection guidance (GO:0097485), axon guidance (GO:0007411), and forebrain neuron differentiation (GO:0021879). Conversely, upregulated proteins were enriched in terms such as the regulation of nervous system processes (GO:0031644) and the response to epidermal growth factor stimulus (GO:0071364) (Fig.53).

In my analysis of synaptic proteins (GO:0045202), I observed a clear downregulation trend, where 22 proteins were significantly suppressed, while only seven were upregulated (Fig.54). Downregulated proteins, such as GRIA2 (AMPA receptor), SYN2 (synapsin), CPLX2 (complexin), SNCA (alpha-synuclein), and SEZ6, are essential for synaptic vesicle function and neurotransmitter activity. Additionally, GO enrichment analysis of downregulated proteins (Fig.54B) identified pathways that include the synaptic vesicle cycle (GO:0099504), vesicle-mediated transport in the synapse (GO:0099003), signal release from the synapse (GO:0099643), neurotransmitter secretion (GO:0007269), and regulation of postsynaptic membrane potential (GO:0060078). These findings collectively support a model suggesting that nFGFR1 reduces synaptic transmission, which may hinder neuronal communication and plasticity in developing organoids.

In summary, proteomic analyses indicate that nFGFR1 upregulation alters neurodevelopmental pathways in cortical organoids through a complex dual-regulatory mechanism. While some transcriptional regulators and signaling factors, such as TBR1 and SLIT2, are upregulated - potentially promoting differentiation and connectivity - others essential for regional brain patterning (BCL11B, FOXG1), axonal formation (EPHA4, PARD3), and synaptic transmission (GRIA2, CPLX2) are downregulated. This dual regulatory effect suggests that nFGFR1 modulates cortical maturation by selectively enhancing and inhibiting neurodevelopmental programs, reshaping both the structural and functional elements of neuronal circuitry.

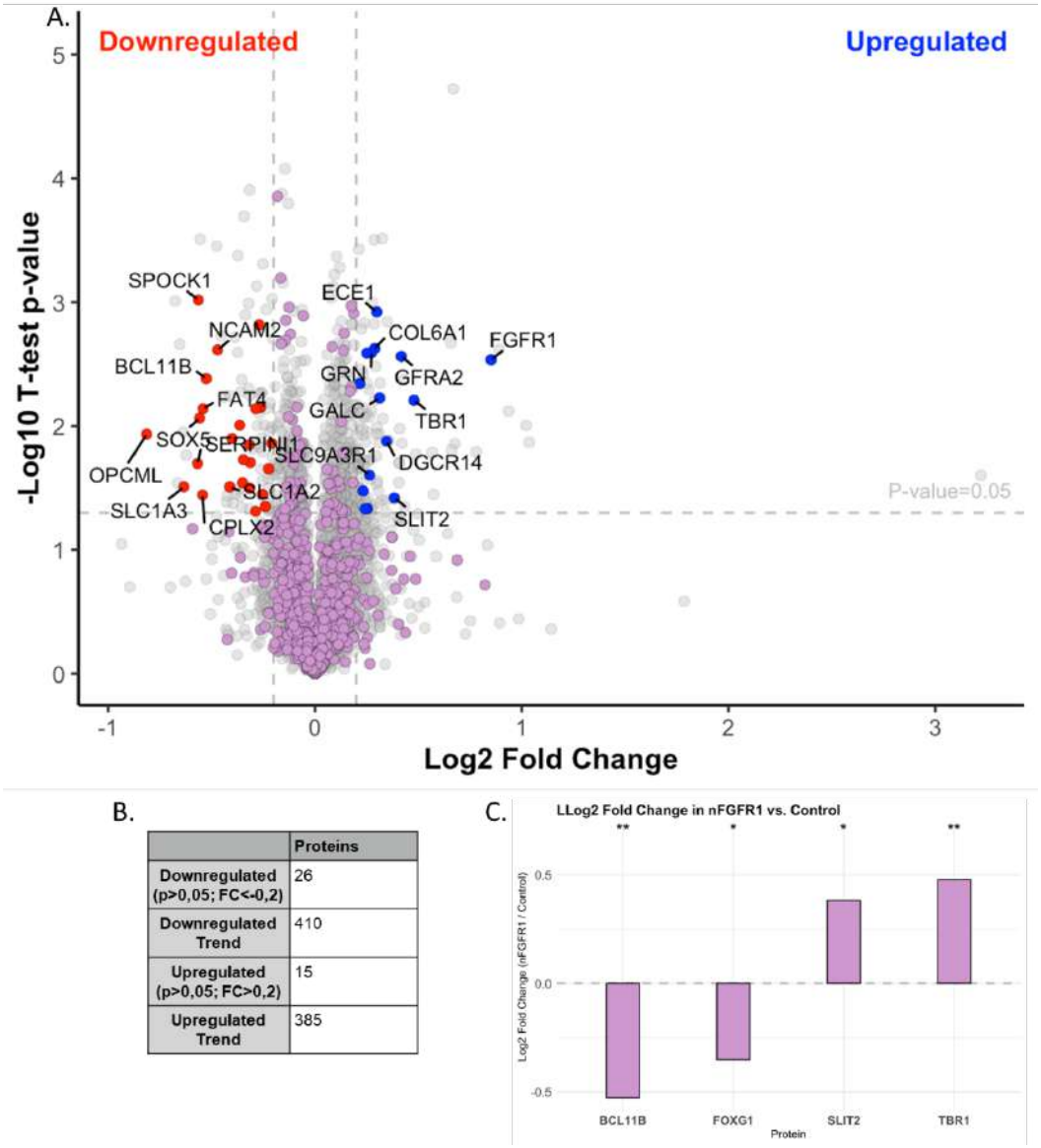

	Proteins
Downregulated (p>0,05; FC<-0,2)	26
Downregulated Trend	410
Upregulated (p>0,05; FC>0,2)	15
Upregulated Trend	385

Fig.48. Proteins involved in neuronal development in hCOs after nFGFR1 upregulation. *A. Volcano plot. A total of 836 proteins related to neuronal development (GO:0048666) were identified in the total proteome (hCOs) treated with DOX and DMSO (control). Proteins related to neuronal development are displayed as purple circles. The x-axis displays log_2 fold changes (DOX vs. control), where positive values reflect upregulation and negative values denote downregulation. The y-axis illustrates $-log_{10}$ p-values from two-tailed t-tests, with greater values indicating stronger statistical validation. Vertical dashed lines represent ±0.2 log_2 fold change, while the horizontal dashed line marks $-log_{10}$ (0.05). Proteins meeting both criteria thresholds (log_2 FC ≥ 0.2; P ≤ 0.05) are marked in blue (upregulation) and in red (downregulation) and are annotated with names. B. Protein Expression Trend Categories. Table classifies each protein into one of four categories based on its log_2 fold-change (FC) and p-value: Significantly Upregulated ($Log_2FC \geq 0.2$; $P \leq 0.05$); Significantly Downregulated ($Log_2FC \leq -0.2$; $P \leq 0.05$); Positive Trend ($0 < Log_2FC$); Negative Trend ($Log_2FC < 0$); C. Plot for Top 4 DEP proteins. The bar graph shows mean ± SD log_2 fold change for the four most strongly regulated proteins associated with neuronal development: FGFR1, NUCKS1 (Upregulated), SOX5, and SPOCK1 (Downregulated). Asterisks denote statistical significance (*P ≤ 0.05; **P ≤ 0.01; ***P ≤ 0.001; ****P ≤ 0.0001).*

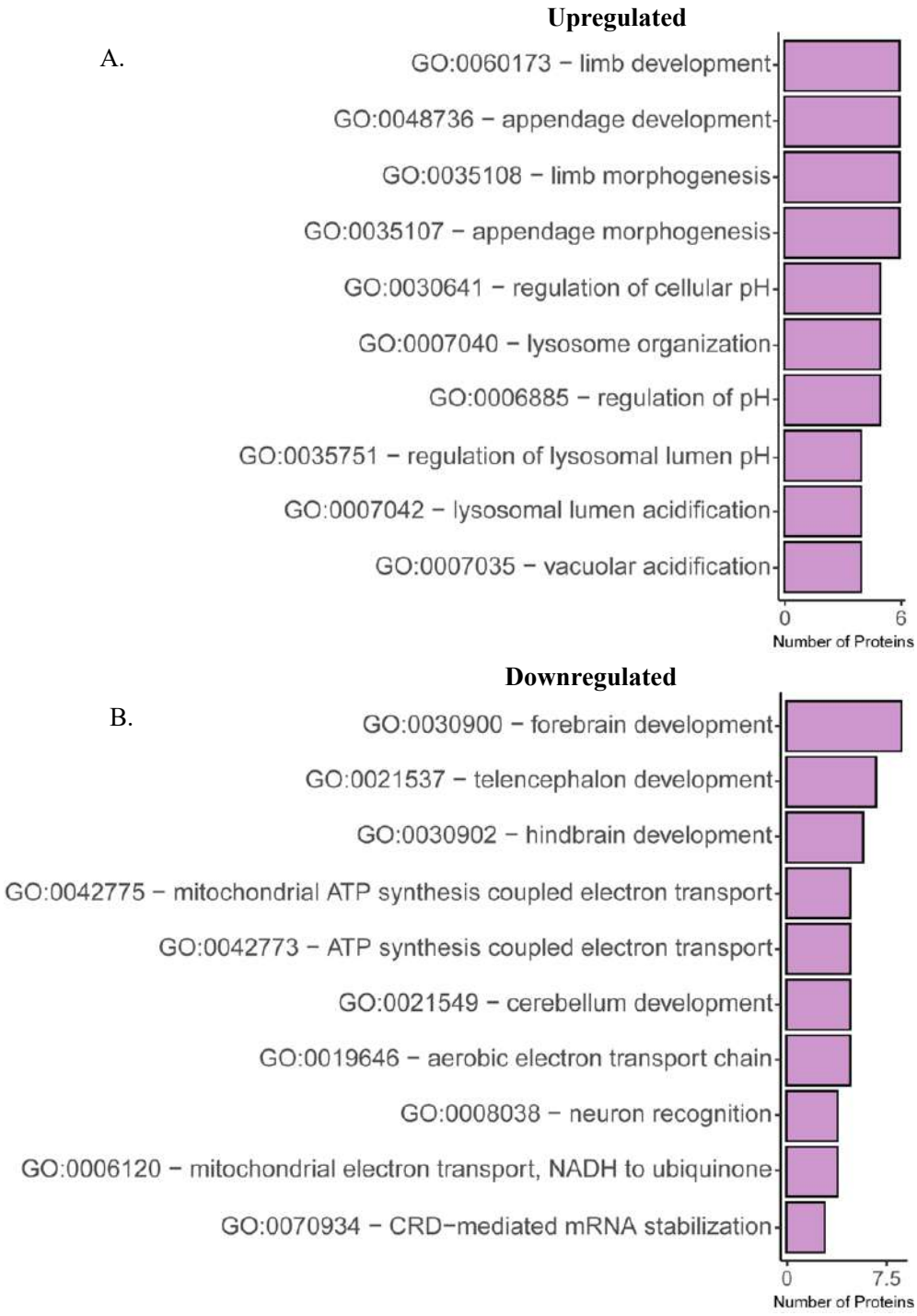

Fig.49. GO enrichment of neuronal development processes after nFGFR1 activation in hCOs*. Bar charts display the top ten GO biological processes (BP) enriched in differentially expressed proteins (DEPs) associated with "neuronal development" (GO:0048666) in 60-day hCOs after nFGFR1 upregulation. Panel A illustrates the ten biological processes significantly enriched among upregulated proteins, while Panel B shows the ten processes enriched among downregulated proteins. Enrichment was assessed using proteins with* $\log_2 FC > 0$ *(upregulated) or* < 0 *(downregulated) and* $P \leq 0.05$*. Each bar reflects the number of differentially expressed proteins linked to that GO term.*

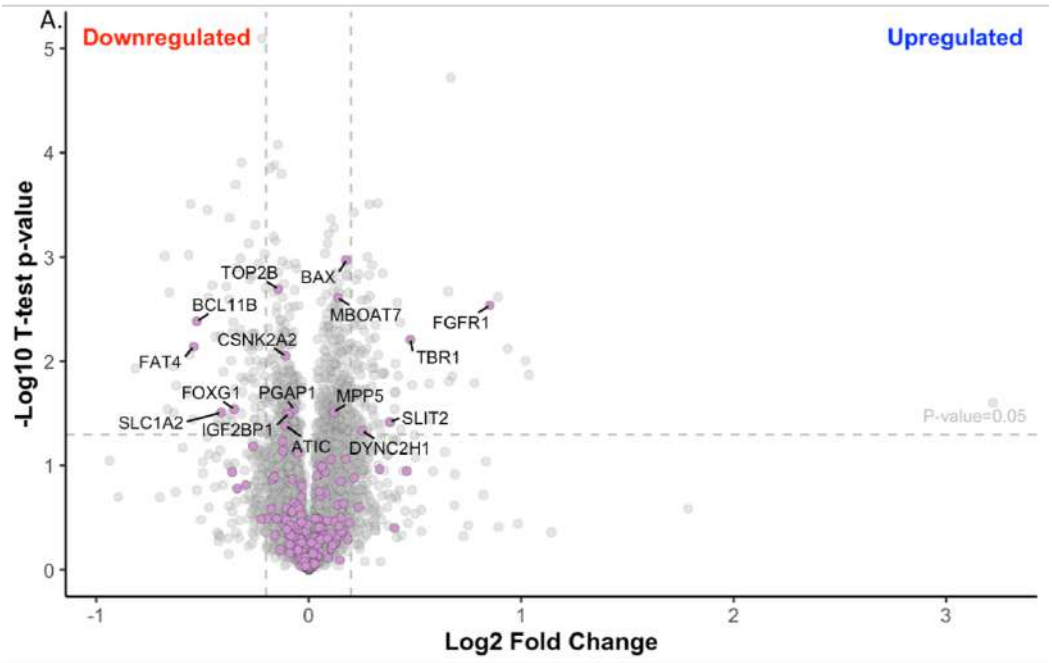

B.

	Proteins
Downregulated (p>0,05; FC<-0,2)	9
Downregulated Trend	71
Upregulated (p>0,05; FC>0,2)	7
Upregulated Trend	70

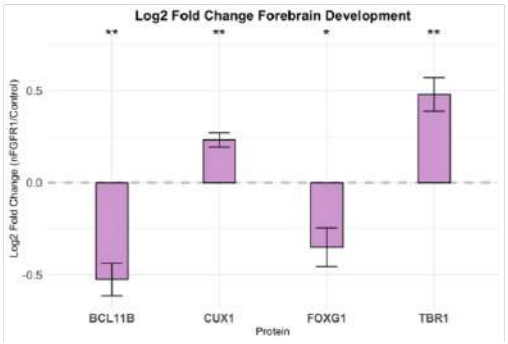

Fig.50. Proteins involved in forebrain development within hCOs following nFGFR1 upregulation. *A. Volcano plot. A total of 157 proteins related to forebrain development (GO:0030900) were identified in the total proteome (hCOs) treated with DOX and DMSO (control). Among these, 7 proteins were significantly upregulated (Log2FC > 0 ; p-value ≤ 0.05), while 9 proteins were significantly downregulated. Proteins related to forebrain development are displayed as purple circles. The x-axis displays log_2 fold changes (DOX vs. control), where positive values reflect upregulation and negative values denote downregulation. The y-axis illustrates $–log_{10}$ p-values from two-tailed t-tests, with greater values indicating stronger statistical validation. Vertical dashed lines represent ±0.2 log_2 fold change, while the horizontal dashed line marks $–log_{10}$ (0.05). Proteins that meet the significance threshold (P ≤ 0.05) are annotated with names. B. Protein Expression Trend Categories. Table classifies each protein into one of four categories based on its log_2 fold-change (FC) and p-value: Significantly Upregulated ($Log_2FC > 0$; P ≤ 0.05); Significantly Downregulated ($Log_2FC < 0$; P ≤ 0.05); Positive Trend ($0 < Log_2FC$); Negative Trend ($Log_2FC < 0$); C. Plot for Top 4 DEP proteins. The bar graph shows mean ± SD log_2 fold change for the four most strongly regulated proteins associated with neuronal development: CUX1, TBR1 (Upregulated), BCL11B, and FOXG1 (Downregulated). Asterisks denote statistical significance (*P ≤ 0.05; **P ≤ 0.01; ***P ≤ 0.001; ****P ≤ 0.0001).*

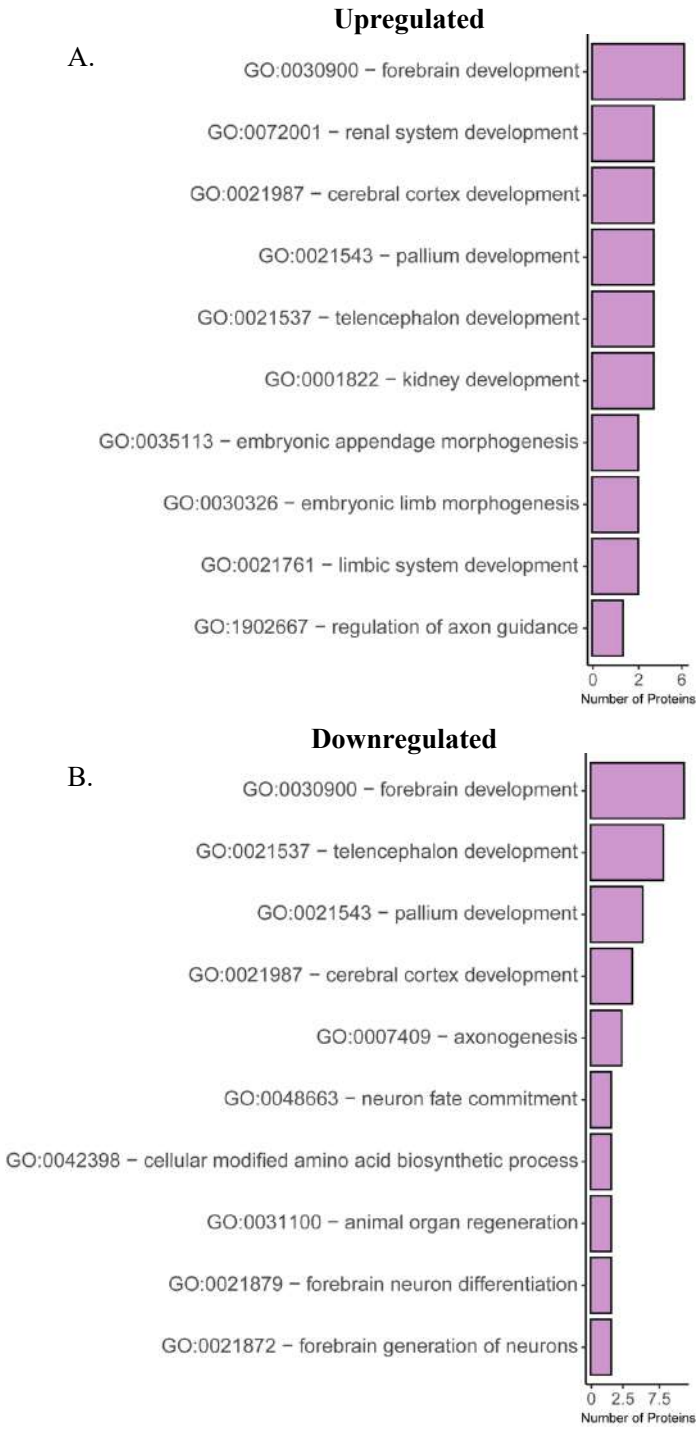

Fig.51. GO enrichment of forebrain development (GO:0030900) processes after nFGFR1 induction in hCOs. *Bar charts illustrate the top ten GO biological processes (BP) enriched in differentially expressed proteins (DEPs) annotated to forebrain development (GO:0030900) in 60-day hCOs following nFGFR1 upregulation. Panel A displays the top ten biological processes significantly enriched among upregulated proteins, while Panel B presents the top ten processes enriched among downregulated proteins. Enrichment was determined using proteins with* $\log_2 FC > 0$ *(upregulated) or* < 0 *(downregulated) and* $P \leq 0.05$*. Each bar represents the number of differentially expressed proteins contributing to that GO term.*

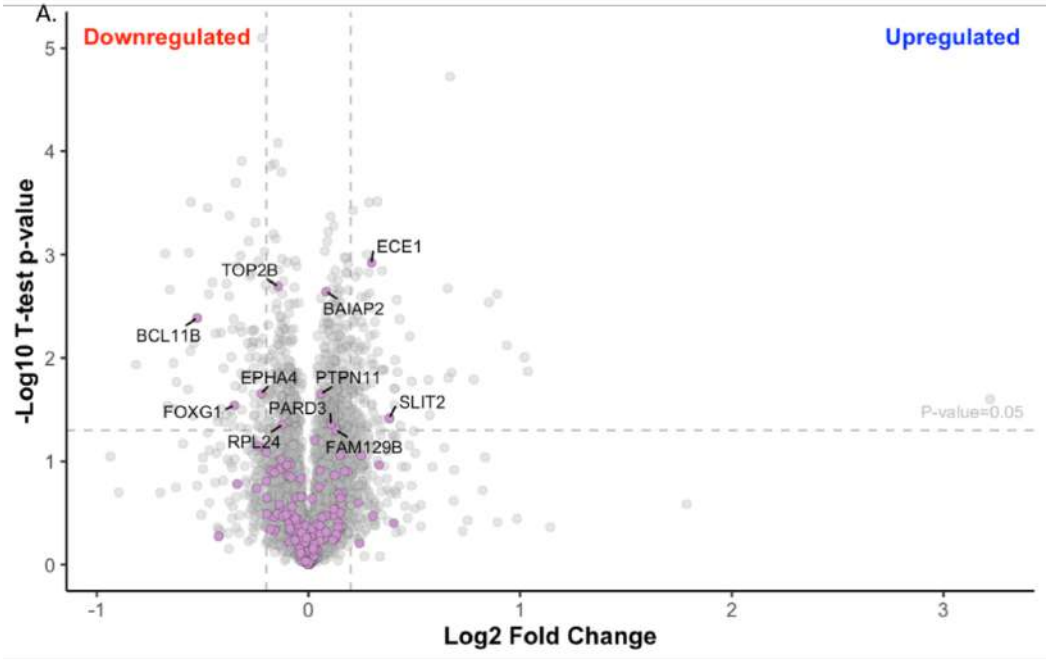

B.

	Proteins
Downregulated (p>0,05; FC<-0,2)	5
Downregulated Trend	78
Upregulated (p>0,05; FC>0,2)	6
Upregulated Trend	67

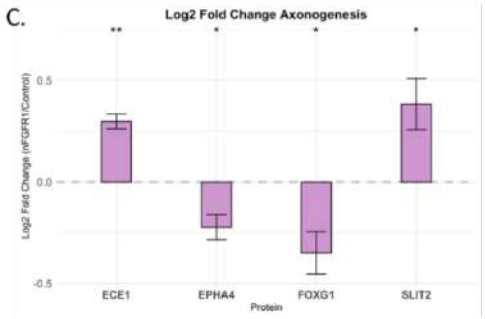

Fig.52. nFGFR1 induction alters the abundance of axonogenesis-related proteins in hCOs. *A. Volcano plot. A total of 156 proteins related to axonogenesis (GO:0007409) were identified in the total proteome (hCOs) treated with DOX and DMSO (control). Among these, six proteins were significantly upregulated (Log2FC > 0 ; p-value ≤ 0.05), while five proteins were significantly downregulated. Proteins related to axonogenesis are displayed as purple circles. The x-axis displays log_2 fold changes (DOX vs. control), where positive values reflect upregulation and negative values denote downregulation. The y-axis illustrates $–log_{10}$ p-values from two-tailed t-tests, with greater values indicating stronger statistical validation. Vertical dashed lines represent ±0.2 log_2 fold change, while the horizontal dashed line marks $–log_{10}$ (0.05). Proteins that meet the significance threshold (P ≤ 0.05) are annotated with names. B. Protein Expression Trend. Table classifies each protein into one of four categories based on its log_2 fold-change (FC) and p-value: Significantly Upregulated ($Log_2FC > 0$; $p < 0.05$); Significantly Downregulated ($Log_2FC < 0$; $P \leq 0.05$); Positive Trend ($0 < Log_2FC$); Negative Trend ($Log_2FC < 0$); C. Plot for Top 4 DEP proteins. The bar graph shows mean ± SD log_2 fold change for the four most strongly regulated proteins associated with axonogenesis: ECE1, SLIT2 (Upregulated), EPHA4, and FOXG1 (Downregulated). Asterisks denote statistical significance (*P ≤ 0.05; **P ≤ 0.01; ***P ≤ 0.001; ****P ≤ 0.0001).*

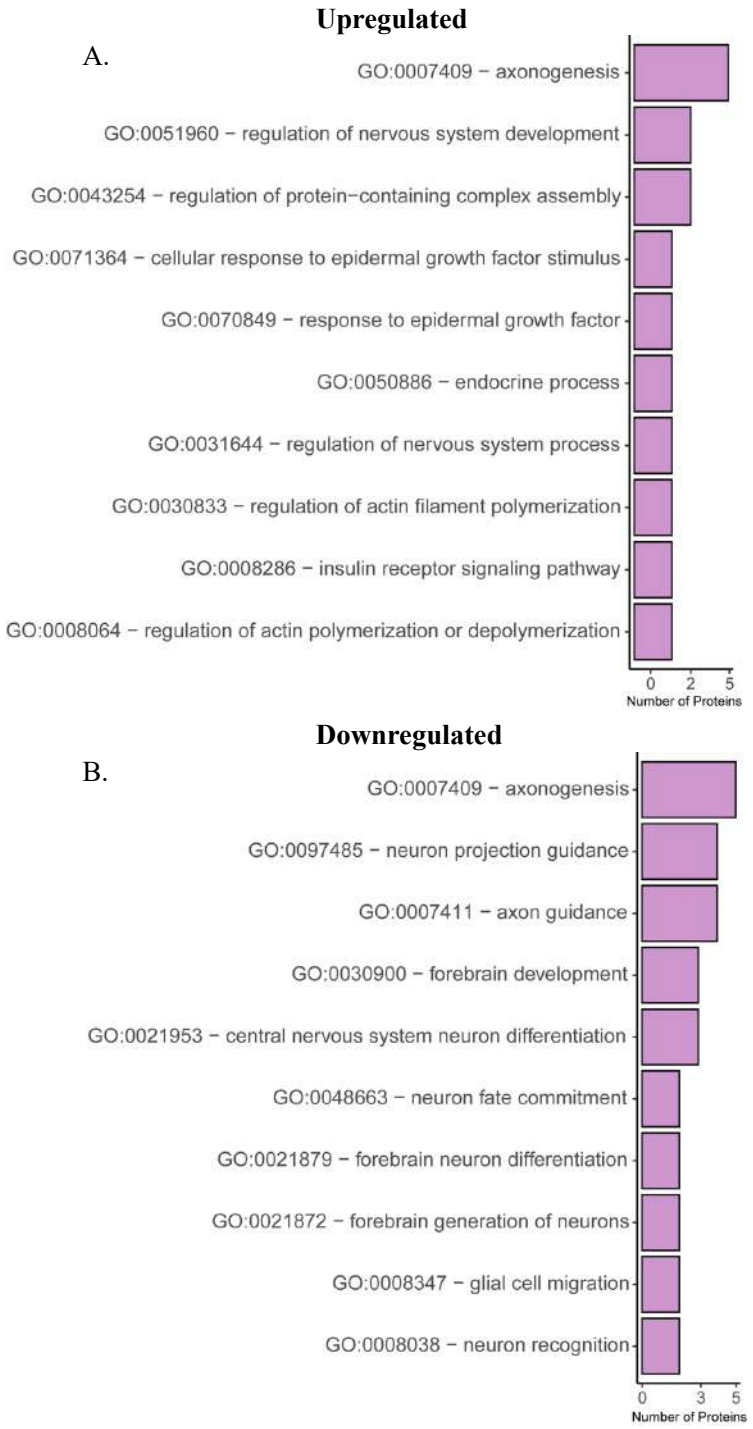

Fig.53. GO enrichment of axonogenesis (GO:0007409) processes after nFGFR1 upregulation in hCOs*. Bar charts illustrate the top ten GO biological processes (BP) enriched in differentially expressed proteins (DEPs) annotated to axonogenesis (GO:0007409) in 60-day hCOs following nFGFR1 upregulation. Panel A displays the top ten biological processes significantly enriched among upregulated proteins, while Panel B presents the top ten processes enriched among downregulated proteins. Enrichment was determined using proteins with* $\log_2 FC > 0$ *(upregulated) or* < 0 *(downregulated;* $P \leq 0.05$*). Each bar represents the number of differentially expressed proteins contributing to that GO term.*

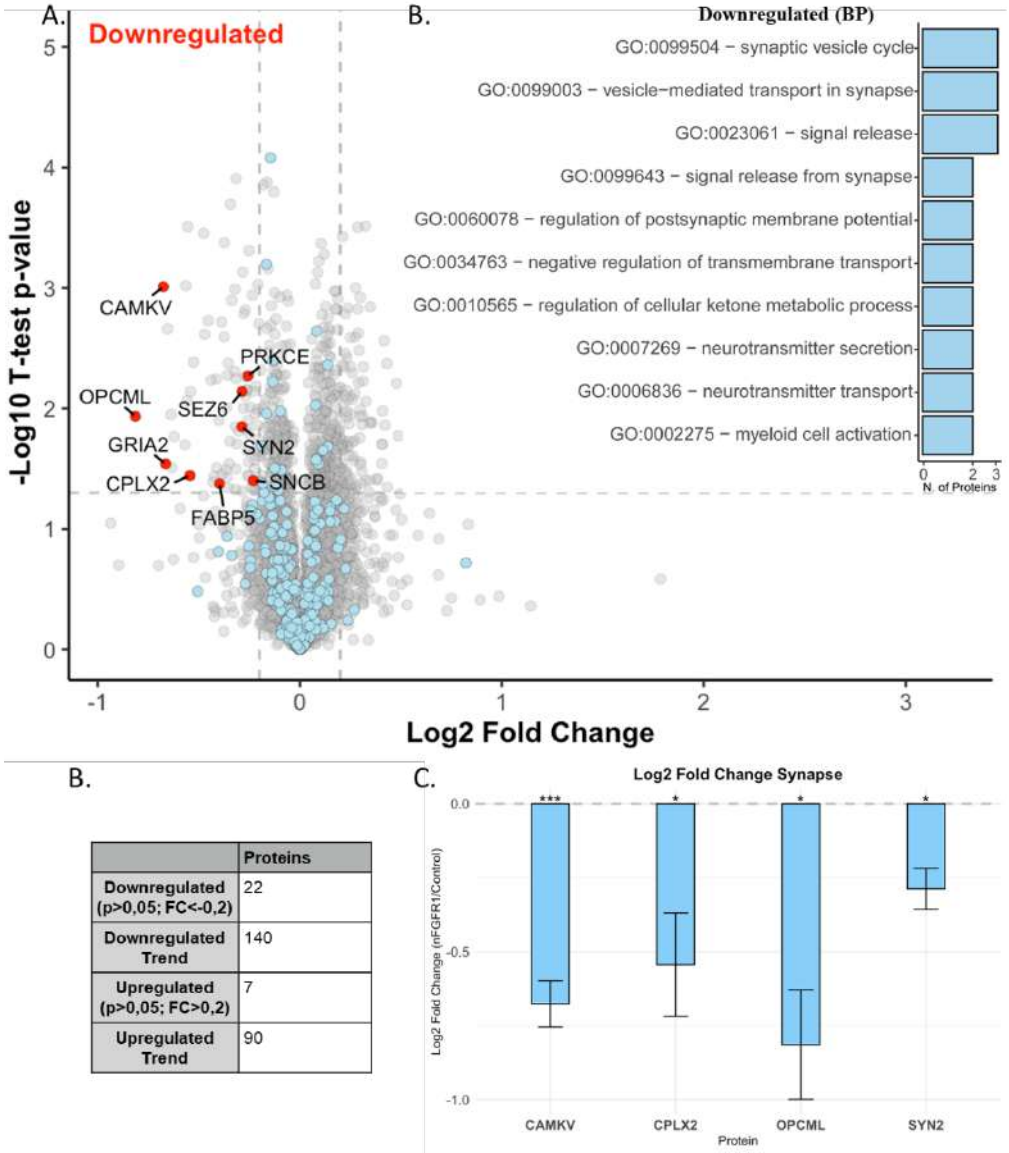

Fig.54. Synaptic Proteins in hCOs following nFGFR1 upregulation. A. Volcano plot. *A total of 230 proteins related to synaptic proteins (GO:0045202) were identified in the total proteome (hCOs) treated with DOX and DMSO (control). Of these, 22 proteins showed significant upregulation (Log2FC > 0 ; p-value ≤ 0.05), and seven proteins were significantly downregulated. Synaptic proteins are displayed as blue circles. The x-axis displays log_2 fold changes (DOX vs. control), where positive values reflect upregulation and negative values denote downregulation. The y-axis illustrates $–log_{10}$ p-values from two-tailed t-tests, with higher values indicating stronger statistical validation. Vertical dashed lines represent ±0.2 log_2 fold change, while the horizontal dashed line marks $–log_{10}$ (0.05). Proteins meeting both criteria thresholds (log_2 FC > 0.2; P ≤ 0.05) are highlighted in red (downregulation) and annotated by name; B. GO Enrichment. Bar charts illustrate the top ten GO biological processes (BP) enriched in downregulated DEPs related to synaptic proteins (GO:0045202) in 60-day hCOs following nFGFR1 upregulation; C. Protein Expression Trend Categories. Table classifies each protein into one of four categories based on its log_2 fold-change (FC) and p-value: Significantly Upregulated ($Log_2FC > 0$; P ≤ 0.05); Significantly Downregulated ($Log_2FC < 0$; P ≤ 0.05); Positive Trend ($0 < Log_2FC$); Negative Trend ($Log_2FC < 0$); D. Plot for Top 4 DEP proteins. The bar graph displays the mean ± SD log_2 fold change for the four top downregulated DEPs synaptic proteins: CAMKV, CPLX, OPCML, and SYN2. Asterisks indicate statistical significance (*P ≤ 0.05; **P ≤ 0.01; ***P ≤ 0.001; ****P ≤ 0.0001).*

5.18. nFGFR1 reprograms mitochondrial and energy metabolism toward glycolysis and lipid metabolism

FGFR1 signaling plays a crucial role in modulating cellular energy metabolism. It has also been demonstrated that FGFR1 influences mitochondrial function and regulation of reactive oxygen species (ROS) response in neuronal systems. Moreover, FGFR signaling has been implicated in balancing glycolysis and fatty acid β-oxidation, coordinating metabolic pathways in a tissue-specific manner (Kar et al., 2023; Xu et al., 2023; Yang et al., 2012). To determine whether nuclear FGFR1 (nFGFR1) contributes to metabolic reprogramming during human cortical development, I performed proteomic profiling in human cortical organoids, focusing on pathways related to mitochondrial dynamics, oxidative phosphorylation, glycolysis, and lipid metabolism.

I identified a total of 607 mitochondrial proteins using the MitoCarta 3.0 database (Fig.55), of which 15 showed significant upregulation and 19 downregulation. Among the upregulated proteins, OXR1 and TXN2 were identified, which are essential for redox regulation, as well as MRPL24, a component of the mitochondrial ribosome. In contrast, several subunits of the electron transport chain, including NDUFA7, NDUFB3, NDUFV1, and COX6C, were downregulated, along with the mitochondrially encoded subunit MT-CO2. This suggests a potential impairment in oxidative phosphorylation (OXPHOS). A general trend of increased expression in mitochondrial proteins was noted, with 371 proteins upregulated compared to 236 that were downregulated (Fig.55B). However, the reduction of essential OXPHOS proteins suggests that energy metabolism may be impaired following nFGFR1 induction in hCOs. Gene ontology (GO) enrichment analysis of upregulated mitochondrial proteins revealed enrichment of terms such as mitochondrial gene expression (GO:0140053), mitochondrial translation (GO:0032543), mitochondrial RNA metabolism (GO:0000959), and mitochondrial organization (GO:0007005). Additionally, metabolic pathways including the amino acid catabolic process (GO:0009063) and cell redox homeostasis were identified (GO:0045454). In contrast, the downregulated proteins were enriched in processes such as oxidative phosphorylation (GO:0006119), mitochondrial ATP synthesis coupled electron transport (GO:0042775), proton motive force-driven mitochondrial ATP synthesis (GO:0042776), and mitochondrial electron transport from NADH to ubiquinone

(GO:0006120) (Fig.56). These changes collectively indicate an energy production imbalance, with increased mitochondrial maintenance and biosynthesis failing to compensate for impaired respiratory capacity.

Among oxidative phosphorylation-related proteins (GO:0006119), I observed a distinct trend of downregulation: out of the 81 identified OXPHOS proteins, 19 were significantly downregulated, while only one, NDUFA3, exhibited significant upregulation (Fig.57). Among the downregulated proteins, key subunits of complex I (e.g., NDUFA7, NDUFB7) and complex IV (COX6C, MT-CO2) were identified, indicating impaired electron transport chain activity. These proteins were enriched in processes such as ATP biosynthesis (GO:0006754), aerobic electron transport (GO:0019646), and purine nucleoside triphosphate biosynthesis (GO:0009145; GO:0009206), suggesting broader bioenergetic deficits following nFGFR1 upregulation in hCOs (Fig.57B).

At the same time, I observed a subtle but coordinated upregulation of proteins associated with the Warburg effect (Fig.58). Out of 57 Warburg-related proteins, six were significantly upregulated (e.g., PKM and SLC16A3), while only one was downregulated. Furthermore, a minor trend toward upregulation was noted, with 27 proteins showing a tendency for downregulation and 36 proteins being upregulated. GO enrichment analysis for upregulated proteins revealed an enrichment of terms such as the glycolytic process (GO:0006096), pyruvate metabolic process (GO:0006090), and ADP catabolic process (GO:0046032), suggesting a metabolic shift towards aerobic glycolysis. Additionally, I found that proteins involved in glucose metabolism (GO:0006006) also showed a trend toward upregulation, with 4 significantly increased expression, such as PKM (pyruvate kinase M, catalyzes the final step of glycolysis), GAA (acid α-glucosidase, a lysosomal enzyme that converts glycogen into glucose), and DCXR (L-xylulose reductase, participates in carbohydrate metabolism) (Fig.59). Together, these changes reflect a switch to glycolysis-based ATP production, likely as a compensatory response to OXPHOS impairment. Collectively, these changes indicate a transition to glycolysis-driven ATP production during neuronal development in the hCO, probably as a compensatory mechanism for OXPHOS dysfunction due to nFGFR1 increased expression.

Finally, I found that glycolipid metabolism-related proteins (GO:0006664) were significantly upregulated in cortical organoids following nFGFR1 upregulation (Fig.60). Of the 25 proteins associated with this pathway, 9 were significantly upregulated while only 2 were significantly downregulated, indicating a trend toward the upregulation of the glycolipid metabolic process proteins. Enzymes like GBA (β-glucocerebrosidase), GALC (galactocerebrosidase), and GM2A (GM2 ganglioside activator protein), which are essential for glycolipid degradation, were significantly upregulated. Additionally, gene ontology enrichment analysis confirmed the activation of several lipid-related biological processes among the upregulated proteins (Fig.60B). These processes included the glycolipid catabolic process (GO:0006689), glycosphingolipid metabolic process (GO:0006687), sphingolipid catabolic process (GO:0046475), membrane lipid catabolic process (GO:0046466), and lipid localization to membrane (GO:1905953). These changes indicate improved lipid metabolism and membrane remodeling following nFGFR1 upregulation, which may facilitate neuronal differentiation or energy compensation in response to reduced oxidative phosphorylation.

In summary, the elevated expression of nFGFR1 in hCOs triggers metabolic reprogramming, characterized by decreased oxidative phosphorylation and upregulated glycolysis, glycolipid metabolism, and mitochondrial biosynthesis functions. This compensatory mechanism enhances cellular resilience by shifting energy production from compromised mitochondrial respiration (OXPHOS) to alternative metabolic pathways that support developmental processes and may impact neuronal function and redox balance.

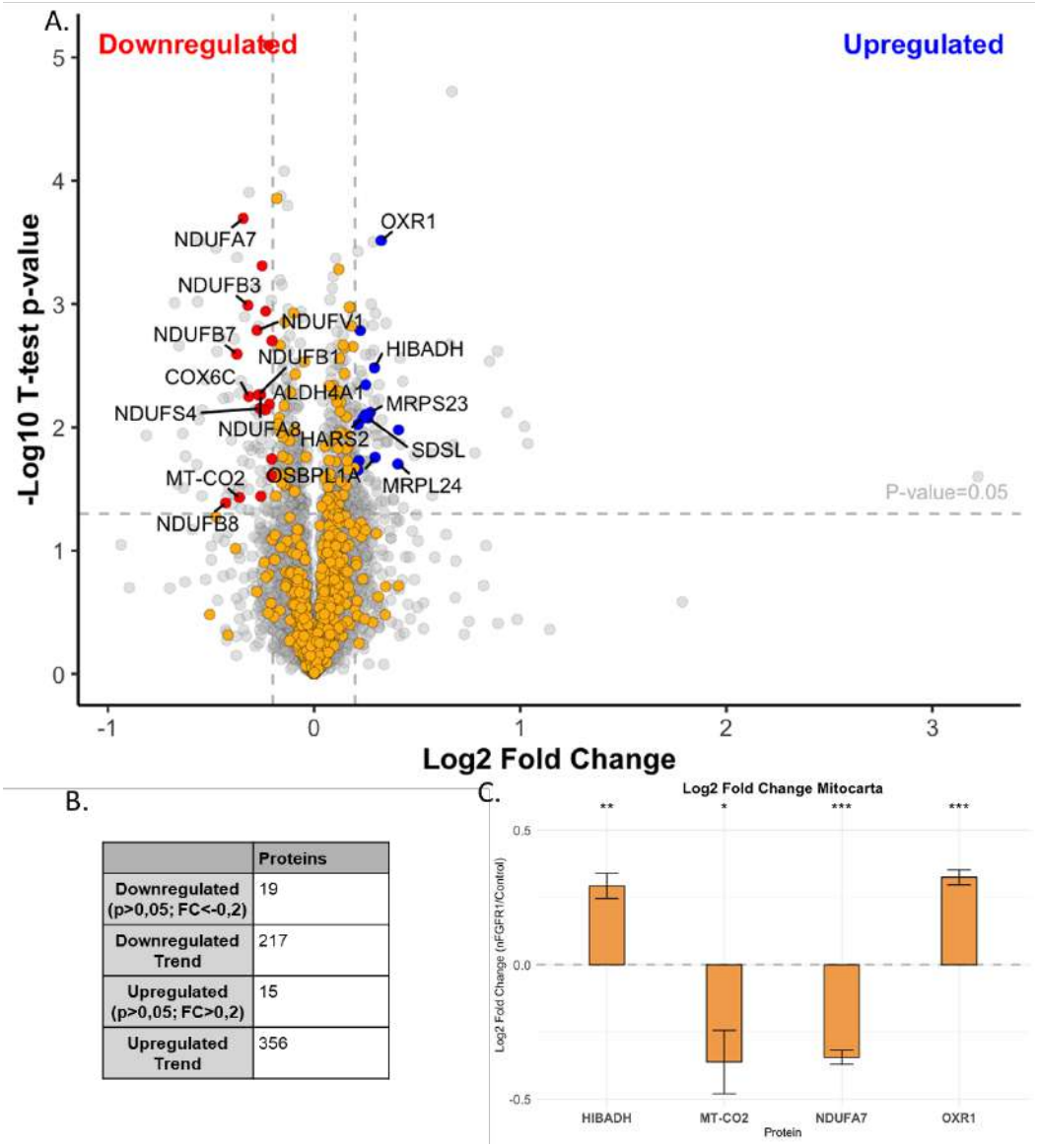

	Proteins
Downregulated (p>0,05; FC<-0,2)	19
Downregulated Trend	217
Upregulated (p>0,05; FC>0,2)	15
Upregulated Trend	356

Fig.55. Mitochondrial proteins in hCOs following nFGFR1 upregulation. *A. Volcano plot. A total of 607 proteins related to mitochondrial proteins were identified in the hCO treated with DOX and DMSO (control), using the MitoCarta 3.0 database. Among these, 15 proteins were significantly upregulated (Log2FC > 0.2, p-value ≤ 0.05), while 19 proteins were significantly downregulated. Mitochondrial proteins are displayed as orange circles. The x-axis displays log_2 fold changes (DOX vs. control), where positive values reflect upregulation and negative values denote downregulation. The y-axis illustrates $–log_{10}$ p-values from two-tailed t-tests, with greater values indicating stronger statistical validation. Vertical dashed lines represent ±0.2 log_2 fold change, while the horizontal dashed line marks $–log_{10}$ (0.05). Proteins meeting both criteria thresholds (log_2 FC > 0.2; P ≤ 0.05) are highlighted in blue (upregulation) or red (downregulation) and annotated by name; B. Protein Expression Trend. Table classifies each protein into one of four categories based on its log_2 fold-change (FC) and p-value: Significantly Upregulated ($Log_2FC \geq 0.2$; $P \leq 0.05$); Significantly Downregulated ($Log_2FC \leq –0.2$; $P \leq 0.05$); Positive Trend ($0 < Log_2FC$); Negative Trend ($Log_2FC < 0$); C. Plot for Top 4 DEP proteins. The bar graph shows mean ± SD log_2 fold change for the four most strongly regulated proteins associated with axonogenesis: HIBADH, OXR1 (Upregulated), MT-CO2, and NDUFA7 (Downregulated). Asterisks denote statistical significance (*P ≤ 0.05; **P ≤ 0.01; ***P ≤ 0.001; ****P ≤ 0.0001).*

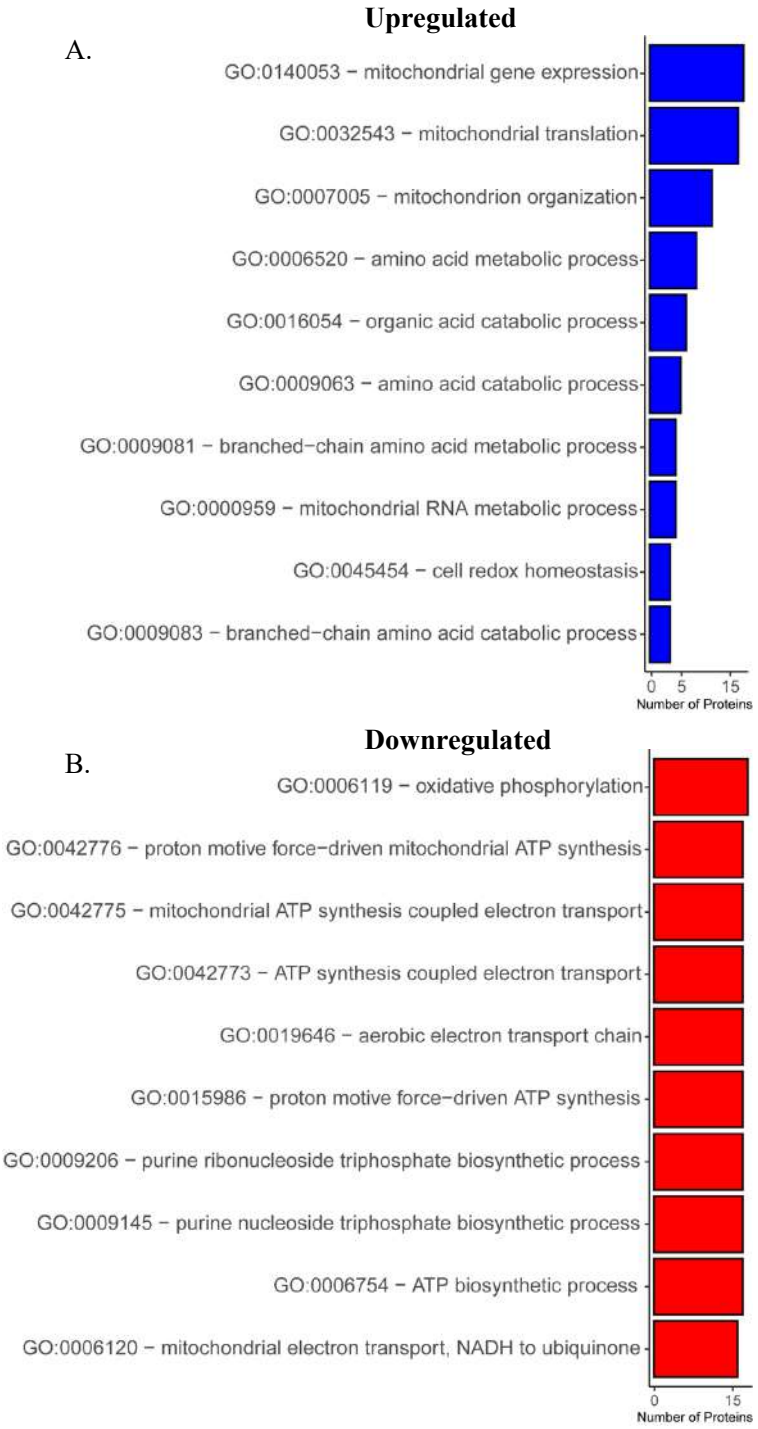

Fig.56. GO enrichment of mitochondrial proteins after nFGFR1 upregulation in hCOs. *Bar charts illustrate the top ten GO biological processes (BP) related to DEPs of mitochondrial proteins using the MitoCarta 3.0 database in 60-day hCOs following nFGFR1 upregulation. Panel A displays the top ten biological processes significantly enriched among upregulated proteins, while Panel B presents the top ten processes enriched among downregulated proteins. Enrichment was determined using proteins with* $\log_2 FC > 0$ *(upregulated) or* < 0 *(downregulated) and* $P \leq 0.05$*. Each bar represents the number of differentially expressed proteins contributing to that GO term.*

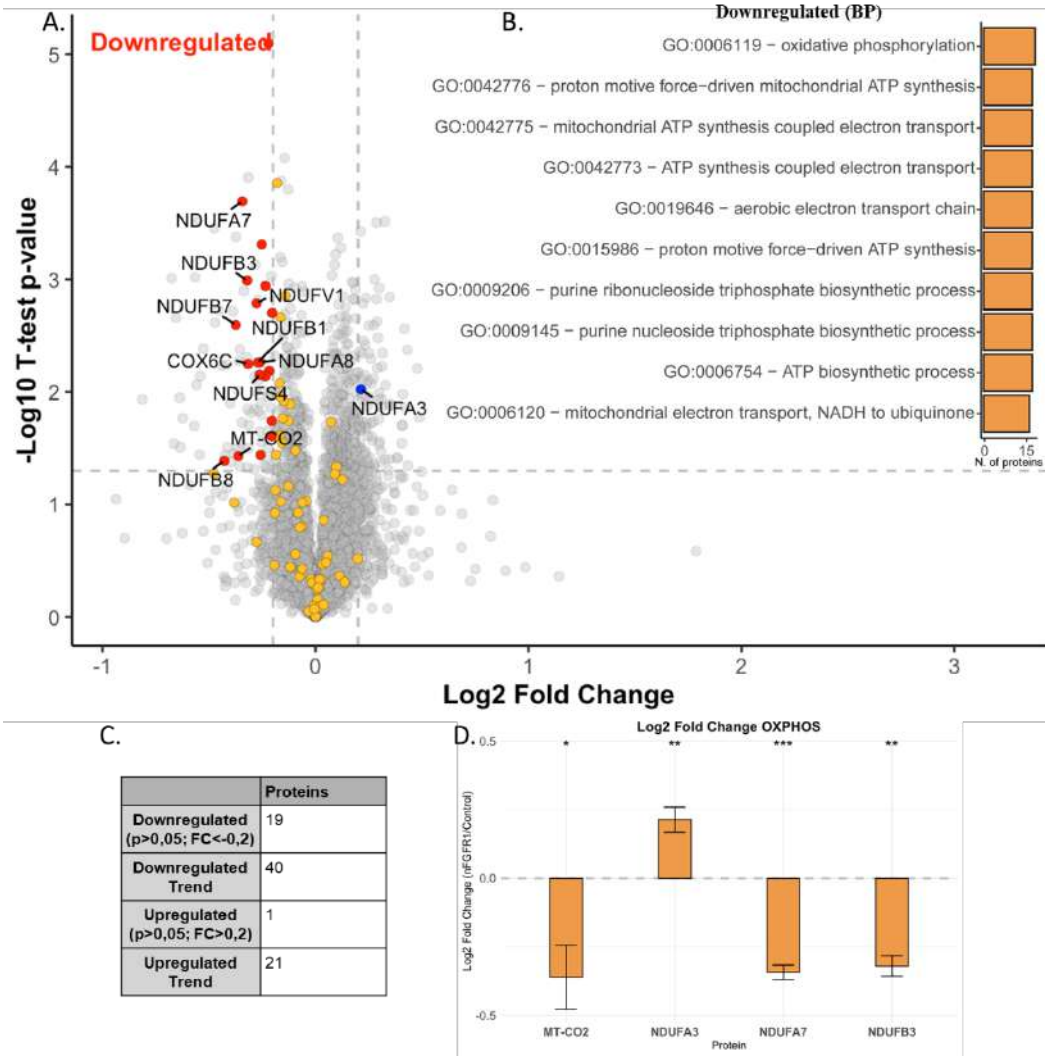

Fig.57. Proteins involved in oxidative phosphorylation in hCOs after nFGFR1 upregulation. *A. Volcano plot. A total of 81 proteins related to oxidative phosphorylation (GO:0006119) were identified in hCOs treated with DOX and DMSO (control). Among these, 19 proteins were significantly downregulated (Log2FC ≤ -0.2, P ≤ 0.05), while only one protein was significantly upregulated. OXPHOS proteins are displayed as orange circles. The x-axis displays log_2 fold changes (DOX vs. control), where positive values reflect upregulation and negative values denote downregulation. The y-axis illustrates $-log_{10}$ p-values from two-tailed t-tests, with greater values indicating stronger statistical validation. Vertical dashed lines represent ±0.2 log_2 fold change, while the horizontal dashed line marks $-log_{10}$ (0.05). Proteins meeting both criteria thresholds (log_2 FC ≥ 0.2; P ≤ 0.05) are highlighted in blue (upregulation) or red (downregulation) and annotated by name; B. GO Enrichment. Bar charts illustrate the top ten GO biological processes (BP) enriched in downregulated DEPs related to oxidative phosphorylation (GO:0006119) in 60-day hCOs following nFGFR1 upregulation; C. Protein Expression Trend Categories. Table classifies each protein into one of four categories based on its log_2 fold-change (FC) and p-value: Significantly Upregulated ($Log_2FC \geq 0.2$; $P \leq 0.05$); Significantly Downregulated ($Log_2FC \leq -0.2$; $P \leq 0.05$); Positive Trend ($0 < Log_2FC$); Negative Trend ($Log_2FC < 0$); D. Plot for Top 4 DEP proteins. The bar graph displays the mean ± SD log_2 fold change for the top differentially expressed proteins (DEPs) of the OXPHOS proteins: MT-CO2, NDUFA7, NDUFB3 (upregulated), and NDUFA3 (downregulated). Asterisks indicate statistical significance (*P ≤ 0.05; **P ≤ 0.01; ***P ≤ 0.001; ****P ≤ 0.0001).*

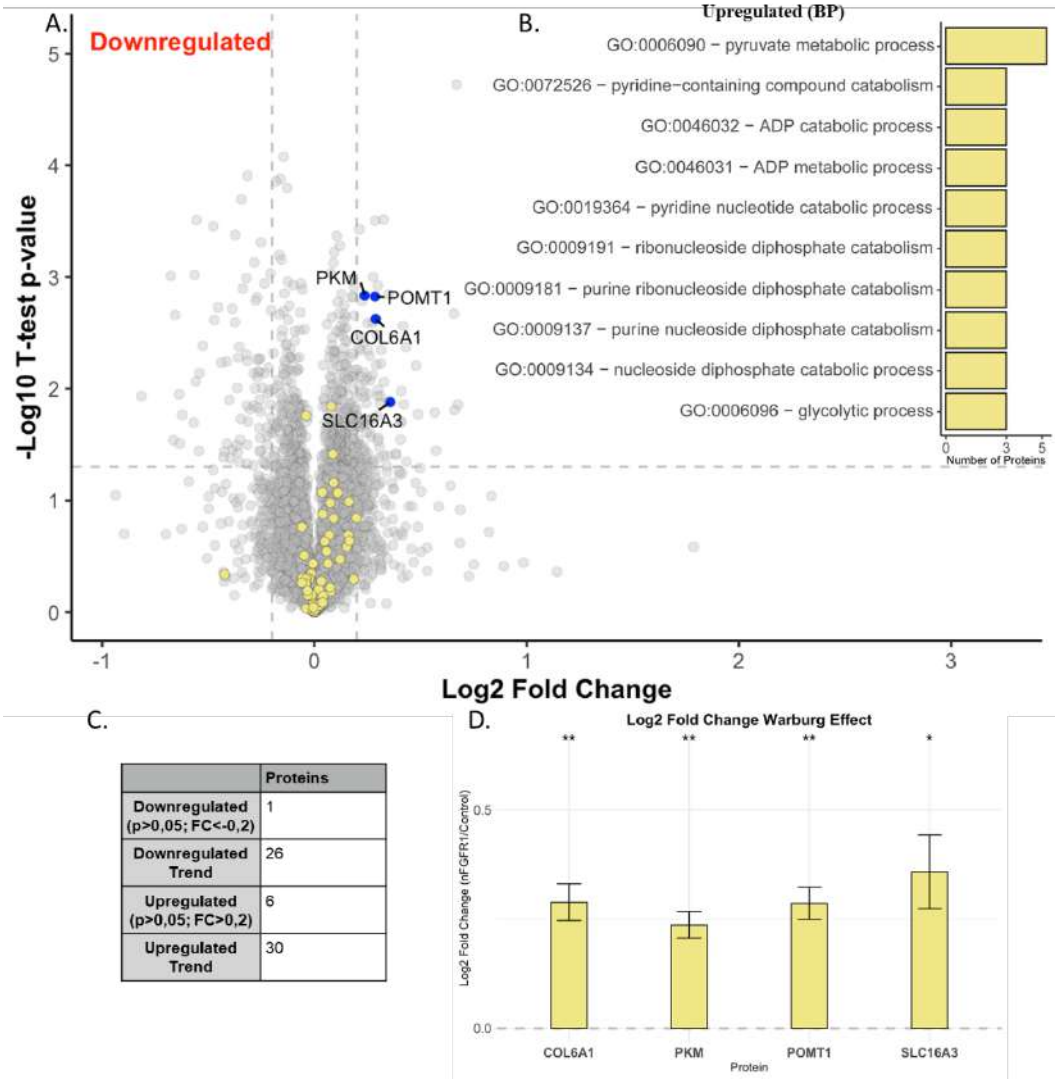

	Proteins
Downregulated (p>0,05; FC<-0,2)	1
Downregulated Trend	26
Upregulated (p>0,05; FC>0,2)	6
Upregulated Trend	30

Fig.58. Proteins associated with the Warburg effect in hCOs following nFGFR1 upregulation. *A. Volcano plot. A total of 57 proteins related to Warburg effect were identified in hCOs treated with DOX and DMSO (control). Among these, 6 proteins were significantly upregulated (Log2FC ≥ 0.2, P ≤ 0.05), while only one protein was significantly downregulated. Warburg effect proteins are displayed as yellow circles. The x-axis displays log_2 fold changes (DOX vs. control), where positive values reflect upregulation and negative values denote downregulation. The y-axis illustrates $–log_{10}$ p-values from two-tailed t-tests, with greater values indicating stronger statistical validation. Vertical dashed lines represent ±0.2 log_2 fold change, while the horizontal dashed line marks $–log_{10}$ (0.05). Proteins meeting both criteria thresholds (log_2 FC ≥ 0.2; P ≤ 0.05) are highlighted in blue (upregulation) and annotated by name; B. GO Enrichment. Bar charts illustrate the top ten GO biological processes (BP) enriched in upregulated DEPs related to the Warburg effect in 60-day hCOs following nFGFR1 upregulation; C. Protein Expression Trend. Table classifies each protein into one of four categories based on its log_2 fold-change (FC) and p-value: Significantly Upregulated ($Log_2FC > 0$; P ≤ 0.05); Significantly Downregulated ($Log_2FC < 0$; P ≤ 0.05); Positive Trend ($0 < Log_2FC$); Negative Trend ($Log_2FC < 0$); D. Plot for Top 4 DEP proteins. The bar graph displays the mean ± SD log_2 fold change for the top 4 upregulated DEPs associated with the Warburg effect proteins: COL6A1, PKM, POMT1, and SLC16A3. Asterisks indicate statistical significance (*P ≤ 0.05; **P ≤ 0.01; ***P ≤ 0.001; ****P ≤ 0.0001).*

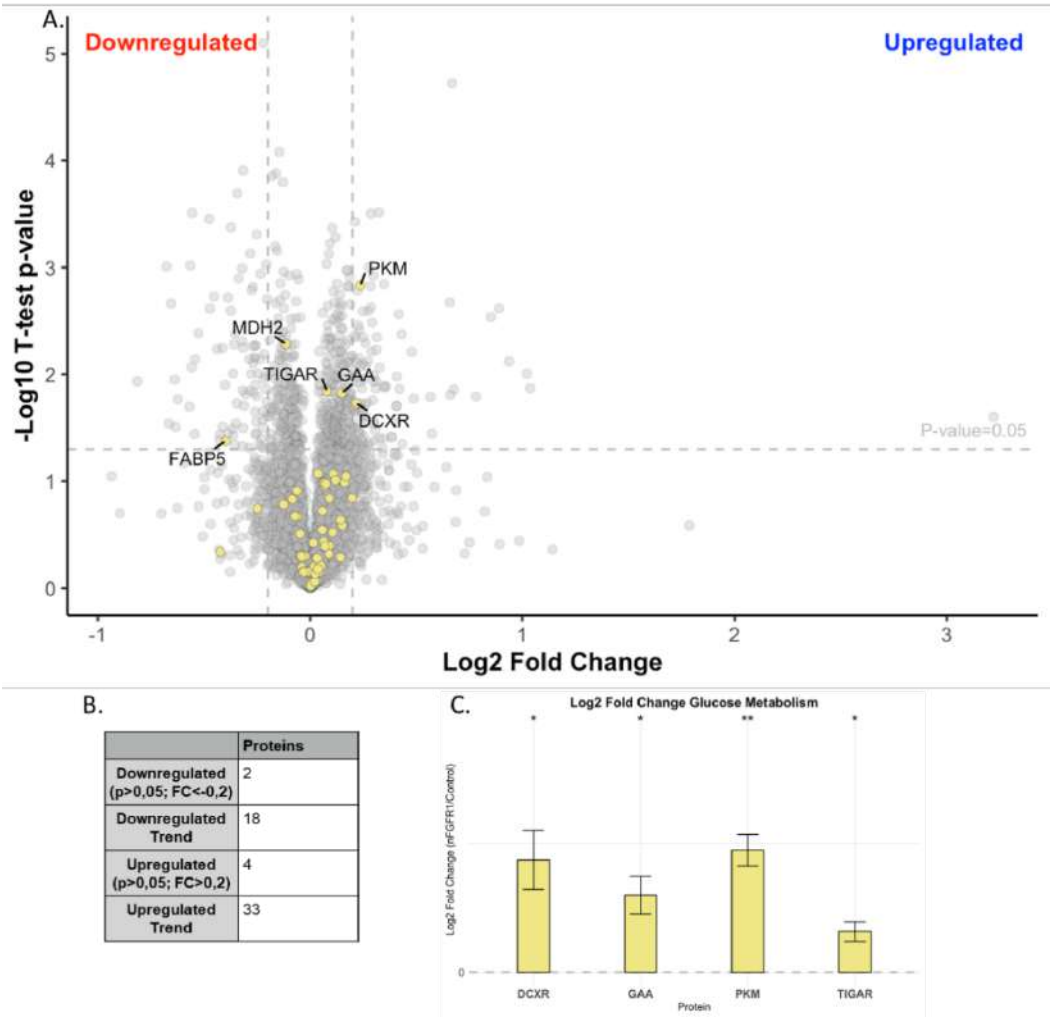

Fig.59. Proteins related to glucose metabolism in hCOs after nFGFR1 upregulation. *A. Volcano plot. A total of 21 proteins related to glucose metabolism (GO:0006006) were identified in hCOs treated with DOX and DMSO (control). Among these, four proteins were significantly upregulated (Log2FC > 0 ; P ≤ 0.05), while two proteins were significantly downregulated. These proteins are displayed as yellow circles. The x-axis displays log_2 fold changes (DOX vs. control), where positive values reflect upregulation and negative values denote downregulation. The y-axis illustrates $–log_{10}$ p-values from two-tailed t-tests, with greater values indicating stronger statistical validation. Vertical dashed lines represent ±0.2 log_2 fold change, while the horizontal dashed line marks $–log_{10}$ (0.05). Proteins that meet the significance threshold (P ≤ 0.05) are annotated with names. B. Protein Expression Trend. Table classifies each protein into one of four categories based on its log_2 fold-change (FC) and p-value: Significantly Upregulated ($Log_2FC > 0$; P ≤ 0.05); Significantly Downregulated ($Log_2FC < 0$; P ≤ 0.05); Positive Trend ($0 < Log_2FC$); Negative Trend ($Log_2FC < 0$); C. Plot for Top 4 DEP proteins. The bar graph displays the mean ± SD log_2 fold change for the top 4 upregulated DEP proteins related to glucose metabolism: DCXR, GAA, PKM, and TIGAR. Asterisks indicate statistical significance (*P ≤ 0.05; **P ≤ 0.01; ***P ≤ 0.001; ****P ≤ 0.0001).*

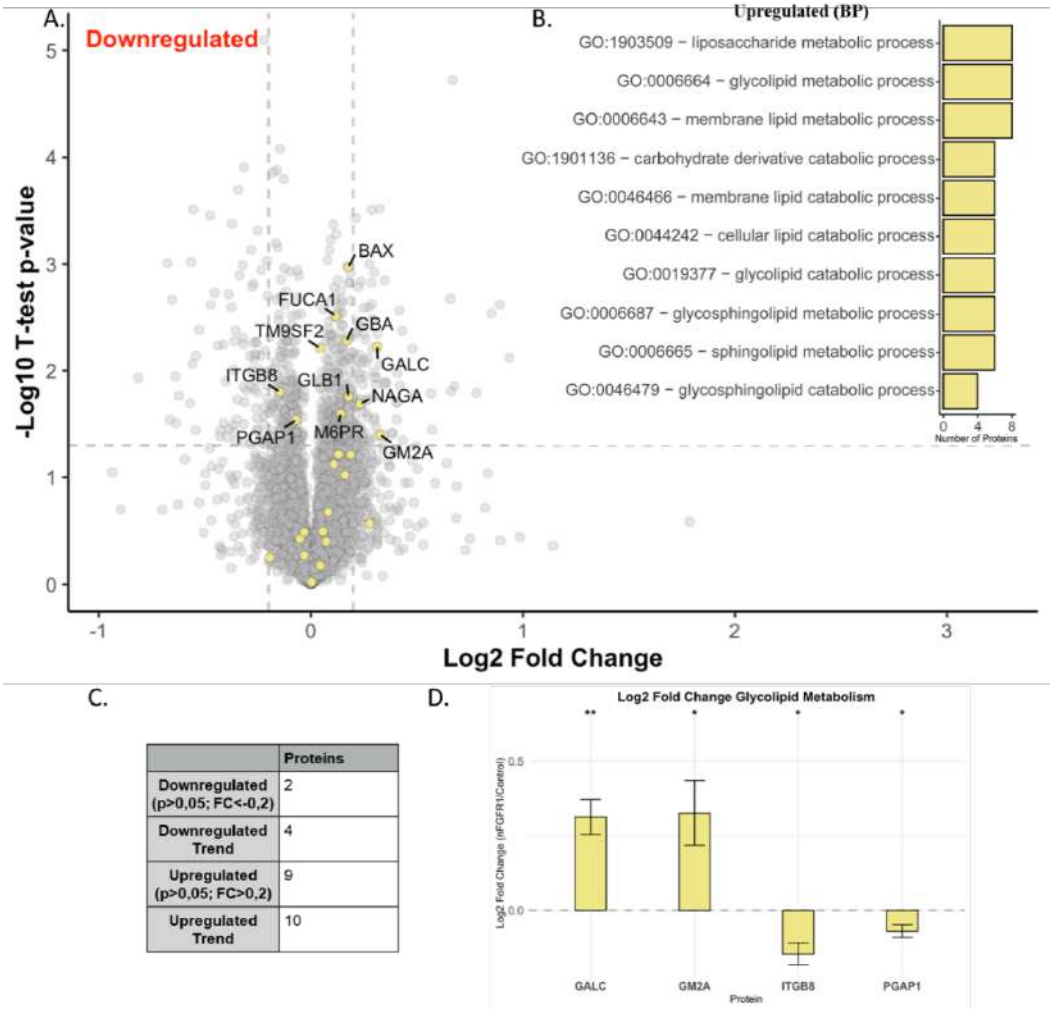

	Proteins
Downregulated (p>0,05; FC<-0,2)	2
Downregulated Trend	4
Upregulated (p>0,05; FC>0,2)	9
Upregulated Trend	10

Fig.60. Proteins related to glycolipid metabolism in hCOs after nFGFR1 upregulation. *A. Volcano plot. A total of 25 proteins related to glycolipid metabolism (GO:0006664) were identified in hCOs treated with DOX and DMSO (control). Among these, nine proteins were significantly upregulated (Log2FC > 0 ; P ≤ 0.05), while only two were significantly downregulated. These proteins are displayed as yellow circles. The x-axis displays log_2 fold changes (DOX vs. control), where positive values reflect upregulation and negative values denote downregulation. The y-axis illustrates $–log_{10}$ p-values from two-tailed t-tests, with greater values indicating stronger statistical validation. Vertical dashed lines represent ±0.2 log_2 fold change, while the horizontal dashed line marks $–log_{10}$ (0.05). Proteins that meet the significance threshold (P ≤ 0.05) are annotated with names. B. GO Enrichment. Bar charts illustrate the top ten GO biological processes (BP) enriched in upregulated DEPs related to glycolipid metabolism (GO:0006664) in 60-day hCOs following nFGFR1 upregulation; C. Protein Expression Trend Categories. Table classifies each protein into one of four categories based on its log_2 fold-change (FC) and p-value: Significantly Upregulated ($Log_2FC > 0$; P ≤ 0.05); Significantly Downregulated ($Log_2FC < 0$; P ≤ 0.05); Positive Trend ($0 < Log_2FC$); Negative Trend ($Log_2FC < 0$); D. Plot for Top 4 DEP proteins. The bar graph displays the mean ± SD log_2 fold change for the top DEP proteins related to glycolipid metabolism: GALC, GM2A (upregulated), and ITGB8, PGAP1 (downregulated). Asterisks indicate statistical significance (*P ≤ 0.05; **P ≤ 0.01; ***P ≤ 0.001; ****P ≤ 0.0001).*

5.19. nFGFR1 alters the balance between autophagy and lysosomal pathways in hCOs

Fibroblast growth factor receptors, including FGFR1, have been shown to influence intracellular trafficking, autophagic signaling, and lysosomal processing, with dysregulation linked to altered cellular homeostasis in both neural and non-neural contexts (Chen et al., 2016; Cho et al., 2004; Haugsten et al., 2008). FGFR1 has also been implicated in promoting protective autophagy in response to stress, independent of classical receptor signaling, and in directing lysosomal and endosomal sorting. To investigate the impact of nuclear FGFR1 (nFGFR1) on autophagic flux, mitophagy, and lysosomal function during cortical development, a comprehensive proteomic analysis was performed in human cortical organoids following inducible nFGFR1 upregulation.

In my study of the proteomic profiling of 60-day-old human cortical organoids (hCOs) after conditional upregulation of nFGFR1, I observed modulation of autophagic and lysosomal pathways. Among 436 proteins associated with autophagy (GO:0006914), 10 proteins were significantly upregulated and three were downregulated (Fig.61). In addition, a clear trend in the expression of autophagy-related proteins was not observed - 199 proteins showed a tendency to be downregulated, whereas 237 were upregulated (Fig.61B). The upregulated factors included TGFBRAP1 (TGF-β receptor-associated protein 1), LAMP2 (lysosome-associated membrane protein 2; which is essential for chaperone-mediated autophagy), and CTSB (cathepsin B; a lysosomal protease involved in protein degradation). This suggests enhanced autophagosome maturation and lysosomal degradation. In contrast, the downregulation of NEDD4L (NEDD4-like E3 ubiquitin ligase, tags proteins for degradation) and VPS13A (vacuolar protein sorting–associated protein 13A, regulates lipid transport) was observed, implying an imbalance in autophagosome turnover and vesicular trafficking following nFGFR1 upregulation (Fig.61C). Furthermore, the GO enrichment analysis revealed a dual trend: processes such as macroautophagy (GO:0016236), vacuole organization (GO:0007033), and autophagosome maturation (GO:0097352) showed upregulation, while pathways like the regulation of autophagy (GO:0010506), regulation of macroautophagy (GO:0016241), and regulation of mitophagy (GO:1901524) were downregulated (Fig.62). This suggests a dysregulated autophagic response due to the increased expression of nFGFR1.

Unlike autophagy proteins, I observed only modest changes in mitophagy-related proteins (GO:0000423) after nFGFR1 upregulation. Among the 107 mitophagy-related proteins, 4 were significantly upregulated and 6 proteins were significantly downregulated (Fig.63). Downregulated proteins such as TOMM22 (translocase of the outer mitochondrial membrane 22; targets nuclear-encoded proteins to mitochondria), HTT (huntingtin), and DNM1L (dynamin-1-like protein; gTPase regulating mitochondrial fission network dynamics) are essential for mitochondrial quality control, suggesting subtle impairments in mitophagic clearance. However, a relatively even distribution of upregulated (n=54) and downregulated (n=52) mitophagy proteins noted. This indicates that the upregulation of nFGFR1 does not significantly impair mitophagy globally but instead leads to minor alterations in mitochondrial quality control mechanisms.

In contrast, lysosomal pathways exhibited a broader activation following nFGFR1 activation. Among the 329 lysosomal proteins (GO:0005764), I identified 18 that were significantly upregulated, including CTSB (cathepsin B), GRN (progranulin, which regulates lysosomal enzyme activity), and GUSB (glucuronidase, a lysosomal hydrolase that degrades glycosaminoglycans). These proteins are essential for lysosomal degradation and lipid metabolism (Fig.64). Conversely, only five proteins were significantly downregulated. GO enrichment of the upregulated proteins revealed an enrichment of terms such as vacuole organization (GO:0007033), lysosome organization (GO:0007040), glycolipid catabolic process (GO:0019377), and regulation of lysosomal lumen pH (GO:0035751). This indicates robust upregulation of lysosomal biogenesis and functionality following nFGFR1 upregulation. On the other hand, the downregulated lysosomal proteins were enriched in GO terms related to RNA and protein localization pathways, including protein localization to the nucleoplasm (GO:1990173) and RNA localization to the nucleus (GO:0090685), suggesting suppression of nuclear-lysosomal communication upon nFGFR1 activation (Fig.65).

In summary, nFGFR1 overexpression in cortical organoids (hCOs) induces divergent dual effects on autophagic networks - it enhances late-stage autophagy and lysosomal degradation while slightly modulating mitophagy at the protein level. This may reflect a compensatory mechanism to maintain cellular homeostasis

during metabolic reprogramming and mitochondrial remodeling triggered by nFGFR1 activity.

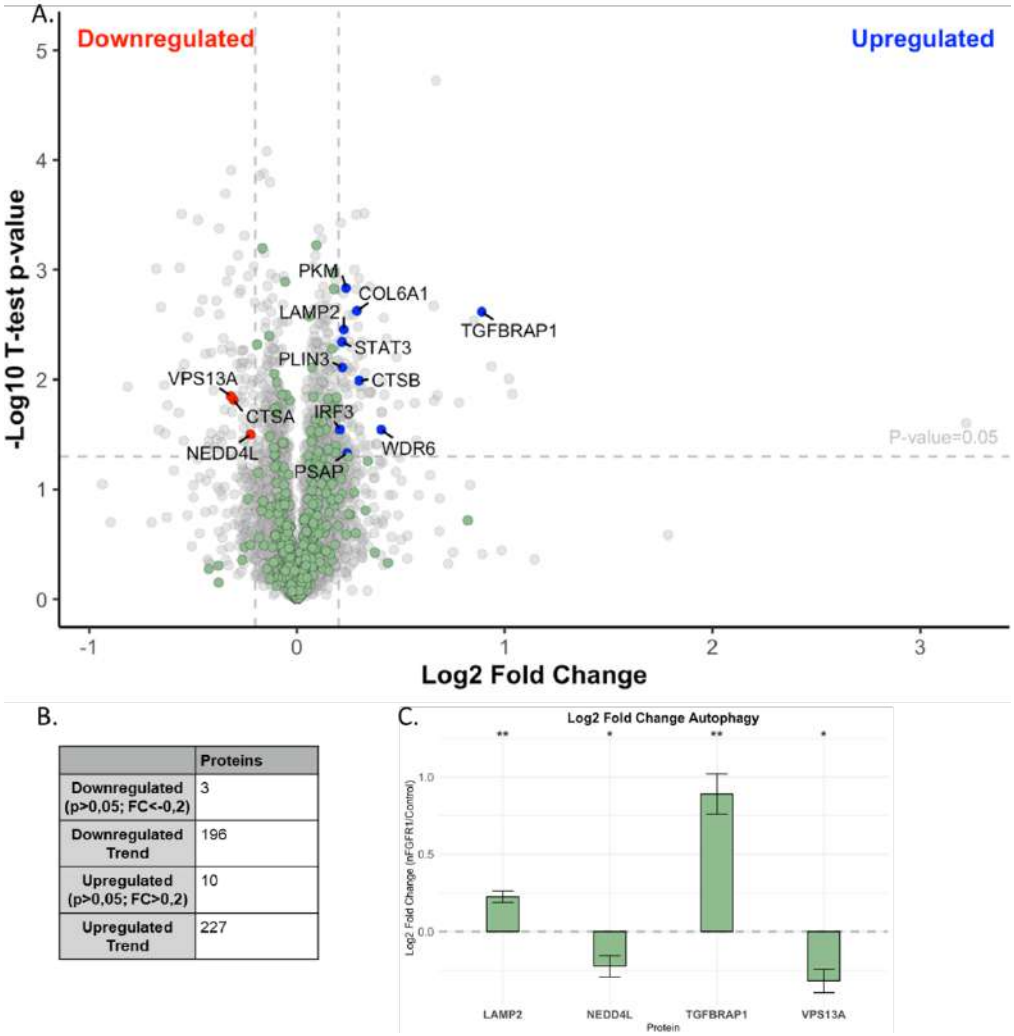

	Proteins
Downregulated (p>0,05; FC<-0,2)	3
Downregulated Trend	196
Upregulated (p>0,05; FC>0,2)	10
Upregulated Trend	227

Fig.61. Proteins associated with autophagy in hCOs following nFGFR1 upregulation. *A. Volcano plot. A total of 436 proteins related to autophagy (GO:0006914) were identified in hCOs treated with DOX and DMSO (control). Among these, 10 proteins were significantly upregulated (Log2FC ≥ 0.2, P ≤ 0.05), while three were significantly downregulated. These proteins are displayed as green circles. The x-axis displays log_2 fold changes (DOX vs. control), where positive values reflect upregulation and negative values denote downregulation. The y-axis illustrates $–log_{10}$ p-values from two-tailed t-tests, with greater values indicating stronger statistical validation. Vertical dashed lines represent ±0.2 log_2 fold change, while the horizontal dashed line marks p = 0.05. Proteins that meet both criteria thresholds (log_2 FC ≥ 0.2; P ≤ 0.05) are highlighted in blue (upregulation) or red (downregulation) and annotated by name; B. Protein Expression Trend Categories. Table classifies each protein into one of four categories based on its log_2 fold-change (FC) and p-value: Significantly Upregulated (Log_2FC ≥ 0.2; P ≤ 0.05); Significantly Downregulated (Log_2FC ≤ –0.2; P ≤ 0.05); Positive Trend (0 < Log_2FC); Negative Trend (Log_2FC < 0); C. Plot for Top 4 DEP proteins. The bar graph displays the mean ± SD log_2 fold change for the top DEPs autophagy proteins: LAMP2, NEDD4L, TGFBRAP1 (upregulated), and VPS13A (downregulated). Asterisks indicate statistical significance (*P ≤ 0.05; **P ≤ 0.01; ***P ≤ 0.001; ****P ≤ 0.0001).*

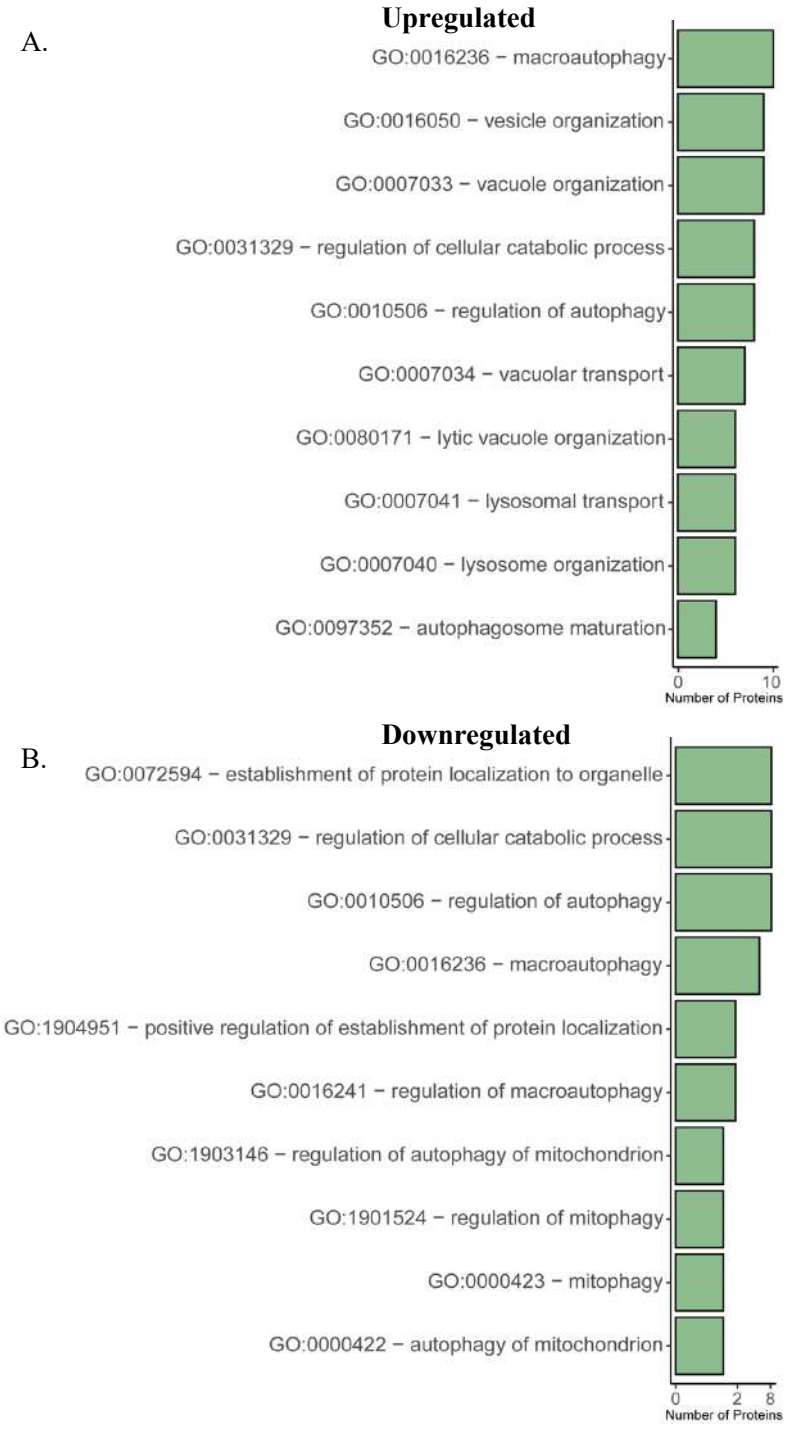

Fig.62. GO enrichment of autophagy proteins following nFGFR1 activation in hCOs. *Bar charts illustrate the top ten GO biological processes (BP) associated with DEPs related to autophagy (GO:0006914) in 60-day hCOs following nFGFR1 upregulation. Panel A displays the top ten biological processes significantly enriched among upregulated proteins, while Panel B presents the top ten processes enriched among downregulated proteins. Enrichment was determined using proteins with* $\log_2 FC > 0$ *(upregulated) or* < 0 *(downregulated) and* $P \leq 0.05$*. Each bar represents the number of differentially expressed proteins contributing to that GO term.*

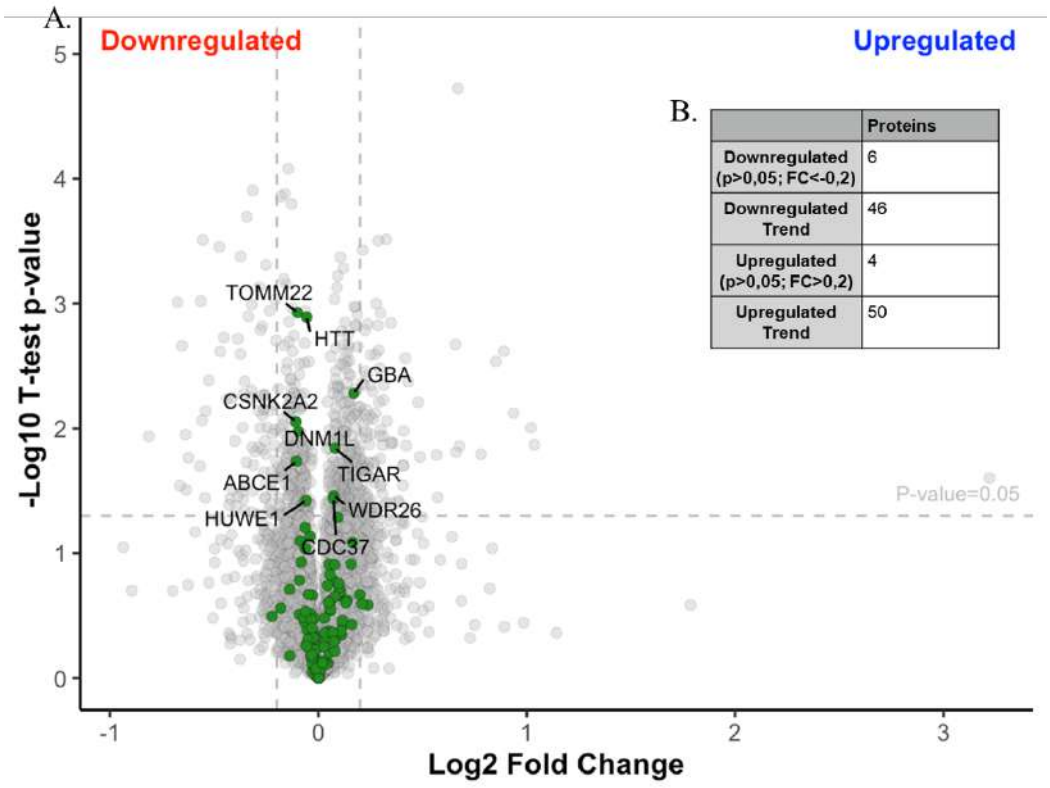

Fig.63. Proteins associated with mitophagy in hCOs following nFGFR1 upregulation. *A. Volcano plot. A total of 96 mitophagy-related proteins (GO:0000423) were identified in hCOs treated with DOX and DMSO (control). Among these, 6 proteins were significantly upregulated (Log2FC > 0 ; P ≤ 0.05), while 4 were significantly downregulated. These proteins are displayed as green circles. The x-axis displays log_2 fold changes (DOX vs. control), where positive values reflect upregulation and negative values denote downregulation. The y-axis illustrates $–log_{10}$ p-values from two-tailed t-tests, with greater values indicating stronger statistical validation. Vertical dashed lines represent ±0.2 log_2 fold change, while the horizontal dashed line marks $–log_{10}$ (0.05). Proteins that meet the significance threshold (P ≤ 0.05) are highlighted by name. B. Protein Expression Trend Categories. Table classifies each protein into one of four categories based on its log_2 fold-change (FC) and p-value: Significantly Upregulated ($Log_2FC > 0$; P ≤ 0.05); Significantly Downregulated ($Log_2FC < 0$; P ≤ 0.05); Positive Trend ($0 < Log_2FC$); Negative Trend ($Log_2FC < 0$).*

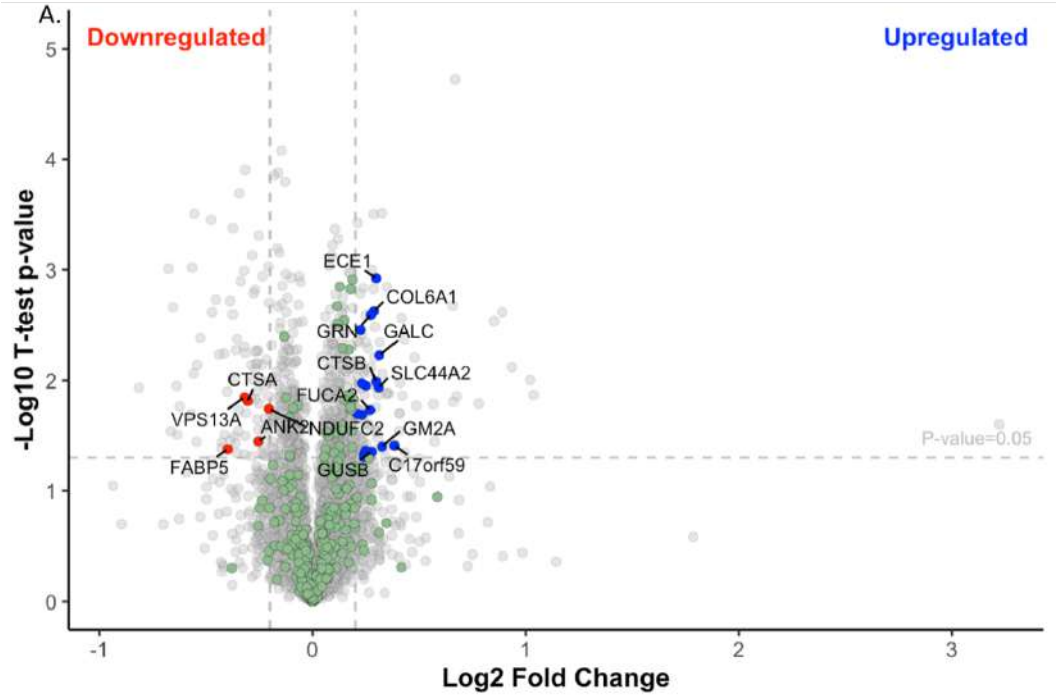

B.

	Proteins
Downregulated (p>0,05; FC<-0,2)	5
Downregulated Trend	127
Upregulated (p>0,05; FC>0,2)	18
Upregulated Trend	179

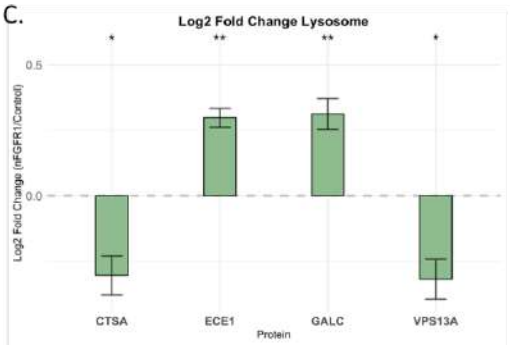

Fig.64. Lysosomal proteins in hCOs following nFGFR1 upregulation. *A. Volcano plot. A total of 329 lysosomal proteins (GO:0005764) were identified in hCOs treated with DOX and DMSO (control). Among these, 18 proteins were significantly upregulated (Log2FC ≥ 0.2, P ≤ 0.05), while five were significantly downregulated. These proteins appear as green circles. The x-axis displays log_2 fold changes (DOX vs. control), where positive values reflect upregulation and negative values denote downregulation. The y-axis illustrates $–log_{10}$ p-values from two-tailed t-tests, with greater values indicating stronger statistical validation. Vertical dashed lines represent ±0.2 log_2 fold change, while the horizontal dashed line marks $–log_{10}$ (0.05). Proteins meeting both criteria thresholds (log_2 FC > 0.2; P ≤ 0.05) are highlighted in blue (upregulation) or red (downregulation) and are annotated with names. B. Protein Expression Trend. Table classifies each protein into one of four categories based on its log_2 fold-change (FC) and p-value: Significantly Upregulated ($Log_2FC \geq 0.2$; $P \leq 0.05$); Significantly Downregulated ($Log_2FC \leq –0.2$; $P \leq 0.05$); Positive Trend ($0 < Log_2FC$); Negative Trend ($Log_2FC < 0$); C. Plot for Top 4 DEP proteins. The bar graph displays the mean ± SD log_2 fold change for the top DEP autophagy proteins: ECE1, GALC (upregulated) and CTSA, VPS13A (downregulated). Asterisks indicate statistical significance (*P ≤ 0.05; **P ≤ 0.01; ***P ≤ 0.001; ****P ≤ 0.0001).*

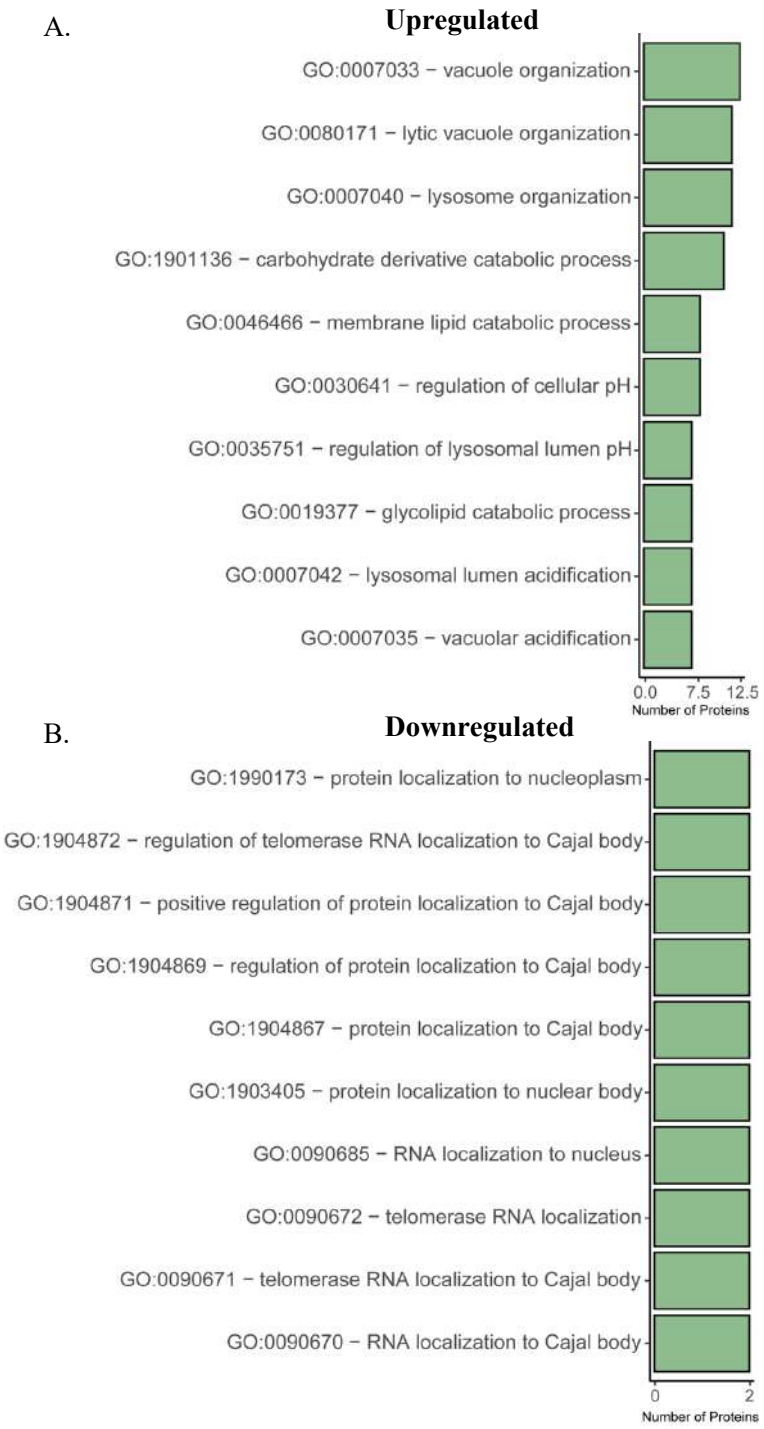

Fig.65. GO enrichment of lysosomal proteins after nFGFR1 induction in hCOs. *Bar charts illustrate the top ten GO biological processes (BP) associated with DEPs lysosomal proteins (GO:0005764) in 60-day hCOs following nFGFR1 upregulation. Panel A displays the top ten biological processes significantly enriched among upregulated proteins, while Panel B presents the top ten processes enriched among downregulated proteins. Enrichment was determined using proteins with log_2 FC > 0 (upregulated) or < 0 (downregulated) and $P \leq 0.05$. Each bar represents the number of differentially expressed proteins contributing to that GO term.*

5.20. nFGFR1 differentially regulates cytoplasmic and mitochondrial translation

Translational regulation plays a critical role in brain development, enabling compartment-specific adaptation of protein synthesis to meet energy demands and facilitate cellular remodeling. Mitochondrial translation, in particular, has emerged as a key axis for neuronal maturation and synaptic plasticity (Borisova et al., 2024; Bruce et al., 2024). Nuclear FGFR1 has been shown to interact with signaling pathways that influence cytoplasmic translation through direct phosphorylation of translational regulators such as RSK (Hu et al., 2004). Moreover, FGFR1 activation has been reported to alleviate translational repression under oxidative stress, supporting proteostasis in models of neurodegenerative neurotoxicity (Ito et al., 2025). To investigate whether nuclear FGFR1 (nFGFR1) differentially affects mitochondrial and cytoplasmic translation, proteomic profiling of human cortical organoids was performed, revealing a coordinated upregulation of mitochondrial translational machinery alongside suppression of cytoplasmic ribosomal processes.

I conducted a proteomic profiling study on 60-day-old human cortical organoids (hCOs) that express increased levels of nuclear FGFR1 (nFGFR1) through doxycycline induction. This study revealed a compartment-specific shift in the cellular translation machinery. I identified a total of 292 proteins associated with the gene ontology term "translation" (GO:0006412), of which 28 were significantly upregulated, while only nine proteins were significantly downregulated (Fig.66). Additionally, the global directionality appeared balanced, with 153 proteins upregulated and 139 downregulated. The GO enrichment analysis indicated that nFGFR1 affects the balance between mitochondrial and cytoplasmic translation pathways: upregulated proteins were predominantly enriched in mitochondrial gene expression (GO:0100153) and translation, including mitochondrial translation (GO:0032543), translational initiation (GO:0043043), regulation of translational initiation (GO:0006446), tRNA aminoacylation for protein translation (GO:0006418), and rRNA processing (GO:0006364). Conversely, downregulated proteins were enriched in cytoplasmic translation–associated processes such as regulation of translation (GO:0006417), translational elongation (GO:0006414) and termination (GO:0006415), ribosome assembly (GO:0042255) and disassembly (GO:0030720), rescue of stalled ribosomes (GO:0072544), protein complex

disassembly (GO:0032984), organelle disassembly (GO:1903008), and mitotic cell-cycle phase transition.

Specifically, I found that proteins involved in mitochondrial translation (GO:0032543) showed an overall increase. Among the 8 mitochondrial translation-related proteins, I observed that 17 were significantly upregulated ($P \leq 0.05$), while no proteins were significantly downregulated (Fig. 67). Notably, several mitochondrial ribosomal proteins, including MRPS26 (mitochondrial 28S ribosomal protein S26), MRPS23 (mitochondrial 28S ribosomal protein S23), MRPS7 (mitochondrial 28S ribosomal protein S7; binds 12S rRNA and aids mRNA decoding in mitochondria), MRPS25 (mitochondrial 28S ribosomal protein S25), and MRPL24 (mitochondrial 39S ribosomal protein L24), as well as YARS2 (a mitochondrial tyrosyl-tRNA synthetase; charges tRNATyr for mitochondrial protein translation), were markedly upregulated, reflecting an enhanced capacity for mitochondrial protein synthesis (Fig.67D). Enrichment analysis further revealed upregulation in mitochondrial gene expression (GO:0140053), mitochondrial RNA metabolism (GO:0000959), mitochondrial transcription (GO:0006390), tRNA aminoacylation (GO:0043039, GO:0006418), amino acid activation (GO:0043038), and ribosomal subunit assembly (GO:0000028), suggesting an enhanced mitochondrial biogenesis and functional adaptation in response to increased nFGFR1 activity (Fig.67B).

In contrast, cytoplasmic translation (GO:0002181) displayed an overall downward trend. Among the 109 cytoplasmic translation-related proteins identified, 84 were downregulated while only 19 were upregulated. The downregulated components included RPL24 and RPL34, both essential members of the large ribosomal subunit, indicating a reduction in cytoplasmic translation (Fig.61).

In summary, these results demonstrate that nuclear FGFR1 orchestrates a divergent translational program in cortical organoids, downregulating cytoplasmic translation while enhancing mitochondrial protein synthesis. This compartment-specific modulation likely reflects a shift in energy demand and proteostasis, possibly due to a compensatory mechanism to sustain mitochondrial function.

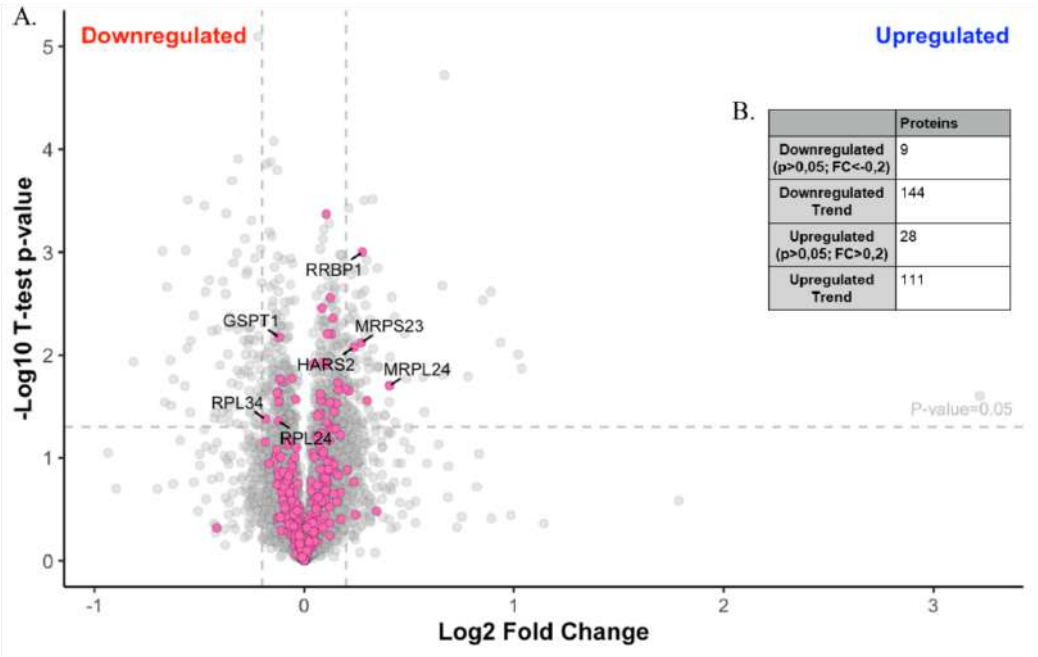

Fig.66. Proteins related to translation proteins (GO:0006412) in hCOs following nFGFR1 upregulation. *A. Volcano plot. A total of translation proteins (GO:0006412) were found in hCOs treated with DOX compared to DMSO (control). Among these, 28 proteins were significantly upregulated ($P \leq 0.05$), while nine were significantly downregulated. Translational proteins appear as pink circles. The x-axis displays log_2 fold changes (DOX vs. control), where positive values reflect upregulation and negative values denote downregulation. The y-axis illustrates $-log_{10}$ p-values from two-tailed t-tests, with greater values indicating stronger statistical validation. Vertical dashed lines represent ± 0.2 log_2 fold change, while the horizontal dashed line marks $-log_{10}$ (0.05). Proteins meeting the significance threshold ($P \leq 0.05$) are annotated with names. B. Protein Expression Trend Categories. Table classifies each protein into one of four categories based on its log_2 fold-change (FC) and p-value: Significantly Upregulated ($Log_2FC > 0$; $P \leq 0.05$); Significantly Downregulated ($Log_2FC < 0$; $P \leq 0.05$); Positive Trend ($0 < Log_2FC$); Negative Trend ($Log_2FC < 0$).*

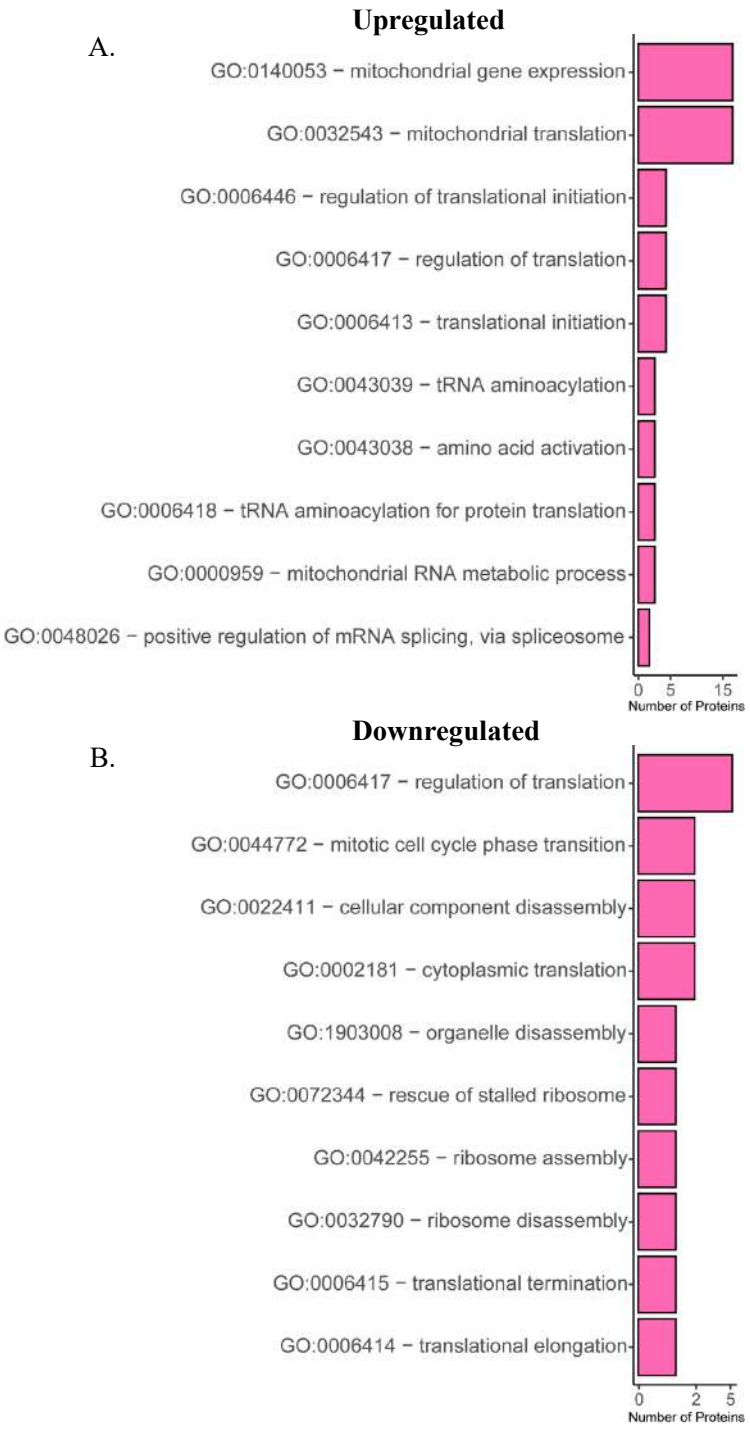

Fig.67. GO enrichment of translational proteins following nFGFR1 activation in hCOs*. Bar charts illustrate the top ten GO biological processes (BP) associated with DEPs related to translation proteins (GO:0006412) in 60-day hCOs following nFGFR1 upregulation. Panel A shows the top ten biological processes that are significantly enriched among upregulated proteins, while Panel B presents the top ten processes that are enriched among downregulated proteins. Enrichment was determined using proteins with* log_2 *fold-change > 0 (upregulated) or < 0 (downregulated) and* $P \leq 0.05$*. Each bar indicates the number of differentially expressed proteins associated with that GO term.*

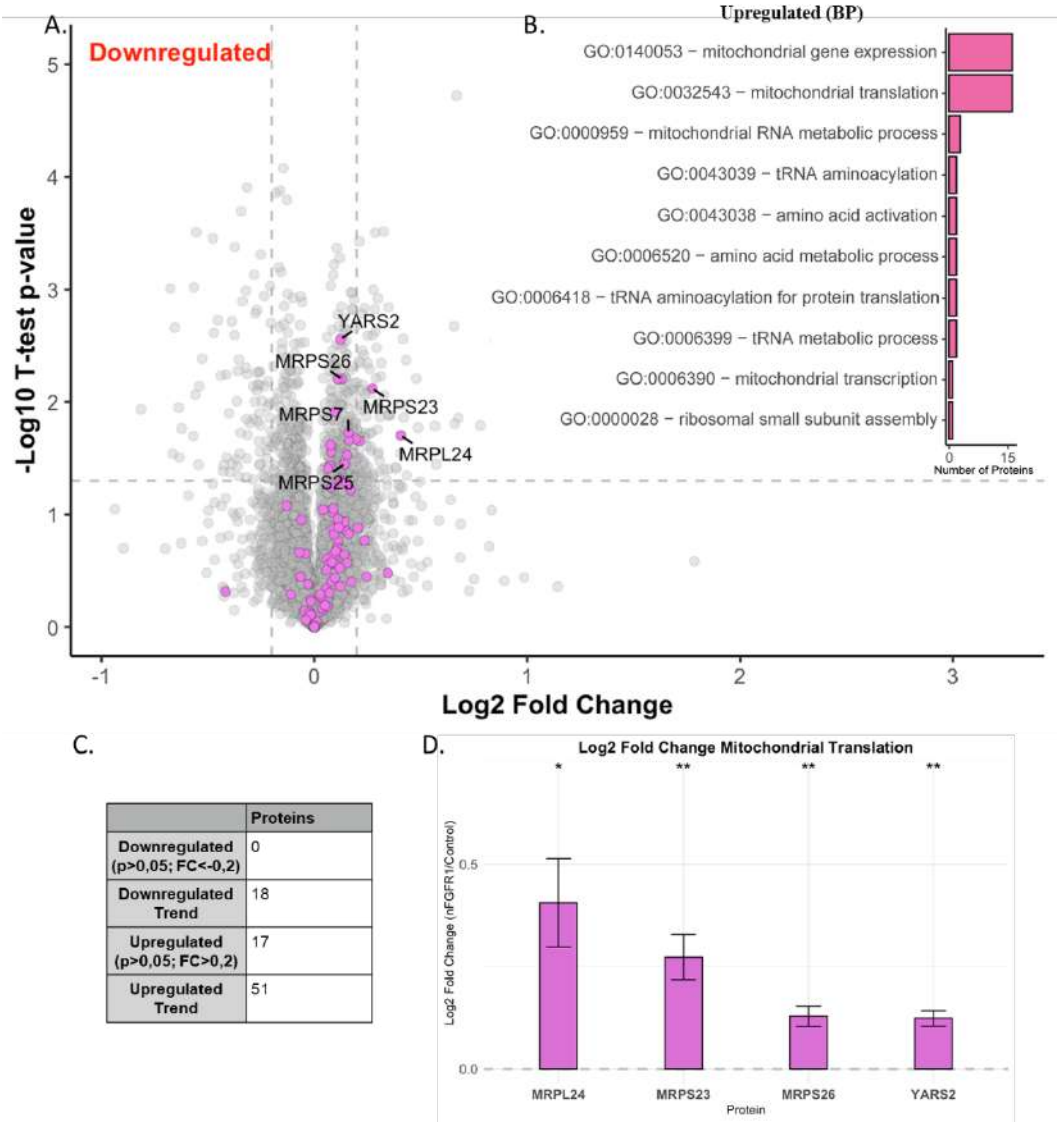

	Proteins
Downregulated (p>0,05; FC<-0,2)	0
Downregulated Trend	18
Upregulated (p>0,05; FC>0,2)	17
Upregulated Trend	51

Fig.68. Proteins related to mitochondrial translation (GO:0032543) in hCOs following nFGFR1 activation. *A. Volcano plot. A total of 86 proteins related to mitochondrial translation (GO:0032543) were identified in hCOs treated with DOX and DMSO (control). Among these, 17 proteins were significantly upregulated ($P \leq 0.05$), while none were significantly downregulated. These proteins are displayed as pink circles. The x-axis displays log_2 fold changes (DOX vs. control), where positive values reflect upregulation and negative values denote downregulation. The y-axis illustrates $-log_{10}$ p-values from two-tailed t-tests, with greater values indicating stronger statistical validation. Vertical dashed lines represent ± 0.2 log_2 fold change, while the horizontal dashed line marks $-log_{10}$ (0.05). Proteins meeting the significance threshold ($P \leq 0.05$) are annotated with names. B. GO Enrichment. Bar charts illustrate the top ten GO biological processes (BP) enriched in upregulated DEPs related to mitochondrial translation (GO:0032543) in 60-day hCOs following nFGFR1 upregulation; C. Protein Expression Trend Categories. Table classifies each protein into one of four categories based on its log_2 fold-change (FC) and p-value: Significantly Upregulated ($Log_2FC > 0$; $P \leq 0.05$); Significantly Downregulated ($Log_2FC < 0$; $P \leq 0.05$); Positive Trend ($0 < Log_2FC$); Negative Trend ($Log_2FC < 0$); D. Plot for Top 4 DEP proteins. The bar graph displays the mean ± SD log_2 fold change for the top four upregulated DEPs mitochondrial translation proteins: MRPL24, MRPS23, MRPS26, and YARS2. Asterisks indicate statistical significance (*$P \leq 0.05$; **$P \leq 0.01$; ***$P \leq 0.001$; ****$P \leq 0.0001$).*

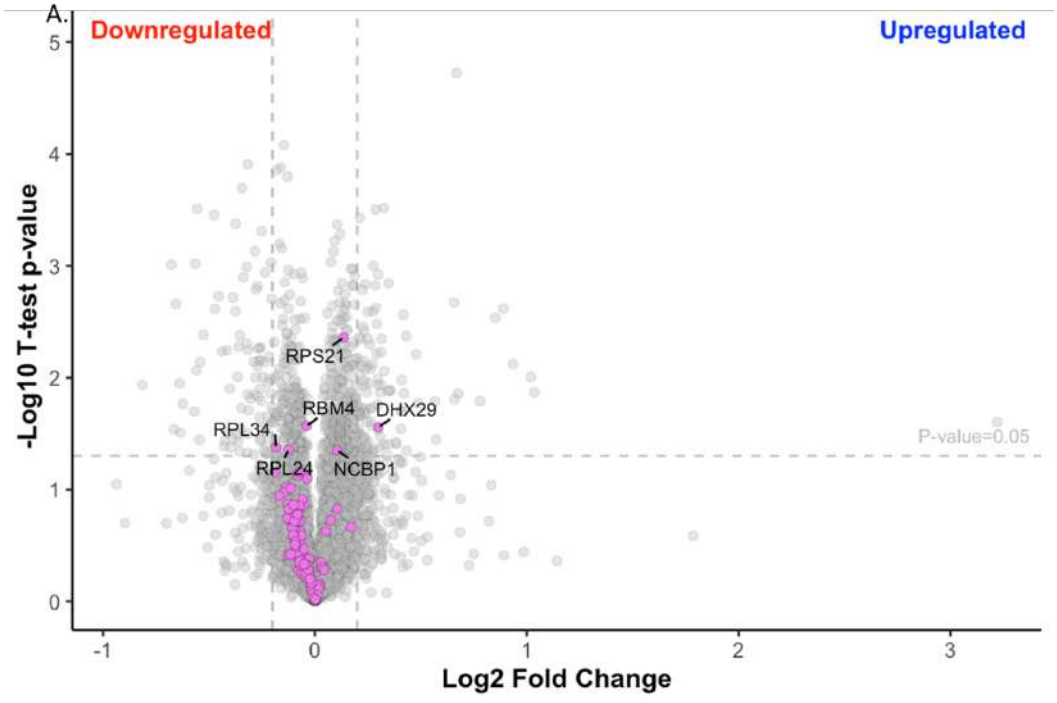

	Proteins
Downregulated (p>0,05; FC<-0,2)	3
Downregulated Trend	84
Upregulated (p>0,05; FC>0,2)	3
Upregulated Trend	19

Fig.69. Proteins associated with cytoplasmic translation (GO:0002181) in hCOs after nFGFR1 activation. *A. Volcano plot. A total of 109 proteins related to cytoplasmic translation (GO:0002181) were identified in hCOs treated with DOX and DMSO (control). These proteins are displayed as pink circles. The x-axis displays log_2 fold changes (DOX vs. control), where positive values reflect upregulation and negative values denote downregulation. The y-axis illustrates $–log_{10}$ p-values from two-tailed t-tests, with greater values indicating stronger statistical validation. Vertical dashed lines represent ±0.2 log_2 fold change, while the horizontal dashed line marks $–log_{10}$ (0.05). Proteins meeting the significance threshold ($P \leq 0.05$) are annotated with names. B. Protein Expression Trend. Table classifies each protein into one of four categories based on its log_2 fold-change (FC) and p-value: Significantly Upregulated ($P \leq 0.05$); Significantly Downregulated ($P \leq 0.05$); Positive Trend ($0 < Log_2FC$); Negative Trend ($Log_2FC < 0$); C. Plot for Top 4 DEP proteins. The bar graph displays the mean ± SD log_2 fold change for the top four DEPs cytoplasmic translation proteins: DHX29, RPS21 (upregulation), and RPL24, RPL34 (downregulation). Asterisks indicate statistical significance (*$P \leq 0.05$; **$P \leq 0.01$; ***$P \leq 0.001$; ****$P \leq 0.0001$).*

5.21. nFGFR1 enhances oxidative stress response proteins without perturbing apoptotic signaling

Reactive oxygen species (ROS) have been recognized as critical modulators of neuronal development, influencing processes ranging from proliferation and differentiation to synaptic plasticity and programmed cell death. FGFR1 signaling has been shown to confer neuroprotection by mitigating oxidative stress, regulating redox homeostasis, and buffering against protein synthesis impairment and p53 accumulation under toxic conditions (Biswas et al., 2022; Ito et al., 2025; Wang et al., 2020). To assess whether nuclear FGFR1 (nFGFR1) influences oxidative resilience and apoptosis during early corticogenesis, I conducted a proteomic analysis in human cortical organoids, revealing a coordinated activation of antioxidant responses alongside a reconfiguration of apoptotic signaling pathways. In the proteomic analysis of 60-day-old human cortical organoids (hCOs), an induction of oxidative stress response pathways and alterations in apoptotic signaling were observed following the upregulation of nFGFR1. Eight proteins were significantly upregulated, while only one was downregulated (Fig.70). Moreover, a general trend of upregulation was noted, with 50 proteins showing increased levels and 29 downregulated. Among the upregulated proteins, OXR1 (oxidation resistance 1), PRDX3 (peroxiredoxin 3, a mitochondrial peroxidase that reduces hydrogen peroxide), PRDX5 (peroxiredoxin 5), and ROMO1 (reactive oxygen species modulator 1, a mitochondrial membrane protein regulating ROS) were included. This indicates the activation of antioxidant defense mechanisms, regulation of mitochondrial redox state, and protection against oxidative damage following nFGFR1 activation.

Next, I examined the GO enrichment of the upregulated proteins associated with the GO term “response to oxidative stress” (GO:0032543). This analysis revealed the upregulation of several stress-related processes, such as “response to reactive oxygen species” (GO:0000302), “cellular response to oxidative stress” (GO:0034599), “response to hydrogen peroxide” (GO:0042542), and “reactive oxygen species metabolic process” (GO:0072593). Additionally, terms such as “response to lipopolysaccharide” (GO:0032496) and “response to molecules of bacterial origin” were also upregulated (GO:0002237) (Fig.70B). These results

suggest that nFGFR1 activates an adaptive redox response to alleviate increased metabolic or mitochondrial stress.

In contrast, I observed that the apoptotic proteins appeared to be more balanced. Out of the 377 apoptosis-related proteins (GO:0006915), 190 showed an upregulation trend and 187 indicated a downregulation trend (Fig.71), with six proteins significantly upregulated and seven significantly downregulated. Both pro-apoptotic and anti-apoptotic proteins were identified within these proteins upon the addition of doxycycline. Among the upregulated proteins, proteins such as OXR1 (oxidation resistance 1; regulates mitochondrial antioxidant defenses), NDUFA13 (Complex I subunit GRIM-19; regulates mitochondrial electron transport), and SLIT2 (Slit Guidance Ligand 2; guidance cue that modulates mitochondrial dynamics and neuroprotection) were detected. On the other hand, proteins that were downregulated included PRKCA (protein kinase C α; promotes cell survival), BCL11B (B-cell cLL/lymphoma 11B; zinc-finger transcription factor that suppresses apoptosis), and CAMK2A (calmodulin-dependent kinase II α; regulates cell death pathways), which are important regulators of apoptotic signaling. (Fig.71C). GO enrichment analysis further illustrated this duality. The downregulated pathways included “regulation of apoptotic signaling pathway” (GO:2001233), “negative regulation of apoptotic signaling pathway” (GO:2001234), “protein localization” (GO:1903829), and “DNA damage checkpoint signaling” (GO:0000077). This suggests a suppression of upstream apoptotic signaling and stress checkpoints. In contrast, the upregulated processes included “intrinsic apoptotic signaling pathway” (GO:0097193), “positive regulation of cysteine-type endopeptidase activity” (GO:2000116), and “positive regulation of hydrolase activity” (GO:0051345), indicating an activation of proteolytic mechanisms (Fig.72A–B).

Overall, the results suggest that nFGFR1 promotes an antioxidant environment within cells while also modifying apoptotic protein pathways. Rather than simply triggering or stopping cell death, nFGFR1 seems to refine apoptotic regulation, minimizing stress-induced apoptosis while permitting the activation of downstream caspase activity. This dual modulation likely promotes neuronal survival and maintains homeostasis in the context of the extensive metabolic reprogramming caused by nuclear FGFR1 signaling.

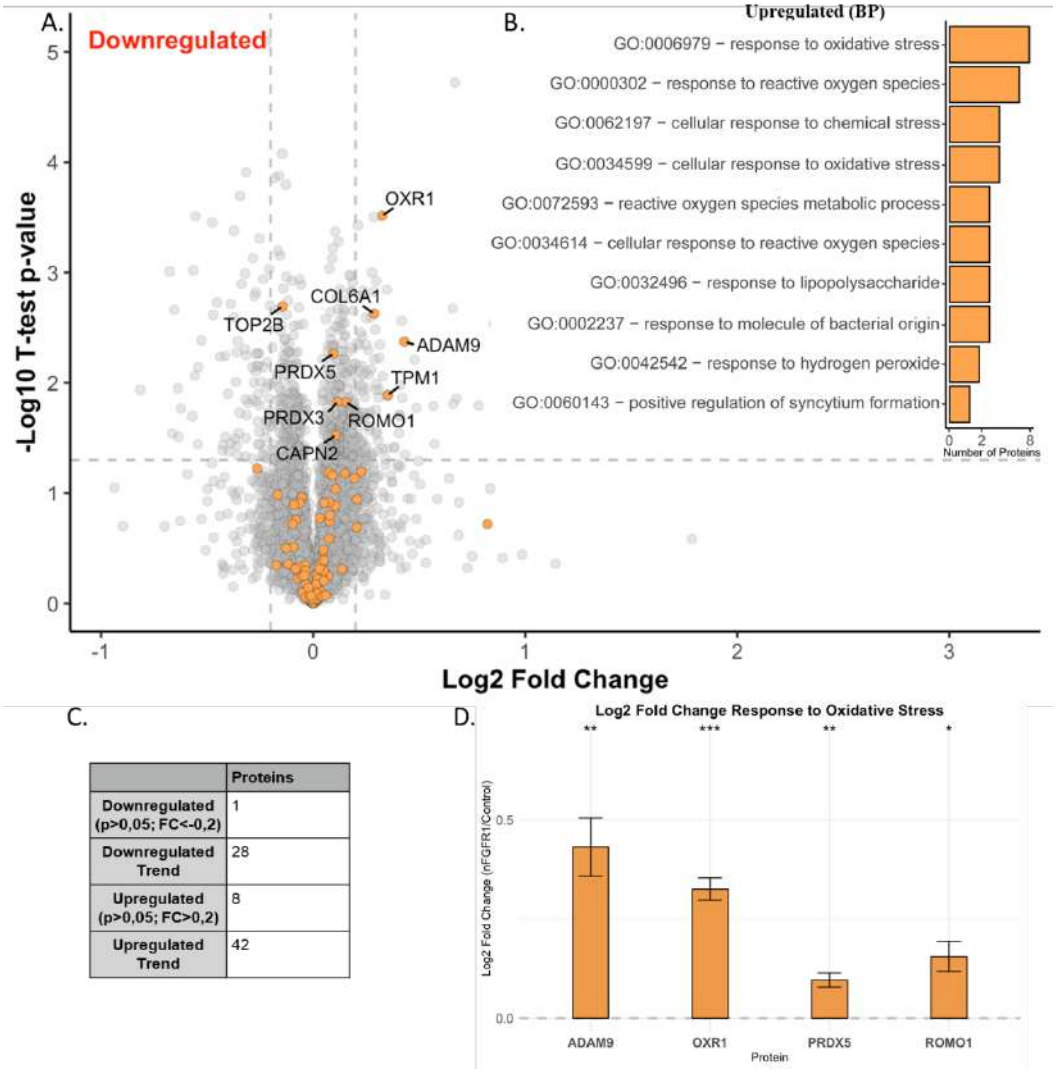

	Proteins
Downregulated (p>0,05; FC<-0,2)	1
Downregulated Trend	28
Upregulated (p>0,05; FC>0,2)	8
Upregulated Trend	42

Fig.70. Proteins related to response to oxidative stress in hCOs following nFGFR1 upregulation. *A. Volcano plot. A total of 70 proteins related to "response to oxidative stress" (GO:0032543), were identified in hCOs treated with DOX and DMSO (control). Among these, eight proteins were significantly upregulated ($P \leq 0.05$), while only one protein was significantly downregulated. These proteins are displayed as orange circles. The x-axis displays log_2 fold changes (DOX vs. control), where positive values reflect upregulation and negative values denote downregulation. The y-axis illustrates $-log_{10}$ p-values from two-tailed t-tests, with greater values indicating stronger statistical validation. Vertical dashed lines represent ±0.2 log_2 fold change, while the horizontal dashed line marks $-log_{10}$ (0.05). Proteins meeting the significance threshold ($P \leq 0.05$) are annotated with names. B. GO Enrichment. Bar charts depict the ten most enriched GO biological processes (BP) related to upregulated DEPs involved in "response to oxidative stress" (GO:0032543) in 60-day hCOs after nFGFR1 upregulation; C. Protein Expression Trend Categories. Table classifies each protein into one of four categories based on its log_2 fold-change (FC) and p-value: Significantly Upregulated ($Log_2FC > 0$; $P \leq 0.05$); Significantly Downregulated ($Log_2FC < 0$; $P \leq 0.05$); Positive Trend ($0 < Log_2FC$); Negative Trend ($Log_2FC < 0$); D. Plot for Top 4 DEP proteins. The bar graph shows the mean ± SD log_2 fold change for the top four upregulated DEPs related to oxidative stress response: ADAM9, OXR1, PRDX5, and ROMO1. Asterisks denote statistical significance (*$P \leq 0.05$; **$P \leq 0.01$; ***$P \leq 0.001$; ****$P \leq 0.0001$).*

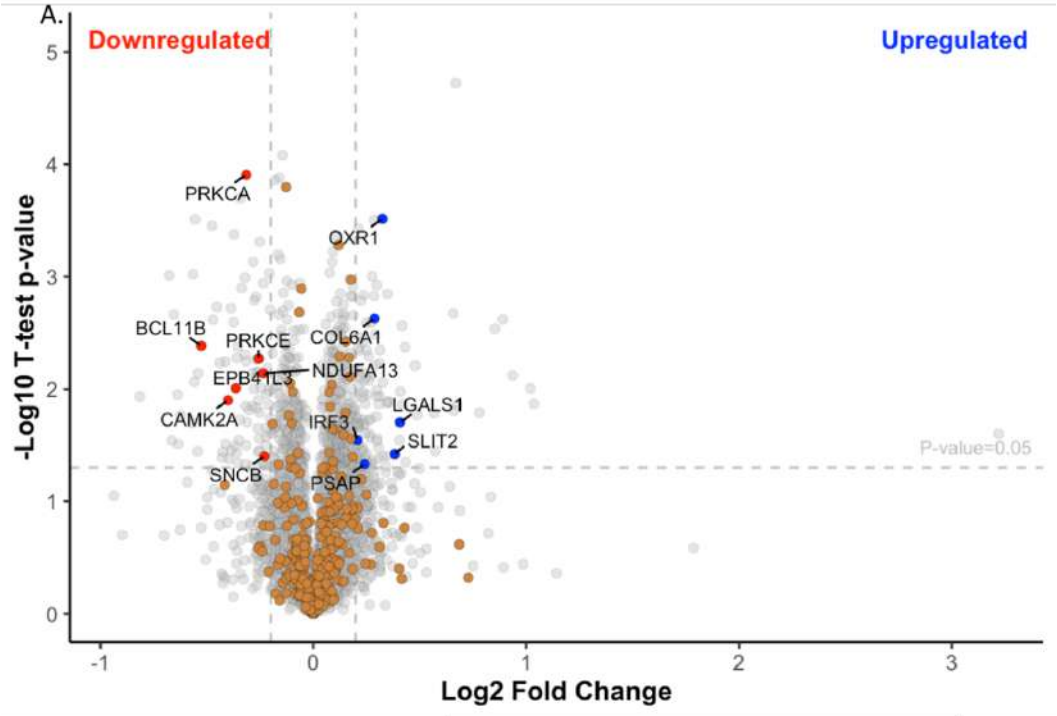

B.

	Proteins
Downregulated (p>0,05; FC<-0,2)	1
Downregulated Trend	28
Upregulated (p>0,05; FC>0,2)	8
Upregulated Trend	42

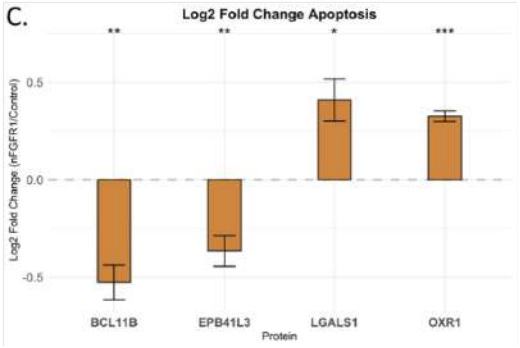

Fig.71. Proteins involved in apoptosis pathways in hCOs after nFGFR1 upregulation. *A. Volcano plot. A total of 377 proteins associated with apoptosis (GO:0006915) were identified in hCOs treated with DOX and DMSO (control). Among these, six proteins were significantly upregulated (Log2FC > 0.2, P ≤ 0.05), while seven proteins were significantly downregulated. These proteins are displayed as brown circles. The x-axis displays log_2 fold changes (DOX vs. control), where positive values reflect upregulation and negative values denote downregulation. The y-axis illustrates $–log_{10}$ p-values from two-tailed t-tests, with greater values indicating stronger statistical validation. Vertical dashed lines represent ±0.2 log_2 fold change, while the horizontal dashed line marks $–log_{10}$ (0.05). Proteins meeting both criteria thresholds (log_2 FC ≥ 0.2; P ≤ 0.05) are highlighted in blue (upregulation) or red (downregulation) and are annotated with names. B. Protein Expression Trend Categories. The table classifies each protein into one of four categories based on its log_2 fold-change (FC) and p-value: Significantly Upregulated ($Log_2FC \geq 0.2$; $p \leq 0.05$); Significantly Downregulated ($Log_2FC \leq –0.2$; $P \leq 0.05$); Positive Trend ($0 < Log_2FC$); Negative Trend ($Log_2FC < 0$).*

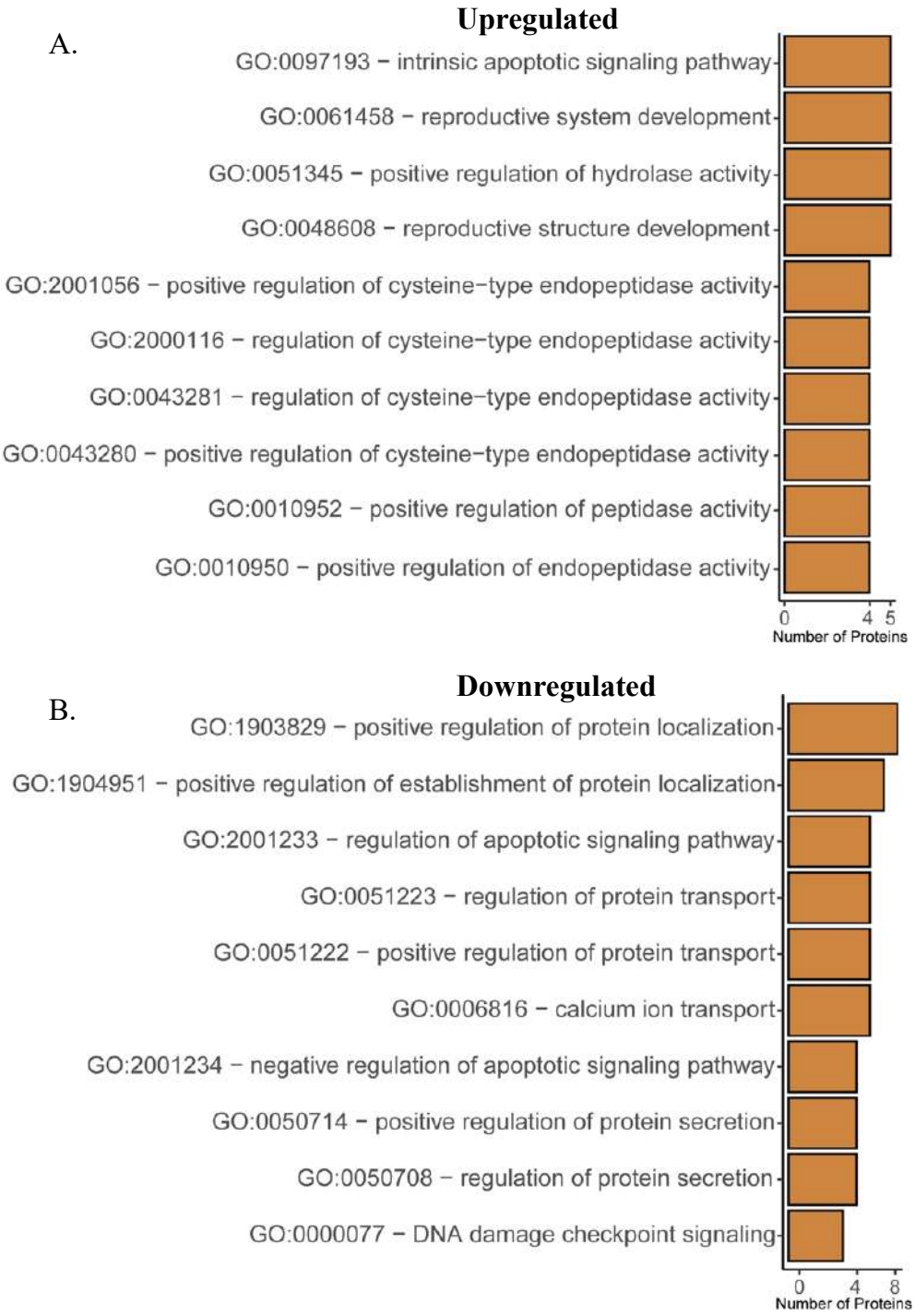

Fig.72. GO enrichment of apoptosis-related proteins (GO:0006915) after nFGFR1 induction in hCOs. *Bar charts illustrate the top ten GO biological processes (BP) associated with DEPs related to apoptosis (GO:0006915) in 60-day hCOs after nFGFR1 upregulation. Panel A shows the top ten biological processes that are significantly enriched among upregulated proteins, while Panel B presents the top ten processes that are enriched among downregulated proteins. Enrichment was determined using proteins with* log_2 *fold-change* > 0 *(upregulated) or* < 0 *(downregulated) and* $P \leq 0.05$*. Each bar indicates the number of differentially expressed proteins associated with that GO term.*

6. Discussion

During the differentiation of embryonic and neural stem cells, a transient accumulation of FGFR1 is observed in the cell nucleus. This process is increased in schizophrenia, leading to premature formation of subcortical neurons and cortical malformations, and expanded in cancer cells with fgfr1 gene duplications, promoting EMT and metastasis.

This dissertation tested the central hypothesis that the accumulation of the nuclear form of the fibroblast growth factor receptor 1 (nFGFR1), which occurs during cortical development in neural stem/progenitor cells (NSPCs) as they differentiate into neuronal lineage cells, governs mitochondrial dynamics and neuronal development during early human brain development. The investigation also addressed the significance of the increased nuclear accumulation of nFGFR1, which is associated with the premature generation of subcortical neurons in schizophrenia neuronal progenitors and could underlie the disruption of mitochondrial processes. I have utilized the previously established recombinant FGFR1(SP-/NLS), in which the FGFR1 signal peptide (SP) was replaced by the Nuclear Localization Signal (NLS), directing the translation of FGFR1 mRNA into ribosomes and the FGFR1 nascent protein into the cytosol, followed by NLS-mediated translocation into the nucleus. This modification eliminates the phase during which the newly synthesized endogenous FGFR1 protein is released from the Golgi and translocated into the nucleus by an NLS-containing ligand (nuclear FGFR1 pathway) or is fully processed by the Golgi and integrated into the plasma membrane (cell surface FGFR1).

Similar to the endogenous nFGFR1, FGFR1(SP-/NLS) associates with chromatin and, along with CBP and other partner proteins, influences gene expression. To test my hypotheses, I engineered an inducible hiPSC$^{\text{Tet3G-FGFR1(SP-/NLS)}}$ line by stably integrating a recombinant Tet3G-regulated FGFR1 transgene (FGFR1(SP-/NLS)) into the CLYBL safe harbor locus. The established hiPSC$^{\text{Tet3G-FGFR1(SP-/NLS)}}$ line maintained expression of pluripotency markers and tri-lineage differentiation potential while enabling doxycycline-inducible expression of nFGFR1 across various hiPSC-derived *in vitro* platforms - embryoid bodies (EBs), neuroepithelial stem (NES) cells, and human cortical organoids (hCOs). My research strategy integrated multi-scale functional assessments, including gene

expression, live-cell reporter imaging, immunofluorescence, morphometric analysis of mitochondria and neuronal rosettes, and proteomic analysis of hCO, to evaluate how nFGFR1 modulates cortical development and mitochondrial regulation across three developmental platforms. I examined changes in NSPCs' proliferation, lineage commitment, mitochondrial morphology, mitophagy, mitochondrial biogenesis, bioenergetics, apoptosis, and global proteomics.

The results indicate that a moderate increase in nFGFR1 expression during early neurogenesis in cortical organoids influences mitochondrial dynamics, neuronal development, and metabolic adaptation by targeting both nuclear and mitochondrial genomes. The up-regulation of FGFR1 selectively enhanced progenitor proliferation and promoted deep-layer neuronal differentiation while diminishing synaptic maturation. At the mitochondrial level, nFGFR1 induced remodeling of mitochondrial networks, enhanced region-specific mitophagy via PINK1–Parkin signaling, and facilitated LC3B autophagosome recruitment, predominantly in cortical plate regions. Notably, these effects did not coincide with changes in mitophagy-related genes and proteins at the global hCO level, suggesting region-specific regulatory mechanisms. While nFGFR1 did not activate mitochondrial biogenesis pathways (e.g., PGC1α promoter activity or mtDNA replication), it increased the expression of the mitochondrial-encoded gene MT-ATP6. This was accompanied by elevated ATP production and mitochondrial membrane potential, indicating that nFGFR1 enhances mitochondrial bioenergetic efficiency rather than mitochondrial biogenesis. Moreover, nFGFR1 elevated ROS levels without triggering apoptosis or integrated stress responses. Cell viability and metabolic activity (ATP levels, membrane potential) increased, indicating that nFGFR1 promotes a state of metabolic resilience and adaptation without compromising cellular equilibrium. Notably, nFGFR1 targets both nuclear and mitochondrial genomes by binding to promoter regions of key mitochondrial regulators and influencing transcriptional programs associated with mitochondrial quality control. The genomic effects of nFGFR1 were associated with global proteomic remodeling, revealing broad shifts in developmental, metabolic, and mitochondrial pathways. Together, these findings advance a new neurodevelopmental model in which nFGFR1 acts as a dual-regulatory role for both mitochondrial and nuclear genomes that integrates developmental and metabolic signals to shape early human cortical development. This research also supports the concept that the overexpression and

increased expression of nFGFR1, observed in schizophrenia NPC, may drive premature subcortical neuronal differentiation and mitochondrial dysfunction. In the following sections, each major result will be reviewed in light of recent literature and interpreted in relation to the original hypothesis, demonstrating the role of nFGFR1 as a dual-genome modulator of developmental and mitochondrial dynamics during human neuronal development.

6.1. Establishment of human induced pluripotent cells with conditional nFGFR1 expression

In this study, I established a doxycycline-inducible human induced pluripotent stem cell line, hiPSC$^{Tet3G\text{-}FGFR1(SP\text{-}/NLS)}$, by targeting the CLYBL (encoding Citramalyl-CoA lyase enzyme) safe harbor locus on human chromosome 13 with a nuclear FGFR1 (nFGFR1) transgene that lacks a signal peptide (SP), driven by a doxycycline-inducible promoter. This allowed for moderate, conditional upregulation of nFGFR1 levels throughout differentiation in various hiPSC$^{Tet3G\text{-}FGFR1(SP\text{-}/NLS)}$ -derived *in vitro* culture models. The system demonstrated the ability to bypass key limitations associated with other safe harbor systems (particularly AAVS1), which have faced gene silencing and gradual loss of transgene expression during directed *in vitro* stem cell differentiation (Bhagwan et al., 2020; Klatt et al., 2020).

The hiPSC$^{Tet3G\text{-}FGFR1(SP\text{-}/NLS)}$ line exhibits typical stem cell morphology, expresses key pluripotent markers (OCT3/4, NANOG, SSEA-4, SOX2), and retains the ability to differentiate into ectodermal, mesodermal, and endodermal lineages. Moreover, NSPC cells differentiated from hiPSC$^{Tet3G\text{-}FGFR1(SP\text{-}/NLS)}$ express neural markers such as PAX6 and Nestin, confirming the maintenance of neural stemness. The CLYBL locus was chosen based on Cerbini et al. (2015), who reported that CLYBL targeting ensured the durability of transgene expression. In my investigation, this targeting sustained transgene expression during neural induction and neuronal development, as evidenced by persistent nFGFR1 inducibility across neuroepithelial NSPCs, embryoid bodies (EBs), and human cortical organoids (hCOs) (Cerbini et al., 2015). An alternative AAVS1 site proved to be more prone to epigenetic silencing and loss of expression upon cell lineage commitment. Although Patterson et al. (2020) reported stable expression of tdTomato under the strong constitutive CAG promoter in the AAVS1 locus, it

experienced promoter-dependent variability when using cell–type–restricted or weaker regulatory elements (Patterson et al., 2020). In line with this, Klatt et al. (2020) showed that myeloid-specific promoters (e.g., MRP8) were silenced in iPSC-derived myeloid cells due to CpG methylation, a mechanism consistent with broader findings on chromatin remodeling during differentiation (Klatt et al., 2020).

In my study, a doxycycline-driven inducible expression of the nuclear form of FGFR1 under the control of the Tet3G promoter allowed for effective and reproducible temporal control. We do not observe promoter leakiness in the absence of doxycycline, indicating that nFGFR1 expression is strictly regulated. Previous studies have shown that promoter leakiness is a common issue that often affects inducible cell lines integrated at the AAVS1 locus (Schmid et al., 2021; Wang et al., 2017). The efficacy of my configuration was also recently demonstrated by Miellet et al. (2024), who utilized the CLYBL locus to introduce DOX-inducible NGN2 in hESCs, resulting in efficient and stable neuronal differentiation (Miellet et al., 2024).

Transgene silencing is a bottleneck for long-term *in vitro* culture systems. Silencing events have been attributed to locus-specific epigenetic regulation and promoter methylation (Cabrera et al., 2022). In this thesis, the combination of CLYBL integration and strong promoter elements likely mitigated such effects, as demonstrated by the stable expression of mApple and nFGFR1 during extended neural differentiation across three different differentiation platforms: embryoid bodies (EBs), neuroepithelial stem (NES) cells, and human cortical organoids (hCOs), lasting at least two months. The ability of the engineered hiPSC$^{FGFR1(SP-/NLS)}$ line to differentiate into neuroepithelial stem (NES) cells and hCOs was preserved, which was essential for successfully modeling human cortical development.

In summary, I have developed the hiPSC$^{FGFR1(SP-/NLS)}$ line, which specifically expresses a nuclear FGFR1 by targeting the CLYBL safe-harbor locus using the TALEN method. The established hiPSC$^{Tet3G-FGFR1(SP-/NLS)}$ line retains pluripotency and can differentiate into all three germ layers. The hiPSC$^{Tet3G-FGFR1(SP-/NLS)}$ line enables effective conditional nFGFR1 overexpression throughout prolonged *in vitro* neuronal differentiation without gene silencing. It serves as an effective

platform to explore the role of nFGFR1 in governing neurodevelopmental and mitochondrial dynamics programs.

6.2. nFGFR1 reduces proliferation and promotes neural stem / progenitor cells (NSPC) differentiation and rosette expansion in hCO

The nFGFR1, by controlling pluripotency and neuronal genes, NSPC proliferation, differentiation, and cell migration into the cortical plate is likely to play a pivotal role in human cortical development (Klimaschewski and Claus, 2021; Ohkubo et al., 2004; Stachowiak et al., 1997; Stachowiak and Stachowiak, 2016). Proliferating NSPCs express primarily a membrane-associated cell surface FGFR1, known to promote cell proliferation. During NSPC differentiation and neuronal development, nFGFR transiently translocates into the cell nucleus, and the nuclear form of FGFR1 (nFGFR1) has been shown to promote neuronal differentiation (Fang et al. 2005). It has been shown that nFGFR1 accumulation is augmented in schizophrenia hCOs, accompanied by premature neuronal differentiation in their subcortical region and cortical malformation (Stachowiak et al., 2017).

In this thesis, I investigated the role of nFGFR1 in hCO, focusing on the effects of nFGFR1 on NSPC proliferation and neuronal differentiation. Overexpression of nFGFR1 significantly decreased the proliferation of NSPC in the periluminal region of the ventricular zone, which contains mitotically active neural stem cells and progenitors surrounding the lumen. This decrease was evidenced by a reduced number of $Ki67^+$ cells next to the rosette's lumen. Notably, there were no significant changes in the numbers of $SOX2^+$ or $PAX6^+$ progenitors in the rosettes, indicating that nFGFR1 shifts the cycling cells to G0 while preserving their progenitor identity. Morphometric analysis showed increased sizes of the hCO and apical rosette areas without changes in the rosette numbers. Thus, nFGFR1 promotes the growth of existing rosettes likely by increasing the number of postmitotic cells, rather than by inducing the formation of new cells or structures in hCO. These observations are consistent with earlier experiments, which showed that transfection or upregulation of the nFGFR1 inhibits cell proliferation and stimulates differentiation of the human medulloblastoma cells, rat PC12 and NPC, mouse ESC, while the nFGFR1 inhibition by dominant negative nFGFR1 (FGFR1(SP-/NLS)(TK-) blocked the cell differentiation (Stachowiak and

Stachowiak, 2016). In mouse ESC, nFGFR1 stimulates transition from the pluripotent state to neuronal differentiation by targeting and inhibiting the pluripotency genes, and genes of the top network controlling cell proliferation and survival, including cyclins (Terranova et al. 2015; Narla et al., 2017). nFGFR1 targets and stimulates mesodermal, endodermal, neural genes and Hox genes, controlling body dimensions and axes and the patterning of the nervous system. As such, nFGFR1 has been established as a "pan-ontogenic" genome regulator, which integrates a plethora of developmental signals through a "feed-forward gate" mechanism (Stachowiak et al., 2003a; M. K. Stachowiak and Stachowiak, 2016).

In this thesis study, the nFGFR1 activation inhibited proliferation, stimulated differentiation of the NSPC and drove rosette expansion in human cortical organoids. These findings align with the earlier reports that the nuclear accumulation of nFGFR1 promotes G0 transition and differentiation of the proliferating cells in contrast to the mitogenic effects of the cell surface FGFR1 (Stachowiak and Stachowiak, 2016). FGFR1 knockout in radial glia, which express largely cell-surface FGFR1, resulted in a significant decline in their proliferation in neurogenic zones and decreased hippocampal volume (Ohkubo et al., 2004). My results also supported a recent study, which showed that FGFR1, particularly in its nuclear form, functions as a transcriptional hub for genes controlling NSPCs' proliferation and differentiation (Klimaschewski and Claus, 2021).

The nFGFR1 reduced NSPC proliferation in hCO could arise through complex mechanisms involving direct transcriptional regulation, chromatin remodeling, and integration of developmental signals. Numerous studies provided mechanistic insights by showing that nFGFR1 directly targets cell cycle regulators such as *TP53* and *E2F1*, while repressing the stemness genes like *SOX2* and *KLF4*. In the Integrative Nuclear FGFR1 Signaling (INFS) pathway, nFGFR1 interacts with transcription co-activators such as CBP (CREB-binding protein) and targets genomic response elements including CRE, AP-1, and NF-κB motifs, enabling nFGFR1 to coordinate the expression of large gene networks involved in cell growth, chromatin organization, and metabolic readiness. nFGFR1 has been asserted a "pan-ontogenic" factor capable of integrating diverse developmental inputs into feed-forward gene expression modules. The pan-ontogenic action of nFGFR1 likely underlies its effects on cell development, mitochondria, and the

metabolism-related effects observed in the present investigation (Narla et al., 2017; Stachowiak et al., 2003b; Terranova et al., 2015).

Study limitations - While my experiments support nFGFR1 participation in human cortical development, several experimental limitations need to be acknowledged. First, the hCO analyses were conducted at a single developmental stage (day 60) and, thus, do not capture the dynamics assigned to different stages of development. Second, my quantitative analysis of cell proliferation focused strictly on the periluminal germinal layer where the NSPCs are located. There were a few Ki67+ cells outside this layer, and their nature will need to be further identified. Additional assays, such as BrdU or EdU incorporation or the FUCCI cell cycle reporter system, could provide further insights into cell cycle kinetics. Most of the imaging and immunofluorescence analyses were performed on fixed samples. Future studies should employ spatio-temporal live imaging to capture the dynamic changes in cell proliferation. Finally, the lineage commitment of differentiating proliferating NSPC and cells migrating out of the periluminal germinal layer could be evaluated further to determine whether nFGFR1 drives expansion of specific neural subtypes in the rosettes. The border of the hCO rossettes could be more precisely delineated with markers such as zonula occludens-1 (ZO-1) and N-cadherin for the apical lumen labeling.

6.3. nFGFR1 accelerates deep-layer neurogenesis and reduces intermediate progenitor pool

Prolonged activation of nFGFR1 in human cortical organoids promoted neuronal differentiation and the generation of deep-layer cortical neurons, similar to that observed in schizophrenia hCO, which overexpresses endogenous nFGFR1 (Narla et al., 2017; Stachowiak et al., 2017). In my study, the immunofluorescence analysis revealed increased numbers of $NeuN^+$ and $CTIP2^+$ postmitotic neurons in the cortical plate, along with a marked rise in $TBR1^+$ cell density and mRNA expression. Additionally, the population of $TBR2^+$ intermediate progenitors was significantly diminished, indicating that nFGFR1 accelerates the transition from progenitor states to differentiated neurons. Notably, these effects occur without changes in general neuronal markers such as *MAP2* or *DCX*, suggesting that nFGFR1 influences specific lineage specification rather than acting pan-neuronally

(Bharali et al., 2005; Fang et al., 2005; Stachowiak et al., 2009). This was further supported by the gene ontology enrichment analysis of the proteomic data from the hCOs, in which nFGFR1 expression was increased with doxycycline treatment. The upregulated pathways included cortical neuron differentiation and axon guidance, enriched with markers such as TBR1 and SLIT2, which is consistent with enhanced deep-layer specification and structural maturation. In contrast, the key regulators of telencephalic identity and neurogenesis, including BCL11B, FOXG1, and EPHA4, were downregulated, along with ontological categories related to forebrain development, axonogenesis, and synaptic transmission.

The results of my investigation demonstrate that increased nFGFR1 expression promotes the differentiation of deep-layer cortical neurons, indicated by an increase in $NeuN^+$, $CTIP2^+$, and $TBR1^+$ cell populations, while reducing the $TBR2^+$ intermediate progenitor pool. This finding closely aligns with previous works that reported nFGFR1 acts as a transcriptional regulator promoting neuronal fate commitment and cortical neuron maturation (Klimaschewski and Claus, 2021; Narla et al., 2017; Stachowiak and Stachowiak, 2016; Terranova et al., 2015). It also aligns with the increased deep TBR1 expression in brain organoids from schizophrenia patients, accompanied by an overexpression of endogenous nFGFR1 and TBR1, along with direct targeting of the TBR1 gene promoter by nFGFR1 (Narla et al., 2017; Stachowiak et al., 2017). The selective increase in deep-layer markers occurred without global changes in general neuronal genes like *MAP2* or *DCX*. Notably, the downregulation of CTIP2 mRNA, despite the increased density of CTIP2+ cells in the cortical plate, suggests a post-transcriptional regulation as part of the nFGFR1 regulatory mechanism (Stachowiak and Stachowiak, 2016). Additionally, the depletion of $TBR2^+$ progenitors supports the model proposed by Gantner et al. (2021) in which nFGFR1 signaling modulates the timing of neuronal differentiation by influencing progenitor pool dynamics. Together, these data indicate that nFGFR1 drives structural neuronal maturation and contributes to a shift in lineage commitment, favoring the generation of postmitotic cortical neurons. However, our data also reveal that the elevated nFGFR1 downregulates critical transcriptional regulators of cortical patterning, including BCL11B, as well as axonogenesis-related proteins (FOXG1, EPHA4, and PARD3). This appears contrary to recent works showing that FGFR1 is essential in maintaining telencephalic identity and proper cortical patterning (Gantner et al., 2021;

Yellapragada et al., 2022). Likely the increase of nFGFR1 needs to be transient to support cortical patterning.

The observed increase in $TBR1^+$ neurons in the cortical plate coincides with the reduction of $TBR2^+$ intermediate progenitors in the rosettes of nFGFR1-overexpressing hCO, is largely consistent with prior findings from different groups. Fagel et al. (2009) showed that FGFR1 activation promotes the generation of $TBR1^+$ excitatory neurons following hypoxic injury, supporting its role in driving neuronal differentiation (Fagel et al., 2009). Similarly, Molnár et al. (2019) emphasized that $TBR1^+$ neurons represent early-born deep-layer excitatory cells arising from radial glia and intermediate progenitors (Molnár et al., 2019). This aligns with the proposition that the expansion of the $TBR1^+$ cell population in the cortical plate occurs at the expense of the premature differentiation of $TBR2^+$ neurons in the subcortical region following nFGFR1 induction. Gantner et al. (2021) reported an opposite effect of exogenous FGF, demonstrating that extended FGF2 treatment delays neuronal differentiation by preserving early progenitor identity *in vitro* (Gantner et al., 2021). This difference may reflect the mode of FGFR1 action (nuclear versus plasma membrane) and the context-specific differences of nFGFR1 function. In my model, nFGFR1 appears to bypass progenitor maintenance by promoting a transition from $TBR2^+$ intermediate progenitors to postmitotic $TBR1^+$ neurons, even at the cost of premature differentiation.

6.4. Regulation of forebrain and axonal development by nFGFR1

The results of proteomic analysis reveal that in hCO, nFGFR1 reprograms pathways related to forebrain development and axonogenesis. The upregulation of TBR1 and SLIT2, both critical for cortical excitatory neuron differentiation and axon guidance, aligns with previous work by Yang et al. (2018), who demonstrated that FGFR1 specifically activates slit1 expression to guide axonal pathfinding in the developing forebrain (Yang et al., 2018). Similarly, Tomé et al. (2023) emphasized FGFR1's central role in promoting axon outgrowth and midline targeting through ligand-dependent mechanisms, particularly involving FGF2 and FGF8. The increased expression of SLIT2 in our dataset indicates that acting specifically in the nucleus, nFGFR1 activates a transcriptional program to promote targeted axon extension. This is further supported by nFGFR1 targeting promoters

of multiple genes in the axon development pathway (Narla et al., 2017; Tomé et al., 2023).

In this investigation, I also observed the downregulation of some axonal and forebrain development markers induced by nFGFR1, including BCL11B, EPHA4, and FOXG1. Together, the results support a model in which nFGFR1 selectively enhances certain aspects of axon guidance and neuronal specification (e.g., SLIT2, TBR1) while selectively suppressing molecular programs for axonal and forebrain development. nFGFR1-induced FOXG1 downregulation observed in my proteomic data could underlie the loss of TBR2+ intermediate progenitors and early neuronal commitment, as FOXG1 has been shown to stimulate the expression of TBR2 and promote NSPC proliferation in the mouse brain (Wang et al., 2022). In this study, I observed a reduction in protein FOXG1 levels in hCO upon nFGFR1 upregulation, which is consistent with the premature neuronal formation at the expense of progenitor expansion. Aberrant FOXG1 expression could also disrupt the homeostasis between glutamatergic and GABAergic neurons (Schäffner et al., 2023).

The nFGFR1-induced upregulation of the deep-layer markers such as TBR1, NeuN, and CTIP2, coinciding with the depletion of the TBR2+ intermediate progenitor pool, suggests that nFGFR1 is a temporal regulator that accelerates neuronal differentiation while limiting progenitor maintenance. Through this mechanism, nFGFR1 could influence the timing of cortical layer formation. Additionally, FGFR1 has been essential for controlling distinct developmental programs in other neuronal and non-neuronal cells, including the auditory epithelium and the telencephalic interneurons (Pirvola et al., 2002; Smith et al., 2014). Therefore, the selective upregulation of deep-layer markers in our organoid model may indicate the unique responsiveness of early cortical domains to nFGFR1-mediated transcriptional programs.

Furthermore, the expression of SLIT2 and TBR1 in my dataset supports a shift toward axonal extension and postmitotic differentiation. However, suppressing upstream regional determinants suggests that elevated nFGFR1 decouples maturation from proper regional patterning. These data collectively indicate that nFGFR1 has a dual function: promoting neuronal commitment and maturation, while also influencing the regional identity landscape. It was previously indicated that nFGFR1 orchestrates neurogenesis through genome-wide regulation

of transcription and chromatin rearrangement (Decker et al., 2021). In line with this, Dhiman et al. (2024) demonstrated that nFGFR1 modulates neurodevelopment by synchronizing transcriptional activity across broad gene activity networks (GANs) and organizing recurring coordination modules (RCMs). This process may facilitate the transition from progenitor to differentiated neuron by coordinating gene activities (Dhiman et al., 2024). Moreover, Decker et al. (2020) revealed that nFGFR1 functions not only as a transcriptional regulator but also as a genomic architect, directly shaping the chromatin landscape through topologically associating domain (TAD) formation and chromatin looping (Decker et al., 2021). The "Genome Archipelago Model" describes how nFGFR1, together with CTCF, mediates spatial genome organization to control multi-gene clusters. This type of control could underlie the observed nFGFR-induced shift toward increased $TBR1^{+}$ neuron formation while turning off gene programs for the TBR2+ intermediate progenitors. Thus, nFGFR1 may modulate region- and stage-specific neurogenic programs at both transcriptional and chromatin structural levels. The observation that $CTIP2^{+}$ cell numbers increase in the hCO cortical layer upon nFGFR1 induction, despite an overall reduction in hCO BCL11B (CTIP2) mRNA and protein levels, suggests that nFGFR1 enhances CTIP2 protein spatially through localized transcription and/or translation of CTIP2 in differentiating deep-layer neurons, even as global hCOs CTIP2 expression decreases.

My investigation highlights the complex role of nFGFR1 in synaptogenesis. Overexpressed nFGFR1 significantly reduces $Synapsin\text{-}2^{+}$ puncta density in the cortical zone, SYP (Synaptophysin) mRNA, and broadly suppresses key synaptic proteins involved in neurotransmitter release, including GRIA2, SYN2, CPLX2, SNCA, and SEZ6, while downregulating pathways critical to synaptic vesicle transport and postsynaptic membrane signaling. The upregulation of nFGFR1 occurs transiently during the differentiation of NSPCs, is maintained during the formation of neuronal pathways and axonal growth, but is reduced and largely reverted to cell surface localization as the axons innervate and establish synaptic contacts with their targets. The suppression of the synaptogenic mechanism and reduced number of synapses in my hCO model may reflect a continued overexpression of nFGFR1. We hypothesize that the persistent nuclear upregulation of nFGFR1 may compromise the molecular framework required for functional synaptic integration. Previous studies have established the role of endogenous

FGFR1 as a critical regulator of synaptogenesis, primarily promoting excitatory presynaptic development and synaptic plasticity (Dabrowski et al., 2015; Terauchi et al., 2010; Umemori et al., 2004; Zhao et al., 2007). For example, Zhao et al. (2007) used FGFR1b mutant mice to show that the loss of FGFR1b significantly reduced excitatory synaptic vesicle formation while leaving inhibitory synapses unaffected, suggesting a selective function for FGFR1 in establishing functional connections (Zhao et al., 2007). Similarly, Umemori et al. (2004) demonstrated that FGF22 FGFR1 activation promotes the clustering of synaptic vesicles and presynaptic differentiation in the developing brain, particularly within the cerebellum and hippocampus (Umemori et al., 2004). It was further shown that ligand-specific activation of FGFR1 and FGFR2 regulates excitatory and inhibitory synapse formation (Terauchi et al., 2010). These molecular changes were verified at both the transcriptomic and proteomic levels.

In summary, the nFGFR1 upregulation specifically initiates the early phases of neuronal development, including the exit of NSPCs from the cell cycle, cell migration, the onset of neuronal differentiation, and the axonal growth program, but it does not lead to robust synaptogenesis. The latter may require a reduction in nFGFR1 signaling, which could be tested by turning off the doxycycline induction of nFGFR1.

One possible mechanism that may influence the neurodevelopmental and synaptogenic effects of the overexpressed nFGFR1 in hCO is the way in which nFGFR1 regulates energy production in hCO. In summary, as discussed in the following sections, upregulated nFGFR1 limits mitochondrial oxidative phosphorylation (OXPHOS) as an energy-producing method and shifts it toward localized aerobic glycolysis and glycolipid metabolism. In my study, nFGFR1 downregulated essential OXPHOS subunits, including NDUFA7, COX6C, and MT-CO2, indicating compromised mitochondrial respiratory function. This downregulation of OXPHOS was accompanied by the upregulation of key glycolytic enzymes like PKM (pyruvate kinase M1/2) and the lactate transporter SLC16A3, as well as other proteins involved in glucose metabolism. Glycolysis is capable of sustaining the energy needs of early neuronogenesis but may not be adequate for the high energy demands of synaptic function.

In summary, my investigation supports the model in which nFGFR1 acts as a global modulator of human cortical neurogenesis by promoting deep-layer

neuronal differentiation, depleting intermediate progenitor populations, activating neurogenic and axon guidance pathways, and influencing neuronal identity and synapse formation.

Study limitations - This study presents new insights into nFGFR1's role in human cortical neurogenesis, but several limitations should be noted. First, all analyses were conducted at a single developmental time point, and further studies will be necessary to decipher the dynamics or stage-specific effects of nFGFR1, particularly at later neuronal maturation (beyond 100 days). Moreover, the use of fixed organoids restricts the resolution of temporal processes and cellular dynamics. Implementing spatio-temporal imaging of hCOs with live-cell reporters activated by cell-type-specific promoters could offer valuable real-time insights into neurogenic lineage dynamics. Additionally, proteomic analyses conducted on bulk organoid samples, which did not allow for determining spatial heterogeneity and cell-type-specific expression. Future studies should integrate single-cell sequencing, spatial transcriptomics, and single-cell proteomics to illuminate region-specific effects of nFGFR1. To better understand the regulatory landscape of neuronal development, future research should utilize epigenomic methods such as ATAC-seq to evaluate chromatin accessibility or CUT&RUN-seq, as well as chromatin analyses like HiC and HiChiP, to identify alterations in chromatin structure. These approaches would provide insight on how nFGFR1 signaling impacts both transcriptional output and post-transcriptional dynamics during human cortical development. The highlighted methodological limitations underscore the necessity for long-term studies employing advanced tools to more deeply elucidate the mechanisms by which nFGFR1 regulates cortical development in a stage- and cell-type-specific manner.

6.5. nFGFR1 modulates mitochondrial morphology and enhances mitophagy via PINK1–Parkin pathway

Mitophagy is widely recognized as a fundamental process in neurogenesis, ensuring the mitochondrial quality control and energy homeostasis necessary for proper neuronal differentiation and neuroprotection (Lou et al., 2020). My research demonstrates that nFGFR1 regulates mitochondrial network dynamics during the development of the human cortex. In the cortical plate, populated mainly by

postmitotic maturing neurons dependent on mitochondrial oxidative phosphorylation (OXPHOS), the expression of nFGFR1 promotes a shift towards smaller, more fragmented mitochondria and a less complex network architecture typically associated with reduced oxidative metabolism or fusion processes, which may not be sufficient for the continued development of cortical connectivity. In human cortical organoid (hCO) layers, nFGFR1 stimulated mitophagy, as evidenced by the mitoKeima assay, along with a region-specific increase in PINK1 and PARKIN levels, and the recruitment of mitochondrial LC3B autophagosomes in the cortical layer of hCOs. However, I did not observe any changes in the global transcript levels of mitophagy genes in whole hCO RNA. Nevertheless, proteomic profiling indicated an overall enrichment in late-stage autophagy and lysosomal biogenesis.

In the subcortical region, where nFGFR1 promoted neuronal differentiation, it also facilitated modest mitochondrial elongation and network branching, indicating enhanced fusion and potentially increased metabolic efficiency. Mitochondrial morphology and dynamics are closely linked to their metabolic functions and neurodevelopmental states. The fused, branched networks support oxidative metabolism in differentiated neurons, while fragmented forms predominate in glycolytic progenitors (Khacho and Slack, 2018; Liu et al., 2024; Romero-Morales et al., 2022).

My investigation collectively suggests that nFGFR1 regulates mitochondrial network morphology, region-specific mitochondrial turnover, and autophagic flux during neuronal development, acting in a region-specific manner. Increased nFGFR1 expression in hCO enhanced elongation and mitochondrial interconnectivity in the ventricular zones, indicating that it promotes mitochondrial expansion during NSPC differentiation and the formation of early neurons. This aligns with previous studies that have shown mitochondrial morphology is closely linked to neurodevelopmental fate decisions, with fused networks supporting stemness and fragmented mitochondria associated with differentiation (Iwata et al., 2020; Khacho and Slack, 2018). Furthermore, the prolonged overexpression of nFGFR1 in the cortical layer may have decreased mitochondrial number, network connectivity, branching, and mitochondrial function by counteracting the effects of endogenous FGFR1, which has been shown to support mitochondrial fusion (Yan et al., 2023). Hu et al. (2018) also found that endogenous FGFR1 regulates

mitochondrial biogenesis in endothelial cells by upregulating the expression of fusion-related proteins OPA1 and MFN2 via microRNA let-7b-5p (Hu et al., 2018). The complex regulation of mitochondrial morphology by nFGFR1 may also be disrupted in schizophrenia, where the overexpression of endogenous nFGFR1 in neurons could result in the underdevelopment of mitochondrial networks and cortical layers.

Together, the findings of this thesis position FGFR1 as a stage-sensitive regulator of mitophagy and mitochondrial quality control, functioning to meet the changing metabolic demands and signaling contexts during the development of the human brain cortex.

6.6. Global hCO proteomic profiling does not reveal a shift in the expression of mitophagy-related proteins

BNIP3 and Parkin are pro-mitophagy factors that mediate the removal of damaged mitochondria, particularly under stress or hypoxic conditions (Zhang and Ney, 2009). The nFGFR1-driven mitophagy may occur through transcriptional control of the mitophagy regulators, as ChIP-seq revealed that nFGFR1 binds to the promoters of *PINK1* and *BNIP3* (Narla et al., 2017; Terranova et al., 2015). Such regulation could occur in selected cells or regions, as global transcript levels of *PINK1*, *BNIP3*, and *SQSTM1* were not significantly changed by nFGFR1 in whole hCO RNA. My assay may not have detected cell-restricted *PINK1*, *BNIP3*, and *SQSTM1* mRNA upregulation. Harbauer et al. (2022) showed that *PINK1* mRNA is cotransported with mitochondria and translated locally in axons, enabling precise mitophagy activation at distal sites (Harbauer et al., 2022). Similarly, Lin et al. (2017) identified that neurons engage early mitochondrial quality control through vesicle-mediated cargo release and transport, independent of full mitophagic degradation, underscoring the compartmental nature of mitochondrial maintenance in neural systems (Lin et al., 2017). Alternatively, the increase in PINK1 and PARKIN proteins, along with the lysosomal LC3B protein, could reflect region-specific post-transcriptional regulation driven by nFGFR1. This regulation selectively engages the translation and/or degradation of the mitophagy proteins in areas with high metabolic demand or mitochondrial turnover needs.

The local translation hypothesis may explain the regional specificity of nFGFR1-induced mitophagy in cortical organoids. As previously shown, neurons possess the capacity for localized translation of mitochondrial proteins directly within axons and dendrites (Harbauer et al., 2022; Kuzniewska et al., 2020; Yousefi et al., 2020). These localized translation events, often triggered by synaptic activity or developmental signals, support rapid mitochondrial remodeling and function without relying on long-range transport. According to this mechanism, nFGFR1 could enhance the localized translation of mitophagy regulators such as PINK1 and Parkin, enabling local autophagy of damaged or excessive mitochondria. This study revealed that nFGFR1 overexpression in hCO leads to a complex modulation of autophagy and lysosomal pathways. Proteomic analyses demonstrated that while overall autophagy-related protein expression remained balanced, there was a distinct upregulation of proteins associated with autophagosome maturation and lysosomal degradation, such as LAMP2 and CTSB. This indicates an enhancement of late-stage autophagy and lysosomal function. The autophagy and lysosomal dynamics are key regulators of neuronal development, supporting stem cell maintenance, differentiation, and fate decisions through metabolic and translational regulation (Calatayud-Baselga et al., 2023; Fleming et al., 2022; Zou et al., 2024). The potential role of nFGFR1 in these processes was indicated by ontological enrichment of the protein translation controlling genes (Narla et al., 2017; Terranova et al., 2015).

In summary, my study revealed that nFGFR1 is a key modulator of mitophagy during early human cortical development. Through the spatially restricted activation of mitophagy in the cortical plate, nFGFR1 induces mitochondrial turnover via the PINK1–Parkin pathway and promotes LC3B-mediated autophagosome engagement. This region-specific activation may reflect a post-transcriptional mode of regulation to meet the varying energy demands of glycolytic neuronal progenitors and differentiating neurons. In addition, proteomic data reveal that nFGFR1 promotes late-stage autophagy and lysosomal biogenesis, suggesting a global role in maintaining organellar homeostasis. These findings establish nFGFR1 as a central modulator linking mitochondrial processes with neurodevelopmental transitions from progenitor to post-mitotic neuronal states.

Study limitations - A key strength of this study is the use of a developmentally relevant 3D organoid model that reliably represents early

cortical development and the selective use of a nuclear form of FGFR1. Moreover, a combination of reporter assays, high-resolution imaging, and biochemical assays enables tracking of mitophagy in live cells and determining the region-specific effects of nFGFR1 on mitochondrial turnover. However, several limitations should be noted. First, the mitophagy markers used in this study (PINK1, Parkin, and mitochondrial LC3B colocalization) provide a snapshot of ongoing mitophagy, rather than evaluating the dynamics of this process. It remains possible that nFGFR1 accelerates the completion of mitophagy or increases the initiation rate. Long-term live-cell time-lapse imaging with mitophagy reporters (e.g., mito-QC or mito-Keima) could facilitate the evaluation of dynamic changes in mitophagy during hCO development following nFGFR1 activation. Additionally, while we determine mitochondrial function using a broad array of assays (increased PINK1/Parkin targeting presumably to damaged organelles), we primarily focused on the effect of nFGFR1 on specific regions of hCO (cortical and subcortical regions and the ventricular zone) or bulk samples (for proteomics and RNA analyses) rather than assessing mitochondrial processes at a single-cell level. Future studies could employ functional mitochondrial assays in FACS-sorted specific neuronal populations. Future work should examine the effect of nFGFR1 across multiple stages of hCO development to evaluate stage-specific effects of nFGFR1 on mitochondrial dynamics.

6.7. nFGFR1 reprograms mitochondrial functions without affecting mitochondrial biogenesis

Contrary to the initial hypothesis, we found no evidence that nFGFR1 activates mitochondrial biogenesis. In hCOs, which lack vascular cells, nFGFR1 produced no significant change in mtDNA copy number or in PGC1α activity, and thus, does not appear to activate mitochondrial biogenesis. In contrast, Wang et al. (2016) demonstrated that FGF21–FGFR1 signaling enhances mitochondrial biogenesis in brain vascular smooth muscle cells while alleviating oxidative stress (Wang et al., 2016). The doxycycline-induced expression of nFGFR1 led to its accumulation in the nuclei and mitochondria. In the mitochondrial genome, nFGFR1 significantly increased *MT-ATP6* mRNA, and a similar trend was observed in *MT-ND2* and *MT-ND5* mRNA, which showed a tendency to be

upregulated. Given nFGFR1's binding to the mtDNA, it could activate mitogenome genes directly in the mitochondrial matrix. Additionally, nFGFR1 may control mitochondrial genes indirectly by controlling the expression of the nuclear DNA-encoded transcription factors, which translocate to the mitochondrial DNA.

The proteomics analysis of nFGFR1-regulated human cortical organoids (hCOs) revealed coordinated alterations in neuronal development, along with significant mitochondrial adaptations. Among the proteins upregulated by elevated nFGFR1 levels, I identified key neuronal developmental regulators, including FGFR1, the receptor tyrosine kinase whose nuclear form drives transcriptional programs in neurogenesis, and TBR1, a T-box transcription factor that plays a crucial role in defining deep-layer cortical neurons in layer 5 and 6 (Crespo et al., 2022); SLIT2 serves as an axon guidance cue that helps direct developing neuron axons to their correct targets (Gohrig et al., 2014); ECE1 is an endopeptidase that contributes to the contraction and relaxation of blood in the brain's vessels (Palmer et al., 2013); BAIAP2, a scaffold protein that regulates the formation of dendritic spines (Kang et al., 2016); CUX1 is essential for dendrite development and the integration of layers II and III neurons in the human brain (Cubelos et al., 2015). Together, these proteins underscore coordinated regulation of neuronal differentiation, migration, and synaptic maturation in response to nFGFR1 upregulation. These upregulated proteins were enriched in Gene Ontology (GO) terms associated with crucial neurodevelopmental processes, including forebrain development (GO:0030900), cerebral cortex formation (GO:0021987), pallium (GO:0021543), and telencephalon development (GO:0021537). Furthermore, these proteins participated in pathways essential for axonal guidance (GO:1902667), axonogenesis (GO:0007409), regulation of neuronal differentiation (GO:0051960), and actin cytoskeletal dynamics (GO:0030833).

In contrast, I noted a significant downregulation of various proteins essential for cortical neuron identity, neuronal migration, synaptic organization, and function. Notably, these included BCL11B (CTIP2), a transcription factor vital for the development and axonal targeting of cortical layer V projection neurons (Du et al., 2022); SOX5 is a crucial regulator that facilitates the exit of neural progenitors from the cell cycle (Stevanovic et al., 2021); NCAM2, which plays a role in synaptic stabilization and neurite outgrowth (Parcerisas et al., 2020; Sheng et al., 2019); and FOXG1 are critical for forebrain patterning and progenitor cell

proliferation. Furthermore, downregulated proteins such as EPHA4, PARD3, FOXC1, GRIA2, SYN2, CPLX2, SNCA, and SEZ6 collectively support essential processes in synaptic vesicle trafficking, neurotransmitter release, postsynaptic organization, and synaptic plasticity (Corradi et al., 2014; Lu et al., 2009; Vargas et al., 2014; Voglewede et al., 2024). This downregulation correlated with enriched GO terms indicating reduced synaptic vesicle cycling (GO:0099504), diminished vesicle-mediated synaptic transport (GO:0099003), impaired synaptic signaling (GO:0099643), and altered neurotransmitter transport (GO:0006836), collectively emphasizing a broad attenuation of synaptic functions.

Alongside these neuronal changes, my analysis uncovered substantial mitochondrial adaptations. Specifically, I observed an increased expression of the oxidative stress protectors OXR1, which are essential for protecting against oxidative stress and suppressing oxidative DNA damage (Matsui et al., 2019), as well as mitochondrial thioredoxin TXN2, a critical regulator of intramitochondrial redox balance during neuronal development (Holzerova et al., 2016). Additionally, the upregulation of nFGFR1 led to in increased levels of mitochondrial ribosomal proteins (MRP), including MRPL24, MRPS26, MRPS23, MRPS7, and MRPS25. These proteins are subunits of the mitochondrial ribosome (mitoribosome), crucial for translating proteins encoded by mitochondrial DNA (Di Nottia et al., 2020); the mitochondrial aminoacyl-tRNA synthetase YARS2 is involved in the proper mitochondrial translation and assembly of respiratory chain complexes in the mitochondria (Jiang et al., 2016).

I also observed coordinated upregulation of metabolic enzymes that support enhanced glycolytic flux and glucose metabolism, including pyruvate kinase M2 (PKM2), a glycolytic enzyme that plays a key role in facilitating the conversion of phosphoenolpyruvate to pyruvate, leading to ATP production (Christofk et al., 2008), and monocarboxylate transporter SLC16A3 (MCT4), which regulates lactate export to maintain redox balance in highly glycolytic cells (Silagi et al., 2020). Furthermore, following increased nFGFR1 expression, I noted an increased expression of proteins involved in intracellular carbohydrate metabolism : acid α-glucosidase (GAA), a lysosomal enzyme that breaks down glycogen (Lee et al., 2018), and dicarbonyl/L-xylulose reductase (DCXR), which is a key enzyme in the pentose metabolism pathway (Yang et al., 2018).

Finally, nFGFR1 induction led to upregulation of lysosomal hydrolases and associated proteins - including glucocerebrosidase (GBA), which regulates glycosphingolipid balance by breaking down glucosylceramide into glucose and ceramide (Smith and Schapira, 2022); galactocerebrosidase (GALC), a lysosomal enzyme that breaks down lipids such as galactosylceramide and galactosylsphingosine (Santambrogio et al., 2012); GM2 activator (GM2A), a lysosomal co-factor essential for the breakdown of GM2 gangliosides (Yoldaş Çelik et al., 2025); and β-glucuronidase (GUSB), a hydrolase involved in the degrading glycosaminoglycans containing glucuronic acid residues (Naz et al., 2013). I also observed an increased expression of other lysosomal proteins following nFGFR1 induction, such as cathepsin B (CTSB), a cysteine protease that is crucial for protein degradation and the regulation of cell death (Xie et al., 2023); progranulin (GRN) is a secreted growth factor involved in regulating lysosome function, including proteolysis and lipid degradation (Simon et al., 2023); lysosome-associated membrane protein 2 (LAMP2) is a lysosomal membrane protein that is crucial for macroautophagy (MA) and chaperone-mediated autophagy (Rothaug et al., 2015); and TGFBRAP1 (TGF-β receptor–associated protein 1), a subunit of the CORVET complex that mediates endosome–lysosome vesicle fusion and facilitates protein trafficking to lysosomes (Sőth et al., 2024). That suggests that nFGFR1 promotes a widespread activation of lysosomal degradation and recycling pathways to address the increased metabolic demands during neuronal development.

GO enrichment highlighted enhanced mitochondrial gene expression (GO:0140053), mitochondrial translation (GO:0032543), mitochondrial RNA metabolism (GO:0000959), and broader mitochondrial organization (GO:0007005), as well as amino acid catabolism (GO:0009063), glycolytic process (GO:0006096), pyruvate metabolism (GO:0006090), ADP catabolism (GO:0046032), glucose metabolism (GO:0006006), sphingolipid and glycolipid catabolism (GO:0006689; GO:0046475), macroautophagy (GO:0016236), vacuole and lysosome organization (GO:0007033; GO:0007040), and “response to reactive oxygen species” (GO:0000302).

In contrast, I identified a downregulation of the electron-transport chain components NDUFA7, NDUFB3, and NDUFV1 (complex I subunits essential for NADH dehydrogenase activity), as well as COX6C and MT-CO2 (complex IV

subunits critical for cytochrome c oxidase function). I also identified noted a downregulation of lipid-transporting proteins such as VPS13A, which mediates interorganelle lipid trafficking (Lees and Reinisch, 2020), and FABP5 (fatty acid-binding protein 5), which maintains lipid signaling and metabolism by binding and transporting long-chain fatty acids within the cytoplasm (Yu et al., 2014). Furthermore, signaling proteins were also suppressed following the upregulation of nFGFR1. This included NEDD4L (HECT-domain E3 ubiquitin ligase), which tags membrane proteins and receptors with ubiquitin, directing them for proteasomal degradation and playing a crucial role in clearing misfolded and damaged proteins (Kim et al., 2021). Meanwhile, PRKCA (Protein kinase C alpha) is a calcium-dependent serine/threonine kinase that regulates neuronal differentiation, maturation, and survival by phosphorylating various substrates (Hapak et al., 2019; Van et al., 2021).

Corresponding GO terms indicated suppression of oxidative phosphorylation (GO:0006119), ATP synthesis–coupled electron transport (GO:0042775), aerobic electron transport (GO:0019646), purine triphosphate biosynthesis (GO:0009145), and regulatory pathways governing autophagy (GO:0010506), macroautophagy (GO:0016241), and mitophagy (GO:1901524). Collectively, these changes suggest that nFGFR1 drives both enhanced mitochondrial biogenesis and a metabolic shift toward glycolysis and lysosomal turnover, while diminishing classical respiratory functions and selective protein-quality control pathways. These alterations imply that nFGFR1 reprograms mitochondrial function, energy metabolism, and protein synthesis to accommodate elevated energetic and biosynthetic demands triggered by enhanced neuronal differentiation driven by nFGFR1 signaling.

Study limitations - Since my TMT-based proteomics analysis was conducted using whole-organoid lysates, these averaged measurements cannot accurately reflect the region- and cell-type-specific dynamics observed in high-resolution imaging studies. As a result, subtle yet biologically significant changes in protein expression within specific neuronal subpopulations or localized areas may have been overlooked. Future analyses employing spatially resolved proteomics or single-cell approaches will be essential to thoroughly elucidate the intricate and localized effects of nFGFR1 signaling. For instance, high-resolution imaging revealed that nuclear FGFR1 (nFGFR1) upregulation specifically

decreased progenitor proliferation within the periluminal region of the ventricular zone, accompanied by structural remodeling of neuronal rosettes. In contrast, proteomics analysis, due to its resolution limits, failed to differentiate these region-specific phenomena, thereby underestimating the localized impact of nFGFR1 signaling. Additionally, microscopy analysis revealed region-specific activation of the PINK1/Parkin mitophagy pathway and increased mitochondrial LC3B localization specifically in the cortical zone after nFGFR1 upregulation. However, global proteomics analysis did not display significant changes in overall mitophagy-related protein levels. This discrepancy emphasizes the limitations of bulk proteomics in capturing spatially restricted mitophagy responses, highlighting the need for complementary spatial analyses.

To address these limitations, I enhanced the global proteomics approach with various functional assays and region-specific analyses. This included a morphometric analysis of mitochondrial morphology and network connectivity using high-resolution confocal microscopy, combined with semi-automated analysis through the Mitochondria Analyzer plugin, which allowed for detailed quantification of mitochondrial structure and connectivity. Additionally, the mitoKeima reporter live imaging assay enabled precise assessment of mitophagy flux on the surface of cortical organoids through ratiometric imaging of healthy mitochondria in the cytoplasm and those engulfed by lysosomes.

These region-specific analyses revealed distinct responses; for example, mitochondrial networks exhibited reduced connectivity and increased fragmentation specifically in the cortical zone upon nFGFR1 induction, while mitochondria in the ventricular zone demonstrated increased branching and elongation. Furthermore, the mitoKeima reporter assay showed a robust increase in mitophagic flux specifically on the surface of hCOs, reinforcing the need for approaches that can dissect these spatially discrete effects.

In summary, high-resolution immunofluorescence analyses of synaptic and neuronal markers provided a cellular-level resolution of neuronal differentiation and synaptic maturation. These techniques facilitated a direct correlation between proteomic signatures and spatially resolved phenotypes.

6.8. How does nucleus-targeted nFGFR1 interact with the mitochondrial genome?

The present study provides further support for the intracellular localization of FGFR1 within the cell nucleus as well as the mitochondria. Additionally, our analysis of earlier ChiPseq data (Narla et al., 2017) shows that, similar to the cell nucleus, FGFR1 binds to DNA in the mitochondria, and that nFGFR1 DNA binding at both sites is upregulated in schizophrenia NSPC, where the endogenous nFGFR1 is also upregulated. This parallel regulation was modeled by transfecting the nucleus-targeted FGFR1(SP-/NLS), which leads to increased receptor accumulation in both the cell nucleus and mitochondria. FGFR1(SP-/NLS) lacks a membrane targeting signal peptide and, like the endogenous nFGFR1, translocates from the cytosol into the nucleus via NLS-mediated nuclear transfer. nFGFR1 has been shown to be actively exported from the nucleus to the cytosol (Lee et al. 2013). The cytosolic nFGFR1 could then translocate through the translocase complexes of the outer membrane (TOM) and the inner mitochondrial membrane (TIM), entering at their adhesion sites (Mårtensson et al., 2019). nFGFR1 could move from the nucleus to the mitochondria's genome alongside its partners, estrogen, retinoic acid receptors, Nur receptors (Baron et al., 2012; Formisano et al., 2017; Lee et al., 2012), as well as CREB Binding Protein (CBP) (X. Fang et al., 2005), CREB, and TFAM, all of which are known to be imported by the TOM complex in a membrane-dependent process (De Rasmo et al., 2009; Lionaki et al., 2016). Lacking a specific mitochondrial targeting sequence, nFGFR could also translocate to mitochondrial DNA through its interaction with heat shock protein 90 (HSP90), similar to connexin-43 or PKCε (Laederich et al., 2011). HSP90 regulates nuclear export and plays a crucial role in nuclear-mitochondrial transport (Lotz et al., 2008).

6.9. FGFR1 affects the expression of RNA and mitochondrial proteins involved in energy metabolism

The nFGFR1 induces FGFR1 protein accumulation within perinuclear mitochondria, as demonstrated by immunofluorescence analysis in EBs. I also observed that nFGFR1 binds to the promoter of the nuclear-coded *TFAM* gene, a master regulator of mtDNA transcription (not shown in this study). By targeting

TFAM and mtDNA, nFGFR1 could enhance local mitochondrial transcription and energy production to support proper neuronal development. Such mechanisms are supported by studies where TFAM silencing in NSPC resulted in mitochondrial dysfunction, activation of ISR, and impaired neurogenesis (Kuroda et al., 2021), while TFAM overexpression alleviated oxidative stress in motor neurons of ALS model mice (Morimoto et al., 2012).

nFGFR1 upregulation increased the levels of *MT-ATP6* mRNA, a mtDNA-encoded subunit of ATP synthase in Complex V, coinciding with elevated ATP levels and mitochondrial membrane potential in NSPCs and EBs. I also observed a similar trend in the expression of *MT-ND2* and *MT-ND5* mtDNA genes. Thus, nFGFR1 may enhance mitochondrial function through the upregulation of mitochondrial DNA genes and their protein products translated within the organelle (Kabala et al., 2022). This aligns with Yousefi et al. (2020), who showed that mitochondria within axons and dendrites can autonomously translate their own genome mRNAs in a compartment-specific manner, independent of nuclear-driven biogenesis (Yousefi et al., 2020). Similarly, Kuzniewska et al. (2020) demonstrated that mitochondrial proteins are synthesized locally at synapses in response to neuronal activity and are incorporated directly into the respiratory chain. Together, these studies support the idea that nFGFR1 may enhance mitochondrial function by promoting the expression of both nuclear and mitochondrial DNA genes. This localized mitochondrial RNA translation may facilitate efficient energy production in metabolically demanding subcellular regions without activating mitochondrial biogenesis.

The proteomic analysis revealed that many electron transport chain subunits were significantly downregulated, including complex I proteins (NDUFA7, NDUFB3, NDUFV1) and complex IV proteins (COX6C, MT-CO2). In line with this, gene ontology (GO) analysis showed an enrichment of downregulated proteins in oxidative phosphorylation and ATP synthesis-coupled electron transport. Upregulated proteins were enriched in categories such as mitochondrial gene expression and mitochondrial translation, along with amino acid catabolism and redox homeostasis. I observed a consistent upregulation of glycolytic enzymes (e.g., PKM, the pyruvate kinase; and SLC16A3, a lactate transporter), known to be associated with the Warburg effect. Moreover, glycolipid proteins were upregulated following nFGFR1 overexpression. Taken together, nFGFR1 drives a metabolic

shift toward glycolysis and lipid metabolism at the expense of OXPHOS, creating a Warburg-like effect to meet the energy demands of developing neurons in hCO. A shift toward glycolysis and away from oxidative phosphorylation may support the biosynthetic needs of proliferative growth and early differentiation by maintaining a less oxidative stress-prone environment. Glycolysis also provides rapid ATP and intermediates for nucleotides, which might be crucial as neural progenitors differentiate. These results align with the findings reported by Lo et al. (2020), who demonstrated that FGFR1 activation *in vitro* promotes aerobic glycolysis to meet biosynthetic demands (Lo et al., 2015). FGFR1 signaling has also been shown to modulate lipid turnover, maintain lipid droplet dynamics, and support phospholipid homeostasis in adipose tissue to accommodate changing energy requirements during cell growth (Yang et al., 2012; Ye et al., 2016). My studies suggest that this effect may be produced by nFGFR1 acting directly in the cell nucleus and mitochondria.

Finally, nFGFR1 overexpression promotes a shift toward glycolysis and lipid metabolism at the expense of OXPHOS during early neuronal differentiation. The nFGFR1 appears to program a transient metabolic state in which the differentiating NSPC progeny relies on rapid, glycolysis- and lipid-driven ATP production to support cell migration and neurite outgrowth. Localized glycolysis near synaptic or neuritic compartments enables rapid and localized ATP synthesis and could thus supplement mitochondrial ATP production (Jang et al., 2016, 2021; Wolfe et al., 2024). However, the nFGFR1-induced metabolic programming toward glycolytic ATP production may not be sufficient to support energy-intensive processes such as synaptic formation and function.

In conclusion, my results indicate that nFGFR1 exerts a context- and compartment-specific influence on human cortical development, regulating proteins that support mitochondrial structure and energetics. The dual regulatory nature of nFGFR1 provides new insight into the molecular balance of neurogenesis and synaptic connectivity.

Study limitations - The quantitative TMT proteomics approach provided us with unbiased insight into how nFGFR1 reshapes metabolism, revealing unexpected trends such as OXPHOS downregulation alongside the upregulation of mitochondrial translation and glycolysis. It allowed us to link functional outputs (ATP, MMP, ROS levels) with global proteome changes. I must emphasize that my

proteomic data represent average protein changes across the entire hCO. Given the region-specific effects of nFGFR1 on mitochondrial morphology, some spatially restricted changes in protein content may occur without detection.

Single-cell or spatial proteomics could help differentiate nFGFR1-induced protein changes in NSPC versus differentiating and mature neurons. Another limitation lies in interpreting metabolic flux based on the proteomics data. While I observed a shift toward glycolysis and a reduction in OXPHOS proteins, it did not directly measure the actual metabolic rates of OXPHOS and glycolysis. An analysis of oxygen consumption rate (OCR) and glycolytic flux using Seahorse XF on FACS-sorted progenitor and post-mitotic neuron populations from dissociated hCOs would provide a quantitative, cell-type-specific assessment of metabolic function. Future studies should also explore global transcriptomic changes upon nFGFR1 upregulation. This would complement our proteomics data and determine whether OXPHOS subunit mRNAs are regulated at the transcriptional or post-transcriptional levels.

In summary, nFGFR1 reprograms cell metabolism to maximize energy production by promoting ATP production and mitochondrial protein synthesis while shifting cellular metabolism toward glycolysis and lipid metabolism. This ensures that developing neurons meet the local energy demands of ongoing processes, such as synapse formation and axonal pruning. Our recent findings that nFGFR1 coordinates the mitochondrial and nuclear genomes (M. Liput, submitted for publication) further support the nFGFR1 pan-mitochondrial function.

6.10. nFGFR1 regulates cellular redox balance without triggering apoptosis

In this study, I investigated whether nFGFR1 modulates cellular redox homeostasis and apoptosis during early human corticogenesis. My findings indicate that overexpression of nFGFR1 enhances oxidative stress response mechanisms, elevates reactive oxygen species (ROS) levels, and supports mitochondrial function without triggering apoptosis in neural progenitor cells and human cortical organoids (hCOs). These data confirm the hypothesis that nFGFR1 regulates redox balance rather than promoting cell death. Previous literature has highlighted the protective role of FGFR1 in neurodegeneration and oxidative stress. A recent study showed

that FGFR1 activation via the β-Klotho axis suppresses iron-dependent lipid peroxidation and neuronal ferroptosis, reduces apoptosis, and decreases iron deposition in spinal cord injury models (Xu et al., 2023). Similarly, activation of FGFR1-ERK-AKT pathways protects neurons from oxidative stress-induced apoptosis (Chuang et al., 2015). Yan et al. (2025) confirmed the neuroprotective role of FGFR1 by showing that its activation via FGF21 suppresses apoptosis through the MEK–ERK signaling pathway. In line with previous studies, our results showed an increased level of ROS in NES cells upon nFGFR1 activation (Yan et al., 2025). However, no significant changes in the density of cleaved caspase-3 in the cortical layer of hCOs were observed, which coincided with the unchanged expression of apoptotic gene expression, such as the BCL2/BAX ratio. Together, these observations indicated that cells were not undergoing stress-induced programmed death. My functional assays showed elevated cell viability and MMP upon nFGFR1 activation, suggesting a beneficial effect of nFGFR1 on mitochondrial function and viability. In line with these findings, I observed an induction of antioxidant and stress response proteins following the increased expression of nFGFR1, including PRDX3 and PRDX5 proteins (mitochondrial antioxidant enzymes), OXR1 (oxidation resistance 1), and TXN2 (thioredoxin-2). Additionally, gene ontology analysis revealed enrichment in cellular redox homeostasis among upregulated processes.

Despite the metabolic and redox changes, nFGFR1 did not induce the integrated stress response (ISR). The ISR is a highly conserved pathway that modulates protein synthesis in reaction to stressors, such as hypoxia, amino acid scarcity, and glucose deprivation (Pakos-Zebrucka et al., 2016). A recent study indicated that FGFR1-FGF21 signaling activates the mitochondrial integrated stress response (mitoISR) specifically during mild-to-moderate cardiac OXPHOS dysfunction (Croon et al., 2022). However, we observed no increase in the levels of ATF4 (an ISR activation marker) protein and mRNA, indicating that the ISR pathway was not activated. This implies that the mitochondrial stress level was inadequate to activate canonical ISR. Mechanistically, our findings suggest that nFGFR1 may induce a state of hormetic stress - mild oxidative stress that activates adaptive protective pathways (Hofbrucker-MacKenzie et al., 2019). Moderate ROS function as signaling molecules that can promote differentiation and adaptive gene expression (Bigarella et al., 2014; Le Belle et al., 2011). Additionally, a transient

elevation of ROS has driven neural stem cells out of quiescence toward differentiation (Adusumilli et al., 2021). By moderately increasing ROS, nFGFR1 could facilitate the transition of neural progenitors into neurons, as observed in our developing hCO.

Study limitations - While our findings indicate that nFGFR1 enhances antioxidant responses and modulates apoptotic signaling without inducing cell death, several limitations should be acknowledged. First, the study focuses on a single developmental time point in cortical organoids (day 60), which limits the ability to determine the balance between oxidative stress resistance and apoptosis modulation throughout neurodevelopment. Long-term analysis at multiple stages would be necessary to determine whether these effects are transient, cumulative, or stage-specific. Second, my functional assays were conducted across different model systems - ROS levels, ATP production, and mitochondrial membrane potential (MMP) were evaluated in NSPC cells and embryoid bodies, while cleaved caspase-3 expression, apoptotic gene expression, and proteomics were carried out on hCOs. This cross-model approach, although valuable for broad biological validation, may introduce variability due to intrinsic differences among the various *in vitro* platforms. Consequently, direct comparisons between oxidative stress responses and apoptosis outcomes across models should be interpreted with caution. Furthermore, despite the observed upregulation of antioxidant proteins like OXR1 and PRDX3, the relationship between redox changes and cell survival remains correlative rather than functionally defined. Future studies should incorporate pharmacological and genetic manipulation of redox regulators to modulate antioxidant capacity and clarify the contribution of redox balance to nFGFR1-mediated neuroprotection. Notably, human iPSC-derived NRF2 knockout models have already been established using CRISPR/Cas9 technology, enabling the *in vitro* assays of oxidative stress responses and redox regulation (Merkert et al., 2023; Zhang et al., 2021).

In conclusion, this thesis demonstrates that nFGFR1 plays a key role in maintaining redox balance during early neuronal development by promoting oxidative stress response mechanisms, elevating reactive oxygen species (ROS) levels, and supporting mitochondrial function without triggering apoptosis. I propose that, through a hormetic mechanism, nFGFR1 modestly elevates ROS levels while activating stress-response pathways, including PRDX3, OXR1, and

TXN2, allowing cells to adapt and differentiate without triggering an integrated stress response or apoptotic signaling. These findings designate nFGFR1 as a metabolic and redox modulator that supports neuronal viability and maturation under physiological stress. Future studies across developmental time points and using functional redox perturbation strategies are essential to decipher the effect of nFGFR1 on redox homeostasis and cell fate regulation. In summary, the nFGFR1 upregulation simultaneously elevates ROS generation (likely due to metabolic shifts) and activates neuroprotective mechanisms, establishing a new equilibrium. nFGFR1 overexpression supports neuronal survival through antioxidant and pro-survival pathways rather than by directly suppressing apoptotic signaling.

6.11. The role of nFGFR1 in regulating cytoplasmic and mitochondrial translation

In this study, I aimed to elucidate the role of nFGFR1 in governing protein translation during early human corticogenesis, using a hCO model. In whole hCO, FGFR1 downregulated cytoplasmic ribosomal proteins, including RPL24 and RPL34, while upregulating levels of mitochondrial translation proteins (MRPS26, MRPS23, MRPL24). This dichotomy suggests that nFGFR1 may differentially influence the translation of cytoplasmic (nDNA-encoded) proteins and mitochondrial (mtDNA-encoded) proteins, enhancing the mitochondrial translation while suppressing cytoplasmic translation. These results support the hypothesis that nFGFR1 contributes to metabolic adaptation and proteostatic remodeling during neurodevelopment. Recent studies have shown the crucial role of protein translation in modulating neuronal identity and function. Borisova et al. (2024) identified increased protein synthesis in neuronal progenitors of later-born Satb2+ neurons, demonstrating that different cortical neuron subpopulations exhibit distinct translation rates (Borisova et al., 2024). Importantly, they identified Ire1α as a key regulator of translation and neuronal polarity, which controls translation through the helicase activity of eIF4A1. This finding is complemented by Pekkurnaz et al. (2022), who demonstrated that the local translation of nuclear-encoded mitochondrial proteins at synapses allows developing neurons to quickly adjust their mitochondrial function to meet local energy demands (Pekkurnaz and Wang, 2022). Thus, regulation of protein turnover (synthesis and degradation) during

corticogenesis could be essential for both defining neuronal identity and maintaining the metabolic flexibility required for neuronal differentiation and maturation. My findings align with previous studies demonstrating the significance of mitochondrial translation in neuronal maturation and synaptic function. Previous studies demonstrated that mitochondrial ribosomal components and RNA processing pathways are upregulated during early brain development, enabling localized translation and energy optimization in neuroepithelial tissues (Agrawal et al., 2018; Bruce et al., 2024). My investigation demonstrated a downregulation of cytoplasmic ribosomal proteins, including RPL24 and RPL34, while mitochondrial translation proteins (MRPS26, MRPS23, MRPL24) were upregulated. This dichotomy suggests a shift in translational capacity to mitochondria at the expense of the cytoplasm and may represent a proteostatic strategy to meet rising energy demands during neuronal differentiation. Similar dynamics have been observed in models where FGFR1 signaling mitigates translational repression during oxidative stress to protect against neuronal cell death (Ito et al., 2025). Mechanistically, the upregulation of mitochondrial translation proteins MRPS26, MRPS23, MRPL24, and YARS2 suggests that nFGFR1 may directly modulate mitochondrial gene expression and ribosome assembly. This possibility aligns with earlier reports indicating that FGFR1 translocates into mitochondria and modulates mitochondrial transcription and biogenesis (Kuzniewska et al., 2020; Srisakuldee et al., 2021; Yan et al., 2023). Additionally, this thesis demonstrates that nFGFR1 targets the mitogenome directly.

Together, these findings implicate nFGFR1 as a central modulator connecting metabolic remodeling and selective mitochondrial turnover to its role in supporting the neurodevelopmental transitions from progenitor to post-mitotic neurons.

7. Summary

- **Generation of inducible hiPSC line**

A human inducible pluripotent stem cell (hiPSC) line was successfully engineered to allow doxycycline-regulated expression of nuclear FGFR1 (nFGFR1). The modified cells maintained pluripotency and the capacity for trilineage differentiation. Conditional overexpression of nFGFR1 was succesfully activated in embryoid bodies (EBs), neuroepithelial stem cells (NES), and cortical organoids (hCOs), indicating stable transgene expression at the CLYBL safe harbor locus without evidence of gene silencing or DNA methylation.

- **Neural progenitor proliferation and rosette morphology**

In cortical organoids, nFGFR1 induction increased the proliferation of neural progenitors ($Ki67^+$) and enlarged the ventricular rosettes. However, the density of progenitor markers SOX2 and PAX6 remained unchanged, suggesting expansion without altering overall progenitor identity.

- **Neuronal differentiation and synaptic maturation**

nFGFR1 promoted differentiation into deep-layer cortical neurons ($CTIP2^+$, $TBR1^+$) while reducing intermediate progenitor populations ($TBR2^+$). Despite enhanced neurogenesis, nFGFR1 impaired synaptic maturation, as shown by decreased Synapsin-1 puncta and lower SYP gene expression.

- **Mitochondrial structure and network dynamics**

In cortical zone, enriched in cortical neurons mostly relying in OXPHOS, nFGFR1 caused mitochondrial fragmentation and reduced network complexity, indicating a shift away from oxidative phosphorylation. In ventricular zone, enriched in glycolytic progenitor cell population, it induced modest mitochondrial elongation, suggesting region-specific effects on mitochondrial morphology.

- **Mitophagy**

nFGFR1 significantly increased mitophagy activity through the PINK1–Parkin pathway and enhanced autophagosome recruitment to mitochondria. These effects were predominantly restricted to the cortical plate and occurred without

significant changes in mitophagy-related gene or protein expression, suggesting a region-specific effect of nFGFR1 or regulation through post-transcriptional mechanisms.

- **Mitochondrial biogenesis and function**

While nFGFR1 did not activate classical mitochondrial biogenesis pathways (PGC1α, mtDNA replication), it increased expression of mt-DNA-coded *MT-ATP6* gene, indicating enhanced energy production without increasing mitochondrial content.

- **Redox Balance and apoptosis**

nFGFR1 increased mitochondrial membrane potential, ATP production, and overall cell viability, despite higher ROS levels. No signs of apoptosis or stress pathway activation were observed, suggesting a role in promoting metabolic adaptation and neuroprotection.

- **Dual genomic targeting**

nFGFR1 localized both to the nucleus and mitochondria. It directly bound promoter regions of nuclear-encoded mitochondrial genes (e.g., TFAM, PINK1) and associated with mitochondrial DNA (mtDNA), suggesting a dual role in regulating both genomes.

- **Global proteomic remodeling**

Proteomic profiling revealed that nFGFR1 overexpression caused broad remodeling of the hCOs proteome. Upregulated pathways included mitochondrial translation, lysosomal-related proteins and neurodevelopment, while synaptic, OXPHOS proteins were downregulated, confirming its broad impact on cellular homeostasis.

8. Conclusions

The following conclusions summarize the main points and restate my thesis:

- nFGFR1 acts as a regulator of early cortical development, promoting progenitor proliferation, neuronal differentiation, and morphogenesis of neural rosettes.
- nFGFR1 modulates mitochondrial network morphology in a region-specific manner, promoting fragmentation and less complex mitochondrial networks in the cortical plate zone and more elongated and interconnected mitochondria in the ventricular zone.
- nFGFR1 enhances mitophagy in a region-specific manner and selectively modulates mitochondrial function, supporting efficient energy production and mitochondrial quality control.
- nFGFR1 promotes metabolic adaptation and cell survival by increasing ATP production and mitochondrial activity without triggering apoptosis.
- nFGFR1 functions as a dual genome regulator, targeting nuclear and mitochondrial DNA, linking transcriptional control to organelle regulation.
- nFGFR1 induces extensive changes in the proteome of hCO, affecting neural development, energy metabolism, autophagy, and synaptic signaling pathways.
- nFGFR1 serves as a master coordinator of neurodevelopmental and metabolic programs in human cortical organoids.

9. References

Abe, P., Molnár, Z., Tzeng, Y. S., Lai, D. M., Arnold, S. J., Stumm, R. (2015). Intermediate progenitors facilitate intracortical progression of thalamocortical axons and interneurons through CXCL12 chemokine signaling. *Journal of Neuroscience*, *35*(38). https://doi.org/10.1523/JNEUROSCI.1488-15.2015

Abed, S., Ebrahimi, A., Fattahi, F., Kouchakali, G., Shekari-Khaniani, M., Mansoori-Derakhshan, S. (2024). The Role of Non-Coding RNAs in Mitochondrial Dysfunction of Alzheimer's Disease. *Journal of Molecular Neuroscience 2024 74:4*, *74*(4), 1–20. https://doi.org/10.1007/S12031-024-02262-Y

Adusumilli, V. S., Walker, T. L., Overall, R. W., Klatt, G. M., Zeidan, S. A., Zocher, S., Kirova, D. G., Ntitsias, K., Fischer, T. J., Sykes, A. M., Reinhardt, S., Dahl, A., Mansfeld, J., Rünker, A. E., Kempermann, G. (2021). ROS Dynamics Delineate Functional States of Hippocampal Neural Stem Cells and Link to Their Activity-Dependent Exit from Quiescence. *Cell Stem Cell*, *28*(2). https://doi.org/10.1016/j.stem.2020.10.019

Agboola, O. S., Hu, X., Shan, Z., Wu, Y., Lei, L. (2021). Brain organoid: a 3D technology for investigating cellular composition and interactions in human neurological development and disease models in vitro. In *Stem Cell Research and Therapy* (Vol. 12, Issue 1). https://doi.org/10.1186/s13287-021-02369-8

Agrawal, A., Pekkurnaz, G., Koslover, E. F. (2018). Spatial control of neuronal metabolism through glucose-mediated mitochondrial transport regulation. *ELife*, *7*. https://doi.org/10.7554/eLife.40986

Aiuti, A., Biasco, L., Scaramuzza, S., Ferrua, F., Cicalese, M. P., Baricordi, C., Dionisio, F., Calabria, A., Giannelli, S., Castiello, M. C., Bosticardo, M., Evangelio, C., Assanelli, A., Casiraghi, M., Di Nunzio, S., Callegaro, L., Benati, C., Rizzardi, P., Pellin, D., … Naldini, L. (2013). Lentiviral hematopoietic stem cell gene therapy in patients with wiskott-aldrich syndrome. *Science*, *341*(6148). https://doi.org/10.1126/science.1233151

Allen, D. E., Donohue, K. C., Cadwell, C. R., Shin, D., Keefe, M. G., Sohal, V. S., Nowakowski, T. J. (2022). Fate mapping of neural stem cell niches reveals distinct origins of human cortical astrocytes. *Science*, *376*(6600). https://doi.org/10.1126/science.abm5224

Anderson, S., Bankier, A. T., Barrell, B. G., De Bruijn, M. H. L., Coulson, A. R., Drouin, J., Eperon, I. C., Nierlich, D. P., Roe, B. A., Sanger, F., Schreier, P. H., Smith, A. J. H., Staden, R., Young, I. G. (1981). Sequence and organization of the human mitochondrial genome. *Nature*, *290*(5806). https://doi.org/10.1038/290457a0

Ashrafi, G., Schlehe, J. S., LaVoie, M. J., Schwarz, T. L. (2014). Mitophagy of damaged mitochondria occurs locally in distal neuronal axons and requires PINK1 and Parkin. *Journal of Cell Biology*, *206*(5). https://doi.org/10.1083/jcb.201401070

Atamian, A., Birtele, M., Hosseini, N., Nguyen, T., Seth, A., Del Dosso, A., Paul, S., Tedeschi, N., Taylor, R., Coba, M. P., Samarasinghe, R., Lois, C., Quadrato, G. (2024). Human cerebellar organoids with functional Purkinje cells. *Cell Stem Cell*, *31*(1). https://doi.org/10.1016/j.stem.2023.11.013

Auer, T. O., Del Bene, F. (2014). CRISPR/Cas9 and TALEN-mediated knock-in approaches in zebrafish. *Methods*, *69*(2). https://doi.org/10.1016/j.ymeth.2014.03.027

Augustyniak, J., Lenart, J., Gaj, P., Kolanowska, M., Jazdzewski, K., Stepien, P. P., Buzanska, L. (2019). Bezafibrate Upregulates Mitochondrial Biogenesis and Influence Neural Differentiation of Human-Induced Pluripotent Stem Cells. *Molecular Neurobiology*, *56*(6). https://doi.org/10.1007/s12035-018-1368-2

Autar, K., Guo, X., Rumsey, J. W., Long, C. J., Akanda, N., Jackson, M., Narasimhan, N. S., Caneus, J., Morgan, D., Hickman, J. J. (2022). A functional hiPSC-cortical neuron differentiation and maturation model and its application to neurological disorders. *Stem Cell Reports*, *17*(1). https://doi.org/10.1016/j.stemcr.2021.11.009

Ayanlaja, A. A., Xiong, Y., Gao, Y., Ji, G., Tang, C., Abdullah, Z., Gao, D. (2017). Distinct features of doublecortin as a marker of neuronal migration and its implications in cancer cell mobility. *Frontiers in Molecular Neuroscience*, *10*. https://doi.org/10.3389/fnmol.2017.00199

Aznauryan, E., Yermanos, A., Kinzina, E., Devaux, A., Kapetanovic, E., Milanova, D., Church, G. M., Reddy, S. T. (2022). Discovery and validation of human genomic safe harbor sites for gene and cell therapies. *Cell Reports Methods*, *2*(1). https://doi.org/10.1016/j.crmeth.2021.100154

Bagley, J. A., Reumann, D., Bian, S., Lévi-Strauss, J., Knoblich, J. A. (2017). Fused cerebral organoids model interactions between brain regions. *Nature Methods*, *14*(7). https://doi.org/10.1038/nmeth.4304

Balafkan, N., Mostafavi, S., Schubert, M., Siller, R., Liang, K. X., Sullivan, G., Bindoff, L. A. (2020). A method for differentiating human induced pluripotent stem cells toward functional cardiomyocytes in 96-well microplates. *Scientific Reports*, *10*(1). https://doi.org/10.1038/s41598-020-73656-2

Ballabio, C., Anderle, M., Gianesello, M., Lago, C., Miele, E., Cardano, M., Aiello, G., Piazza, S., Caron, D., Gianno, F., Ciolfi, A., Pedace, L., Mastronuzzi, A., Tartaglia, M., Locatelli, F., Ferretti, E., Giangaspero, F., Tiberi, L. (2020). Modeling medulloblastoma in vivo and with human cerebellar organoids. *Nature Communications*, *11*(1). https://doi.org/10.1038/s41467-019-13989-3

Barel, O., Malicdan, M. C. V., Ben-Zeev, B., Kandel, J., Pri-Chen, H., Stephen, J., Castro, I. G., Metz, J., Atawa, O., Moshkovitz, S., Ganelin, E., Barshack, I., Polak-Charcon, S., Nass, D., Marek-Yagel, D., Amariglio, N., Shalva, N., Vilboux, T., Ferreira, C., … Anikster, Y. (2017). Deleterious variants in TRAK1 disrupt mitochondrial movement and cause fatal encephalopathy. *Brain*, *140*(3). https://doi.org/10.1093/brain/awx002

Barker, S. J., Raju, R. M., Milman, N. E. P., Wang, J., Davila-Velderrain, J., Gunter-Rahman, F., Parro, C. C., Bozzelli, P. L., Abdurrob, F., Abdelaal, K., Bennett, D. A., Kellis, M., Tsai, L. H. (2021). MEF2 is a key regulator of cognitive potential and confers resilience to neurodegeneration. *Science Translational Medicine*, *13*(618). https://doi.org/10.1126/SCITRANSLMED.ABD7695

Baron, O., Förthmann, B., Lee, Y. W., Terranova, C., Ratzka, A., Stachowiak, E. K., Grothe, C., Claus, P., Stachowiak, M. K. (2012). Cooperation of nuclear fibroblast growth factor receptor 1 and Nurr1 offers new interactive mechanism in postmitotic development of mesencephalic dopaminergic neurons. *Journal of Biological Chemistry*, *287*(24). https://doi.org/10.1074/jbc.M112.347831

Becerra-Calixto, A., Mukherjee, A., Ramirez, S., Sepulveda, S., Sinha, T., Al-Lahham, R., De Gregorio, N., Gherardelli, C., Soto, C. (2023). Lewy Body-like Pathology and Loss of Dopaminergic Neurons in Midbrain Organoids Derived from Familial Parkinson's Disease Patient. *Cells*, *12*(4). https://doi.org/10.3390/cells12040625

Bedogni, F., Hodge, R. D., Elsen, G. E., Nelson, B. R., Daza, R. A. M., Beyer, R. P., Bammler, T. K., Rubenstein, J. L. R., Hevner, R. F. (2010). Tbr1 regulates regional and laminar identity of postmitotic neurons in developing neocortex. *Proceedings of the National Academy of Sciences of the United States of America*, *107*(29). https://doi.org/10.1073/pnas.1002285107

Benes, F. M. (2004). The role of apoptosis in neuronal pathology in schizophrenia and bipolar disorder. In *Current Opinion in Psychiatry* (Vol. 17, Issue 3). https://doi.org/10.1097/00001504-200405000-00006

Bernal, A., Arranz, L. (2018). Nestin-expressing progenitor cells: function, identity and therapeutic implications. In *Cellular and Molecular Life Sciences* (Vol. 75, Issue 12). https://doi.org/10.1007/s00018-018-2794-z

Bershteyn, M., Nowakowski, T. J., Pollen, A. A., Di Lullo, E., Nene, A., Wynshaw-Boris, A., Kriegstein, A. R. (2017). Human iPSC-Derived Cerebral Organoids

Model Cellular Features of Lissencephaly and Reveal Prolonged Mitosis of Outer Radial Glia. *Cell Stem Cell*, *20*(4). https://doi.org/10.1016/j.stem.2016.12.007

Bhaduri, A., Andrews, M. G., Mancia Leon, W., Jung, D., Shin, D., Allen, D., Jung, D., Schmunk, G., Haeussler, M., Salma, J., Pollen, A. A., Nowakowski, T. J., Kriegstein, A. R. (2020). Cell stress in cortical organoids impairs molecular subtype specification. *Nature*, *578*(7793). https://doi.org/10.1038/s41586-020-1962-0

Bhagwan, J. R., Denning, C., Collins, E., Mosqueira, D., Bakar, M., Johnson, B. B., Thompson, A., Smith, J. G. W. (2020). Variable expression and silencing of CRISPR-Cas9 targeted transgenes identifies the AAVS1 locus as not an entirely safe harbour. *F1000Research*, *8*. https://doi.org/10.12688/f1000research.19894.2

Bharali, D. J., Klejbor, I., Stachowiak, E. K., Dutta, P., Roy, I., Kaur, N., Bergey, E. J., Prasad, P. N., Stachowiak, M. K. (2005). Organically modified silica nanoparticles: A nonviral vector for in vivo gene delivery and expression in the brain. *Proceedings of the National Academy of Sciences of the United States of America*, *102*(32). https://doi.org/10.1073/pnas.0504926102

Bhardwaj, A., Nain, V. (2021). TALENs—an indispensable tool in the era of CRISPR: a mini review. In *Journal of Genetic Engineering and Biotechnology* (Vol. 19, Issue 1). https://doi.org/10.1186/s43141-021-00225-z

Bigarella, C. L., Liang, R., Ghaffari, S. (2014). Stem cells and the impact of ROS signaling. *Development (Cambridge)*, *141*(22). https://doi.org/10.1242/dev.107086

Birey, F., Andersen, J., Makinson, C. D., Islam, S., Wei, W., Huber, N., Fan, H. C., Metzler, K. R. C., Panagiotakos, G., Thom, N., O'Rourke, N. A., Steinmetz, L. M., Bernstein, J. A., Hallmayer, J., Huguenard, J. R., Pasca, S. P. (2017). Assembly of functionally integrated human forebrain spheroids. *Nature*, *545*(7652). https://doi.org/10.1038/nature22330

Biswas, K., Alexander, K., Francis, M. M. (2022). Reactive Oxygen Species: Angels and Demons in the Life of a Neuron. *NeuroSci*, *3*(1). https://doi.org/10.3390/neurosci3010011

Bolaños, N. A., Faravelli, I., Faits, T., Andreadis, S., Trattaro, S., Kastli, R., Adiconis, X., Bella, D. J. Di, Tegtmeyer, M., Nehme, R., Levin, J. Z., Regev, A., Arlotta, P. (2023). Multi-donor human cortical Chimeroids reveal individual susceptibility to neurotoxic triggers. *BioRxiv*.

Borisova, E., Newman, A. G., Couce Iglesias, M., Dannenberg, R., Schaub, T., Qin, B., Rusanova, A., Brockmann, M., Koch, J., Daniels, M., Turko, P., Jahn, O., Kaplan, D. R., Rosário, M., Iwawaki, T., Spahn, C. M. T., Rosenmund, C., Meierhofer, D., Kraushar, M. L., … Ambrozkiewicz, M. C. (2024). Protein translation rate determines neocortical neuron fate. *Nature Communications 2024 15:1*, *15*(1), 1–25. https://doi.org/10.1038/s41467-024-49198-w

Bosone, C., Castaldi, D., Burkard, T. R., Guzman, S. J., Wyatt, T., Cheroni, C., Caporale, N., Bajaj, S., Bagley, J. A., Li, C., Sorre, B., Villa, C. E., Testa, G., Krenn, V., Knoblich, J. A. (2024). A polarized FGF8 source specifies frontotemporal signatures in spatially oriented cell populations of cortical assembloids. *Nature Methods 2024 21:11*, *21*(11), 2147–2159. https://doi.org/10.1038/s41592-024-02412-5

Brenes, A. J., Griesser, E., Sinclair, L. V., Davidson, L., Prescott, A. R., Singh, F., Hogg, E. K. J., Espejo-Serrano, C., Jiang, H., Yoshikawa, H., Platani, M., Swedlow, J., Findlay, G. M., Cantrell, D. A., Lamond, A. I. (2024). Proteomic and functional comparison between human induced and embryonic stem cells. *ELife*, *13*.

Bruce, H., Halpern, M. E., Monfries, C., Suleyman, O., Hamid, F., Houart, C. (2024). *A cleaved cytosolic FOXG1 promotes excitatory neurogenesis by modulation of mitochondrial translation – a new therapeutic target for brain disorders*. https://doi.org/10.1101/2024.08.13.607559

Cabrera, A., Edelstein, H. I., Glykofrydis, F., Love, K. S., Palacios, S., Tycko, J., Zhang, M., Lensch, S., Shields, C. E., Livingston, M., Weiss, R., Zhao, H., Haynes, K. A., Morsut, L., Chen, Y. Y., Khalil, A. S., Wong, W. W., Collins, J. J., Rosser, S. J., … Deans, T. L. (2022). The sound of silence: Transgene silencing in mammalian cell engineering. In *Cell Systems* (Vol. 13, Issue 12). https://doi.org/10.1016/j.cels.2022.11.005

Caceres, A., Banker, G., Steward, O., Binder, L., Payne, M. (1984). MAP2 is localized to the dendrites of hippocampal neurons which develop in culture. *Developmental Brain Research*, *13*(2). https://doi.org/10.1016/0165-3806(84)90167-6

Cakir, B., Xiang, Y., Tanaka, Y., Kural, M. H., Parent, M., Kang, Y. J., Chapeton, K., Patterson, B., Yuan, Y., He, C. S., Raredon, M. S. B., Dengelegi, J., Kim, K. Y., Sun, P., Zhong, M., Lee, S., Patra, P., Hyder, F., Niklason, L. E., … Park, I. H. (2019). Engineering of human brain organoids with a functional vascular-like system. *Nature Methods*, *16*(11). https://doi.org/10.1038/s41592-019-0586-5

Cakir, B., Tanaka, Y., Kiral, F. R., Xiang, Y., Dagliyan, O., Wang, J., Lee, M., Greaney, A. M., Yang, W. S., duBoulay, C., Kural, M. H., Patterson, B., Zhong, M., Kim, J., Bai, Y., Min, W., Niklason, L. E., Patra, P., Park, I. H. (2022). Expression of the transcription factor PU.1 induces the generation of microglia-like cells in human cortical organoids. *Nature Communications*, *13*(1). https://doi.org/10.1038/s41467-022-28043-y

Calatayud-Baselga, I., Casares-Crespo, L., Franch-Ibáñez, C., Guijarro-Nuez, J., Sanz, P., Mira, H. (2023). Autophagy drives the conversion of developmental neural stem cells to the adult quiescent state. *Nature Communications*, *14*(1). https://doi.org/10.1038/s41467-023-43222-1

Calvo-Garrido, J., Winn, D., Maffezzini, C., Wedell, A., Freyer, C., Falk, A., Wredenberg, A. (2021). Protocol for the derivation, culturing, and differentiation of human iPS-cell-derived neuroepithelial stem cells to study neural differentiation in vitro. *STAR Protocols*, *2*(2). https://doi.org/10.1016/j.xpro.2021.100528

Camp, J. G., Badsha, F., Florio, M., Kanton, S., Gerber, T., Wilsch-Bräuninger, M., Lewitus, E., Sykes, A., Hevers, W., Lancaster, M., Knoblich, J. A., Lachmann, R., Pääbo, S., Huttner, W. B., Treutlein, B. (2015). Human cerebral organoids recapitulate gene expression programs of fetal neocortex development. *Proceedings of the National Academy of Sciences of the United States of America*, *112*(51). https://doi.org/10.1073/pnas.1520760112

Cerbini, T., Funahashi, R., Luo, Y., Liu, C., Park, K., Rao, M., Malik, N., Zou, J. (2015a). Transcription activator-like effector nuclease (TALEN)-mediated CLYBL targeting enables enhanced transgene expression and one-step generation of dual reporter human induced pluripotent stem cell (iPSC) and neural stem cell (NSC) lines. *PLoS ONE*, *10*(1). https://doi.org/10.1371/journal.pone.0116032

Chaudhry, A., Shi, R., Luciani, D. S. (2020). A pipeline for multidimensional confocal analysis of mitochondrial morphology, function, and dynamics in pancreatic β-cells. *American Journal of Physiology - Endocrinology and Metabolism*, *318*(2). https://doi.org/10.1152/ajpendo.00457.2019

Chaudhuri, T. R., Lin, Q., Stachowiak, E. K., Rosario, S. R., Spernyak, J. A., Ma, W. W., Stachowiak, M. K., Greene, M. K., Quinn, G. P., McDade, S. S., Clynes, M., Scott, C. J., Straubinger, R. M. (2024). Dual-Hit Strategy for Therapeutic Targeting of Pancreatic Cancer in Patient-Derived Xenograft Tumors. *Clinical Cancer Research*, *30*(7). https://doi.org/10.1158/1078-0432.CCR-23-0131

Chen, B., Wang, S. S., Hattox, A. M., Rayburn, H., Nelson, S. B., McConnell, S. K. (2008). The Fezf2-Ctip2 genetic pathway regulates the fate choice of subcortical projection neurons in the developing cerebral cortex. *Proceedings of the National Academy of Sciences of the United States of America*, *105*(32). https://doi.org/10.1073/pnas.0804918105

Chen, X., Saiyin, H., Liu, Y., Wang, Y., Li, X., Ji, R., Ma, L. (2022). Human striatal organoids derived from pluripotent stem cells recapitulate striatal development and compartments. *PLoS Biology*, *20*(11). https://doi.org/10.1371/journal.pbio.3001868

Chen, Y., Xie, X., Li, X., Wang, P., Jing, Q., Yue, J., Liu, Y., Cheng, Z., Li, J., Song, H., Li, G., Liu, R., Wang, J. (2016). FGFR antagonist induces protective autophagy in FGFR1-amplified breast cancer cell. *Biochemical and Biophysical Research Communications*, *474*(1). https://doi.org/10.1016/j.bbrc.2016.03.017

Chioni, A. M., Grose, R. (2012). FGFR1 cleavage and nuclear translocation regulates breast cancer cell behavior. *Journal of Cell Biology*, *197*(6). https://doi.org/10.1083/jcb.201108077

Cho, J. Y., Guo, C., Torello, M., Lunstrum, G. P., Iwata, T., Deng, C., Horton, W. A. (2004). Defective lysosomal targeting of activated fibroblast growth factor receptor 3 in achondroplasia. *Proceedings of the National Academy of Sciences of the United States of America*, *101*(2). https://doi.org/10.1073/pnas.2237184100

Christofk, H. R., Vander Heiden, M. G., Harris, M. H., Ramanathan, A., Gerszten, R. E., Wei, R., Fleming, M. D., Schreiber, S. L., Cantley, L. C. (2008). The M2 splice isoform of pyruvate kinase is important for cancer metabolism and tumour growth. *Nature*, *452*(7184). https://doi.org/10.1038/nature06734

Chuang, J. I., Huang, J. Y., Tsai, S. J., Sun, H. S., Yang, S. H., Chuang, P. C., Huang, B. M., Ching, C. H. (2015). FGF9-induced changes in cellular redox status and HO-1 upregulation are FGFR-dependent and proceed through both ERK and AKT to induce CREB and Nrf2 activation. *Free Radical Biology and Medicine*, *89*. https://doi.org/10.1016/j.freeradbiomed.2015.08.011

Cimmino, F., Montella, A., Tirelli, M., Avitabile, M., Lasorsa, V. A., Visconte, F., Cantalupo, S., Maiorino, T., De Angelis, B., Morini, M., Castellano, A., Locatelli, F., Capasso, M., Iolascon, A. (2022). FGFR1 is a potential therapeutic target in neuroblastoma. *Cancer Cell International*, *22*(1). https://doi.org/10.1186/s12935-022-02587-x

Claflin, K. E., Sullivan, A. I., Naber, M. C., Flippo, K. H., Morgan, D. A., Neff, T. J., Jensen-Cody, S. O., Zhu, Z., Zingman, L. V., Rahmouni, K., Potthoff, M. J. (2022). Pharmacological FGF21 signals to glutamatergic neurons to enhance leptin action and lower body weight during obesity. *Molecular Metabolism*, *64*. https://doi.org/10.1016/j.molmet.2022.101564

Clark, J. F., Soriano, P. (2024). Diverse Fgfr1 signaling pathways and endocytic trafficking regulate early mesoderm development. *BioRxiv*, 2024.02.16.580629. https://doi.org/10.1101/2024.02.16.580629

Coelho, P., Fão, L., Mota, S., Rego, A. C. (2022). Mitochondrial function and dynamics in neural stem cells and neurogenesis: Implications for neurodegenerative diseases. In *Ageing Research Reviews* (Vol. 80). https://doi.org/10.1016/j.arr.2022.101667

Coetzee, A. S., Carter, E. P., Rodríguez-Fernández, L., Heward, J., Wang, Q., Karim, S. A., Boughetane, L., Milton, C., Uyulur, F., Morton, J. P., Kocher, H. M., Grose, R. P. (2023). Nuclear FGFR1 promotes pancreatic stellate cell-driven invasion through up-regulation of Neuregulin 1. *Oncogene*, *42*(7). https://doi.org/10.1038/s41388-022-02513-5

Coleman, S. J., Chioni, A. M., Ghallab, M., Anderson, R. K., Lemoine, N. R., Kocher, H. M., Grose, R. P. (2014). Nuclear translocation of FGFR1 and FGF2 in pancreatic stellate cells facilitates pancreatic cancer cell invasion. *EMBO Molecular Medicine*, *6*(4). https://doi.org/10.1002/emmm.201302698

Collado, M. S., Cole, B. K., Figler, R. A., Lawson, M., Manka, D., Simmers, M. B., Hoang, S., Serrano, F., Blackman, B. R., Sinha, S., Wamhoff, B. R. (2017). Exposure of induced pluripotent stem cell-derived vascular endothelial and smooth muscle cells in coculture to hemodynamics induces primary vascular cell-

like phenotypes. *Stem Cells Translational Medicine*, *6*(8). https://doi.org/10.1002/sctm.17-0004

Comps-Agrar, L., Dunshee, D. R., Eaton, D. L., Sonoda, J. (2015). Unliganded fibroblast growth factor receptor 1 forms density-independent dimers. *Journal of Biological Chemistry*, *290*(40). https://doi.org/10.1074/jbc.M115.681395

Corradi, A., Fadda, M., Piton, A., Patry, L., Marte, A., Rossi, P., Cadieux-Dion, M., Gauthier, J., Lapointe, L., Mottron, L., Valtorta, F., Rouleau, G. A., Fassio, A., Benfenati, F., Cossette, P. (2014). SYN2 is an autism predisposing gene: Loss-offunction mutations alter synaptic vesicle cycling and axon outgrowth. *Human Molecular Genetics*, *23*(1). https://doi.org/10.1093/hmg/ddt401

Crespo, I., Pignatelli, J., Kinare, V., Méndez-Gómez, H. R., Esgleas, M., Román, M. J., Canals, J. M., Tole, S., Vicario, C. (2022). Tbr1 Misexpression Alters Neuronal Development in the Cerebral Cortex. *Molecular Neurobiology*, *59*(9). https://doi.org/10.1007/s12035-022-02936-x

Croon, M., Szczepanowska, K., Popovic, M., Lienkamp, C., Senft, K., Brandscheid, C. P., Bock, T., Gnatzy-Feik, L., Ashurov, A., Acton, R. J., Kaul, H., Pujol, C., Rosenkranz, S., Krüger, M., Trifunovic, A. (2022). FGF21 modulates mitochondrial stress response in cardiomyocytes only under mild mitochondrial dysfunction. *Science Advances*, *8*(14). https://doi.org/10.1126/sciadv.abn7105

Cubelos, B., Briz, C. G., Esteban-Ortega, G. M., Nieto, M. (2015). Cux1 and Cux2 selectively target basal and apical dendritic compartments of layer II-III cortical neurons. *Developmental Neurobiology*, *75*(2). https://doi.org/10.1002/dneu.22215

Cuomo, A. S. E., Seaton, D. D., McCarthy, D. J., Martinez, I., Bonder, M. J., Garcia-Bernardo, J., Amatya, S., Madrigal, P., Isaacson, A., Buettner, F., Knights, A., Natarajan, K. N., Agu, C. A., Alderton, A., Danecek, P., Denton, R., Durbin, R., Gaffney, D. J., Goncalves, A., … Stegle, O. (2020). Single-cell RNA-sequencing of differentiating iPS cells reveals dynamic genetic effects on gene expression. *Nature Communications*, *11*(1). https://doi.org/10.1038/s41467-020-14457-z

Dabrowski, A., Terauchi, A., Strong, C., Umemori, H. (2015). Distinct sets of FGF receptors sculpt excitatory and inhibitory synaptogenesis. *Development (Cambridge)*, *142*(10). https://doi.org/10.1242/dev.115568

Dabrowski, A., Umemori, H. (2016). Buttressing a balanced brain: Target-derived FGF signaling regulates excitatory/inhibitory tone and adult neurogenesis within the maturating hippocampal network. In *Neurogenesis* (Vol. 3, Issue 1). https://doi.org/10.1080/23262133.2016.1168504

Dai, S., Zhou, Z., Chen, Z., Xu, G., Chen, Y. (2019). Fibroblast growth factor receptors (Fgfrs): Structures and small molecule inhibitors. *Cells*, *8*(6). https://doi.org/10.3390/cells8060614

De Rasmo, D., Signorile, A., Roca, E., Papa, S. (2009). CAMP response element-binding protein (CREB) is imported into mitochondria and promotes protein synthesis. *FEBS Journal*, *276*(16). https://doi.org/10.1111/j.1742-4658.2009.07133.x

Deacon, T. W., Pakzaban, P., Isacson, O. (1994). The lateral ganglionic eminence is the origin of cells committed to striatal phenotypes: neural transplantation and developmental evidence. *Brain Research*, *668*(1–2). https://doi.org/10.1016/0006-8993(94)90526-6

Decker, B., Liput, M., Abdellatif, H., Yergeau, D., Bae, Y., Jornet, J. M., Stachowiak, E. K., Stachowiak, M. K. (2021). Global genome conformational programming during neuronal development is associated with ctcf and nuclear fgfr1-the genome archipelago model. *International Journal of Molecular Sciences*, *22*(1). https://doi.org/10.3390/ijms22010347

DeGiosio, R. A., Grubisha, M. J., MacDonald, M. L., McKinney, B. C., Camacho, C. J., Sweet, R. A. (2022). More than a marker: potential pathogenic functions of MAP2. *Frontiers in Molecular Neuroscience*, *15*. https://doi.org/10.3389/fnmol.2022.974890

Delerive, P., Wu, Y., Burris, T. P., Chin, W. W., Suen, C. S. (2002). PGC-1 functions as a transcriptional coactivator for the retinoid X receptors. *Journal of Biological Chemistry*, *277*(6). https://doi.org/10.1074/jbc.M109409200

Delgado, R. N., Allen, D. E., Keefe, M. G., Mancia Leon, W. R., Ziffra, R. S., Crouch, E. E., Alvarez-Buylla, A., Nowakowski, T. J. (2022). Individual human cortical progenitors can produce excitatory and inhibitory neurons. *Nature*, *601*(7893). https://doi.org/10.1038/s41586-021-04230-7

Deng, C., Bedford, M., Li, C., Xu, X., Yang, X., Dunmore, J., Leder, P. (1997). Fibroblast growth factor receptor-1 (FGFR-1) is essential for normal neural tube and limb development. *Developmental Biology*, *185*(1). https://doi.org/10.1006/dbio.1997.8553

Deng, C. X., Wynshaw-Boris, A., Shen, M. M., Daugherty, C., Ornitz, D. M., Leder, P. (1994). Murine FGFR-1 is required for early postimplantation growth and axial organization. *Genes and Development*, *8*(24). https://doi.org/10.1101/gad.8.24.3045

Devine, M. J., Norkett, R., Kittler, J. T. (2016). DISC1 is a coordinator of intracellular trafficking to shape neuronal development and connectivity. In *Journal of Physiology* (Vol. 594, Issue 19). https://doi.org/10.1113/JP272187

Dhiman, S., Manoj, N., Liput, M., Sangwan, A., Diehl, J., Balcerak, A., Sudhakar, S., Augustyniak, J., Jornet, J. M., Bae, Y., Stachowiak, E. K., Dutta, A., Stachowiak, M. K. (2024). Systems Genome: Coordinated Gene Activity Networks, Recurring Coordination Modules, and Genome Homeostasis in Developing Neurons. *International Journal of Molecular Sciences*, *25*(11), 5647. https://doi.org/10.3390/IJMS25115647/S1

Di Lullo, E., Kriegstein, A. R. (2017). The use of brain organoids to investigate neural development and disease. In Nature Reviews Neuroscience (Vol. 18, Issue 10). https://doi.org/10.1038/nrn.2017.107

Di Nottia, M., Marchese, M., Verrigni, D., Mutti, C. D., Torraco, A., Oliva, R., Fernandez-Vizarra, E., Morani, F., Trani, G., Rizza, T., Ghezzi, D., Ardissone, A., Nesti, C., Vasco, G., Zeviani, M., Minczuk, M., Bertini, E., Santorelli, F. M., Carrozzo, R. (2020). A homozygous MRPL24 mutation causes a complex movement disorder and affects the mitoribosome assembly. *Neurobiology of Disease*, *141*. https://doi.org/10.1016/j.nbd.2020.104880

Dong, Y., Zhuang, X. X., Wang, Y. T., Tan, J., Feng, D., Li, M., Zhong, Q., Song, Z., Shen, H. M., Fang, E. F., Lu, J. H. (2023). Chemical mitophagy modulators: Drug development strategies and novel regulatory mechanisms. In *Pharmacological Research* (Vol. 194). https://doi.org/10.1016/j.phrs.2023.106835

Du, H., Wang, Z., Guo, R., Yang, L., Liu, G., Zhang, Z., Xu, Z., Tian, Y., Yang, Z., Li, X., Chen, B. (2022). Transcription factors Bcl11a and Bcl11b are required for the production and differentiation of cortical projection neurons. *Cerebral Cortex*, *32*(17). https://doi.org/10.1093/cercor/bhab437

Duncan, J. G., Finck, B. N. (2008). The PPARα-PGC-1α Axis Controls Cardiac Energy Metabolism in Healthy and Diseased Myocardium. *PPAR Research*, *2008*(1), 253817. https://doi.org/10.1155/2008/253817

Dunham-Ems, S. M., Pudavar, H. E., Myers, J. M., Maher, P. A., Prasad, P. N., Stachowiak, M. K. (2006). Factors controlling fibroblast growth factor receptor-1′s cytoplasmic trafficking and its regulation as revealed by FRAP analysis. *Molecular Biology of the Cell*, *17*(5). https://doi.org/10.1091/mbc.E05-08-0749

Esteban-Martínez, L., Sierra-Filardi, E., McGreal, R. S., Salazar-Roa, M., Mariño, G., Seco, E., Durand, S., Enot, D., Graña, O., Malumbres, M., Cvekl, A., Cuervo, A. M., Kroemer, G., Boya, P. (2017). Programmed mitophagy is essential for the glycolytic switch during cell differentiation. *The EMBO Journal*, *36*(12). https://doi.org/10.15252/embj.201695916

Fagel, D. M., Ganat, Y., Cheng, E., Silbereis, J., Ohkubo, Y., Ment, L. R., Vaccarino, F. M. (2009). Fgfr1 is required for cortical regeneration and repair after perinatal

hypoxia. *Journal of Neuroscience*, *29*(4). https://doi.org/10.1523/JNEUROSCI.4516-08.2009

Fang, E. F., Hou, Y., Palikaras, K., Adriaanse, B. A., Kerr, J. S., Yang, B., Lautrup, S., Hasan-Olive, M. M., Caponio, D., Dan, X., Rocktäschel, P., Croteau, D. L., Akbari, M., Greig, N. H., Fladby, T., Nilsen, H., Cader, M. Z., Mattson, M. P., Tavernarakis, N., Bohr, V. A. (2019). Mitophagy inhibits amyloid-β and tau pathology and reverses cognitive deficits in models of Alzheimer's disease. *Nature Neuroscience*, *22*(3). https://doi.org/10.1038/s41593-018-0332-9

Fang, X., Stachowiak, E. K., Dunham-Ems, S. M., Klejbor, I., Stachowiak, M. K. (2005). Control of CREB-binding protein signaling by nuclear fibroblast growth factor receptor-1: A novel mechanism of gene regulation. *Journal of Biological Chemistry*, *280*(31). https://doi.org/10.1074/jbc.M504400200

Farrell, B., Breeze, A. L. (2018). Structure, activation and dysregulation of fibroblast growth factor receptor kinases: Perspectives for clinical targeting. In *Biochemical Society Transactions* (Vol. 46, Issue 6). https://doi.org/10.1042/BST20180004

Feliciano, P., Matos, H., Andrade, R., Bykhovskaia, M. (2017). Synapsin II regulation of GABAergic synaptic transmission is dependent on interneuron subtype. *Journal of Neuroscience*, *37*(7). https://doi.org/10.1523/JNEUROSCI.0844-16.2016

Feng, Y., He, D., Yao, Z., Klionsky, D. J. (2014). The machinery of macroautophagy. In *Cell Research* (Vol. 24, Issue 1). https://doi.org/10.1038/cr.2013.168

Fernandopulle, M. S., Prestil, R., Grunseich, C., Wang, C., Gan, L., Ward, M. E. (2018). Transcription Factor–Mediated Differentiation of Human iPSCs into Neurons. *Current Protocols in Cell Biology*, *79*(1). https://doi.org/10.1002/cpcb.51

Flandin, P., Kimura, S., Rubenstein, J. L. R. (2010a). The progenitor zone of the ventral medial ganglionic eminence requires Nkx2-1 to generate most of the globus pallidus but few neocortical interneurons. *Journal of Neuroscience*, *30*(8). https://doi.org/10.1523/JNEUROSCI.4228-09.2010

Fleck, J. S., Sanchís-Calleja, F., He, Z., Santel, M., Boyle, M. J., Camp, J. G., Treutlein, B. (2021). Resolving organoid brain region identities by mapping single-cell genomic data to reference atlases. Cell Stem Cell, 28(6). https://doi.org/10.1016/j.stem.2021.02.015

Fleming, A., Bourdenx, M., Fujimaki, M., Karabiyik, C., Krause, G. J., Lopez, A., Martín-Segura, A., Puri, C., Scrivo, A., Skidmore, J., Son, S. M., Stamatakou, E., Wrobel, L., Zhu, Y., Cuervo, A. M., Rubinsztein, D. C. (2022). The different autophagy degradation pathways and neurodegeneration. In *Neuron* (Vol. 110, Issue 6). https://doi.org/10.1016/j.neuron.2022.01.017

Foldynova-Trantirkova, S., Wilcox, W. R., Krejci, P. (2012). Sixteen years and counting: The current understanding of fibroblast growth factor receptor 3 (FGFR3) signaling in skeletal dysplasias. In *Human Mutation* (Vol. 33, Issue 1). https://doi.org/10.1002/humu.21636

Fontecha-barriuso, M., Martin-sanchez, D., Martinez-moreno, J. M., Monsalve, M., Ramos, A. M., Sanchez-niño, M. D., Ruiz-ortega, M., Ortiz, A., Sanz, A. B. (2020). The role of PGC-1α and mitochondrial biogenesis in kidney diseases. In *Biomolecules* (Vol. 10, Issue 2). https://doi.org/10.3390/biom10020347

Formisano, L., Stauffer, K. M., Young, C. D., Bhola, N. E., Guerrero-Zotano, A. L., Jansen, V. M., Estrada, M. M., Hutchinson, K. E., Giltnane, J. M., Schwarz, L. J., Lu, Y., Balko, J. M., Deas, O., Cairo, S., Judde, J. G., Mayer, I. A., Sanders, M., Dugger, T. C., Bianco, R., … Arteaga, C. L. (2017). Association of FGFR1 with ERα maintains ligand-independent ER transcription and mediates resistance to estrogen deprivation in ER+ breast cancer. *Clinical Cancer Research*, *23*(20). https://doi.org/10.1158/1078-0432.CCR-17-1232

Frank, S., Skryabin, B. V., Greber, B. (2013). A modified TALEN-based system for robust generation of knock-out human pluripotent stem cell lines and disease models. *BMC Genomics*, *14*(1). https://doi.org/10.1186/1471-2164-14-773

Gabler, L., Jaunecker, C. N., Katz, S., van Schoonhoven, S., Englinger, B., Pirker, C., Mohr, T., Vician, P., Stojanovic, M., Woitzuck, V., Laemmerer, A., Kirchhofer, D., Mayr, L., LaFranca, M., Erhart, F., Grissenberger, S., Wenninger-Weinzierl, A., Sturtzel, C., Kiesel, B., … Berger, W. (2022). Fibroblast growth factor receptor 4 promotes glioblastoma progression: a central role of integrin-mediated cell invasiveness. *Acta Neuropathologica Communications*, *10*(1). https://doi.org/10.1186/s40478-022-01363-2

Gantner, C. W., Hunt, C. P. J., Niclis, J. C., Penna, V., McDougall, S. J., Thompson, L. H., Parish, C. L. (2021). FGF-MAPK signaling regulates human deep-layer corticogenesis. *Stem Cell Reports*, *16*(5). https://doi.org/10.1016/j.stemcr.2021.03.014

Garone, C., De Giorgio, F., Carli, S. (2024). Mitochondrial metabolism in neural stem cells and implications for neurodevelopmental and neurodegenerative diseases. In *Journal of Translational Medicine* (Vol. 22, Issue 1). https://doi.org/10.1186/s12967-024-05041-w

Gędaj, A., Gregorczyk, P., Żukowska, D., Chorążewska, A., Ciura, K., Kalka, M., Porębska, N., Opaliński, Ł. (2024). Glycosylation of FGF/FGFR: An underrated sweet code regulating cellular signaling programs. *Cytokine Growth Factor Reviews*, *77*, 39–55. https://doi.org/10.1016/J.CYTOGFR.2024.04.001

Geisler, S., Holmström, K. M., Skujat, D., Fiesel, F. C., Rothfuss, O. C., Kahle, P. J., Springer, W. (2010). PINK1/Parkin-mediated mitophagy is dependent on VDAC1 and p62/SQSTM1. *Nature Cell Biology*, *12*(2). https://doi.org/10.1038/ncb2012

Gelman, D. M., Martini, F. J., Nóbrega-Pereira, S., Pierani, A., Kessaris, N., Marín, O. (2009). The embryonic preoptic area is a novel source of cortical GABAergic interneurons. *Journal of Neuroscience*, *29*(29). https://doi.org/10.1523/JNEUROSCI.0604-09.2009

Georgakopoulos, N. D., Wells, G., Campanella, M. (2017). The pharmacological regulation of cellular mitophagy. In *Nature Chemical Biology* (Vol. 13, Issue 2). https://doi.org/10.1038/nchembio.2287

Gerdes, J., Schwab, U., Lemke, H., Stein, H. (1983). Production of a mouse monoclonal antibody reactive with a human nuclear antigen associated with cell proliferation. *International Journal of Cancer*, *31*(1). https://doi.org/10.1002/ijc.2910310104

Ghafouri-Fard, S., Safarzadeh, A., Taheri, M., Jamali, E. (2023). Identification of diagnostic biomarkers via weighted correlation network analysis in colorectal cancer using a system biology approach. *Scientific Reports*, *13*(1). https://doi.org/10.1038/s41598-023-40953-5

Giandomenico, S. L., Mierau, S. B., Gibbons, G. M., Wenger, L. M. D., Masullo, L., Sit, T., Sutcliffe, M., Boulanger, J., Tripodi, M., Derivery, E., Paulsen, O., Lakatos, A., Lancaster, M. A. (2019). Cerebral organoids at the air–liquid interface generate diverse nerve tracts with functional output. *Nature Neuroscience*, *22*(4). https://doi.org/10.1038/s41593-019-0350-2

Goetz, R., Mohammadi, M. (2013). Exploring mechanisms of FGF signalling through the lens of structural biology. In *Nature Reviews Molecular Cell Biology* (Vol. 14, Issue 3). https://doi.org/10.1038/nrm3528

Gohrig, A., Detjen, K. M., Hilfenhaus, G., Korner, J. L., Welzel, M., Arsenic, R., Schmuck, R., Bahra, M., Wu, J. Y., Wiedenmann, B., Fischer, C. (2014). Axon guidance factor SLIT2 inhibits neural invasion and metastasis in pancreatic cancer. *Cancer Research*, *74*(5). https://doi.org/10.1158/0008-5472.CAN-13-1012

Goldsmith, J., Ordureau, A., Harper, J. W., Holzbaur, E. L. F. (2022). Brain-derived autophagosome profiling reveals the engulfment of nucleoid-enriched mitochondrial fragments by basal autophagy in neurons. *Neuron*, *110*(6). https://doi.org/10.1016/j.neuron.2021.12.029

Gomes, A. R., Fernandes, T. G., Vaz, S. H., Silva, T. P., Bekman, E. P., Xapelli, S., Duarte, S., Ghazvini, M., Gribnau, J., Muotri, A. R., Trujillo, C. A., Sebastião, A. M., Cabral, J. M. S., Diogo, M. M. (2020). Modeling Rett Syndrome With Human Patient-Specific Forebrain Organoids. *Frontiers in Cell and Developmental Biology*, *8*. https://doi.org/10.3389/fcell.2020.610427

Gorman, A. M., Ceccatelli, S., Orrenius, S. (2000). Role of mitochondria in neuronal apoptosis. *Developmental Neuroscience*, *22*(5–6). https://doi.org/10.1159/000017460

Götz, M., Huttner, W. B. (2005). The cell biology of neurogenesis. In *Nature Reviews Molecular Cell Biology* (Vol. 6, Issue 10). https://doi.org/10.1038/nrm1739

Gregorczyk, P., Porębska, N., Żukowska, D., Chorążewska, A., Gędaj, A., Malinowska, A., Otlewski, J., Zakrzewska, M., Opaliński, Ł. (2023). N-glycosylation acts as a switch for FGFR1 trafficking between the plasma membrane and nuclear envelope. *Cell Communication and Signaling*, *21*(1). https://doi.org/10.1186/s12964-023-01203-3

Groth, C., Lardelli, M. (2002). The structure and function of vertebrate fibroblast growth factor receptor 1. *International Journal of Developmental Biology*, *46*(4 SPEC.).

Guénantin, A. C., Briand, N., Capel, E., Dumont, F., Morichon, R., Provost, C., Stillitano, F., Jeziorowska, D., Siffroi, J. P., Hajjar, R. J., Fève, B., Hulot, J. S., Collas, P., Capeau, J., Vigouroux, C. (2017). Functional human beige adipocytes from induced pluripotent stem cells. *Diabetes*, *66*(6). https://doi.org/10.2337/db16-1107

Gureev, A. P., Shaforostova, E. A., Popov, V. N. (2019). Regulation of mitochondrial biogenesis as a way for active longevity: Interaction between the Nrf2 and PGC-1α signaling pathways. In *Frontiers in Genetics* (Vol. 10, Issue MAY). https://doi.org/10.3389/fgene.2019.00435

Gusel'nikova, V. V., Korzhevskiy, D. E. (2015). NeuN as a neuronal nuclear antigen and neuron differentiation marker. In *Acta Naturae* (Vol. 7, Issue 2). https://doi.org/10.32607/20758251-2015-7-2-42-47

Hacein-Bey-Abina, S., Pai, S.-Y., Gaspar, H. B., Armant, M., Berry, C. C., Blanche, S., Bleesing, J., Blondeau, J., de Boer, H., Buckland, K. F., Caccavelli, L., Cros, G., De Oliveira, S., Fernández, K. S., Guo, D., Harris, C. E., Hopkins, G., Lehmann, L. E., Lim, A., … Thrasher, A. J. (2014). A Modified γ-Retrovirus Vector for X-Linked Severe Combined Immunodeficiency. *New England Journal of Medicine*, *371*(15). https://doi.org/10.1056/nejmoa1404588

Hafner, A.-L. (2014). Human induced pluripotent stem cells: A new source for brown and white adipocytes. *World Journal of Stem Cells*, *6*(4). https://doi.org/10.4252/wjsc.v6.i4.467

Hanna, R. A., Quinsay, M. N., Orogo, A. M., Giang, K., Rikka, S., Gustafsson, Å. B. (2012). Microtubule-associated protein 1 light chain 3 (LC3) interacts with Bnip3 protein to selectively remove endoplasmic reticulum and mitochondria via autophagy. *Journal of Biological Chemistry*, *287*(23). https://doi.org/10.1074/jbc.M111.322933

Hansen, D. V., Lui, J. H., Flandin, P., Yoshikawa, K., Rubenstein, J. L., Alvarez-Buylla, A., Kriegstein, A. R. (2013). Non-epithelial stem cells and cortical interneuron production in the human ganglionic eminences. *Nature Neuroscience*, *16*(11). https://doi.org/10.1038/nn.3541

Hansen, D. V., Lui, J. H., Parker, P. R. L., Kriegstein, A. R. (2010). Neurogenic radial glia in the outer subventricular zone of human neocortex. *Nature*, *464*(7288). https://doi.org/10.1038/nature08845

Hapak, S. M., Rothlin, C. V., Ghosh, S. (2019). aPKC in neuronal differentiation, maturation and function. In *Neuronal Signaling* (Vol. 3, Issue 3). https://doi.org/10.1042/NS20190019

Hara, T., Nakamura, K., Matsui, M., Yamamoto, A., Nakahara, Y., Suzuki-Migishima, R., Yokoyama, M., Mishima, K., Saito, I., Okano, H., Mizushima, N. (2006).

Suppression of basal autophagy in neural cells causes neurodegenerative disease in mice. *Nature*, *441*(7095). https://doi.org/10.1038/nature04724

Harbauer, A. B., Hees, J. T., Wanderoy, S., Segura, I., Gibbs, W., Cheng, Y., Ordonez, M., Cai, Z., Cartoni, R., Ashrafi, G., Wang, C., Perocchi, F., He, Z., Schwarz, T. L. (2022). Neuronal mitochondria transport Pink1 mRNA via synaptojanin 2 to support local mitophagy. *Neuron*, *110*(9). https://doi.org/10.1016/j.neuron.2022.01.035

Haubensak, W., Attardo, A., Denk, W., Huttner, W. B. (2004). Neurons arise in the basal neuroepithelium of the early mammalian telencephalon: A major site of neurogenesis. *Proceedings of the National Academy of Sciences of the United States of America*, *101*(9). https://doi.org/10.1073/pnas.0308600100

Haugsten, E. M., Małecki, J., Bjørklund, S. M. S., Olsnes, S., Wesche, J. (2008). Ubiquitination of fibroblast growth factor receptor 1 is required for its intracellular sorting but not for its endocytosis. *Molecular Biology of the Cell*, *19*(8). https://doi.org/10.1091/mbc.E07-12-1219

He, Z., Maynard, A., Jain, A., Gerber, T., Petri, R., Lin, H. C., Santel, M., Ly, K., Dupré, J. S., Sidow, L., Sanchis Calleja, F., Jansen, S. M. J., Riesenberg, S., Camp, J. G., Treutlein, B. (2022). Lineage recording in human cerebral organoids. *Nature Methods*, *19*(1). https://doi.org/10.1038/s41592-021-01344-8

Hevner, R. F. (2019). Intermediate progenitors and Tbr2 in cortical development. In *Journal of Anatomy* (Vol. 235, Issue 3). https://doi.org/10.1111/joa.12939

Hevner, R. F., Hodge, R. D., Daza, R. A. M., Englund, C. (2006). Transcription factors in glutamatergic neurogenesis: Conserved programs in neocortex, cerebellum, and adult hippocampus. In *Neuroscience Research* (Vol. 55, Issue 3). https://doi.org/10.1016/j.neures.2006.03.004

Hinsch, C. L., Venkata, J. K., Hsu, T., Dammai, V. (2023). Controlled Plasma Membrane Delivery of FGFR1 and Modulation of Signaling by a Novel Regulated Anterograde RTK Transport Pathway. *Cancers*, *15*(24). https://doi.org/10.3390/cancers15245837

Hiranuma, M., Okuda, Y., Fujii, Y., Richard, J. P., Watanabe, T. (2024). Characterization of human iPSC-derived sensory neurons and their functional assessment using multi electrode array. *Scientific Reports*, *14*(1). https://doi.org/10.1038/s41598-024-55602-8

Hitosugi, T., Fan, J., Chung, T. W., Lythgoe, K., Wang, X., Xie, J., Ge, Q., Gu, T. L., Polakiewicz, R. D., Roesel, J. L., Chen, G. Z., Boggon, T. J., Lonial, S., Fu, H., Khuri, F. R., Kang, S., Chen, J. (2011). Tyrosine Phosphorylation of Mitochondrial Pyruvate Dehydrogenase Kinase 1 Is Important for Cancer Metabolism. *Molecular Cell*, *44*(6). https://doi.org/10.1016/j.molcel.2011.10.015

Hodneland Nilsson, L. I., Nitschke Pettersen, I. K., Nikolaisen, J., Micklem, D., Avsnes Dale, H., Vatne Røsland, G., Lorens, J., Tronstad, K. J. (2015). A new live-cell reporter strategy to simultaneously monitor mitochondrial biogenesis and morphology. *Scientific Reports*, *5*. https://doi.org/10.1038/srep17217

Hofbrucker-MacKenzie, S. A., Sivaprakasam, I., Ji, Y., Kessels, M. M., Qualmann, B. (2019). Neuronal Stress and Its Hormetic Aspects. *The Science of Hormesis in Health and Longevity*, 171–180. https://doi.org/10.1016/B978-0-12-814253-0.00015-2

Holzerova, E., Danhauser, K., Haack, T. B., Kremer, L. S., Melcher, M., Ingold, I., Kobayashi, S., Terrile, C., Wolf, P., Schaper, J., Mayatepek, E., Baertling, F., Friedmann Angeli, J. P., Conrad, M., Strom, T. M., Meitinger, T., Prokisch, H., Distelmaier, F. (2016). Human thioredoxin 2 deficiency impairs mitochondrial redox homeostasis and causes early-onset neurodegeneration. *Brain*, *139*(2). https://doi.org/10.1093/brain/awv350

Hu, Q., Li, J., Nitta, K., Kitada, M., Nagai, T., Kanasaki, K., Koya, D. (2018a). FGFR1 is essential for N-acetyl-seryl-aspartyl-lysyl-proline regulation of mitochondrial

dynamics by upregulating microRNA let-7b-5p. *Biochemical and Biophysical Research Communications*, *495*(3). https://doi.org/10.1016/j.bbrc.2017.12.089

Hu, Y., Fang, X., Dunham, S. M., Prada, C., Stachowiak, E. K., Stachowiak, M. K. (2004). 90-kDa ribosomal S6 kinase is a direct target for the nuclear fibroblast growth factor receptor 1 (FGFR1): Role in FGFR1 signaling. *Journal of Biological Chemistry*, *279*(28). https://doi.org/10.1074/jbc.M311144200

Huang, S., Jin, Y., Zhang, L., Zhou, Y., Chen, N., Wang, W. (2024). PPAR gamma and PGC-1alpha activators protect against diabetic nephropathy by suppressing the inflammation and NF-kappaB activation. *Nephrology*, *29*(12), 858–872. https://doi.org/10.1111/NEP.14381

Huang, W. K., Wong, S. Z. H., Pather, S. R., Nguyen, P. T. T., Zhang, F., Zhang, D. Y., Zhang, Z., Lu, L., Fang, W., Chen, L., Fernandes, A., Su, Y., Song, H., Ming, G. li. (2021). Generation of hypothalamic arcuate organoids from human induced pluripotent stem cells. *Cell Stem Cell*, *28*(9). https://doi.org/10.1016/j.stem.2021.04.006

Huang, W. T., Chen, X. J., Lin, Y. K., Shi, J. F., Li, H., Wu, H. Di, Jiang, R. L., Chen, S., Wang, X., Tan, X. X., Chen, K. Y., Wang, P. (2024). FGF17 protects cerebral ischemia reperfusion-induced blood-brain barrier disruption via FGF receptor 3-mediated PI3K/AKT signaling pathway. *European Journal of Pharmacology*, *971*. https://doi.org/10.1016/j.ejphar.2024.176521

Inglis-Broadgate, S. L., Thomson, R. E., Pellicano, F., Tartaglia, M. A., Pontikis, C. C., Cooper, J. D., Iwata, T. (2005). FGFR3 regulates brain size by controlling progenitor cell proliferation and apoptosis during embryonic development. *Developmental Biology*, *279*(1). https://doi.org/10.1016/j.ydbio.2004.11.035

Inigo, J. R., Chandra, D. (2022). The mitochondrial unfolded protein response (UPRmt): shielding against toxicity to mitochondria in cancer. In *Journal of Hematology and Oncology* (Vol. 15, Issue 1). https://doi.org/10.1186/s13045-022-01317-0

Irion, S., Luche, H., Gadue, P., Fehling, H. J., Kennedy, M., Keller, G. (2007). Identification and targeting of the ROSA26 locus in human embryonic stem cells. *Nature Biotechnology*, *25*(12). https://doi.org/10.1038/nbt1362

Ito, T., Ohuchi, K., Kurita, H., Murakami, T., Takizawa, S., Fujimaki, A., Murata, J., Oida, Y., Hozumi, I., Kitaichi, K., Inden, M. (2025a). Activated Fibroblast Growth Factor Receptor 1 Mitigated Poly-PR–Induced Oxidative Stress and Protein Translational Impairment. *Biological and Pharmaceutical Bulletin*, *48*(2), 93–100. https://doi.org/10.1248/BPB.B24-00794

Iwata, R., Casimir, P., Vanderhaeghen, P. (2020). Mitochondrial dynamics in postmitotic cells regulate neurogenesis. *Science*, *369*(6505), 858–862. https://doi.org/10.1126/science.aba9760

Jacob, F., Pather, S. R., Huang, W. K., Zhang, F., Wong, S. Z. H., Zhou, H., Cubitt, B., Fan, W., Chen, C. Z., Xu, M., Pradhan, M., Zhang, D. Y., Zheng, W., Bang, A. G., Song, H., Carlos de la Torre, J., Ming, G. li. (2020). Human Pluripotent Stem Cell-Derived Neural Cells and Brain Organoids Reveal SARS-CoV-2 Neurotropism Predominates in Choroid Plexus Epithelium. *Cell Stem Cell*, *27*(6). https://doi.org/10.1016/j.stem.2020.09.016

Jacobi, A., Loy, K., Schmalz, A. M., Hellsten, M., Umemori, H., Kerschensteiner, M., Bareyre, F. M. (2015). FGF 22 signaling regulates synapse formation during post-injury remodeling of the spinal cord. *The EMBO Journal*, *34*(9). https://doi.org/10.15252/embj.201490578

Jang, S. R., Nelson, J. C., Bend, E. G., Rodríguez-Laureano, L., Tueros, F. G., Cartagenova, L., Underwood, K., Jorgensen, E. M., Colón-Ramos, D. A. (2016). Glycolytic Enzymes Localize to Synapses under Energy Stress to Support Synaptic Function. *Neuron*, *90*(2). https://doi.org/10.1016/j.neuron.2016.03.011

Jang, S. R., Xuan, Z., Lagoy, R. C., Jawerth, L. M., Gonzalez, I. J., Singh, M., Prashad, S., Kim, H. S., Patel, A., Albrecht, D. R., Hyman, A. A., Colón-Ramos, D. A. (2021). Phosphofructokinase relocalizes into subcellular compartments with

liquid-like properties in vivo. *Biophysical Journal*, *120*(7). https://doi.org/10.1016/j.bpj.2020.08.002

Jensen-Cody, S. O., Flippo, K. H., Claflin, K. E., Yavuz, Y., Sapouckey, S. A., Walters, G. C., Usachev, Y. M., Atasoy, D., Gillum, M. P., Potthoff, M. J. (2020). FGF21 Signals to Glutamatergic Neurons in the Ventromedial Hypothalamus to Suppress Carbohydrate Intake. *Cell Metabolism*, *32*(2). https://doi.org/10.1016/j.cmet.2020.06.008

Jerber, J., Seaton, D. D., Cuomo, A. S. E., Kumasaka, N., Haldane, J., Steer, J., Patel, M., Pearce, D., Andersson, M., Bonder, M. J., Mountjoy, E., Ghoussaini, M., Lancaster, M. A., Marioni, J. C., Merkle, F. T., Gaffney, D. J., Stegle, O. (2021). Population-scale single-cell RNA-seq profiling across dopaminergic neuron differentiation. *Nature Genetics*, *53*(3). https://doi.org/10.1038/s41588-021-00801-6

Jiang, H., Kang, S. U., Zhang, S., Karuppagounder, S., Xu, J., Lee, Y. K., Kang, B. G., Lee, Y., Zhang, J., Pletnikova, O., Troncoso, J. C., Pirooznia, S., Andrabi, S. A., Dawson, V. L., Dawson, T. M. (2016). Adult conditional knockout of PGC-1α leads to loss of dopamine neurons. *ENeuro*, *3*(4). https://doi.org/10.1523/ENEURO.0183-16.2016

Johansson, P. A., Adami, A., Jakobsson, J. (2022). CRISPRi-mediated transcriptional silencing in iPSCs for the study of human brain development. *STAR Protocols*, *3*(2). https://doi.org/10.1016/j.xpro.2022.101285

Jukkola, T., Lahti, L., Naserke, T., Wurst, W., Partanen, J. (2006). FGF regulated gene-expression and neuronal differentiation in the developing midbrain-hindbrain region. *Developmental Biology*, *297*(1). https://doi.org/10.1016/j.ydbio.2006.05.002

Kabala, A. M., Binko, K., Godard, F., Charles, C., Dautant, A., Baranowska, E., Skoczen, N., Gombeau, K., Bouhier, M., Becker, H. D., Ackerman, S. H., Steinmetz, L. M., Tribouillard-Tanvier, D., Kucharczyk, R., di Rago, J. P. (2022). Assembly-dependent translation of subunits 6 (Atp6) and 9 (Atp9) of ATP synthase in yeast mitochondria. *Genetics*, *220*(3). https://doi.org/10.1093/genetics/iyac007

Kanatani, S., Yozu, M., Tabata, H., Nakajima, K. (2008). COUP-TFII is preferentially expressed in the caudal ganglionic eminence and is involved in the caudal migratory stream. *Journal of Neuroscience*, *28*(50). https://doi.org/10.1523/JNEUROSCI.2132-08.2008

Kang, J., Park, H., Kim, E. (2016). IRSp53/BAIAP2 in dendritic spine development, NMDA receptor regulation, and psychiatric disorders. In *Neuropharmacology* (Vol. 100). https://doi.org/10.1016/j.neuropharm.2015.06.019

Kang, M., Garg, V., Hadjantonakis, A. K. (2017). Lineage Establishment and Progression within the Inner Cell Mass of the Mouse Blastocyst Requires FGFR1 and FGFR2. *Developmental Cell*, *41*(5). https://doi.org/10.1016/j.devcel.2017.05.003

Kar, S., Maji, N., Sen, K., Roy, S., Maity, A., Dastidar, S. G., Nath, S., Basu, G., Basu, M. (2023). Reprogramming of glucose metabolism via PFKFB4 is critical in FGF16-driven invasion of breast cancer cells. *Bioscience Reports*, *43*(8). https://doi.org/10.1042/BSR20230677

Karbassi, E., Padgett, R., Bertero, A., Reinecke, H., Klaiman, J. M., Yang, X., Hauschka, S. D., Murry, C. E. (2024). Targeted CRISPR activation is functional in engineered human pluripotent stem cells but undergoes silencing after differentiation into cardiomyocytes and endothelium. *Cellular and Molecular Life Sciences*, *81*(1). https://doi.org/10.1007/s00018-023-05101-2

Khacho, M., Slack, R. S. (2018). Mitochondrial dynamics in the regulation of neurogenesis: From development to the adult brain. In *Developmental Dynamics* (Vol. 247, Issue 1). https://doi.org/10.1002/dvdy.24538

Kim, H. J., Joe, Y., Rah, S. Y., Kim, S. K., Park, S. U., Park, J., Kim, J., Ryu, J., Cho, G. J., Surh, Y. J., Ryter, S. W., Kim, U. H., Chung, H. T. (2018). Carbon monoxide-induced TFEB nuclear translocation enhances mitophagy/mitochondrial biogenesis in hepatocytes and ameliorates inflammatory liver injury. *Cell Death and Disease*, *9*(11). https://doi.org/10.1038/s41419-018-1112-x

Kim, J. A., Berlow, N. E., Lathara, M., Bharathy, N., Martin, L. R., Purohit, R., Cleary, M. M., Liu, Q., Michalek, J. E., Srinivasa, G., Cole, B. L., Chen, S. D., Keller, C. (2022). Sensitization of osteosarcoma to irradiation by targeting nuclear FGFR1. *Biochemical and Biophysical Research Communications*, *621*. https://doi.org/10.1016/j.bbrc.2022.07.002

Kim, J., Imaizumi, K., Jurjuț, O., Kelley, K. W., Wang, D., Thete, M. V., Hudacova, Z., Amin, N. D., Levy, R. J., Scherrer, G., Pașca, S. P. (2025). Human assembloid model of the ascending neural sensory pathway. *Nature 2025*, 1–11. https://doi.org/10.1038/s41586-025-08808-3

Kim, T. H., Chokkalla, A. K., Vemuganti, R. (2021). Deletion of ubiquitin ligase Nedd4l exacerbates ischemic brain damage. *Journal of Cerebral Blood Flow and Metabolism*, *41*(5). https://doi.org/10.1177/0271678X20943804

Kinnart, I., Manders, L., Heyninck, T., Imberechts, D., Praschberger, R., Schoovaerts, N., Verfaillie, C., Verstreken, P., Vandenberghe, W. (2024). Elevated α-synuclein levels inhibit mitophagic flux. *Npj Parkinson's Disease*, *10*(1), 1–15. https://doi.org/10.1038/S41531-024-00696-0;SUBJMETA=1718,375,617,631,692,80;KWRD=CELL+BIOLOGY,PARKINSON

Kiral, F. R., Cakir, B., Tanaka, Y., Kim, J., Yang, W. S., Wehbe, F., Kang, Y. J., Zhong, M., Sancer, G., Lee, S. H., Xiang, Y., Park, I. H. (2023). Generation of ventralized human thalamic organoids with thalamic reticular nucleus. *Cell Stem Cell*, *30*(5). https://doi.org/10.1016/j.stem.2023.03.007

Klatt, D., Cheng, E., Hoffmann, Di., Santilli, G., Thrasher, A. J., Brendel, C., Schambach, A. (2020). Differential Transgene Silencing of Myeloid-Specific Promoters in the AAVS1 Safe Harbor Locus of Induced Pluripotent Stem Cell-Derived Myeloid Cells. *Human Gene Therapy*, *31*(3–4). https://doi.org/10.1089/hum.2019.194

Klejbor, I., Myers, J. M., Hausknecht, K., Corso, T. D., Gambino, A. S., Morys, J., Maher, P. A., Hard, R., Richards, J., Stachowiak, E. K., Stachowiak, M. K. (2006). Fibroblast growth factor receptor signaling affects development and function of dopamine neurons - Inhibition results in a schizophrenia-like syndrome in transgenic mice. *Journal of Neurochemistry*, *97*(5). https://doi.org/10.1111/j.1471-4159.2006.03754.x

Klimaschewski, L., Claus, P. (2021). Fibroblast Growth Factor Signalling in the Diseased Nervous System. In *Molecular Neurobiology* (Vol. 58, Issue 8). https://doi.org/10.1007/s12035-021-02367-0

Kodroń, A., Mussulini, B. H., Pilecka, I., Chacińska, A. (2021). The ubiquitin-proteasome system and its crosstalk with mitochondria as therapeutic targets in medicine. In *Pharmacological Research* (Vol. 163). https://doi.org/10.1016/j.phrs.2020.105248

Komatsu, M., Waguri, S., Chiba, T., Murata, S., Iwata, J. I., Tanida, I., Ueno, T., Koike, M., Uchiyama, Y., Kominami, E., Tanaka, K. (2006). Loss of autophagy in the central nervous system causes neurodegeneration in mice. *Nature*, *441*(7095). https://doi.org/10.1038/nature04723

Koo, B., Choi, B., Park, H., Yoon, K. J. (2019). Past, Present, and Future of Brain Organoid Technology. In *Molecules and Cells* (Vol. 42, Issue 9). https://doi.org/10.14348/molcells.2019.0162

Kosodo, Y., Suetsugu, T., Suda, M., Mimori-Kiyosue, Y., Toida, K., Baba, S. A., Kimura, A., Matsuzaki, F. (2011). Regulation of interkinetic nuclear migration

by cell cycle-coupled active and passive mechanisms in the developing brain. *EMBO Journal*, *30*(9). https://doi.org/10.1038/emboj.2011.81

Kotin, R. M., Linden, R. M., Berns, K. I. (1992). Characterization of a preferred site on human chromosome 19q for integration of adeno-associated virus DNA by non-homologous recombination. *The EMBO Journal*, *11*(13). https://doi.org/10.1002/j.1460-2075.1992.tb05614.x

Kühlbrandt, W. (2015). Structure and function of mitochondrial membrane protein complexes. In *BMC Biology* (Vol. 13, Issue 1). https://doi.org/10.1186/s12915-015-0201-x

Kumar, V., Goutam, R. S., Park, S., Lee, U., Kim, J. (2021). Functional roles of fgf signaling in early development of vertebrate embryos. In *Cells* (Vol. 10, Issue 8). https://doi.org/10.3390/cells10082148

Kuroda, R., Tominaga, K., Kasashima, K., Kuroiwa, K., Sakashita, E., Hayakawa, H., Kouki, T., Ohno, N., Kawai, K., Endo, H. (2021). Loss of mitochondrial transcription factor A in neural stem cells leads to immature brain development and triggers the activation of the integral stress response in vivo. *PLoS ONE*, *16*(7 July). https://doi.org/10.1371/journal.pone.0255355

Kurowski, A., Molotkov, A., Soriano, P. (2019). FGFR1 regulates trophectoderm development and facilitates blastocyst implantation. *Developmental Biology*, *446*(1). https://doi.org/10.1016/j.ydbio.2018.12.008

Kuzniewska, B., Cysewski, D., Wasilewski, M., Sakowska, P., Milek, J., Kulinski, T. M., Winiarski, M., Kozielewicz, P., Knapska, E., Dadlez, M., Chacinska, A., Dziembowski, A., Dziembowska, M. (2020). Mitochondrial protein biogenesis in the synapse is supported by local translation. *EMBO Reports*, *21*(8). https://doi.org/10.15252/embr.201948882

Kvajo, M., McKellar, H., Arguello, P. A., Drew, L. J., Moore, H., MacDermott, A. B., Karayiorgou, M., Gogos, J. A. (2008). A mutation in mouse Disc1 that models a schizophrenia risk allele leads to specific alterations in neuronal architecture and cognition. *Proceedings of the National Academy of Sciences of the United States of America*, *105*(19). https://doi.org/10.1073/pnas.0802615105

Laederich, M. B., Degnin, C. R., Lunstrum, G. P., Holden, P., Horton, W. A. (2011). Fibroblast Growth Factor Receptor 3 (FGFR3) is a strong Heat shock protein 90 (Hsp90) client: Implications for therapeutic manipulation. *Journal of Biological Chemistry*, *286*(22). https://doi.org/10.1074/jbc.M110.206151

Lahti, L., Saarimäki-Vire, J., Rita, H., Partanen, J. (2011). FGF signaling gradient maintains symmetrical proliferative divisions of midbrain neuronal progenitors. *Developmental Biology*, *349*(2). https://doi.org/10.1016/j.ydbio.2010.11.008

Lam, W. K., Lindblom, R. S. J., Milky, B., Mazzachi, P., Hadian-Jazi, M., Küng, C., Khuu, G., Uoselis, L., Nguyen, T. N., Skulsuppaisarn, M., Saunders, T. L., Schmidt, M. F., Dewson, G., Fogel, A. I., Bardy, C., Lazarou, M. (2024). Presynapses are mitophagy pit stops that prevent axon degeneration. *BioRxiv*, 2024.09.09.611943. https://doi.org/10.1101/2024.09.09.611943

Lancaster, M. A., Knoblich, J. A. (2014). Generation of cerebral organoids from human pluripotent stem cells. *Nature Protocols*, *9*(10). https://doi.org/10.1038/nprot.2014.158

Lancaster, M. A., Renner, M., Martin, C. A., Wenzel, D., Bicknell, L. S., Hurles, M. E., Homfray, T., Penninger, J. M., Jackson, A. P., Knoblich, J. A. (2013). Cerebral organoids model human brain development and microcephaly. *Nature*, *501*(7467). https://doi.org/10.1038/nature12517

Latoszek, E., Piechota, M., Liszewska, E., Hansíková, H., Klempíř, J., Mühlbäck, A., Landwehrmeyer, G. B., Kuznicki, J., Czeredys, M. (2022). Generation of three human iPSC lines from patients with Huntington's disease with different CAG lengths and human control iPSC line from a healthy donor. *Stem Cell Research*, *64*. https://doi.org/10.1016/j.scr.2022.102931

Lautrup, S., Sinclair, D. A., Mattson, M. P., Fang, E. F. (2019). NAD+ in Brain Aging and Neurodegenerative Disorders. In *Cell Metabolism* (Vol. 30, Issue 4). https://doi.org/10.1016/j.cmet.2019.09.001

Lavdas, A. A., Grigoriou, M., Pachnis, V., Parnavelas, J. G. (1999). The medial ganglionic eminence gives rise to a population of early neurons in the developing cerebral cortex. *Journal of Neuroscience*, *19*(18). https://doi.org/10.1523/jneurosci.19-18-07881.1999

Le Belle, J. E., Orozco, N. M., Paucar, A. A., Saxe, J. P., Mottahedeh, J., Pyle, A. D., Wu, H., Kornblum, H. I. (2011). Proliferative neural stem cells have high endogenous ROS levels that regulate self-renewal and neurogenesis in a PI3K/Akt-dependant manner. *Cell Stem Cell*, *8*(1). https://doi.org/10.1016/j.stem.2010.11.028

Lee, N. C., Hwu, W. L., Muramatsu, S. I., Falk, D. J., Byrne, B. J., Cheng, C. H., Shih, N. C., Chang, K. L., Tsai, L. K., Chien, Y. H. (2018). A Neuron-Specific Gene Therapy Relieves Motor Deficits in Pompe Disease Mice. *Molecular Neurobiology*, *55*(6). https://doi.org/10.1007/s12035-017-0763-4

Lee, Y. W., Terranova, C., Birkaya, B., Narla, S., Kehoe, D., Parikh, A., Dong, S., Ratzka, A., Brinkmann, H., Aletta, J. M., Tzanakakis, E. S., Stachowiak, E. K., Claus, P., Stachowiak, M. K. (2012). A novel nuclear FGF Receptor-1 partnership with retinoid and Nur receptors during developmental gene programming of embryonic stem cells. *Journal of Cellular Biochemistry*, *113*(9). https://doi.org/10.1002/jcb.24170

Lees, J. A., Reinisch, K. M. (2020). Inter-organelle lipid transfer: a channel model for Vps13 and chorein-N motif proteins. In *Current Opinion in Cell Biology* (Vol. 65). https://doi.org/10.1016/j.ceb.2020.02.008

Lehtinen, M. K., Zappaterra, M. W., Chen, X., Yang, Y. J., Hill, A. D., Lun, M., Maynard, T., Gonzalez, D., Kim, S., Ye, P., D'Ercole, A. J., Wong, E. T., LaMantia, A. S., Walsh, C. A. (2011). The Cerebrospinal Fluid Provides a Proliferative Niche for Neural Progenitor Cells. *Neuron*, *69*(5). https://doi.org/10.1016/j.neuron.2011.01.023

Lenaz, G. (2001). The mitochondrial production of reactive oxygen species: Mechanisms and implications in human pathology. In *IUBMB Life* (Vol. 52, Issues 3–5). https://doi.org/10.1080/15216540152845957

Lendahl, U., Zimmerman, L. B., McKay, R. D. G. (1990). CNS stem cells express a new class of intermediate filament protein. *Cell*, *60*(4). https://doi.org/10.1016/0092-8674(90)90662-X

Lewitus, E., Kelava, I., Huttner, W. B. (2013). Conical expansion of the outer subventricular zone and the role of neocortical folding in evolution and development. *Frontiers in Human Neuroscience*, *JUL*. https://doi.org/10.3389/fnhum.2013.00424

Li, C., Xu, X., Nelson, D. K., Williams, T., Kuehn, M. R., Deng, C. X. (2005). FGFR1 function at the earliest stages of mouse limb development plays an indispensable role in subsequent autopod morphogenesis. *Development*, *132*(21). https://doi.org/10.1242/dev.02065

Li, J., Hua, Y., Miyagawa, S., Zhang, J., Li, L., Liu, L., Sawa, Y. (2020). HiPSC-derived cardiac tissue for disease modeling and drug discovery. In *International Journal of Molecular Sciences* (Vol. 21, Issue 23). https://doi.org/10.3390/ijms21238893

Li, J., Shi, S., Srivastava, S. P., Kitada, M., Nagai, T., Nitta, K., Kohno, M., Kanasaki, K., Koya, D. (2017). FGFR1 is critical for the anti-endothelial mesenchymal transition effect of N-Acetyl-seryl-Aspartyl-lysyl-proline via induction of the MAP4K4 pathway. *Cell Death and Disease*, *8*(8). https://doi.org/10.1038/cddis.2017.353

Li, J., Yang, D., Li, Z., Zhao, M., Wang, D., Sun, Z., Wen, P., Dai, Y., Gou, F., Ji, Y., Zhao, D., Yang, L. (2023). PINK1/Parkin-mediated mitophagy in

neurodegenerative diseases. In *Ageing Research Reviews* (Vol. 84). https://doi.org/10.1016/j.arr.2022.101817

Li, K., Zheng, Y., Cai, S., Fan, Z., Yang, J., Liu, Y., Liang, S., Song, M., Du, S., Qi, L. (2024). The subventricular zone structure, function and implications for neurological disease. *Genes & Diseases*, *12*(3), 101398. https://doi.org/10.1016/J.GENDIS.2024.101398,

Liang, K. X., Kristiansen, C. K., Mostafavi, S., Vatne, G. H., Zantingh, G. A., Kianian, A., Tzoulis, C., Høyland, L. E., Ziegler, M., Perez, R. M., Furriol, J., Zhang, Z., Balafkan, N., Hong, Y., Siller, R., Sullivan, G. J., Bindoff, L. A. (2020). Disease-specific phenotypes in iPSC -derived neural stem cells with POLG mutations. *EMBO Molecular Medicine*, *12*(10). https://doi.org/10.15252/emmm.202012146

Liang, K. X., Vatne, G. H., Kristiansen, C. K., Ievglevskyi, O., Kondratskaya, E., Glover, J. C., Chen, A., Sullivan, G. J., Bindoff, L. A. (2021). N-acetylcysteine amide ameliorates mitochondrial dysfunction and reduces oxidative stress in hiPSC-derived dopaminergic neurons with POLG mutation. *Experimental Neurology*, *337*. https://doi.org/10.1016/j.expneurol.2020.113536

Lie, P. P. Y., Nixon, R. A. (2019). Lysosome trafficking and signaling in health and neurodegenerative diseases. In *Neurobiology of Disease* (Vol. 122). https://doi.org/10.1016/j.nbd.2018.05.015

Lim, M. S., Lee, S. Y., Park, C. H. (2015). FGF8 is essential for functionality of induced neural precursor cell-derived dopaminergic neurons. *International Journal of Stem Cells*, *8*(2). https://doi.org/10.15283/ijsc.2015.8.2.228

Lin, C. C., Wieteska, L., Poncet-Montange, G., Suen, K. M., Arold, S. T., Ahmed, Z., Ladbury, J. E. (2023). The combined action of the intracellular regions regulates FGFR2 kinase activity. *Communications Biology*, *6*(1). https://doi.org/10.1038/s42003-023-05112-6

Lin, C., Chen, P. Y., Chan, H. C., Huang, Y. P., Chang, N. W. (2018). Peroxisome proliferator-activated receptor alpha accelerates neuronal differentiation and this might involve the mitogen-activated protein kinase pathway. *International Journal of Developmental Neuroscience*, *71*. https://doi.org/10.1016/j.ijdevneu.2018.08.006

Lin, H., Lin, S., Shi, L., Xu, G., Lin, M., Li, S., Chen, J., Li, Z., Nakazibwe, C., Xiao, Y., Li, X., Pan, X., Wang, C. (2024). FGFR1 governs iron homeostasis via regulating intracellular protein degradation pathways of IRP2 in prostate cancer cells. *Communications Biology 2024 7:1*, *7*(1), 1–13. https://doi.org/10.1038/s42003-024-06704-6

Lin, M. Y., Cheng, X. T., Tammineni, P., Xie, Y., Zhou, B., Cai, Q., Sheng, Z. H. (2017). Releasing Syntaphilin Removes Stressed Mitochondria from Axons Independent of Mitophagy under Pathophysiological Conditions. *Neuron*, *94*(3). https://doi.org/10.1016/j.neuron.2017.04.004

Lionaki, E., Gkikas, I., Tavernarakis, N. (2016). Differential protein distribution between the nucleus and mitochondria: Implications in aging. In *Frontiers in Genetics* (Vol. 7, Issue SEP). https://doi.org/10.3389/fgene.2016.00162

Liu, J. C., Zhao, X. Y., Wu, M. L., Shi, Y. F., Huang, Z. P., Fang, L. P., Zhu, C., Peng, X., Shi, Z. L., Lan, L. J., Ji, W. L., Luo, L., Feng, L., Zhang, Z. L., Xu, D. E., Li, S., Qin, Z. H., Sun, Y. Y., Schachner, M., Ma, Q. H. (2024a). GPR50 regulates neuronal development as a mitophagy receptor. *Cell Death & Disease 2024 15:8*, *15*(8), 1–17. https://doi.org/10.1038/s41419-024-06978-y

Liu, Y., Cao, M., Cai, Y., Li, X., Zhao, C., Cui, R. (2020). Dissecting the Role of the FGF19-FGFR4 Signaling Pathway in Cancer Development and Progression. In *Frontiers in Cell and Developmental Biology* (Vol. 8). https://doi.org/10.3389/fcell.2020.00095

Liu, Y., Thyagarajan, B., Lakshmipathy, U., Xue, H., Lieu, P., Fontes, A., MacArthur, C. C., Scheyhing, K., Rao, M. S., Chesnut, J. D. (2009). Generation of platform human embryonic stem cell lines that allow efficient targeting at a predetermined

genomic location. *Stem Cells and Development*, *18*(10). https://doi.org/10.1089/scd.2009.0047

Lo, A. K. F., Dawson, C. W., Young, L. S., Ko, C. W., Hau, P. M., Lo, K. W. (2015). Activation of the FGFR1 signalling pathway by the Epstein-Barr virus-encoded LMP1 promotes aerobic glycolysis and transformation of human nasopharyngeal epithelial cells. *Journal of Pathology*, *237*(2). https://doi.org/10.1002/path.4575

Lom, B., Höpker, V., McFarlane, S., Bixby, J. L., Holt, C. E. (1998). Fibroblast growth factor receptor signaling in Xenopus retinal axon extension. *Journal of Neurobiology*, *37*(4). https://doi.org/10.1002/(SICI)1097-4695(199812)37:4<633::AID-NEU11>3.0.CO;2-L

Lotz, G. P., Brychzy, A., Heinz, S., Obermann, W. M. J. (2008). A novel HSP90 chaperone complex regulates intracellular vesicle transport. *Journal of Cell Science*, *121*(5). https://doi.org/10.1242/jcs.015610

Lou, G., Palikaras, K., Lautrup, S., Scheibye-Knudsen, M., Tavernarakis, N., Fang, E. F. (2020). Mitophagy and Neuroprotection. In *Trends in Molecular Medicine* (Vol. 26, Issue 1). https://doi.org/10.1016/j.molmed.2019.07.002

Lu, W., Shi, Y., Jackson, A. C., Bjorgan, K., During, M. J., Sprengel, R., Seeburg, P. H., Nicoll, R. A. (2009). Subunit Composition of Synaptic AMPA Receptors Revealed by a Single-Cell Genetic Approach. *Neuron*, *62*(2). https://doi.org/10.1016/j.neuron.2009.02.027

Lui, J. H., Hansen, D. V., Kriegstein, A. R. (2011a). Development and evolution of the human neocortex. In *Cell* (Vol. 146, Issue 1). https://doi.org/10.1016/j.cell.2011.06.030

Lv, M., Wang, C., Li, F., Peng, J., Wen, B., Gong, Q., Shi, Y., Tang, Y. (2017). Structural insights into the recognition of phosphorylated FUNDC1 by LC3B in mitophagy. *Protein and Cell*, *8*(1). https://doi.org/10.1007/s13238-016-0328-8

Ma, D. K., Ponnusamy, K., Song, M. R., Ming, G. L., Song, H. (2009). Molecular genetic analysis of FGFR1 signalling reveals distinct roles of MAPK and PLC1 activation for self-renewal of adult neural stem cells. *Molecular Brain*, *2*(1), 1–14. https://doi.org/10.1186/1756-6606-2-16/FIGURES/6

Ma, T., Zhang, Q., Cai, Y., You, Y., Rubenstein, J. L. R., Yang, Z. (2012). A subpopulation of dorsal lateral/caudal ganglionic eminence-derived neocortical interneurons expresses the transcription factor Sp8. *Cerebral Cortex*, *22*(9). https://doi.org/10.1093/cercor/bhr296

Maniou, E., Farah, F., Marshall, A. R., Crane-Smith, Z., Krstevski, A., Stathopoulou, A., Greene, N. D. E., Copp, A. J., Galea, G. L. (2023). Caudal Fgfr1 disruption produces localised spinal mis-patterning and a terminal myelocystocele-like phenotype in mice. *Development (Cambridge)*, *150*(19). https://doi.org/10.1242/dev.202139

Mansueto, G., Armani, A., Viscomi, C., D'Orsi, L., De Cegli, R., Polishchuk, E. V., Lamperti, C., Di Meo, I., Romanello, V., Marchet, S., Saha, P. K., Zong, H., Blaauw, B., Solagna, F., Tezze, C., Grumati, P., Bonaldo, P., Pessin, J. E., Zeviani, M., Ballabio, A. (2017). Transcription Factor EB Controls Metabolic Flexibility during Exercise. *Cell Metabolism*, *25*(1). https://doi.org/10.1016/j.cmet.2016.11.003

Marín, O., Anderson, S. A., Rubenstein, J. L. R. (2000). Origin and molecular specification of striatal interneurons. *Journal of Neuroscience*, *20*(16). https://doi.org/10.1523/jneurosci.20-16-06063.2000

Mårtensson, C. U., Priesnitz, C., Song, J., Ellenrieder, L., Doan, K. N., Boos, F., Floerchinger, A., Zufall, N., Oeljeklaus, S., Warscheid, B., Becker, T. (2019). Mitochondrial protein translocation-associated degradation. *Nature*, *569*(7758). https://doi.org/10.1038/s41586-019-1227-y

Martínez-Cerdeño, V., Noctor, S. C., Kriegstein, A. R. (2006). The role of intermediate progenitor cells in the evolutionary expansion of the cerebral cortex. *Cerebral Cortex*, *16*(SUPPL. 1). https://doi.org/10.1093/cercor/bhk017

Martínez-Fernández, L., González-Muniesa, P., Sáinz, N., Laiglesia, L. M., Escoté, X., Martínez, J. A., Moreno-Aliaga, M. J. (2019). Maresin 1 Regulates Hepatic FGF21 in Diet-Induced Obese Mice and in Cultured Hepatocytes. *Molecular Nutrition and Food Research*, *63*(24). https://doi.org/10.1002/mnfr.201900358

Matsui, A., Kobayashi, J., Kanno, S. I., Hashiguchi, K., Miyaji, M., Yoshikawa, Y., Yasui, A., Zhang-Akiyama, Q. M. (2019). Oxidation resistance 1 prevents genome instability through maintenance of G2/M arrest in gamma-ray-irradiated cells. *Journal of Radiation Research*, *61*(1). https://doi.org/10.1093/jrr/rrz080

Meng, X., Yao, D., Imaizumi, K., Chen, X., Kelley, K. W., Reis, N., Thete, M. V., Arjun McKinney, A., Kulkarni, S., Panagiotakos, G., Bassik, M. C., Pașca, S. P. (2023). Assembloid CRISPR screens reveal impact of disease genes in human neurodevelopment. *Nature*, *622*(7982). https://doi.org/10.1038/s41586-023-06564-w

Merkert, S., Haase, A., Dahlmann, J., Göhring, G., Waqas, F. H., Pessler, F., Martin, U., Olmer, R. (2023). Generation of two human NRF2 knockout iPSC clones using CRISPR/Cas9 editing. *Stem Cell Research*, *69*. https://doi.org/10.1016/j.scr.2023.103090

Metzler, E., Escobar, H., Sunaga-Franze, D. Y., Sauer, S., Diecke, S., Spuler, S. (2022). Generation of hiPSC-Derived Skeletal Muscle Cells: Exploiting the Potential of Skeletal Muscle-Derived hiPSCs. *Biomedicines*, *10*(5). https://doi.org/10.3390/BIOMEDICINES10051204

Miellet, S., St Clair-Glover, M., Maddock, M., Dottori, M. (2024). Generation of a gene-edited H9 embryonic stem cell line carrying a DOX-inducible NGN2 expression cassette in the CLYBL locus. *Stem Cell Research*, *75*. https://doi.org/10.1016/j.scr.2024.103312

Millar, J. K., James, R., Christie, S., Porteous, D. J. (2005). Disrupted in Schizophrenia 1 (DISC1): Subcellular targeting and induction of ring mitochondria. *Molecular and Cellular Neuroscience*, *30*(4). https://doi.org/10.1016/j.mcn.2005.08.021

Miller, I., Min, M., Yang, C., Tian, C., Gookin, S., Carter, D., Spencer, S. L. (2018). Ki67 is a Graded Rather than a Binary Marker of Proliferation versus Quiescence. *Cell Reports*, *24*(5). https://doi.org/10.1016/j.celrep.2018.06.110

Mitchell, J. M., Nemesh, J., Ghosh, S., Handsaker, R. E., Mello, C. J., Meyer, D., Raghunathan, K., Rivera, H. de, Tegtmeyer, M., Hawes, D., Neumann, A., Nehme, R., Eggan, K., McCarroll, S. A. (2020). Mapping genetic effects on cellular phenotypes with "cell villages." *BioRxiv*.

Miura, Y., Li, M. Y., Birey, F., Ikeda, K., Revah, O., Thete, M. V., Park, J. Y., Puno, A., Lee, S. H., Porteus, M. H., Pașca, S. P. (2020). Generation of human striatal organoids and cortico-striatal assembloids from human pluripotent stem cells. *Nature Biotechnology*, *38*(12). https://doi.org/10.1038/s41587-020-00763-w

Miyata, T., Okamoto, M., Shinoda, T., Kawaguchi, A. (2015). Interkinetic nuclear migration generates and opposes ventricular-zone crowding: Insight into tissue mechanics. In *Frontiers in Cellular Neuroscience* (Vol. 8, Issue JAN). https://doi.org/10.3389/fncel.2014.00473

Miyoshi, G., Hjerling-Leffler, J., Karayannis, T., Sousa, V. H., Butt, S. J. B., Battiste, J., Johnson, J. E., Machold, R. P., Fishell, G. (2010). Genetic fate mapping reveals that the caudal ganglionic eminence produces a large and diverse population of superficial cortical interneurons. *Journal of Neuroscience*, *30*(5). https://doi.org/10.1523/JNEUROSCI.4515-09.2010

Molnár, Z., Clowry, G. J., Šestan, N., Alzu'bi, A., Bakken, T., Hevner, R. F., Hüppi, P. S., Kostović, I., Rakic, P., Anton, E. S., Edwards, D., Garcez, P., Hoerder-Suabedissen, A., Kriegstein, A. (2019). New insights into the development of the human cerebral cortex. In *Journal of Anatomy* (Vol. 235, Issue 3). https://doi.org/10.1111/joa.13055

Molotkov, A., Mazot, P., Brewer, J. R., Cinalli, R. M., Soriano, P. (2017). Distinct Requirements for FGFR1 and FGFR2 in Primitive Endoderm Development and

Exit from Pluripotency. *Developmental Cell*, *41*(5). https://doi.org/10.1016/j.devcel.2017.05.004

Morimoto, N., Miyazaki, K., Kurata, T., Ikeda, Y., Matsuura, T., Kang, D., Ide, T., Abe, K. (2012). Effect of mitochondrial transcription factor a overexpression on motor neurons in amyotrophic lateral sclerosis model mice. *Journal of Neuroscience Research*, *90*(6). https://doi.org/10.1002/jnr.23000

Mummidi, S., Ahuja, S. S., Gonzalez, E., Anderson, S. A., Santiago, E. N., Stephan, K. T., Craig, F. E., O'Connell, P., Tryon, V., Clark, R. A., Dolan, M. J., Ahuja, S. K. (1998). Genealogy of the CCR5 locus and chemokine system gene variants associated with altered rates of HIV-1 disease progression. *Nature Medicine*, *4*(7). https://doi.org/10.1038/nm0798-786

Myers, J. M., Martins, G. G., Ostrowski, J., Stachowiak, M. K. (2003). Nuclear trafficking of FGFR1: A role for the transmembrane domain. *Journal of Cellular Biochemistry*, *88*(6), 1273–1291. https://doi.org/10.1002/JCB.10476

Narendra, D. P., Jin, S. M., Tanaka, A., Suen, D. F., Gautier, C. A., Shen, J., Cookson, M. R., Youle, R. J. (2010). PINK1 is selectively stabilized on impaired mitochondria to activate Parkin. *PLoS Biology*, *8*(1). https://doi.org/10.1371/journal.pbio.1000298

Narendra, D. P., Youle, R. J. (2011). Targeting mitochondrial dysfunction: Role for PINK1 and parkin in mitochondrial quality control. In *Antioxidants and Redox Signaling* (Vol. 14, Issue 10). https://doi.org/10.1089/ars.2010.3799

Narla, S. T., Lee, Y. W., Benson, C. A., Sarder, P., Brennand, K. J., Stachowiak, E. K., Stachowiak, M. K. (2017a). Common developmental genome deprogramming in schizophrenia — Role of Integrative Nuclear FGFR1 Signaling (INFS). *Schizophrenia Research*, *185*. https://doi.org/10.1016/j.schres.2016.12.012

Narsinh, K. H., Plews, J., Wu, J. C. (2011). Comparison of human induced pluripotent and embryonic stem cells: Fraternal or identical twins? In *Molecular Therapy* (Vol. 19, Issue 4). https://doi.org/10.1038/mt.2011.41

Naz, H., Islam, A., Waheed, A., Sly, W. S., Ahmad, F., Hassan, M. I. (2013). Human β-glucuronidase: Structure, function, and application in enzyme replacement therapy. *Rejuvenation Research*, *16*(5). https://doi.org/10.1089/rej.2013.1407

Neavin, D. R., Steinmann, A. M., Farbehi, N., Chiu, H. S., Daniszewski, M. S., Arora, H., Bermudez, Y., Moutinho, C., Chan, C. L., Bax, M., Tyebally, M., Gnanasambandapillai, V., Lam, C. E., Nguyen, U., Hernández, D., Lidgerwood, G. E., Graham, R. M., Hewitt, A. W., Pébay, A., Powell, J. E. (2023). A village in a dish model system for population-scale hiPSC studies. *Nature Communications*, *14*(1). https://doi.org/10.1038/s41467-023-38704-1

Nery, S., Fishell, G., Corbin, J. G. (2002). The caudal ganglionic eminence is a source of distinct cortical and subcortical cell populations. *Nature Neuroscience*, *5*(12). https://doi.org/10.1038/nn971

Nies, V. J. M., Struik, D., Liu, S., Liu, W., Kruit, J. K., Downes, M., van Zutphen, T., Verkade, H. J., Evans, R. M., Jonker, J. W. (2022). Autocrine FGF1 signaling promotes glucose uptake in adipocytes. *Proceedings of the National Academy of Sciences of the United States of America*, *119*(40). https://doi.org/10.1073/pnas.2122382119

Niethammer, P., Delling, M., Sytnyk, V., Dityatev, A., Fukami, K., Schachner, M. (2002). Cosignaling of NCAM via lipid rafts and the FGF receptor is required for neuritogenesis. *Journal of Cell Biology*, *157*(3). https://doi.org/10.1083/jcb.200109059

Nissanka, N., Moraes, C. T. (2018). Mitochondrial DNA damage and reactive oxygen species in neurodegenerative disease. In *FEBS Letters* (Vol. 592, Issue 5). https://doi.org/10.1002/1873-3468.12956

Nóbrega-Pereira, S., Gelman, D., Bartolini, G., Pla, R., Pierani, A., Marín, O. (2010). Origin and molecular specification of globus pallidus neurons. *Journal of Neuroscience*, *30*(8). https://doi.org/10.1523/JNEUROSCI.4023-09.2010

Noctor, S. C., Flint, A. C., Weissman, T. A., Dammerman, R. S., Kriegstein, A. R. (2001). Neurons derived from radial glial cells establish radial units in neocortex. *Nature*, *409*(6821). https://doi.org/10.1038/35055553

Noctor, S. C., Martinez-Cerdeño, V., Ivic, L., Kriegstein, A. R. (2004). Cortical neurons arise in symmetric and asymmetric division zones and migrate through specific phases. *Nature Neuroscience*, *7*(2). https://doi.org/10.1038/nn1172

Noctor, S. C., Martínez-Cerdeño, V., Kriegstein, A. R. (2007). Contribution of intermediate progenitor cells to cortical histogenesis. In *Archives of Neurology* (Vol. 64, Issue 5). https://doi.org/10.1001/archneur.64.5.639

Norkett, R., Modi, S., Birsa, N., Atkin, T. A., Ivankovic, D., Pathania, M., Trossbach, S. V., Korth, C., Hirst, W. D., Kittler, J. T. (2016). DISC1-dependent regulation of mitochondrial dynamics controls the morphogenesis of complex neuronal dendrites. *Journal of Biological Chemistry*, *291*(2). https://doi.org/10.1074/jbc.M115.699447

Nowakowski, T. J., Bhaduri, A., Pollen, A. A., Alvarado, B., Mostajo-Radji, M. A., Di Lullo, E., Haeussler, M., Sandoval-Espinosa, C., Liu, S. J., Velmeshev, D., Ounadjela, J. R., Shuga, J., Wang, X., Lim, D. A., West, J. A., Leyrat, A. A., Kent, W. J., Kriegstein, A. R. (2017). Spatiotemporal gene expression trajectories reveal developmental hierarchies of the human cortex. *Science*, *358*(6368). https://doi.org/10.1126/science.aap8809

Nowakowski, T. J., Pollen, A. A., Sandoval-Espinosa, C., Kriegstein, A. R. (2016). Transformation of the Radial Glia Scaffold Demarcates Two Stages of Human Cerebral Cortex Development. *Neuron*, *91*(6). https://doi.org/10.1016/j.neuron.2016.09.005

Oberholzer, Z., Loubser, C., Nikitina, N. V. (2024). Fgf17: A regulator of the mid/hind brain boundary in mammals. *Differentiation*, *140*, 100813. https://doi.org/10.1016/J.DIFF.2024.100813

Ohkubo, Y., Uchida, A. O., Shin, D., Partanen, J., Vaccarino, F. M. (2004). Fibroblast growth factor receptor 1 is required for the proliferation of hippocampal progenitor cells and for hippocampal growth in mouse. *Journal of Neuroscience*, *24*(27). https://doi.org/10.1523/JNEUROSCI.1140-04.2004

Ohmachi, S., Mikami, T., Konishi, M., Miyake, A., Itoh, N. (2003). Preferential neurotrophic activity of fibroblast growth factor-20 for dopaminergic neurons through fibroblast growth factor receptor-1c. *Journal of Neuroscience Research*, *72*(4). https://doi.org/10.1002/jnr.10592

Olsson, M., Campbell, K., Wictorin, K., Björklund, A. (1995). Projection neurons in fetal striatal transplants are predominantly derived from the lateral ganglionic eminence. *Neuroscience*, *69*(4). https://doi.org/10.1016/0306-4522(95)00325-D

Osman, C., Voelker, D. R., Langer, T. (2011). Making heads or tails of phospholipids in mitochondria. In *Journal of Cell Biology* (Vol. 192, Issue 1). https://doi.org/10.1083/jcb.201006159

Pakos-Zebrucka, K., Koryga, I., Mnich, K., Ljujic, M., Samali, A., Gorman, A. M. (2016). The integrated stress response. *EMBO Reports*, *17*(10). https://doi.org/10.15252/embr.201642195

Palmer, J. C., Tayler, H. M., Love, S. (2013). Endothelin-converting enzyme-1 activity, endothelin-1 production, and free radical-dependent vasoconstriction in Alzheimer's disease. *Journal of Alzheimer's Disease*, *36*(3). https://doi.org/10.3233/JAD-130383

Palser, A. L., Norman, A. L., Saffell, J. L., Reynolds, R. (2009). Neural cell adhesion molecule stimulates survival of premyelinating oligodendrocytes via the fibroblast growth factor receptor. *Journal of Neuroscience Research*, *87*(15). https://doi.org/10.1002/jnr.22248

Pamies, D., Block, K., Lau, P., Gribaldo, L., Pardo, C. A., Barreras, P., Smirnova, L., Wiersma, D., Zhao, L., Harris, G., Hartung, T., Hogberg, H. T. (2018). Rotenone exerts developmental neurotoxicity in a human brain spheroid model. *Toxicology*

and Applied Pharmacology, *354*, 101–114. https://doi.org/10.1016/J.TAAP.2018.02.003

Papapetrou, E. P., Schambach, A. (2016). Gene insertion into genomic safe harbors for human gene therapy. In *Molecular Therapy* (Vol. 24, Issue 4). https://doi.org/10.1038/mt.2016.38

Parcerisas, A., Pujadas, L., Ortega-Gascó, A., Perelló-Amorós, B., Viais, R., Hino, K., Figueiro-Silva, J., La Torre, A., Trullás, R., Simó, S., Lüders, J., Soriano, E. (2020). NCAM2 Regulates Dendritic and Axonal Differentiation through the Cytoskeletal Proteins MAP2 and 14-3-3. *Cerebral Cortex*, *30*(6). https://doi.org/10.1093/cercor/bhz342

Parrotta, E. I., Lucchino, V., Zannino, C., Valente, D., Scalise, S., Benedetto, G. L., Iazzetta, M. R., Talarico, M., Conforti, F., Agostino, S. Di, Fiorenzano, A., Quattrone, A., Cuda, G., Quattrone, A. (2024). Mosaic midbrain organoids: a new tool to study Progressive Supranuclear Palsy and advancing clinical neurology research. *BioRxiv*, 2024.06.03.597136. https://doi.org/10.1101/2024.06.03.597136

Pașca, A. M., Park, J. Y., Shin, H. W., Qi, Q., Revah, O., Krasnoff, R., O'Hara, R., Willsey, A. J., Palmer, T. D.,Pașca, S. P. (2019). Human 3D cellular model of hypoxic brain injury of prematurity. *Nature Medicine*, *25*(5). https://doi.org/10.1038/s41591-019-0436-0

Pasca, A. M., Sloan, S. A., Clarke, L. E., Tian, Y., Makinson, C. D., Huber, N., Kim, C. H., Park, J. Y., O'Rourke, N. A., Nguyen, K. D., Smith, S. J., Huguenard, J. R., Geschwind, D. H., Barres, B. A., Pasca, S. P. (2015). Functional cortical neurons and astrocytes from human pluripotent stem cells in 3D culture. *Nature Methods*, *12*(7). https://doi.org/10.1038/nmeth.3415

Pașca, S. P., Arlotta, P., Bateup, H. S., Camp, J. G., Cappello, S., Gage, F. H., Knoblich, J. A., Kriegstein, A. R., Lancaster, M. A., Ming, G. L., Muotri, A. R., Park, I. H., Reiner, O., Song, H., Studer, L., Temple, S., Testa, G., Treutlein, B., Vaccarino, F. M. (2022). A nomenclature consensus for nervous system organoids and assembloids. *Nature*, *609*(7929). https://doi.org/10.1038/s41586-022-05219-6

Patterson, K., Linask, K. L., Beers, J., Zou, J. (2020). Generation of two tdTomato reporter induced pluripotent stem cell lines (NHLBIi003-A-1 and NHLBIi003-A-2) by AAVS1 safe harbor gene-editing. *Stem Cell Research*, *42*. https://doi.org/10.1016/j.scr.2019.101673

Patton, M. H., Thomas, K. T., Bayazitov, I. T., Newman, K. D., Kurtz, N. B., Robinson, C. G., Ramirez, C. A., Trevisan, A. J., Bikoff, J. B., Peters, S. T., Pruett-Miller, S. M., Jiang, Y., Schild, A. B., Nityanandam, A., Zakharenko, S. S. (2024). Synaptic plasticity in human thalamocortical assembloids. *BioRxiv*, 2024.02.01.578421. https://doi.org/10.1101/2024.02.01.578421

Pebworth, M. P., Ross, J., Andrews, M., Bhaduri, A., Kriegstein, A. R. (2021a). Human intermediate progenitor diversity during cortical development. *Proceedings of the National Academy of Sciences of the United States of America*, *118*(26). https://doi.org/10.1073/pnas.2019415118

Pekkurnaz, G., Wang, X. (2022). Mitochondrial heterogeneity and homeostasis through the lens of a neuron. *Nature Metabolism*, *4*(7). https://doi.org/10.1038/s42255-022-00594-w

Pellegrini, L., Bonfio, C., Chadwick, J., Begum, F., Skehel, M., Lancaster, M. A. (2020). Human CNS barrier-forming organoids with cerebrospinal fluid production. *Science*, *369*(6500). https://doi.org/10.1126/science.aaz5626

Pellenz, S., Phelps, M., Tang, W., Hovde, B. T., Sinit, R. B., Fu, W., Li, H., Chen, E., Monnat, R. J. (2019). New Human Chromosomal Sites with "Safe Harbor" Potential for Targeted Transgene Insertion. *Human Gene Therapy*, *30*(7). https://doi.org/10.1089/hum.2018.169

Peng, H., Moffett, J., Myers, J., Fang, X., Stachowiak, E. K., Maher, P., Kratz, E., Hines, J., Fluharty, S. J., Mizukoshi, E., Bloom, D. C., Stachowiak, M. K. (2001). Novel

nuclear signaling pathway mediates activation of fibroblast growth factor-2 gene by type 1 and type 2 angiotensin II receptors. *Molecular Biology of the Cell*, *12*(2). https://doi.org/10.1091/mbc.12.2.449

Peng, W. C., Lin, X., Torres, J. (2009). The strong dimerization of the transmembrane domain of the fibroblast growth factor receptor (FGFR) is modulated by C-terminal juxtamembrane residues. *Protein Science*, *18*(2). https://doi.org/10.1002/pro.65

Perez, R. K., Gordon, M. G., Subramaniam, M., Kim, M. C., Hartoularos, G. C., Targ, S., Sun, Y., Ogorodnikov, A., Bueno, R., Lu, A., Thompson, M., Rappoport, N., Dahl, A., Lanata, C. M., Matloubian, M., Maliskova, L., Kwek, S. S., Li, T., Slyper, M., … Ye, C. J. (2022). Single-cell RNA-seq reveals cell type-specific molecular and genetic associations to lupus. *Science*, *376*(6589). https://doi.org/10.1126/science.abf1970

Petazzi, P., Menéndez, P., Sevilla, A. (2022). CRISPR/Cas9–Mediated Gene Knockout and Knockin Human iPSCs. In *Methods in Molecular Biology* (Vol. 2454). https://doi.org/10.1007/7651_2020_337

Petersilie, L., Kafitz, K. W., Neu, L. A., Heiduschka, S., Le, S., Prigione, A., Rose, C. R. (2024). Protocol for the generation of cultured cortical brain organoid slices. *STAR Protocols*, *5*(3). https://doi.org/10.1016/J.XPRO.2024.103212

Pirou, C., Montazer-Torbati, F., Jah, N., Delmas, E., Lasbleiz, C., Mignotte, B., Renaud, F. (2017). FGF1 protects neuroblastoma SH-SY5Y cells from p53-dependent apoptosis through an intracrine pathway regulated by FGF1 phosphorylation. *Cell Death and Disease*, *8*(8). https://doi.org/10.1038/CDDIS.2017.404

Pirvola, U., Ylikoski, J., Trokovic, R., Hébert, J. M., McConnell, S. K., Partanen, J. (2002). FGFR1 is required for the development of the auditory sensory epithelium. *Neuron*, *35*(4). https://doi.org/10.1016/S0896-6273(02)00824-3

Plotnikov, A. N., Schlessinger, J., Hubbard, S. R., Mohammadi, M. (1999). Structural basis for FGF receptor dimerization and activation. *Cell*, *98*(5). https://doi.org/10.1016/S0092-8674(00)80051-3

Pollen, A. A., Nowakowski, T. J., Chen, J., Retallack, H., Sandoval-Espinosa, C., Nicholas, C. R., Shuga, J., Liu, S. J., Oldham, M. C., Diaz, A., Lim, D. A., Leyrat, A. A., West, J. A., Kriegstein, A. R. (2015). Molecular Identity of Human Outer Radial Glia during Cortical Development. *Cell*, *163*(1). https://doi.org/10.1016/j.cell.2015.09.004

Poole, L. P., Bock-Hughes, A., Berardi, D. E., Macleod, K. F. (2021). ULK1 promotes mitophagy via phosphorylation and stabilization of BNIP3. *Scientific Reports*, *11*(1). https://doi.org/10.1038/s41598-021-00170-4

Popova, G., Soliman, S. S., Kim, C. N., Keefe, M. G., Hennick, K. M., Jain, S., Li, T., Tejera, D., Shin, D., Chhun, B. B., McGinnis, C. S., Speir, M., Gartner, Z. J., Mehta, S. B., Haeussler, M., Hengen, K. B., Ransohoff, R. R., Piao, X., Nowakowski, T. J. (2021). Human microglia states are conserved across experimental models and regulate neural stem cell responses in chimeric organoids. Cell Stem Cell, 28(12). https://doi.org/10.1016/j.stem.2021.08.015

Porębska, N., Latko, M., Kucińska, M., Zakrzewska, M., Otlewski, J., Opaliński, Ł. (2019). Targeting cellular trafficking of fibroblast growth factor receptors as a strategy for selective cancer treatment. In *Journal of Clinical Medicine* (Vol. 8, Issue 1). https://doi.org/10.3390/jcm8010007

Prondzynski, M., Berkson, P., Trembley, M. A., Tharani, Y., Shani, K., Bortolin, R. H., Sweat, M. E., Mayourian, J., Yucel, D., Cordoves, A. M., Gabbin, B., Hou, C., Anyanwu, N. J., Nawar, F., Cotton, J., Milosh, J., Walker, D., Zhang, Y., Lu, F., … Pu, W. T. (2024). Efficient and reproducible generation of human iPSC-derived cardiomyocytes and cardiac organoids in stirred suspension systems. *Nature Communications 2024 15:1*, *15*(1), 1–17. https://doi.org/10.1038/s41467-024-50224-0

Pu, J., Frescas, D., Zhang, B., Feng, J. (2015). Utilization of TALEN and CRISPR/Cas9 technologies for gene targeting and modification. *Experimental Biology and Medicine*, *240*(8). https://doi.org/10.1177/1535370215584932

Qian, X., Nguyen, H. N., Jacob, F., Song, H., Ming, G. L. (2017). Using brain organoids to understand Zika virus-induced microcephaly. *Development (Cambridge)*, *144*(6). https://doi.org/10.1242/dev.140707

Qian, X., Su, Y., Adam, C. D., Deutschmann, A. U., Pather, S. R., Goldberg, E. M., Su, K., Li, S., Lu, L., Jacob, F., Nguyen, P. T. T., Huh, S., Hoke, A., Swinford-Jackson, S. E., Wen, Z., Gu, X., Pierce, R. C., Wu, H., Briand, L. A., … Ming, G. li. (2020). Sliced Human Cortical Organoids for Modeling Distinct Cortical Layer Formation. *Cell Stem Cell*, *26*(5). https://doi.org/10.1016/j.stem.2020.02.002

Quadrato, G., Nguyen, T., Macosko, E. Z., Sherwood, J. L., Yang, S. M., Berger, D. R., Maria, N., Scholvin, J., Goldman, M., Kinney, J. P., Boyden, E. S., Lichtman, J. W., Williams, Z. M., McCarroll, S. A., Arlotta, P. (2017). Cell diversity and network dynamics in photosensitive human brain organoids. *Nature*, *545*(7652). https://doi.org/10.1038/nature22047

Ramachandra, C. J. A., Shahbazi, M., Kwang, T. W. X., Choudhury, Y., Bak, X. Y., Yang, J., Wang, S. (2011). Efficient recombinase-mediated cassette exchange at the AAVS1 locus in human embryonic stem cells using baculoviral vectors. *Nucleic Acids Research*, *39*(16). https://doi.org/10.1093/nar/gkr409

Rath, S., Sharma, R., Gupta, R., Ast, T., Chan, C., Durham, T. J., Goodman, R. P., Grabarek, Z., Haas, M. E., Hung, W. H. W., Joshi, P. R., Jourdain, A. A., Kim, S. H., Kotrys, A. V., Lam, S. S., McCoy, J. G., Meisel, J. D., Miranda, M., Panda, A., … Mootha, V. K. (2021). MitoCarta3.0: An updated mitochondrial proteome now with sub-organelle localization and pathway annotations. *Nucleic Acids Research*, *49*(D1). https://doi.org/10.1093/nar/gkaa1011

Reilly, J. F., Maher, P. A. (2001). Importin β-mediated nuclear import of fibroblast growth factor receptor: Role in cell proliferation. *Journal of Cell Biology*, *152*(6). https://doi.org/10.1083/jcb.152.6.1307

Reumann, D., Krauditsch, C., Novatchkova, M., Sozzi, E., Wong, S. N., Zabolocki, M., Priouret, M., Doleschall, B., Ritzau-Reid, K. I., Piber, M., Morassut, I., Fieseler, C., Fiorenzano, A., Stevens, M. M., Zimmer, M., Bardy, C., Parmar, M., Knoblich, J. A. (2023). In vitro modeling of the human dopaminergic system using spatially arranged ventral midbrain–striatum–cortex assembloids. *Nature Methods*, *20*(12). https://doi.org/10.1038/s41592-023-02080-x

Richter-Dennerlein, R., Dennerlein, S., Rehling, P. (2015). Integrating mitochondrial translation into the cellular context. *Nature Reviews Molecular Cell Biology*, *16*(10). https://doi.org/10.1038/nrm4051

Romero-Morales, A. I., Robertson, G. L., Rastogi, A., Rasmussen, M. L., Temuri, H., McElroy, G. S., Chakrabarty, R. P., Hsu, L., Almonacid, P. M., Millis, B. A., Chandel, N. S., Cartailler, J. P., Gama, V. (2022a). Human iPSC-derived cerebral organoids model features of Leigh syndrome and reveal abnormal corticogenesis. *Development (Cambridge)*, *149*(20). https://doi.org/10.1242/dev.199914

Rothaug, M., Stroobants, S., Schweizer, M., Peters, J., Zunke, F., Allerding, M., D'Hooge, R., Saftig, P., Blanz, J. (2015). LAMP-2 deficiency leads to hippocampal dysfunction but normal clearance of neuronal substrates of chaperone-mediated autophagy in a mouse model for Danon disease. *Acta Neuropathologica Communications*, *3*. https://doi.org/10.1186/s40478-014-0182-y

Ruan, L., Zhou, C., Jin, E., Kucharavy, A., Zhang, Y., Wen, Z., Florens, L., Li, R. (2017). Cytosolic proteostasis through importing of misfolded proteins into mitochondria. *Nature*, *543*(7645). https://doi.org/10.1038/nature21695

Saarimäki-Vire, J., Peltopuro, P., Lahti, L., Naserke, T., Blak, A. A., Weisenhorn, D. M. V., Yu, K., Ornitz, D. M., Wurst, W., Partanen, J. (2007). Fibroblast growth factor

receptors cooperate to regulate neural progenitor properties in the developing midbrain and hindbrain. *Journal of Neuroscience*, *27*(32). https://doi.org/10.1523/JNEUROSCI.0192-07.2007

Saffell, J. L., Williams, E. J., Mason, I. J., Walsh, F. S., Doherty, P. (1997). Expression of a dominant negative FGF receptor inhibits axonal growth and FGF receptor phosphorylation stimulated by CAMs. *Neuron*, *18*(2). https://doi.org/10.1016/S0896-6273(00)80264-0

Sakaguchi, H., Kadoshima, T., Soen, M., Narii, N., Ishida, Y., Ohgushi, M., Takahashi, J., Eiraku, M., Sasai, Y. (2015). Generation of functional hippocampal neurons from self-organizing human embryonic stem cell-derived dorsomedial telencephalic tissue. *Nature Communications*, *6*. https://doi.org/10.1038/ncomms9896

Sakaguchi, K., Lorenzi, M. V., Bottaro, D. P., Miki, T. (1999). The Acidic Domain and First Immunoglobulin-Like Loop of Fibroblast Growth Factor Receptor 2 Modulate Downstream Signaling through Glycosaminoglycan Modification. *Molecular and Cellular Biology*, *19*(10). https://doi.org/10.1128/mcb.19.10.6754

Santambrogio, S., Ricca, A., Maderna, C., Ieraci, A., Aureli, M., Sonnino, S., Kulik, W., Aimar, P., Bonfanti, L., Martino, S., Gritti, A. (2012). The galactocerebrosidase enzyme contributes to maintain a functional neurogenic niche during early post-natal CNS development. *Human Molecular Genetics*, *21*(21). https://doi.org/10.1093/hmg/dds313

Sarabipour, S., Hristova, K. (2016). Mechanism of FGF receptor dimerization and activation. *Nature Communications*, *7*. https://doi.org/10.1038/ncomms10262

Sarrafha, L., Neavin, D. R., Parfitt, G. M., Kruglikov, I. A., Whitney, K., Reyes, R., Coccia, E., Kareva, T., Goldman, C., Tipon, R., Croft, G., Crary, J. F., Powell, J. E., Blanchard, J., Ahfeldt, T. (2023). Novel human pluripotent stem cell-derived hypothalamus organoids demonstrate cellular diversity. *IScience*, *26*(9). https://doi.org/10.1016/j.isci.2023.107525

Sawada, T., Barbosa, A. R., Araujo, B., McCord, A. E., D'Ignazio, L., Benjamin, K. J. M., Sheehan, B., Zabolocki, M., Feltrin, A., Arora, R., Brandtjen, A. C., Kleinman, J. E., Hyde, T. M., Bardy, C., Weinberger, D. R., Paquola, A. C. M., Erwin, J. A. (2024). Recapitulation of Perturbed Striatal Gene Expression Dynamics of Donors' Brains With Ventral Forebrain Organoids Derived From the Same Individuals With Schizophrenia. *The American Journal of Psychiatry*, *181*(6). https://doi.org/10.1176/appi.ajp.20220723

Scandella, V., Petrelli, F., Moore, D. L., Braun, S. M. G., Knobloch, M. (2023). Neural stem cell metabolism revisited: a critical role for mitochondria. In *Trends in Endocrinology and Metabolism* (Vol. 34, Issue 8). https://doi.org/10.1016/j.tem.2023.05.008

Schäffner, I., Wittmann, M. T., Vogel, T., Lie, D. C. (2023). Differential vulnerability of adult neurogenic niches to dosage of the neurodevelopmental-disorder linked gene Foxg1. *Molecular Psychiatry*, *28*(1). https://doi.org/10.1038/s41380-022-01497-8

Schmid, B., Holst, B., Poulsen, U., Jørring, I., Clausen, C., Rasmussen, M., Mau-Holzmann, U. A., Steeg, R., Nuthall, H., Ebneth, A., Cabrera-Socorro, A. (2021). Generation of two gene edited iPSC-lines carrying a DOX-inducible NGN2 expression cassette with and without GFP in the AAVS1 locus. *Stem Cell Research*, *52*. https://doi.org/10.1016/j.scr.2021.102240

Schmidt, O., Pfanner, N., Meisinger, C. (2010). Mitochondrial protein import: From proteomics to functional mechanisms. In *Nature Reviews Molecular Cell Biology* (Vol. 11, Issue 9). https://doi.org/10.1038/nrm2959

Scholzen, T., Gerdes, J. (2000). The Ki-67 protein: From the known and the unknown. In *Journal of Cellular Physiology* (Vol. 182, Issue 3). https://doi.org/10.1002/(SICI)1097-4652(200003)182:3<311::AID-JCP1>3.0.CO;2-9

Schöndorf, D. C., Ivanyuk, D., Baden, P., Sanchez-Martinez, A., De Cicco, S., Yu, C., Giunta, I., Schwarz, L. K., Di Napoli, G., Panagiotakopoulou, V., Nestel, S., Keatinge, M., Pruszak, J., Bandmann, O., Heimrich, B., Gasser, T., Whitworth, A. J., Deleidi, M. (2018). The NAD+ Precursor Nicotinamide Riboside Rescues Mitochondrial Defects and Neuronal Loss in iPSC and Fly Models of Parkinson's Disease. *Cell Reports*, *23*(10). https://doi.org/10.1016/j.celrep.2018.05.009

Schreiber, S. N., Emter, R., Hock, M. B., Knutti, D., Cardenas, J., Podvinec, M., Oakeley, E. J., Kralli, A. (2004). The estrogen-related receptor α (ERRα) functions in PPARγ coactivator 1α (PGC-1α)-induced mitochondrial biogenesis. *Proceedings of the National Academy of Sciences of the United States of America*, *101*(17), 6472–6477. https://doi.org/10.1073/PNAS.0308686101/SUPPL_FILE/08686TABLE2.PDF

Sebastian, R., Jin, K., Pavon, N., Bansal, R., Potter, A., Song, Y., Babu, J., Gabriel, R., Sun, Y., Aronow, B., Pak, C. H. (2023). Schizophrenia-associated NRXN1 deletions induce developmental-timing- and cell-type-specific vulnerabilities in human brain organoids. *Nature Communications*, *14*(1). https://doi.org/10.1038/s41467-023-39420-6

Sepehrimanesh, M., Ding, B. (2020). Generation and optimization of highly pure motor neurons from human induced pluripotent stem cells via lentiviral delivery of transcription factors. *American Journal of Physiology - Cell Physiology*, *319*(4). https://doi.org/10.1152/AJPCELL.00279.2020

Servetto, A., Kollipara, R., Formisano, L., Lin, C. C., Lee, K. M., Sudhan, D. R., Gonzalez-Ericsson, P. I., Chatterjee, S., Guerrero-Zotano, A., Mendiratta, S., Akamatsu, H., James, N., Bianco, R., Hanker, A. B., Kittler, R., Arteaga, C. L. (2021). Nuclear FGFR1 regulates gene transcription and promotes antiestrogen resistance in ERþ breast cancer. *Clinical Cancer Research*, *27*(15), 4379–4396. https://doi.org/10.1158/1078-0432.CCR-20-3905/672118/AM/NUCLEAR-FGFR1-REGULATES-GENE-TRANSCRIPTION-AND

Sessa, A., Mao, C. an, Hadjantonakis, A. K., Klein, W. H., Broccoli, V. (2008). Tbr2 Directs Conversion of Radial Glia into Basal Precursors and Guides Neuronal Amplification by Indirect Neurogenesis in the Developing Neocortex. *Neuron*, *60*(1). https://doi.org/10.1016/j.neuron.2008.09.028

Shearer, R. F., Saunders, D. N. (2015). Experimental design for stable genetic manipulation in mammalian cell lines: Lentivirus and alternatives. In *Genes to Cells* (Vol. 20, Issue 1). https://doi.org/10.1111/gtc.12183

Sheng, L., Leshchyns'ka, I., Sytnyk, V. (2019). Neural Cell Adhesion Molecule 2 (NCAM2)-Induced c-Src-Dependent Propagation of Submembrane Ca2+ Spikes Along Dendrites Inhibits Synapse Maturation. *Cerebral Cortex*, *29*(4), 1439–1459. https://doi.org/10.1093/CERCOR/BHY041

Shi, Y. J., Shi, M., Xiao, L. J., Li, L., Zou, L. H., Li, C. Y., Zhang, Q. J., Zhou, L. F., Ji, X. C., Huang, H., Xi, Y., Liu, L., Zhang, H. Y., Zhao, G., Ma, L. (2018). Inhibitive effects of FGF2/FGFR1 pathway on astrocyte-mediated inflammation in vivo and in vitro after infrasound exposure. *Frontiers in Neuroscience*, *12*(AUG). https://doi.org/10.3389/fnins.2018.00582

Shin, D., Kim, C. N., Ross, J., Hennick, K. M., Wu, S. R., Paranjape, N., Leonard, R., Wang, J. C., Keefe, M. G., Pavlovic, B. J., Donohue, K. C., Moreau, C., Wigdor, E. M., Larson, H. H., Allen, D. E., Cadwell, C. R., Bhaduri, A., Popova, G., Bearden, C. E., … Nowakowski, T. J. (2024). Thalamocortical organoids enable in vitro modeling of 22q11.2 microdeletion associated with neuropsychiatric disorders. *Cell Stem Cell*, *31*(3). https://doi.org/10.1016/j.stem.2024.01.010

Shin, S., Kim, S. H., Shin, S. W., Grav, L. M., Pedersen, L. E., Lee, J. S., Lee, G. M. (2020). Comprehensive Analysis of Genomic Safe Harbors as Target Sites for Stable Expression of the Heterologous Gene in HEK293 Cells. *ACS Synthetic Biology*, *9*(6). https://doi.org/10.1021/acssynbio.0c00097

Short, M. I., Fohner, A. E., Skjellegrind, H. K., Beiser, A., Gonzales, M. M., Satizabal, C. L., Austin, T. R., Longstreth, W. T., Bis, J. C., Lopez, O., Hveem, K., Selbæk, G., Larson, M. G., Yang, Q., Aparicio, H. J., McGrath, E. R., Gerszten, R. E., Decarli, C. S., Psaty, B. M., … Seshadri, S. (2023). Proteome Network Analysis Identifies Potential Biomarkers for Brain Aging. *Journal of Alzheimer's Disease*, *96*(4). https://doi.org/10.3233/JAD-230145

Sidhaye, J., Trepte, P., Sepke, N., Novatchkova, M., Schutzbier, M., Dürnberger, G., Mechtler, K., Knoblich, J. A. (2023). Integrated transcriptome and proteome analysis reveals posttranscriptional regulation of ribosomal genes in human brain organoids. *ELife*, *12*. https://doi.org/10.7554/elife.85135

Silagi, E. S., Novais, E. J., Bisetto, S., Telonis, A. G., Snuggs, J., Le Maitre, C. L., Qiu, Y., Kurland, I. J., Shapiro, I. M., Philp, N. J., Risbud, M. V. (2020). Lactate Efflux From Intervertebral Disc Cells Is Required for Maintenance of Spine Health. *Journal of Bone and Mineral Research*, *35*(3). https://doi.org/10.1002/jbmr.3908

Silva, T. P., Fernandes, T. G., Nogueira, D. E. S., Rodrigues, C. A. V., Bekman, E. P., Hashimura, Y., Jung, S., Lee, B., Carmo-Fonseca, M., Cabral, J. M. S. (2020). Scalable generation of mature cerebellar organoids from human pluripotent stem cells and characterization by immunostaining. *Journal of Visualized Experiments*, *2020*(160). https://doi.org/10.3791/61143

Simon, M. J., Logan, T., DeVos, S. L., Di Paolo, G. (2023). Lysosomal functions of progranulin and implications for treatment of frontotemporal dementia. In *Trends in Cell Biology* (Vol. 33, Issue 4). https://doi.org/10.1016/j.tcb.2022.09.006

Sin, J., Andres, A. M., Taylo R, D. J. R., Weston, T., Hiraumi, Y., Stotland, A., Kim, B. J., Huang, C., Doran, K. S., Gottlieb, R. A. (2016). Mitophagy is required for mitochondrial biogenesis and myogenic differentiation of C2C12 myoblasts. *Autophagy*, *12*(2). https://doi.org/10.1080/15548627.2015.1115172

Sliter, D. A., Martinez, J., Hao, L., Chen, X., Sun, N., Fischer, T. D., Burman, J. L., Li, Y., Zhang, Z., Narendra, D. P., Cai, H., Borsche, M., Klein, C., Youle, R. J. (2018). Parkin and PINK1 mitigate STING-induced inflammation. *Nature*, *561*(7722). https://doi.org/10.1038/s41586-018-0448-9

Sloan, S. A., Andersen, J., Paşca, A. M., Birey, F., Paşca, S. P. (2018). Generation and assembly of human brain region–specific three-dimensional cultures. *Nature Protocols*, *13*(9). https://doi.org/10.1038/s41596-018-0032-7

Smith, K. M., Maragnoli, M. E., Phull, P. M., Tran, K. M., Choubey, L., Vaccarino, F. M. (2014). Fgfr1 inactivation in the mouse telencephalon results in impaired maturation of interneurons expressing parvalbumin. *PLoS ONE*, *9*(8). https://doi.org/10.1371/journal.pone.0103696

Smith, L., Schapira, A. H. V. (2022). GBA Variants and Parkinson Disease: Mechanisms and Treatments. In *Cells* (Vol. 11, Issue 8). https://doi.org/10.3390/cells11081261

Smits, L. M., Reinhardt, L., Reinhardt, P., Glatza, M., Monzel, A. S., Stanslowsky, N., Rosato-Siri, M. D., Zanon, A., Antony, P. M., Bellmann, J., Nicklas, S. M., Hemmer, K., Qing, X., Berger, E., Kalmbach, N., Ehrlich, M., Bolognin, S., Hicks, A. A., Wegner, F., … Schwamborn, J. C. (2019). Modeling Parkinson's disease in midbrain-like organoids. *Npj Parkinson's Disease*, *5*(1). https://doi.org/10.1038/s41531-019-0078-4

Somredngan, S., Thong-Asa, W. (2017). Neurological changes in vulnerable brain areas of chronic cerebral hypoperfusion mice. *Annals of Neurosciences*, *24*(4). https://doi.org/10.1159/000481789

Son, G., Han, J. (2018). Roles of mitochondria in neuronal development. In *BMB Reports* (Vol. 51, Issue 11). https://doi.org/10.5483/BMBRep.2018.51.11.226

Song, H., Zhu, J., Li, P., Han, F., Fang, L., Yu, P. (2021). Metabolic flexibility maintains proliferation and migration of FGFR signaling–deficient lymphatic endothelial cells. *Journal of Biological Chemistry*, *279*(4). https://doi.org/10.1016/j.jbc.2021.101149

Sőth, Á., Molnár, M., Lőrincz, P., Simon-Vecsei, Z., Juhász, G. (2024). CORVET-specific subunit levels determine the balance between HOPS/CORVET endosomal tethering complexes. *Scientific Reports*, *14*(1). https://doi.org/10.1038/S41598-024-59775-0,

Srisakuldee, W., Nickel, B. E., Fandrich, R. R., Zhang, F., Pasumarthi, K. B. S., Kardami, E. (2021a). A cardiac mitochondrial fgfr1 mediates the antithetical effects of fgf2 isoforms on permeability transition. *Cells*, *10*(10). https://doi.org/10.3390/cells10102735

Srivastava, S. P., Kanasaki, K., Goodwin, J. E. (2020). Loss of Mitochondrial Control Impacts Renal Health. In *Frontiers in Pharmacology* (Vol. 11). https://doi.org/10.3389/fphar.2020.543973

Srivatsan, S. R., McFaline-Figueroa, J. L., Ramani, V., Saunders, L., Cao, J., Packer, J., Pliner, H. A., Jackson, D. L., Daza, R. M., Christiansen, L., Zhang, F., Steemers, F., Shendure, J., Trapnell, C. (2020). Massively multiplex chemical transcriptomics at single-cell resolution. *Science*, *367*(6473). https://doi.org/10.1126/science.aax6234

Stachowiak, E. K., Benson, C. A., Narla, S. T., Dimitri, A., Chuye, L. E. B., Dhiman, S., Harikrishnan, K., Elahi, S., Freedman, D., Brennand, K. J., Sarder, P., Stachowiak, M. K. (2017). Cerebral organoids reveal early cortical maldevelopment in schizophrenia—computational anatomy and genomics, role of FGFR1. *Translational Psychiatry*, *7*(11). https://doi.org/10.1038/s41398-017-0054-x

Stachowiak, E. K., Fang, X., Myers, J., Dunham, S., Stachowiak, M. K. (2003a). cAMP-induced differentiation of human neuronal progenitor cells is mediated by nuclear fibroblast growth factor receptor-1 (FGFR1). *Journal of Neurochemistry*, *84*(6). https://doi.org/10.1046/j.1471-4159.2003.01624.x

Stachowiak, E. K., Maher, P. A., Tucholski, J., Mordechai, E., Joy, A., Moffett, J., Coons, S., Stachowiak, M. K. (1997). Nuclear accumulation of fibroblast growth factor receptors in human glial cells - Association with cell proliferation. *Oncogene*, *14*(18). https://doi.org/10.1038/sj.onc.1201057

Stachowiak, E. K., Roy, I., Lee, Y. W., Capacchietti, M., Aletta, J. M., Prasad, P. N., Stachowiak, M. K. (2009). Targeting novel integrative nuclear FGFR1 signaling by nanoparticle- mediated gene transfer stimulates neurogenesis in the adult brain. *Integrative Biology*, *1*(5–6). https://doi.org/10.1039/b902617g

Stachowiak, M. K., Fang, X., Myers, J. M., Dunham, S. M., Berezney, R., Maher, P. A., Stachowiak, E. K. (2003b). Integrative Nuclear FGFR1 Signaling (INFS) as a Part of a Universal "Feed-Forward-And-Gate" Signaling Module That Controls Cell Growth and Differentiation. In *Journal of Cellular Biochemistry* (Vol. 90, Issue 4). https://doi.org/10.1002/jcb.10606

Stachowiak, M. K., Maher, P. A., Joy, A., Mordechai, E., Stachowiak, E. K. (1996). Nuclear accumulation of fibroblast growth factor receptors is regulated by multiple signals in adrenal medullary cells. *Molecular Biology of the Cell*, *7*(8). https://doi.org/10.1091/mbc.7.8.1299

Stachowiak, M. K., Stachowiak, E. K. (2016). Evidence-Based Theory for Integrated Genome Regulation of Ontogeny-An Unprecedented Role of Nuclear FGFR1 Signaling. In *Journal of Cellular Physiology* (Vol. 231, Issue 6). https://doi.org/10.1002/jcp.25298

Statharakos, N. (2025). Link between the mechanism of mitophagy and schizophrenia: A narrative review. *Psychiatrike = Psychiatriki*. https://doi.org/10.22365/JPSYCH.2025.008

Stavoe, A. K. H., Holzbaur, E. L. F. (2019). Autophagy in neurons. In *Annual Review of Cell and Developmental Biology* (Vol. 35). https://doi.org/10.1146/annurev-cellbio-100818-125242

Stehling, O., Lill, R. (2013). The role of mitochondria in cellular iron-sulfur protein biogenesis: Mechanisms, connected processes, and diseases. *Cold Spring Harbor Perspectives in Biology*, *5*(8). https://doi.org/10.1101/cshperspect.a011312

Stevanovic, M., Drakulic, D., Lazic, A., Ninkovic, D. S., Schwirtlich, M., Mojsin, M. (2021). SOX Transcription Factors as Important Regulators of Neuronal and Glial Differentiation During Nervous System Development and Adult Neurogenesis. In *Frontiers in Molecular Neuroscience* (Vol. 14). https://doi.org/10.3389/fnmol.2021.654031

Strittmatter, L., Li, Y., Nakatsuka, N. J., Calvo, S. E., Grabarek, Z., Mootha, V. K. (2014). CLYBL is a polymorphic human enzyme with malate synthase and β-methylmalate synthase activity. *Human Molecular Genetics*, *23*(9). https://doi.org/10.1093/hmg/ddt624

Su, N., Jin, M., Chen, L. (2014). Role of FGF/FGFR signaling in skeletal development and homeostasis: Learning from mouse models. In *Bone Research* (Vol. 2). https://doi.org/10.1038/boneres.2014.3

Subramaniam, S. (2020). Exaggerated mitophagy: A weapon of striatal destruction in the brain? In *Biochemical Society Transactions* (Vol. 48, Issue 2). https://doi.org/10.1042/BST20191283

Suh, J., Kim, D.-H., Kim, S.-J., Cho, N.-C., Lee, Y.-H., Jang, J.-H., Surh, Y.-J. (2022). Nuclear Localization of Fibroblast Growth Factor Receptor 1 in Breast Cancer Cells Interacting with Cancer Associated Fibroblasts. *Journal of Cancer Prevention*, *27*(1). https://doi.org/10.15430/jcp.2022.27.1.68

Sun, N., Malide, D., Liu, J., Rovira, I. I., Combs, C. A., Finkel, T. (2017). A fluorescence-based imaging method to measure in vitro and in vivo mitophagy using mt-Keima. *Nature Protocols*, *12*(8). https://doi.org/10.1038/nprot.2017.060

Sussel, L., Marin, O., Kimura, S., Rubenstein, J. L. R. (1999). Loss of Nkx2.1 homeobox gene function results in a ventral to dorsal molecular respecification within the basal telencephalon: Evidence for a transformation of the pallidum into the striatum. *Development*, *126*(15). https://doi.org/10.1242/dev.126.15.3359

Szybowska, P., Haugsten, E. M., Wiedlocha, A. (2021). The canonical FGF-FGFR signaling system at the molecular level. *Postepy Higieny i Medycyny Doswiadczalnej*, *75*(1), 711–719. https://doi.org/10.2478/AHEM-2021-0024

Takahashi, K., Tanabe, K., Ohnuki, M., Narita, M., Ichisaka, T., Tomoda, K., Yamanaka, S. (2007). Induction of Pluripotent Stem Cells from Adult Human Fibroblasts by Defined Factors. *Cell*, *131*(5). https://doi.org/10.1016/j.cell.2007.11.019

Takahashi, K., Yamanaka, S. (2006). Induction of Pluripotent Stem Cells from Mouse Embryonic and Adult Fibroblast Cultures by Defined Factors. *Cell*, *126*(4). https://doi.org/10.1016/j.cell.2006.07.024

Tanaka, Y., Park, I. H. (2021). Regional specification and complementation with non-neuroectodermal cells in human brain organoids. In *Journal of Molecular Medicine* (Vol. 99, Issue 4). https://doi.org/10.1007/s00109-021-02051-9

Tatsuta, T., Scharwey, M., Langer, T. (2014). Mitochondrial lipid trafficking. In *Trends in Cell Biology* (Vol. 24, Issue 1). https://doi.org/10.1016/j.tcb.2013.07.011

Taverna, E., Huttner, W. B. (2010). Neural progenitor nuclei IN motion. In *Neuron* (Vol. 67, Issue 6). https://doi.org/10.1016/j.neuron.2010.08.027

Tekirdag, K., Cuervo, A. M. (2018). Chaperone-mediated autophagy and endosomal microautophagy: Joint by a chaperone. In *Journal of Biological Chemistry* (Vol. 293, Issue 15). https://doi.org/10.1074/jbc.R117.818237

Terauchi, A., Gavin, E., Wilson, J., Umemori, H. (2017). Selective Inactivation of Fibroblast Growth Factor 22 (FGF22) in CA3 Pyramidal Neurons Impairs Local Synaptogenesis and Affective Behavior Without Affecting Dentate Neurogenesis. *Frontiers in Synaptic Neuroscience*, *9*. https://doi.org/10.3389/fnsyn.2017.00017

Terauchi, A., Johnson-Venkatesh, E. M., Bullock, B., Lehtinen, M. K., Umemori, H. (2016). Retrograde fibroblast growth factor 22 (FGF22) signaling regulates insulin-like growth factor 2 (IGF2) expression for activity-dependent synapse stabilization in the mammalian brain. *ELife*, *5*(APRIL2016). https://doi.org/10.7554/eLife.12151

Terauchi, A., Johnson-Venkatesh, E. M., Toth, A. B., Javed, D., Sutton, M. A., Umemori, H. (2010). Distinct FGFs promote differentiation of excitatory and inhibitory synapses. *Nature*, *465*(7299). https://doi.org/10.1038/nature09041

Terranova, C., Narla, S. T., Lee, Y. W., Bard, J., Parikh, A., Stachowiak, E. K., Tzanakakis, E. S., Buck, M. J., Birkaya, B., Stachowiak, M. K. (2015a). Global developmental gene programing involves a nuclear form of fibroblast growth factor receptor-1 (FGFR1). *PLoS ONE*, *10*(4). https://doi.org/10.1371/journal.pone.0123380

Thiel, G. (1993). Synapsin I, Synapsin II, and Synaptophysin: Marker Proteins of Synaptic Vesicles. *Brain Pathology*, *3*(1). https://doi.org/10.1111/j.1750-3639.1993.tb00729.x

Thisse, B., Thisse, C. (2005). Functions and regulations of fibroblast growth factor signaling during embryonic development. *Developmental Biology*, *287*(2). https://doi.org/10.1016/j.ydbio.2005.09.011

Tiscornia, G., Singer, O., Verma, I. M. (2006). Production and purification of lentiviral vectors. *Nature Protocols*, *1*(1). https://doi.org/10.1038/nprot.2006.37

Tomczak, A., Mortensen, J. M., Winnenburg, R., Liu, C., Alessi, D. T., Swamy, V., Vallania, F., Lofgren, S., Haynes, W., Shah, N. H., Musen, M. A., Khatri, P. (2018). Interpretation of biological experiments changes with evolution of the Gene Ontology and its annotations. *Scientific Reports*, *8*(1). https://doi.org/10.1038/s41598-018-23395-2

Tomé, D., Dias, M. S., Correia, J., Almeida, R. D. (2023). Fibroblast growth factor signaling in axons: from development to disease. In *Cell Communication and Signaling* (Vol. 21, Issue 1). https://doi.org/10.1186/s12964-023-01284-0

Trokovic, R., Trokovic, N., Hernesniemi, S., Pirvola, U., Vogt Weisenhorn, D. M., Rossant, J., McMahon, A. P., Wurst, W., Partanen, J. (2003). FGFR1 is independently required in both developing mid- and hindbrain for sustained response to isthmic signals. *EMBO Journal*, *22*(8). https://doi.org/10.1093/emboj/cdg169

Tsai, L. H., Gleeson, J. G. (2005). Nucleokinesis in neuronal migration. In *Neuron* (Vol. 46, Issue 3). https://doi.org/10.1016/j.neuron.2005.04.013

Tseng, C. S., Chao, Y. W., Liu, Y. H., Huang, Y. S., Chao, H. W. (2023). Dysregulated proteostasis network in neuronal diseases. In *Frontiers in Cell and Developmental Biology* (Vol. 11). https://doi.org/10.3389/fcell.2023.1075215

Umemori, H., Linhoff, M. W., Ornitz, D. M., Sanes, J. R. (2004). FGF22 and its close relatives are presynaptic organizing molecules in the mammalian brain. *Cell*, *118*(2). https://doi.org/10.1016/j.cell.2004.06.025

Vaccarino, F. M., Schwartz, M. L., Raballo, R., Rhee, J., Lyn-Cook, R. (1999). Fibroblast growth factor signaling regulates growth and morphogenesis at multiple steps during brain development. In *Current topics in developmental biology* (Vol. 46). https://doi.org/10.1016/s0070-2153(08)60329-4

Van, A. A. N., Kunkel, M. T., Baffi, T. R., Lordén, G., Antal, C. E., Banerjee, S., Newton, A. C. (2021). Protein kinase C fusion proteins are paradoxically loss of function in cancer. *Journal of Biological Chemistry*, *296*. https://doi.org/10.1016/j.jbc.2021.100445

Vargas, L. M., Leal, N., Estrada, L. D., González, A., Serrano, F., Araya, K., Gysling, K., Inestrosa, N. C., Pasquale, E. B., Alvarez, A. R. (2014). EphA4 activation of c-Abl mediates synaptic loss and LTP blockade caused by amyloid-β oligomers. *PLoS ONE*, *9*(3). https://doi.org/10.1371/journal.pone.0092309

Velmeshev, D., Chavali, M., Nowakowski, T. J., Bhade, M., Mayer, S., Goyal, N., Alvarado, B., Mancia, W., Wang, S., Speir, M., Haeussler, M., Rowitch, D., Alvarez-Buylla, A., Huang, E. J., Paredes, M., Kriegstein #, A. (2021). Molecular diversity and lineage commitment of human interneuron progenitors. *BioRxiv*.

Voglewede, M. M., Ozsen, E. N., Ivak, N., Bernabucci, M., Tang, R., Sun, M., Pang, Z. P., Zhang, H. (2024). Loss of the polarity protein Par3 promotes dendritic spine neoteny and enhances learning and memory. *IScience*, *27*(7), 110308. https://doi.org/10.1016/J.ISCI.2024.110308

Walshe, J., Mason, I. (2000). Expression of FGFR1, FGFR2 and FGFR3 during early neural development in the chick embryo. *Mechanisms of Development*, *90*(1). https://doi.org/10.1016/S0925-4773(99)00225-7

Wang, C., Li, Y., Li, H., Zhang, Y., Ying, Z., Wang, X., Zhang, T., Zhang, W., Fan, Z., Li, X., Ma, J., Pan, X. (2020). Disruption of FGF Signaling Ameliorates Inflammatory Response in Hepatic Stellate Cells. *Frontiers in Cell and Developmental Biology*, *8*. https://doi.org/10.3389/fcell.2020.00601

Wang, C., Ward, M. E., Chen, R., Liu, K., Tracy, T. E., Chen, X., Xie, M., Sohn, P. D., Ludwig, C., Meyer-Franke, A., Karch, C. M., Ding, S., Gan, L. (2017). Scalable Production of iPSC-Derived Human Neurons to Identify Tau-Lowering Compounds by High-Content Screening. *Stem Cell Reports*, *9*(4). https://doi.org/10.1016/j.stemcr.2017.08.019

Wang, C., Youle, R. J. (2009). The role of mitochondria in apoptosis. In *Annual Review of Genetics* (Vol. 43). https://doi.org/10.1146/annurev-genet-102108-134850

Wang, D. X., Huang, W. T., Shi, J. F., Liu, F., Jiang, W. Y., Chen, K. Y., Zhang, S. Y., Li, X. K., Lin, L. (2025). FGF21, a modulator of astrocyte reactivity, protects against ischemic brain injury through anti-inflammatory and neurotrophic pathways. *Acta Pharmacologica Sinica*, 1–18. https://doi.org/10.1038/S41401-024-01462-X;KWRD=BIOMEDICINE

Wang, F., Kan, M., Yan, G., Xu, J., McKeehan, W. L. (1995). Alternately spliced NH2-terminal immunoglobulin-like loop I in the ectodomain of the fibroblast growth factor (FGF) receptor 1 lowers affinity for both heparin and FGF-1. *Journal of Biological Chemistry*, *270*(17). https://doi.org/10.1074/jbc.270.17.10231

Wang, J., Zhai, H. R., Ma, S. F., Shi, H. Z., Zhang, W. J., Yun, Q., Liu, W. J., Liu, Z. Z., Zhang, W. N. (2022). FOXG1 Contributes Adult Hippocampal Neurogenesis in Mice. *International Journal of Molecular Sciences*, *23*(23). https://doi.org/10.3390/ijms232314979

Wang, X., Bajpai, A. K., Gu, Q., Ashbrook, D. G., Starlard-Davenport, A., Lu, L. (2023). Weighted gene co-expression network analysis identifies key hub genes and pathways in acute myeloid leukemia. *Frontiers in Genetics*, *14*. https://doi.org/10.3389/fgene.2023.1009462

Wang, X. M., Xiao, H., Liu, L. L., Cheng, D., Li, X. J., Si, L. Y. (2016). FGF21 represses cerebrovascular aging via improving mitochondrial biogenesis and inhibiting p53 signaling pathway in an AMPK-dependent manner. *Experimental Cell Research*, *346*(2). https://doi.org/10.1016/j.yexcr.2016.06.020

Wang, Y., Li, G., Stanco, A., Long, J. E., Crawford, D., Potter, G. B., Pleasure, S. J., Behrens, T., Rubenstein, J. L. R. (2011). CXCR4 and CXCR7 Have Distinct Functions in Regulating Interneuron Migration. *Neuron*, *69*(1). https://doi.org/10.1016/j.neuron.2010.12.005

Wang, Y. M., Qiu, M. Y., Liu, Q., Tang, H., Gu, H. F. (2021). Critical role of dysfunctional mitochondria and defective mitophagy in autism spectrum disorders. In *Brain Research Bulletin* (Vol. 168). https://doi.org/10.1016/j.brainresbull.2020.12.022

Wells, M. F., Nemesh, J., Ghosh, S., Mitchell, J. M., Salick, M. R., Mello, C. J., Meyer, D., Pietilainen, O., Piccioni, F., Guss, E. J., Raghunathan, K., Tegtmeyer, M., Hawes, D., Neumann, A., Worringer, K. A., Ho, D., Kommineni, S., Chan, K., Peterson, B. K., … McCarroll, S. A. (2023). Natural variation in gene expression

and viral susceptibility revealed by neural progenitor cell villages. *Cell Stem Cell*, *30*(3). https://doi.org/10.1016/j.stem.2023.01.010

Wichterle, H., Garcia-Verdugo, J. M., Herrera, D. G., Alvarez-Buylla, A. (1999). Young neurons from medial ganglionic eminence disperse in adult and embryonic brain. *Nature Neuroscience*, *2*(5). https://doi.org/10.1038/8131

Wichterle, H., Turnbull, D. H., Nery, S., Fishell, G., Alvarez-Buylla, A. (2001). In utero fate mapping reveals distinct migratory pathways and fates of neurons born in the mammalian basal forebrain. *Development*, *128*(19). https://doi.org/10.1242/dev.128.19.3759

Wolfe, A. D., Koberstein, J. N., Smith, C. B., Stewart, M. L., Gonzalez, I. J., Hammarlund, M., Hyman, A. A., Stork, P. J. S., Goodman, R. H., Colón-Ramos, D. A. (2024). Local and dynamic regulation of neuronal glycolysis in vivo. *Proceedings of the National Academy of Sciences of the United States of America*, *121*(3). https://doi.org/10.1073/pnas.2314699121

Woodbury, M. E., Ikezu, T. (2014). Fibroblast growth factor-2 signaling in neurogenesis and neurodegeneration. In *Journal of Neuroimmune Pharmacology* (Vol. 9, Issue 2). https://doi.org/10.1007/s11481-013-9501-5

Wu, P. R., Cho, K. K. A., Vogt, D., Sohal, V. S., Rubenstein, J. L. R. (2017). The cytokine CXCL12 promotes basket interneuron inhibitory synapses in the medial prefrontal cortex. *Cerebral Cortex*, *27*(9). https://doi.org/10.1093/cercor/bhw230

Wu, W., Tian, W., Hu, Z., Chen, G., Huang, L., Li, W., Zhang, X., Xue, P., Zhou, C., Liu, L., Zhu, Y., Zhang, X., Li, L., Zhang, L., Sui, S., Zhao, B., Feng, D. (2014). ULK1 translocates to mitochondria and phosphorylates FUNDC1 to regulate mitophagy. *EMBO Reports*, *15*(5). https://doi.org/10.1002/embr.201438501

Wu, Y., Cheng, J., Qi, J., Hang, C., Dong, R., Low, B. C., Yu, H., Jiang, X. (2024). Three-dimensional liquid metal-based neuro-interfaces for human hippocampal organoids. *Nature Communications 2024 15:1*, *15*(1), 1–15. https://doi.org/10.1038/s41467-024-48452-5

Wu, Y. kuan, Ren, Z. nan, Zhu, S. long, Wu, Y. zhou, Wang, G., Zhang, H., Chen, W., He, Z., Ye, X. long, Zhai, Q. xiao. (2022). Sulforaphane ameliorates non-alcoholic fatty liver disease in mice by promoting FGF21/FGFR1 signaling pathway. *Acta Pharmacologica Sinica*, *43*(6). https://doi.org/10.1038/s41401-021-00786-2

Xiang, Y., Tanaka, Y., Cakir, B., Patterson, B., Kim, K. Y., Sun, P., Kang, Y. J., Zhong, M., Liu, X., Patra, P., Lee, S. H., Weissman, S. M., Park, I. H. (2019). hESC-Derived Thalamic Organoids Form Reciprocal Projections When Fused with Cortical Organoids. *Cell Stem Cell*, *24*(3). https://doi.org/10.1016/j.stem.2018.12.015

Xiang, Y., Tanaka, Y., Patterson, B., Kang, Y. J., Govindaiah, G., Roselaar, N., Cakir, B., Kim, K. Y., Lombroso, A. P., Hwang, S. M., Zhong, M., Stanley, E. G., Elefanty, A. G., Naegele, J. R., Lee, S. H., Weissman, S. M., Park, I. H. (2017). Fusion of Regionally Specified hPSC-Derived Organoids Models Human Brain Development and Interneuron Migration. *Cell Stem Cell*, *21*(3). https://doi.org/10.1016/j.stem.2017.07.007

Xie, Y., Liu, J., Kang, R., Tang, D. (2020a). Mitophagy Receptors in Tumor Biology. In *Frontiers in Cell and Developmental Biology* (Vol. 8). https://doi.org/10.3389/fcell.2020.594203

Xie, Y., Su, N., Yang, J., Tan, Q., Huang, S., Jin, M., Ni, Z., Zhang, B., Zhang, D., Luo, F., Chen, H., Sun, X., Feng, J. Q., Qi, H., Chen, L. (2020b). FGF/FGFR signaling in health and disease. In *Signal Transduction and Targeted Therapy* (Vol. 5, Issue 1). https://doi.org/10.1038/s41392-020-00222-7

Xie, Z., Zhao, M., Yan, C., Kong, W., Lan, F., Narengaowa, Zhao, S., Yang, Q., Bai, Z., Qing, H., Ni, J. (2023). Cathepsin B in programmed cell death machinery: mechanisms of execution and regulatory pathways. In *Cell Death and Disease* (Vol. 14, Issue 4). https://doi.org/10.1038/s41419-023-05786-0

Xu, T., Zhu, Q., Huang, Q., Gu, Q., Zhu, Y., Tang, M., Tian, S., Wang, L., Yan, F., Ge, J., Sha, W., Lin, X. (2023). FGF21 prevents neuronal cell ferroptosis after spinal cord injury by activating the FGFR1/β-Klotho pathway. *Brain Research Bulletin*, *202*. https://doi.org/10.1016/j.brainresbull.2023.110753

Yamagishi, M., Okamaoto, H. (2009). Competition for ligands between FGFR1 and FGFR4 regulates *Xenopus* neural development. *The International Journal of Developmental Biology*, *54*(1), 93–104. https://doi.org/10.1387/IJDB.092849MY

Yamaguchi, T. P., Harpal, K., Henkemeyer, M., Rossant, J. (1994). fgfr-1 is required for embryonic growth and mesodermal patterning during mouse gastrulation. *Genes and Development*, *8*(24). https://doi.org/10.1101/gad.8.24.3032

Yan, B., Mei, Z., Tang, Y., Song, H., Wu, H., Jing, Q., Zhang, X., Yan, C., Han, Y. (2023). FGF21-FGFR1 controls mitochondrial homeostasis in cardiomyocytes by modulating the degradation of OPA1. *Cell Death and Disease*, *14*(5). https://doi.org/10.1038/s41419-023-05842-9

Yan, Q., Li, X. J., Wang, Q. Q., Jia, W., Wang, S. L. (2025). FGF21 Exhibits Neuroprotective Effects by Promoting 5-HT1AR-FGFR1 Heteroreceptor Complexes and Triggering MEK1/2-ERK1/2 Signaling Pathway. *Molecular Neurobiology*, *62*(5), 6369–6382. https://doi.org/10.1007/S12035-024-04673-9/FIGURES/7

Yang, C., Wang, C., Ye, M., Jin, C., He, W., Wang, F., McKeehan, W. L., Luo, Y. (2012). Control of lipid metabolism by adipocyte FGFR1-mediated adipohepatic communication during hepatic stress. *Nutrition and Metabolism*, *9*. https://doi.org/10.1186/1743-7075-9-94

Yang, J. L. J., Bertolesi, G. E., Hehr, C. L., Johnston, J., McFarlane, S. (2018). Fibroblast growth factor receptor 1 signaling transcriptionally regulates the axon guidance cue slit1. *Cellular and Molecular Life Sciences*, *75*(19). https://doi.org/10.1007/s00018-018-2824-x

Yang, M., Fu, J. D., Zou, J., Sridharan, D., Zhao, M. T., Singh, H., Krigman, J., Khan, M., Xin, G., Sun, N. (2022). Assessment of mitophagy in human iPSC-derived cardiomyocytes. *Autophagy*, *18*(10). https://doi.org/10.1080/15548627.2022.2037920

Yazar, S., Alquicira-Hernandez, J., Wing, K., Senabouth, A., Gordon, M. G., Andersen, S., Lu, Q., Rowson, A., Taylor, T. R. P., Clarke, L., Maccora, K., Chen, C., Cook, A. L., Ye, C. J., Fairfax, K. A., Hewitt, A. W., Powell, J. E. (2022). Single-cell eQTL mapping identifies cell type-specific genetic control of autoimmune disease. *Science*, *376*(6589). https://doi.org/10.1126/science.abf3041

Ye, M., Lu, W., Wang, X., Wang, C., Abbruzzese, J. L., Liang, G., Li, X., Luo, Y. (2016). FGF21-FGFR1 coordinates phospholipid homeostasis, lipid droplet function, and ER stress in obesity. *Endocrinology*, *157*(12). https://doi.org/10.1210/en.2016-1710

Yellapragada, V., Eskici, N., Wang, Y., Madhusudan, S., Vaaralahti, K., Tuuri, T., Raivio, T. (2022). FGF8–FGFR1 signaling regulates human GnRH neuron differentiation in a time- and dose-dependent manner. *DMM Disease Models and Mechanisms*, *15*(8). https://doi.org/10.1242/dmm.049436

Yoldaş Çelik, M., Köşeci, B., Burgaç, E., Yararbaş, K. (2025). GM2 activator deficiency: An ultra-rare disorder with a new case and review of 22 published cases. *Molecular Genetics and Metabolism Reports*, *43*, 101225. https://doi.org/10.1016/J.YMGMR.2025.101225

Yoon, K., Nery, S., Rutlin, M. L., Radtke, F., Fishell, G., Gaiano, N. (2004). Fibroblast growth factor receptor signaling promotes radial glial identity and interacts with Notch1 signaling in telencephalic progenitors. *Journal of Neuroscience*, *24*(43). https://doi.org/10.1523/JNEUROSCI.0993-04.2004

Yoon, S. J., Elahi, L. S., Paşca, A. M., Marton, R. M., Gordon, A., Revah, O., Miura, Y., Walczak, E. M., Holdgate, G. M., Fan, H. C., Huguenard, J. R., Geschwind, D.

H., Pașca, S. P. (2019). Reliability of human cortical organoid generation. *Nature Methods*, *16*(1). https://doi.org/10.1038/s41592-018-0255-0

Yousefi, R., Fornasiero, E. F., Cyganek, L., Jakobs, S., Rizzoli, S. O., Rehling, P., Pacheu-Grau, D. (2020). Local translation in synaptic mitochondria influences synaptic transmission. *BioRxiv*.

Yu, S., Levi, L., Casadesus, G., Kunos, G., Noy, N. (2014). Fatty Acid-binding Protein 5 (FABP5) Regulates Cognitive Function Both by Decreasing Anandamide Levels and by Activating the Nuclear Receptor Peroxisome Proliferator-activated Receptor β/δ (PPARβ/δ) in the Brain. *Journal of Biological Chemistry*, *289*(18), 12748–12758. https://doi.org/10.1074/JBC.M114.559062

Yu, X., Zecevic, N. (2011). Dorsal radial glial cells have the potential to generate cortical interneurons in human but not in mouse brain. *Journal of Neuroscience*, *31*(7). https://doi.org/10.1523/JNEUROSCI.5249-10.2011

Yu, Y., Zeng, Z., Xie, D., Chen, R., Sha, Y., Huang, S., Cai, W., Chen, W., Li, W., Ke, R., Sun, T. (2021). Interneuron origin and molecular diversity in the human fetal brain. *Nature Neuroscience*, *24*(12). https://doi.org/10.1038/s41593-021-00940-3

Yu, Z., Lin, L., Jiang, Y., Chin, I., Wang, X., Li, X., Lo, E. H., Wang, X. (2019). Recombinant FGF21 Protects Against Blood-Brain Barrier Leakage Through Nrf2 Upregulation in Type 2 Diabetes Mice. *Molecular Neurobiology*, *56*(4). https://doi.org/10.1007/s12035-018-1234-2

Zecevic, N., Chen, Y., Filipovic, R. (2005). Contributions of cortical subventricular zone to the development of the human cerebral cortex. *Journal of Comparative Neurology*, *491*(2). https://doi.org/10.1002/cne.20714

Zhang, J., Ney, P. A. (2009). Role of BNIP3 and NIX in cell death, autophagy, and mitophagy. In *Cell Death and Differentiation* (Vol. 16, Issue 7). https://doi.org/10.1038/cdd.2009.16

Zhang, T., Xue, L., Li, L., Tang, C., Wan, Z., Wang, R., Tan, J., Tan, Y., Han, H., Tian, R., Billiar, T. R., Tao, W. A., Zhang, Z. (2016). BNIP3 protein suppresses PINK1 kinase proteolytic cleavage to promote mitophagy. *Journal of Biological Chemistry*, *291*(41). https://doi.org/10.1074/jbc.M116.733410

Zhang, Y., Ma, K., Song, S., Elam, M. B., Cook, G. A., Park, E. A. (2004). Peroxisomal Proliferator-activated Receptor-γ Coactivator-1α (PGC-1α) Enhances the Thyroid Hormone Induction of Carnitine Palmitoyltransferase I (CPT-Iα). *Journal of Biological Chemistry*, *279*(52), 53963–53971. https://doi.org/10.1074/JBC.M406028200

Zhang, Z., Fu, C., Liu, J., Sai, X., Qin, C., Di, T., Yang, Y., Wu, Y., Bian, T. (2021). Hypermethylation of the Nrf2 Promoter Induces Ferroptosis by Inhibiting the Nrf2-GPX4 Axis in COPD. *International Journal of COPD*, *16*. https://doi.org/10.2147/COPD.S340113

Zhao, H. H., Haddad, G. (2024). Brain organoid protocols and limitations. *Frontiers in Cellular Neuroscience*, *18*. https://doi.org/10.3389/FNCEL.2024.1351734,

Zhao, M., Li, D., Shimazu, K., Zhou, Y. X., Lu, B., Deng, C. X. (2007). Fibroblast Growth Factor Receptor-1 is Required for Long-Term Potentiation, Memory Consolidation, and Neurogenesis. *Biological Psychiatry*, *62*(5). https://doi.org/10.1016/j.biopsych.2006.10.019

Zhao, T., Pellegrini, L., van der Hee, B., Boekhorst, J., Fernandes, A., Brugman, S., van Baarlen, P., Wells, J. M. (2025). Choroid plexus organoids reveal mechanisms of Streptococcus suis translocation at the blood-cerebrospinal fluid barrier. *Fluids and Barriers of the CNS*, *22*(1), 1–17. https://doi.org/10.1186/S12987-025-00627-Y/FIGURES/7

Zhen, Y., Liu, K., Shi, L., Shah, S., Xu, Q., Ellis, H., Balasooriya, E. R., Kreuzer, J., Morris, R., Baldwin, A. S., Juric, D., Haas, W., Bardeesy, N. (2024). FGFR inhibition blocks NF-κB-dependent glucose metabolism and confers metabolic

vulnerabilities in cholangiocarcinoma. *Nature Communications 2024 15:1*, *15*(1), 1–17. https://doi.org/10.1038/s41467-024-47514-y

Zheng, X., Boyer, L., Jin, M., Mertens, J., Kim, Y., Ma, L., Ma, L., Hamm, M., Gage, F. H., Hunter, T. (2016). Metabolic reprogramming during neuronal differentiation from aerobic glycolysis to neuronal oxidative phosphorylation. *ELife*, *5*(JUN2016). https://doi.org/10.7554/eLife.13374

Zhou, Y. (2012). Cortical development and asymmetric cell divisions. In *Frontiers in Biology* (Vol. 7, Issue 4). https://doi.org/10.1007/s11515-012-1235-x

Zou, W., Lv, Y., Zhang, S., Li, L., Sun, L., Jiao, J. (2024). Lysosomal dynamics regulate mammalian cortical neurogenesis. *Developmental Cell*, *59*(1). https://doi.org/10.1016/j.devcel.2023.11.021